ARS JOURNAL

RUSSIAN SUPPLEMENT

J. George Adashko, Editor

Published Under National Science Foundation Grant-in-Aid

Formation of a Shock Discontinuity Ahead of a Flame Front

G. D. SALAMANDRA and
O. A. TSUKHANOVA

THE COMBUSTION of gases, in spite of the apparent simplicity, is so complicated a process that many phenomena that accompany it have not been sufficiently investigated. One such phenomenon is the formation of the shock discontinuity ahead of a flame front.

In addition to being of theoretical interest, a study of this process also has great practical significance, since the presence of a shock discontinuity ahead of a flame front is the condition for the transition of a slow combustion wave to a detonation. The rate of acceleration of the flame determines where the shock wave (and consequently the transition into detonation) occurs relative to the ignition point in the combustion chamber. In the first approximation the problem of the motion of a gas ahead of the flame front can be reduced to the problem of motion of gas in front of a piston, accelerated in accordance with the same law that governs the actual propagation of the flame. The problem of the combustion of a gas contained in an infinite cylinder, bounded on one end by an accelerated piston, was first solved by Hugoniot at the end of the 19th century.

In solving this problem, Hugoniot started with the equation of motion of an ideal gas, obtained from conservation laws in the following form

$$\frac{\partial^2 u}{\partial t^2} = \varphi\left(\frac{\partial u}{\partial x}\right)\frac{\partial^2 u}{\partial x^2} \qquad [1]$$

where

$$\varphi\left(\frac{\partial u}{\partial x}\right) = a^2\left(1 + \frac{\partial u}{\partial x}\right)^{-\gamma-1} \qquad [2]$$

Here u is the displacement of a point that has a coordinate x at the instant t, $\gamma = c_p/c_v$, and a is the velocity of sound in the unburned mixture. Disturbances travel in front of the accelerated piston in the tube, and a discontinuity, namely a shock wave, is produced where these disturbances meet each other. According to Hugoniot, two elementary disturbances produced by the piston at instants that are close to each other will meet at a distance

$$X = \frac{2a^2\{1 + [(\gamma - 1)/2a]v\}^{2\gamma/(\gamma-1)}}{(\gamma + 1)(\partial v/\partial t)} \qquad [3]$$

where

t = time of excitation of a given disturbance in the gas
v = velocity of motion of the piston at the instant t

Hugoniot has shown that all the elementary disturbances meet at one point only if the piston moves in a special way, namely, if the velocity of the piston changes with time as

$$v = \frac{2a}{\gamma - 1}\left(1 - \frac{at}{X}\right)^{-\frac{(\gamma-1)}{(\gamma+1)}} - \frac{2a}{\gamma - 1} \qquad [4]$$

In the general case, the disturbances produced by the moving piston will be concentrated not in one section of the tube, but over a certain length of the tube.

It must be noted that by reducing the problem of the motion of a gas ahead of the flame front to a problem of the motion of a gas ahead of a piston, the flame is assumed to have properties of a solid wall, which compresses the gas in front of it.

The time interval within which the elementary disturbance sent by the flame evolves into a shock wave is determined by the character of the variation of the flame velocity during the combustion process. The almost complete lack of experimental data on the formation of a shock discontinuity ahead of a flame front, makes it difficult to check the validity of reducing the complex problem of motion of gas ahead of a flame front to the simpler and already solved problem of the motion of gas in front of a piston.

It should be noted that in most studies of unsteady combustion or of the transition from slow combustion into detonation, the process is usually recorded by direct photography of the intrinsic radiation of the burning mixture.

The formation of a shock wave ahead of the flame front is not accompanied by intrinsic radiation, and therefore in order to follow all the details of this process, it must be examined optically, and the visible processes that occur in the unburned mixture become decisive. It is best to investigate a hydrogen-oxygen mixture, since the combustion process in such mixtures is so rapid, that the shock discontinuity is formed a comparatively short distance from the ignition point in the combustion chamber.

To be able to trace all the phases of the process of shock wave production, it is necessary to use high speed photography. The best known version of high speed photography is "spark photography," in which the subject is illuminated by a series of electric sparks produced by discharging a capacitor through the illuminating spark gap.

A distinguishing feature of spark apparatus is the simplicity of the spark circuit, the ease of synchronization of the light flashes with the investigated process, and the possibility of varying the frequency of the photographs over a wide range. A spark discharge, lasting 10^{-6} sec, insures a sufficiently short exposure time, making it possible to obtain sharp photographs even with very fast processes. Inasmuch as the speed of propagation of the elementary disturbances that evolve into a shock wave does not exceed 1000 m/sec, we have deemed it advisable to use, in our particular investigation, a spark device capable of taking a total of about 100 frames at a rate of 50,000 to 70,000 frames per sec.

1 Experimental Setup

The experimental setup for studying the process of shock discontinuity formation ahead of the flame front consisted of an optical section to visualize the disturbances that occur in the gas during the combustion of the mixture, an electrical section to produce a series of sufficiently intense short duration electric flashes, and a photographic section to record

Translated from "Physical Gasdynamics," USSR Acad. Sci., pp. 151–162.

the process. The IAB-451 mirror-meniscus apparatus was used to make the disturbances in the gas visible.

The light source used to take pictures by the scanning method was a PZh-26 lamp. During high speed spark photography, the lamp was replaced by a discharge gap. In the latter case the source of light was a series of illuminating sparks. The number of sparks in the series and their repetition frequency were determined by the parameters of the electric circuit.

The diagram of the electric section of the spark apparatus is shown in Fig. 1. The power supply, consisting of a high voltage transformer *Tr*, which steps up the voltage to 27 kv, and of a rectifier *Kp*, is disconnected prior to taking the picture. Thus the source of electric energy is the 1-μf capacitor C_1. When switch *P* is closed, capacitor C_1 is discharged and charges capacitor C_2, which has a rating of 0.125 μf. Whenever the voltage across capacitor C_2 reaches a value sufficient to break down the spark gap, a spark is produced in the gap *F*. Using an inductance $L = 2$ h, a total of 150 to 200 spark flashes were produced at a repetition rate of approximately 50,000 per sec. Kozachenko, using an installation of this type, was able to vary the taking rate from 5000 to 100,000 frames per sec by varying the inductance from 10 to 0.5 h. This spark circuit is convenient in operation. True, a certain difficulty is caused by the need of preparing a set of inductors designed for rather high voltage. This is why the inductor was later replaced by a resistor. If the resistor is chosen sufficiently large and C_2 sufficiently small, the capacitor C_2 will discharge into the illuminating spark gap much more rapidly than it is charged through the resistance. This guarantees good quenching of the spark. By varying the resistance it is possible to adjust the picture-taking frequency over a wide range. With 27 kv across capacitor C_1, and with $C_1 = 2.7$ μf and $C_2 = 0.125$ μf, the breakdown voltage of the gap approximately 15 kv, and the resistance 1200 ohms, the repetition rate of the flashes reaches 50,000 per sec, the total number of flashes being approximately 200. The explosion was synchronized with the series of illuminating flashes by means of a special pendulum switch.

To obtain bright illuminating flashes, a special discharge gap was designed, a so-called "linear source of light," shown in Fig. 2. The electrodes of the gap are a brass plate *5*, clamped on both ends by fiber plates *9*, and the second electrode is a tungsten rod *10*, which can be moved by means of a micrometer screw *11*. Light strikes the slit of the optical setup through a Plexiglas covered window cut through the forward portion of the discharge assembly. Valve *7* allows one to pump the air out of the discharge assembly and to fill it with hydrogen. In spite of the very low light yield of a hydrogen discharge, this gas was chosen, since it permits taking pictures at a high frequency. The explosion process was recorded on a film having a speed of 250 GOST (=Russian standard) units, placed on the outer surface of a uniformly

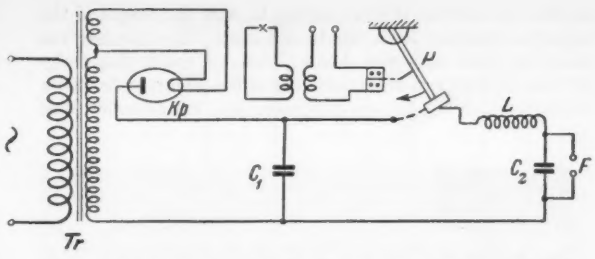

Fig. 1 Diagram of electrical section of the spark assembly

rotating drum driven by a synchronous motor. To determine the speed of the moving film, an intermittent source of light, which produced a series of lines on the film, was photographed simultaneously outside the field of the image. The speed of the film could be determined from the repetition frequency of the light flashes by measuring the distance between the time markers. In our case the film moved at a speed of 45 m/sec. The pulsating source of light for the time markers was a neon lamp MN-7, fed from a 50–500 cycle frequency converter. To prevent the time markers from becoming superimposed on each other, a shutter was placed in front of the neon lamp, which in turn was placed in a special tube; the shutter was closed after each revolution.

The object lens used was an *f*/1.4, 13.5-cm focal length "Sonnar" telephoto lens. It was already noted in the foregoing that the process was photographed by two methods: A scanning method, and spark motion-picture photography. In the former case a continuous source of light was used. To prevent superimposed images, a focal-plane type shutter was placed in the path of the light and was closed after each revolution. The unique construction of the shutter made it possible to synchronize the operation of the shutter with the process. In the case of spark photography there was no need for a shutter. To prevent superimposed frames, the size of capacitor C_1 was chosen such that the entire series of illuminating flashes took place within a single revolution of the photorecording drum.

2 Explosion Chamber and Sequence of Experiments

To explain the effect of the shape of the chamber cross section on the process of formation of a shock wave in front of the flame front, the behavior of the process in round and rectangular chambers was compared. The area of the transverse cross section of both chambers was kept constant. Chambers in which the combustible mixture was burned consisted of several sections joined with flanges. By using a different

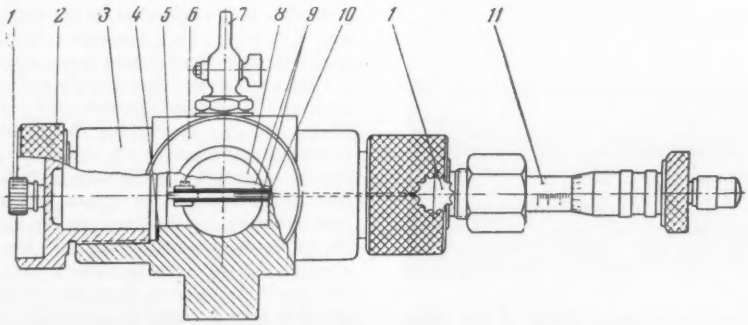

Fig. 2 Discharge assembly, "linear source of light"

number of sections, it was possible to vary the length of the explosion chamber from 280 to 608 mm. The chamber was closed on both ends with cover plates. A spark plug to ignite the mixture was mounted in one of the plates, and a valve, through which the air was evacuated and the chamber filled with the explosive mixture, was mounted in the other plate. The process was photographed through side openings cut in one of the sections of the chamber.

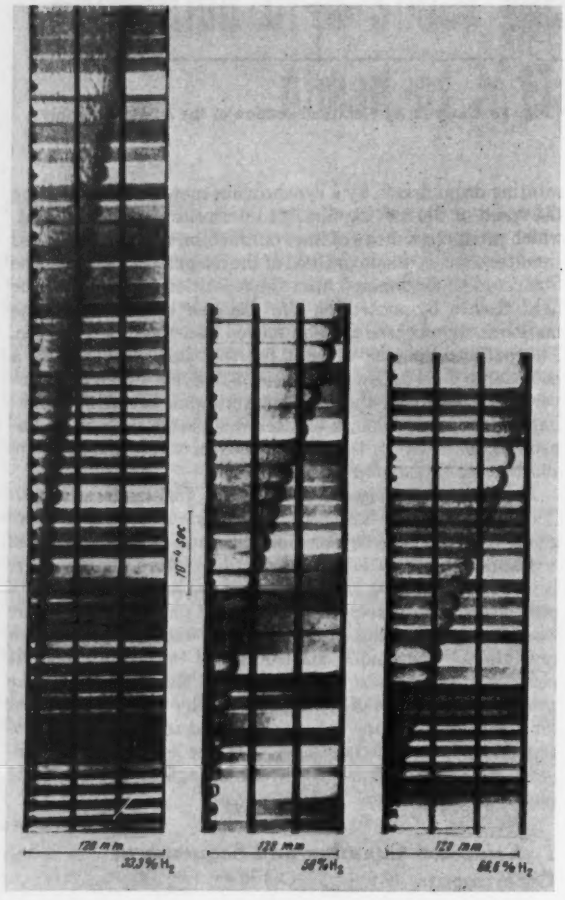

Fig. 3 Instantaneous photographs of the combustion of hydrogen-oxygen mixtures in the first section of a rectangular chamber

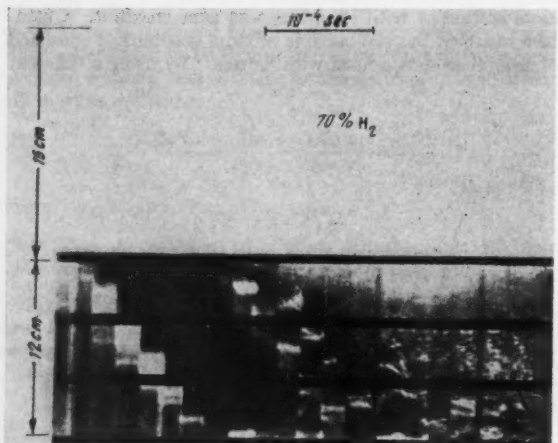

Fig. 4 Formation of shock discontinuity ahead of the flame front

The openings were covered with plane-parallel optical-glass plates, secured to the body of the chamber with the aid of slotted covers. The cross pieces of the covers served as scale markers. The combustible mixture was compounded by volume and stored in a gas holder without being dried before filling the chamber. We investigated the combustion of hydrogen-oxygen mixtures containing 25, 33.3, 50, 66.6 and 70 per cent hydrogen.

After the chamber was filled with the explosive mixture, the electric section of the apparatus was turned on. The capacitor bank was charged to 27 kv, after which the motor of the drum camera was turned on and the latch, which maintained the pendulum of the synchronizing device in a horizontal position, was actuated. The falling pendulum switch closes the high voltage circuit of the spark assembly. Simultaneously, the tail piece of the pendulum opens the circuit of the primary winding of the transformer, producing a spark that ignites the mixture. Approximately 200 different phases of the investigated process were recorded on the uniformly moving film of the photorecorder.

The first series of experiments was carried out in chambers long enough to permit a shock wave to be formed before the disturbances, produced by the front of the flame in the unburned gas, reached the end of the chamber.

The second series of experiments was carried out in a short chamber. In this case a shock wave is formed as a result of cumulation of disturbances reflected from the end of the chamber.

3 Description of the Experimental Material and Analysis of the Results

a Formation of Shock Wave Ahead of the Flame Front

Fig. 3 shows a series of instantaneous photographs of the combustion of hydrogen-oxygen mixtures in the first section of a rectangular chamber measuring 19 × 37 mm.

The photographs show that the flame propagates from left to right as the film moves in a vertical direction. The two black strips parallel to the time axis are scale markers, spaced 38 mm apart. The photographs were taken against a so-called "gray" background.

As can be seen from the photographs, the initially hemispherical flame front is gradually drawn out and becomes meniscus shaped. As the flame propagates, the flame front recorded on the photograph becomes somewhat thicker, showing development of a flame front surface with the meniscus shape retained.

The flame front is preceded by traveling disturbances, which are quite clearly seen on photographs of Fig. 4, which characterize the development of the process of combustion of a hydrogen-oxygen mixture containing 70 per cent hydrogen in the second section of a chamber 480 mm long. The distance from the point of ignition to the start of the section viewed was 160 mm. The developing shock wave appears as a gradually narrowing bright zone, which changes finally into a thin line, evidencing the formation of a shock discontinuity. The shock discontinuity is formed approximately 25 cm from the spark plug that ignites the mixture. In a mixture containing 50 per cent hydrogen, the shock discontinuity is formed at a distance of 29 to 30 cm, and in a mixture with a still greater oxygen content, the elementary disturbances sent by the flame evolve into a shock wave 57 to 58 cm from the spark plug. If the flame front traveling through the tube can be likened to a piston that compresses the gas in front of it, then the already available Hugoniot solution can be used to determine the distance from the ignition to the place of formation of the shock discontinuity.

To estimate the value of X in Equation [3] for the case of propagation of the flame in a tube, it is necessary to know the speed and acceleration of the flame, the γ of the mixture, and the velocity of sound propagation in the unburned mixture. The velocity of sound is calculated from the formula

$$a = \sqrt{9.81\gamma R_{cm} T}$$

where

T = absolute temperature of the mixture
$R_{cm} = R_{O_2} \cdot R_{H_2}/(\alpha R_{O_2} + \beta R_{H_2})$
R_{O_2} = 26.5 m/deg
R_{H_2} = 420 m/deg
α = fraction of the hydrogen in the mixture
β = fraction of oxygen in the mixture

For the hydrogen-oxygen mixtures of interest to us, the velocity of sound at 20 C has the following values:

H_2, per cent in mixture	a, m/sec
70	567
66.6	535
50	448
33.3	394

The velocity and acceleration of the flame at any instant of time can be readily found experimentally. During the first instants after the ignition of the mixture, the speed of the flame first increases and then remains constant, after which it gradually decreases and drops sharply at the instant when the flame makes contact with the walls of the chamber. This is followed by a new increase in the speed of flame propagation. In a rectangular chamber, by virtue of the fact that the flame front first touches the upper and lower walls and then the side walls of the chamber, it is impossible to establish a reduction in the speed of flame propagation due to the increase in heat transfer during contact between the flame and the walls. In later instants of time the speed of flame propagation increases as the flame advances in the tube, in both round and rectangular chambers. If one disregards the stage during which the flame propagates from ignition to contact with the wall, the path covered by the flame in a time t can be represented by the empirical formula

$$x = at^b + c \qquad [5]$$

where

x = path, m
t = time, sec
a, b, c = quantities that depend on the concentration of the mixture and structural features of the chamber

Differentiating Equation [5] with respect to t, we can readily find the velocity and acceleration of the flame at any instant of time. Figs. 5a and 5b illustrate the acceleration as a function of time for hydrogen-oxygen flames in round and rectangular chambers.

It is easy to note that the acceleration of the flame depends on the structural features of the chamber, and depends for each given chamber on the concentration of the mixture. Whereas in a rectangular chamber the combustion process proceeds in such a way that the acceleration of the flame diminishes with time for all the hydrogen-oxygen mixtures considered, in a round chamber of equal transverse area as the rectangular chamber, the dependence of the acceleration of the flame on the concentration varies quite pronouncedly. In fact, in a mixture containing 70 per cent hydrogen, the acceleration of the flame increases with time; in a mixture containing 50 per cent hydrogen, the flame propagates with equal acceleration, and in a mixture with a still greater content of oxygen, the acceleration diminishes gradually as the flame moves in the chamber. Since the variation of the acceleration of the flame should be greatly affected by the distance from the ignition point to the place where the shock discontinuity is generated, it can be deduced without calculation that the conditions in a round chamber are obviously more favorable for the occurrence of a shock discontinuity than in a rectangular chamber. By way of example let us calculate at what distance from the ignition point will there be encountered the disturbances propagated by the flame front during the instant $t = 10^{-4}$ sec for the case of a combustion of a mixture containing 70 per cent hydrogen in a round chamber.

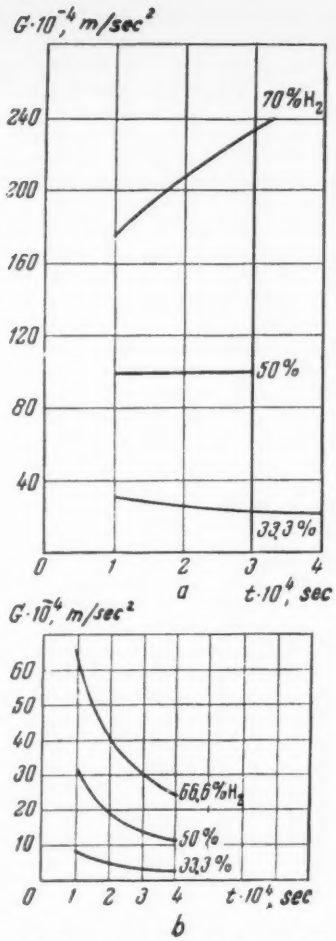

Fig. 5 Change in acceleration of flame with time

Inserting the corresponding values of v and γ in the formula for X, and taking into account the fact that the velocity of sound in the unburned mixture is 567 m/sec, we obtain X = 22.5 cm. Considering that at the instant $t = 10^{-4}$ sec the front of the flame is at a distance 2.4 cm from the edge of the chamber, the distance from the point of ignition to the point of "generation" of the shock discontinuity is 24.9 cm. This value is in good agreement with experiment, thus confirming the correctness of the idealization we have assumed for the process. The solution of this problem becomes particularly clear if the graphic method of characteristics is employed.

b Use of the Graphic Method of Characteristics in the Solution of the Problem of Unsteady One-Dimensional Flow of Gas Ahead of the Flame Front

Without dwelling on the derivation of the equation of

characteristics, which is covered in detail in (2 and 3),[1] let us proceed to solve the problem of interest to us.

A flame front propagates in a hydrogen-oxygen mixture contained in a tube at constant pressure and temperature. The flame propagation is described by the curve OA in the (x, t) plane. It is required to find the state of the gas ahead of the flame front. Let us make the corresponding graphic construction. The sonic disturbances at the instants of time 1, 2, 3, 4, 5, 6, 7 and 8 are determined in the (v, a) plane by the characteristic represented in Fig. 6c by a straight line making an angle 45 deg with the v and a axes. This angle is determined by the choice of the scale of the ordinate axis.

The sonic disturbances traveling from points 1, 2, 3, . . ., 8 (Fig. 6a) are determined as the ordinates of the points, the abscissas of which are the corresponding values of the velocity of the flame front.

Let us call attention to one peculiarity in our problem. Usually, in the solution of the problem of motion of a gas in front of a piston moving in a tube, it is the first disturbance, produced by the piston at the initial instant of time and propagating with the velocity of sound in the unburned gas, which plays the major role. In the ignition of a mixture by even a very weak spark, a disturbance is also produced in the gas and propagates at the velocity of sound, but this is where the analogy ends. Experience shows that the first disturbance, produced in the gas by an ignition spark, usually does not participate in the formation of a sufficiently intense shock wave. Therefore, in solving the problem by the method of characteristics, this disturbance should not be taken into account. The results of the calculations of the sonic disturbances, produced by the front of the flame in later instants of time, are listed in Table 1.

As can be seen from the diagram, the characteristics that emerge at the instants of time 1 and 2 are parallel, since the flame velocity in this section remains constant. The flame velocity decreases then, causing a diverging bundle of characteristics. Starting with the instant $t = 10^{-4}$ sec, the flame velocity increases. The characteristics that emerge at the instants 4, 5, 6, 7 and 8 intersect at a distance $\simeq$24.5 cm. The calculation is in good agreement with experiment. Analogous calculations were made for combustion of a mixture containing 50 and 33.3 per cent hydrogen.

Calculations carried out by the same method show that when a flame propagates in a rectangular chamber, the shock discontinuity is formed at a considerably greater distance from the point of ignition than if the same mixture is ignited in a round chamber.

The results of the construction made by us are presented in Table 2.

It is easy to note that the distance from the point of ignition to the point of formation of the shock discontinuity depends substantially on the structural features of the chamber.

For equal transverse areas, a shock discontinuity is produced in the round chamber at half the distance from the point of ignition than when the same mixture is ignited in a rectangular chamber.

To relate the distance from the point of ignition to the point of production of a shock wave and the time of its occurrence with the fuel characteristics of the mixture, we make use of the formulas obtained by Hugoniot to calculate the values of X and T. According to Hugoniot

$$X \sim \frac{a^2}{dv/dt} \qquad T \sim \frac{a}{dv/dt}$$

It has been shown previously that the acceleration of the flame, which enters into the denominators of both expressions, is a function of the construction of the chamber, and is determined for a given chamber by the concentration of the combustible mixture.

[1] Numbers in parentheses indicate References at end of paper.

Table 1

Point	v, m/sec	$\frac{2}{\gamma - 1} a$, m/sec	a, m/sec	$v + a$, m/sec
1	300	3135	627	927
2	300	3135	627	927
3	200	3035	607	807
4	141	2976	595	736
5	187	3022	604	791
6	235	3070	614	849
7	282	3117	623	905
8	334	3169	634	968

Calculation shows that during that time when the front of the flame generates disturbances in the unburned mixture that cumulate in a shock wave, the acceleration of the flame, in the range of concentrations of interest to us, is proportional to the square of the percentage of hydrogen in the mixture and, consequently

$$X \sim \frac{a^2}{m^2} \qquad T \sim \frac{a}{m}$$

Fig. 7 shows the dependence of X on a^2/m^2. The abscissas represent the square of the ratio of the velocity of sound to the percentage of hydrogen, while the ordinates represent the distance from the point of ignition to the point of generation of the shock discontinuity. The open circles denote the values of X that correspond to the process in a round chamber, while the filled ones are for a rectangular chamber.

So far we have not considered the process of formation of the shock wave in chambers that are not sufficiently long. In short chambers the elementary disturbances, generated by an accelerated flame, do not have a chance to cumulate into a shock wave before they intersect the end of the chamber. The formation of the shock discontinuity in a short chamber is therefore complicated by the participation of disturbances reflected from the end of the chamber.

c Formation of Shock Wave in a Short Chamber

The shock wave is formed at a definite length of the chamber. If the disturbances produced by the flame in the unburned gas do not have time to cumulate into a shock wave prior to encountering the end of the chamber, the shock discontinuity may occur as a result of addition of the disturbances that are reflected from the end of the chamber or from the front of the flame. Elementary disturbances, as a rule, do not pass through the front of the flame, and are re-

Table 2

	Round chamber		Rectangular chamber
Per cent H_2 in mixture	Distance from ignition point to point of formation of shock wave, cm (calculated)	Distance from ignition point to point of formation of shock wave, cm (experimental)	Distance from ignition point to point of formation of shock wave, cm (calculated)
70	24.5	25–26	. . .
66.6	. . .	. . .	60
50	28.5	29–30	69
33.3	56	$\approx$58	121

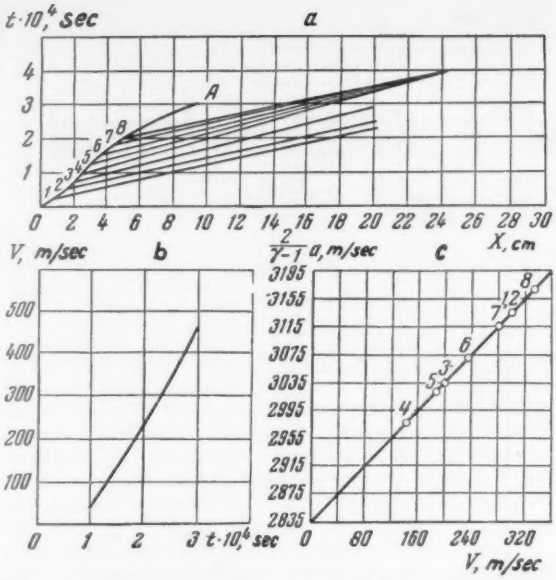

Fig. 6 Solution of the problem of unsteady one-dimensional flow of gas ahead of the flame front by the method of characteristics

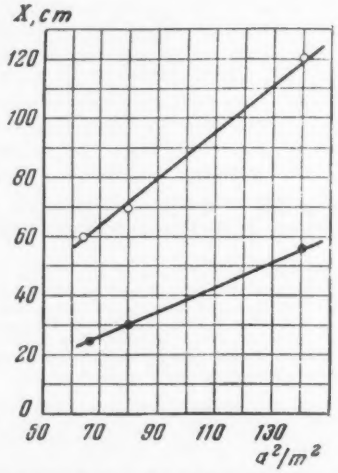

Fig. 7 Dependence of the value of X on the square of the ratio of the velocity of sound to the percentage of hydrogen

flected from it as from a solid wall. Fig. 8 shows the process of formation of a shock discontinuity in the combustion of a mixture containing 33 per cent H_2 in a chamber 280 mm long. In the left half of the diagram is shown the trace of motion of the flame front in the first section of the chamber. The developing shock wave is clearly seen ahead of the flame front that appears in the field of view on the twelfth frame. On the first frames it has the form of a rather broad light zone. After reflection from the end of the chamber the disturbance propagates in the opposite direction and is recorded on the photograph in the form of a gradually narrowing dark zone. In addition to the formed shock wave, the photograph shows clearly the disturbances produced by the flame front in the unburned gas. Propagating between the flame front and the end of the chamber, they form a dense grid of disturbances that do not interact with each other.

Since the flame front behaves like a solid wall with respect to the elementary disturbances, it is possible, when calculating the state of the gas between the front of a flame and the wall,

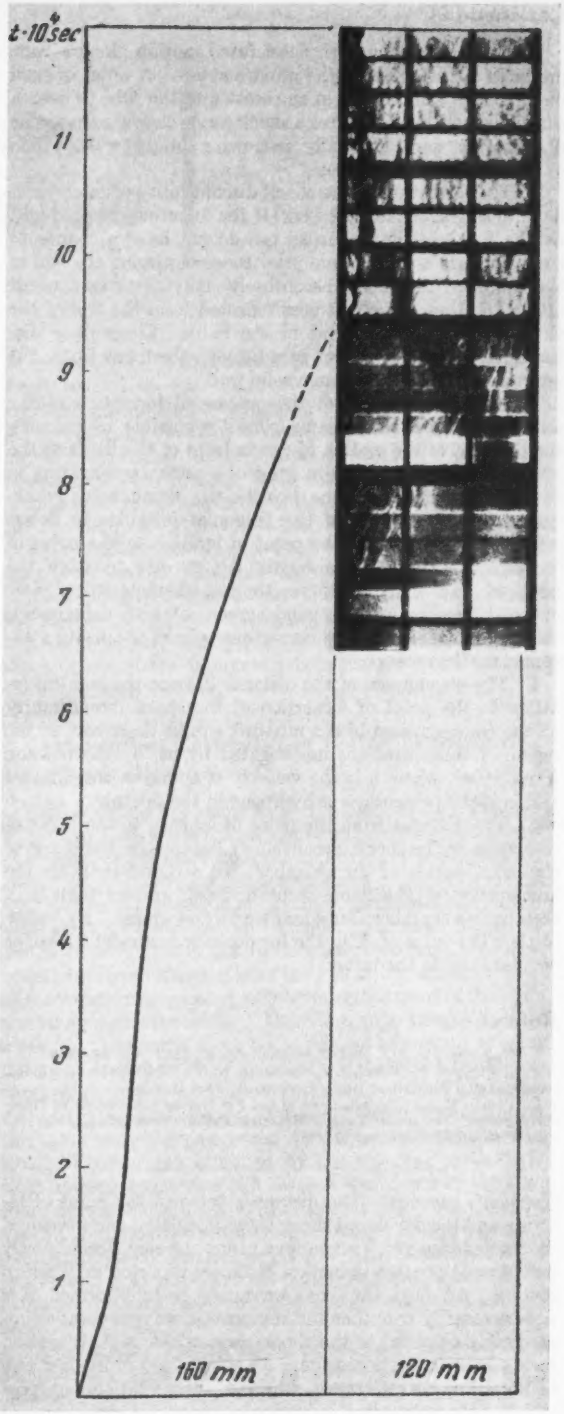

Fig. 8 Formation of shock discontinuity in a short chamber

to solve the problem by the graphic method of characteristics, by likening the flame to a piston. Fig. 9 shows the corresponding constructions for the case represented in the photograph. The law of propagation of the flame is specified by curve OA. The position of the wall is noted by a vertical line with coordinate $X = 25$ mm. Comparison of Figs. 8 and 9a shows that the calculation of the place of formation of the shock wave in a short chamber is in good agreement with experiment.

Conclusions

1 A flame moving with accelerated motion along a tube produces disturbances in the unburned gas. A series of such disturbances, cumulating in one section of the tube or over a certain length of it, produces a shock wave, clearly seen on the photographs as a gradually narrowing bright zone, which finally becomes a thin line.

2 The formation of the shock discontinuity occurs over a definite length of the chamber. If the disturbances produced by the flame in the unburned gas do not have a chance to cumulate into a shock wave prior to encountering the end of the chamber, the shock discontinuity may occur as a result of the addition of disturbances reflected from the end of the chamber or from the front of the flame. Elementary disturbances, as a rule, do not pass through the flame front, but are reflected from it as from a solid wall.

3 In the calculation of the process of formation of the shock wave ahead of the flame front it is possible, by reducing the problem of the motion of gas in front of the flame to the problem of motion of gas in front of a piston accelerating in accordance with the same law as the flame actually accelerates, to make use of the Hugoniot formulas to determine the distance from the point of ignition to the point of formation of the shock discontinuity, or else to solve the problem graphically by the method of characteristics. Our own calculations were in good agreement with experiment, this being evidence of the correctness of the idealization assumed for the process.

4 The dependence of the distance X from the point of ignition to the point of formation of the shock discontinuity on the concentration of the mixture, can be described, in the region of concentrations investigated by us, by the relation $X \sim a^2/m^2$, where a is the velocity of sound in the mixture and m is the percentage of hydrogen in the mixture.

5 The distance from the point of ignition to the point of formation of the shock discontinuity depends on the shape of the cross section of the chamber. In a round chamber the acceleration of the flame front is much greater than in a rectangular chamber (for equal transverse areas). By virtue of this, the value of X in the former case is almost 2.5 times smaller than in the latter.

References

1 Hugoniot, H., *J. J. Ecole Polytechn.*, vol. 57, 1887; vol. 58, 1889.

2 Kochin, N. E., Kibel', I. A. and Roze, N. V., "Teoreticheskaya gidromekhanika" (Theoretical Hydromechanics), Part II, 1948.

3 Popov, V. A., "Certain Laws of the Pre-Detonation Section of Flame Propagation," *Izv. Akad. Nauk SSSR, Otd. Tekhn. Nauk (Bull. Acad. Sci. USSR, Div. Tech. Sci.)*, no. 10. 1953.

Reviewer's comment: The distances between the point of ignition and the developed shock wave calculated and measured by Salamandra and Tsukhanova cannot be compared directly with the detonation induction distances reported in Western studies. Although the shock wave may be fully formed, it is not necessarily true that the combustion wave is located immediately adjacent to the shock wave which is the situation for a stable detonation wave. As pointed out in the last two of the following references, different interpretations are possible for the detonation induction distance. It would appear that this work may add another interpretation to the list.

With the exception of the original work of Hugoniot, no references of related research conducted outside the USSR are given in this paper. The following references are suggested to obtain information on related studies.

—Loren E. Bollinger
The Ohio State University

Laffitte, P. and Dumanois, P., *Compt. Rend.*, vol. 183, 1926, p. 284.

Laffite, P., *Compt. Rend.*, vol. 186, p. 951.

Chu, Boa-Teh, "On the Generation of Pressure Waves at a Plane Flame Front," in "Fourth Symposium on Combustion," The Williams and Wilkins Co., Baltimore, 1953, pp. 603–612.

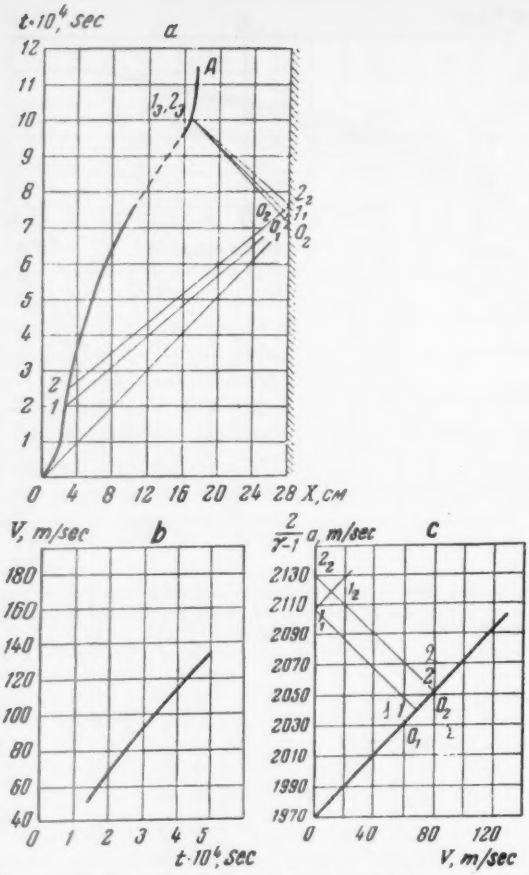

Fig. 9 Determination of the place of formation of a shock discontinuity by the method of characteristics

Schmidt, E., Steinicke, H. and Neubert, U., "Flame and Schlieren Photographs of Combustion Waves in Tubes," in "Fourth Symposium on Combustion," The Williams and Wilkins Co., Baltimore, 1953, pp. 658–666.

Bollinger, L. E. and Edse, R., "Measurement of Detonation Induction Distances in Hydrogen-Oxygen and Acetylene-Oxygen-Nitrogen Mixtures at Normal and Elevated Initial Pressures and Temperatures," Wright Air Development Center Tech. Rep. 57–414, ASTIA no. AD 130 874, June 1957.

Adams, G. K. and Pack, D. C., "Some Observations on the Problem of Transition Between Deflagration and Detonation," in "Seventh Symposium (International) on Combustion," Butterworths Scientific Publications, London, 1959, pp. 812–819.

Brinkley, S. R., Jr. and Lewis, B., "On the Transition from Deflagration to Detonation," in "Seventh Symposium (International) on Combustion," Butterworths Scientific Publications, London, 1959, pp. 807–811.

Martin, F. J. and White, D. R., "The Formation and Structure of Gaseous Detonation Waves," in "Seventh Symposium (International) on Combustion," Butterworths Scientific Publications, London, 1959, pp. 856–865.

Oppenheim, A. K. and Stern, R. A., "On the Development of Gaseous Detonation—Analysis of Wave Interaction Phenomena," in "Seventh Symposium (International) on Combustion," Butterworths Scientific Publications, London, 1959, pp. 837–850.

Bollinger, L. E. and Edse, R., "Detonation Induction Distances in Combustible Gaseous Mixtures at Atmospheric and Elevated Initial Pressures, I Methane-Oxygen, II Carbon Monoxide-Oxygen, III Hydrogen-Oxygen," Wright Air Development Center Tech. Rep. 58–591, ASTIA no. AD 208–325, March 1959.

Bollinger, L. E., Fong, M. C. and Edse, R., "Detonation Induction Distances in Combustible Gaseous Mixtures at Atmospheric and Elevated Initial Pressures. IV Hydrogen-Nitric Oxide, V Hydrogen-Oxygen-Diluent, VI Theoretical Analysis," Wright Air Development Center Tech. Rep. 59–437, Aug. 1959.

Edse, R., "Propagation of Shock Waves Through Chemically Reacting Gas Mixtures," Proceedings, American Rocket Society Meeting on Propellant Thermodynamics and Handling, Ohio State University, July 20–21, 1959.

Gross, R. A. and Oppenheim, A. K., "Recent Advances in Gaseous Detonation," ARS Journal, vol. 29, no. 3, March 1959, pp. 173–179.

Bollinger, L. E., Fong, M. C. and Edse, R., "Theoretical Analysis and Experimental Measurements of Detonation Induction Distances at Atmospheric and Elevated Initial Pressures," ARS preprint no. 922–59.

Bollinger, L. E. and Edse, R., "Effect of Initial Pressure and Temperature on the Detonation Induction Distances in Hydrogen-Oxygen and Acetylene-Oxygen-Nitrogen Mixtures," American Rocket Society Meeting on Propellant Thermodynamics and Handling, Columbus, July 20–21, 1959.

Interaction Between a Flame and a Shock Discontinuity

G. D. SALAMANDRA

THE PROCESS of flame propagation in a closed chamber is accompanied by a wave process. The acoustic waves are the cause of one of the unique propagations of the flame, namely, vibrational combustion. The ripples of the flame are connected with phenomena of hydrodynamic character that occur during combustion, which are much more intense than pure acoustic phenomena. The first attempt to attribute the occurrence of flame ripples to purely mechanic interaction of the disturbances that arise in the gas with the front of the flame was made by Dixon, who attributed the flame ripples to the interaction between the reflected sound wave and the front of the flame. By using Dixon's method to plot the path of the sound wave, Sokolik found no agreement between the reflected wave and the place where the flame is rippled, which is quite understandable, since the sound wave is a wave of infinitesimally small amplitude and cannot cause finite ripples of the flame. Flame ripples are due to the action of shock waves on the front of the flame. In spite of the fact that the combustion with ripples has long interested the researchers, the problem of the investigation of the interaction of the flame front with the shock wave is still not being given enough attention at the present time. Most investigations devoted to this problem pertain to a single particular case, which indeed is of great practical and theoretical interest, namely the case where the interaction of the shock wave with the flame of the front results in a detonation wave. Completely opposed to this is the problem of interaction between a shock wave and the flame front without detonation propagation of the flame. Without dwelling in detail on the mechanism of formation of shock waves ahead of the flame front, considered elsewhere,[1] we note that since the shock discontinuity occurs at a definite position in the chamber, the front of the flame can interact both with the shock wave that is being formed and with shock waves that have already been formed. The interaction process will have, in either case, its own characteristic features. To follow the details of this process, it is necessary to visualize the processes occurring in a fresh mixture and not accompanied by intrinsic glow. During the process of interaction, changes occur both in the flame front and in the shock wave, and to record the process it is necessary to use high speed motion picture photography, which makes it possible to examine all its phases.

A detailed description of the optical portion of the equipment with which one can make visible even weak disturbances produced by the flame in a fresh mixture has been given.[1] The same article describes the high speed spark apparatus, which yields up to 200 different phases of the investigated process at a rate of 50,000 frames per sec.

We used the apparatus to investigate the interaction between the front of a flame propagating in closed chambers and a shock wave produced ahead of the flame front as a result of cumulation of disturbances, produced by the flame in the fresh gas. Use was made of hydrogen-oxygen mixtures, containing 25, 33.3, 50, 66.6 and 70 per cent hydrogen. The combustion chamber length varied from 280 to 480 mm. The pictures were taken through windows cut in the side walls of rectangular chambers 19 × 37 mm. The windows of the chambers were covered with optical glass. The metal strips used to clamp the glass to the body of the chamber were used as scale markers, which were fixed on the photographs in the form of dark strips, parallel to the time axis. The process was photographed by two methods: The method of scanning, and the method of high speed motion picture photography.

After these preliminary remarks, let us proceed to examine the problem of the interaction between the flame front and the shock discontinuity.

1 Interaction Between the Flame Front and the Shock Discontinuity

Fig. 1 shows photographs of the process of combustion of hydrogen-oxygen mixtures, containing 50 per cent hydrogen in a chamber 280 mm long, obtained by the scanning method. Recorded to the left are the development of the process in the first section of a two-section chamber, and to the right are the processes near the second end surface. The flame accelerated in the tube excites in the fresh mixture disturbances which cumulate, after reflection from the end of the chamber, into a shock wave which passes freely through the front of the flame, almost stopping the latter. The flame, so to speak, "splashes away." The second shock wave, formed as a result of cumulation of disturbances propagated by the flame in later instants of time, will be reflected by the end of the chamber and will encounter the already "splashed" flame, through which this shock wave also passes freely, pushing its front back somewhat. Photographs obtained by the scanning method disclose nothing concerning the changes that occur in the flame front during the process of this interaction. Fig. 2 shows a series of photographs of the same process, obtained by spark photography at 50,000 frames per sec. The disturbances that evolve into a shock wave are seen distinctly ahead of the flame front, which has a clearly pronounced meniscus shaped form.

The encounter between the shock wave and the front of the flame is accompanied not only by a reduction in the speed of propagation of the flame, but also by a deformation of the latter. A small indention appears in the heretofore meniscus shaped front of the flame, which now assumes a characteristic tulip-like shape. After the passage of the shock wave through the front of the flame, a long comet-like loop stretches out behind the flame front, in which the mixture is afterburned. The unique shape of the "loop" is evidence of a definite distribution of the velocity field of the stream, of the flow, accompanying the shock wave. The front of the flame acquires a cellular structure. The total surface of the front increases and this, in turn, increases the rate of propagation of the flame. Gradually the flame front again acquires a meniscus shape. The second shock wave, encountering the

---

Translated from "Physical Gasdynamics," USSR Acad. Sci., pp. 163–166.

[1] Salamandra, G. D. and Tsukhanova, O. A., "Production of Shock Discontinuity Ahead of a Flame Front," ARS JOURNAL, vol. 30, no. 1, Jan. 1960, pp. 66–72.

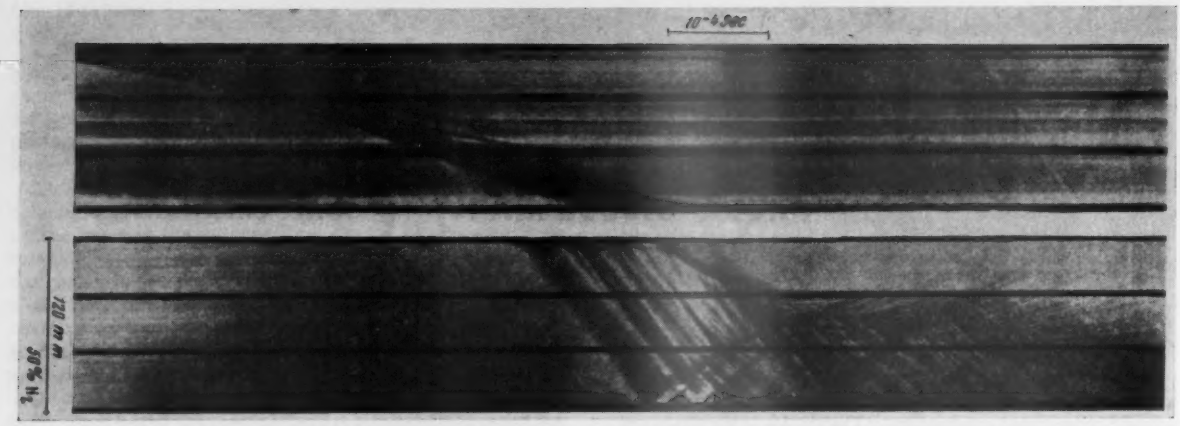

Fig. 1 Scanning of the combustion of a hydrogen-oxygen mixture

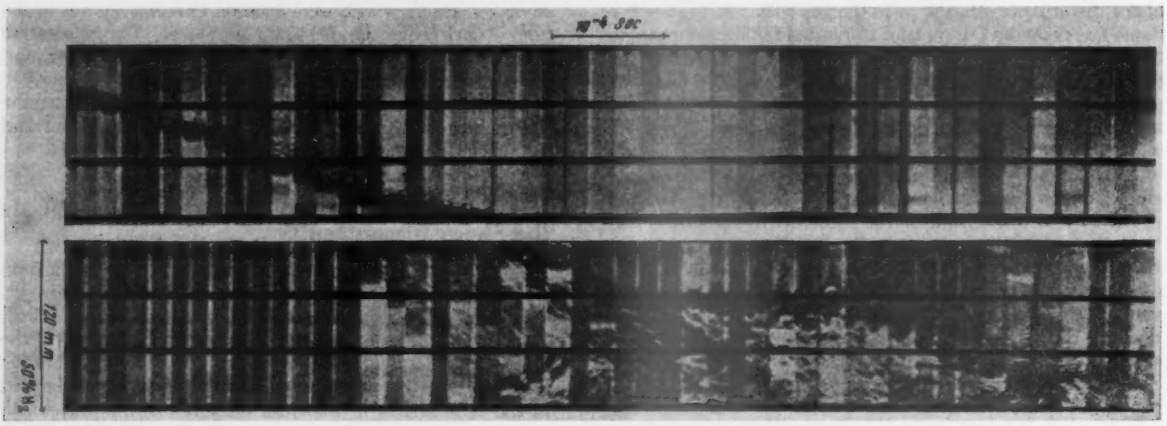

Fig. 2 Series of spark photographs of the same process

front of the flame and accompanying the comet-like "loop," is in itself deformed somewhat after passing through the region in which the mixture is afterburned. Frames 35 to 37 of photograph 2b shows clearly the curving of the front of the shock wave, following the comet-like "loop." Upon leaving this zone, the front of the shock wave again becomes flat. Since the shock wave traveling ahead of the front encounters the flame several times before the latter reaches the end of the chamber, the process of variation of the shape of the front of the flame during combustion with ripples is periodic in character.

We considered above the interaction between the flame front and the shock wave, producing the so-called combustion with ripples. At a sufficient length of the combustion chamber, the flame front may catch up with the shock wave before the latter reaches the end of the chamber. Under certain conditions imposed on the intensity of the shock wave and on the speed of the reaction inside the flame front, such an interaction between the wave and the flame front results in the formation of a detonation wave. The transition into a detonation wave is observed also during combustion of the mixture in a chamber, the length of which is less than the length of the predetonation path. For this transition it is essential that there exists an intense shock wave and that the mean velocity of the reaction be capable of maintaining the propagation of the detonation front.

The existence of an intense shock wave is a necessary but not sufficient condition for the transition from slow combustion into detonation, as evidenced by the series of photographs in Figs. 3a and b, which record the combustion of a mixture containing 50 per cent hydrogen near the end surface of a chamber 480 mm long. In spite of the fact that in both cases a shock wave of the same intensity travels in opposition to the front of the flame, in the former case the process is such that the encounter between the shock wave and the flame front does not lead to the formation of a detonation wave. In the second case the slow combustion does change into detonation. Unfortunately, the photographs did not register the interaction between the wave and the flame front, since the latter took place in a section of the chamber obscured from view.

2 Interaction Between the Forming Shock Wave and the Flame Front

If the shock wave passes freely through the flame front, the latter behaves like a deformable wall with respect to the forming shock wave. The process of the interaction between the forming shock wave and the flame front can be followed on the series of photographs (Fig. 4) which show the combustion of a mixture containing 33.3 per cent hydrogen in a chamber 280 mm long. The forming shock wave, traveling opposite to the flame front, can be seen in the form of a gradually narrowing dark zone. After encountering the flame front, it deforms

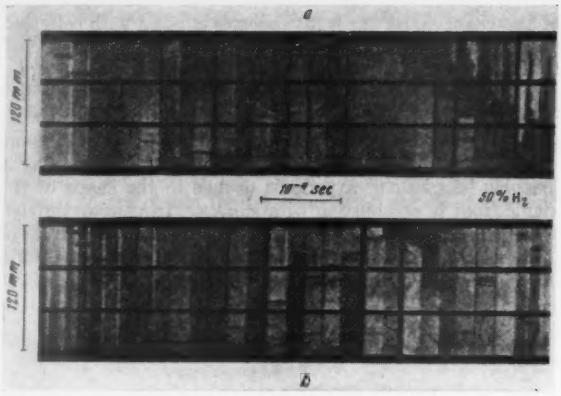

Fig. 3 Interaction between flame front and shock wave

the latter and cannot pass through it. The photographs show clearly how a meniscus shaped flame front becomes tulip shaped under the influence of a shock wave. The deformation of the flame front when a wave is reflected from it is probably the cause of the change of the angle of inclination of the front of the forming shock wave to the chamber axis after the reflection.

The interaction between the forming shock wave and the front of the flame can lead to the formation of a new ignition center ahead of the flame front. This process is quite noticeable on the series of photographs (Fig. 5a) showing the combustion of a mixture containing 25 per cent hydrogen in the second section of a 280-mm long chamber. The new ignition center, the appearance of which is quite noticeable starting with the fourth frame, has the form of a gradually broadening dark region. This is followed by a bright region—the compression region, contained between two combustion centers. The occurrance of the new center is due apparently not to the ignition of the mixture by compression in the wave, but by the injection of the reaction products in the fresh mixture, as evidenced by the thin bridge between the new ignition center with the flame front.

As can be seen from the photographs, the production of a new ignition center does not change substantially the character of the combustion. The interaction between the second forming shock wave and the flame front leads, as can be seen from the last frames of the photograph 5, to a new change in the form of the front and to a sharp increase of its surface, owing to the appearance of the cellular structure. The cellular structure is particularly clearly pronounced on photographs (Fig. 5b) of the combustion of the same mixture in the second section of the three-section chamber, 480 mm long.

An examination of the above experimental data leads to the following conclusions.

1 The forming shock discontinuity, traveling in opposition to the flame, does not as a rule pass through the flame, but is reflected from it. The encounter between the forming shock

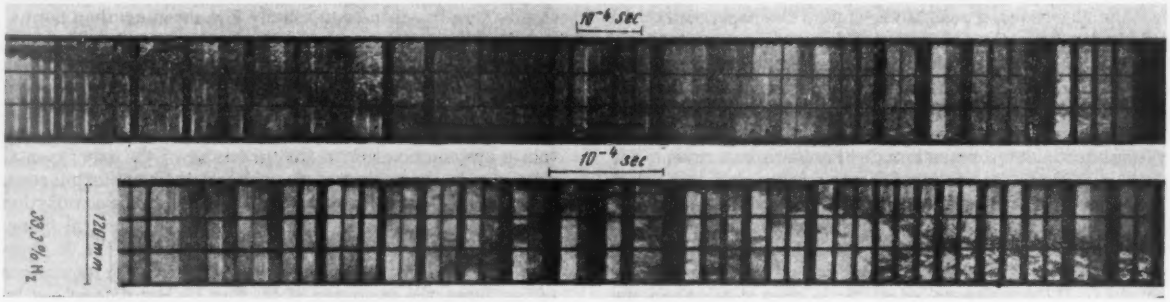

Fig. 4 Interaction between flame front and forming shock wave

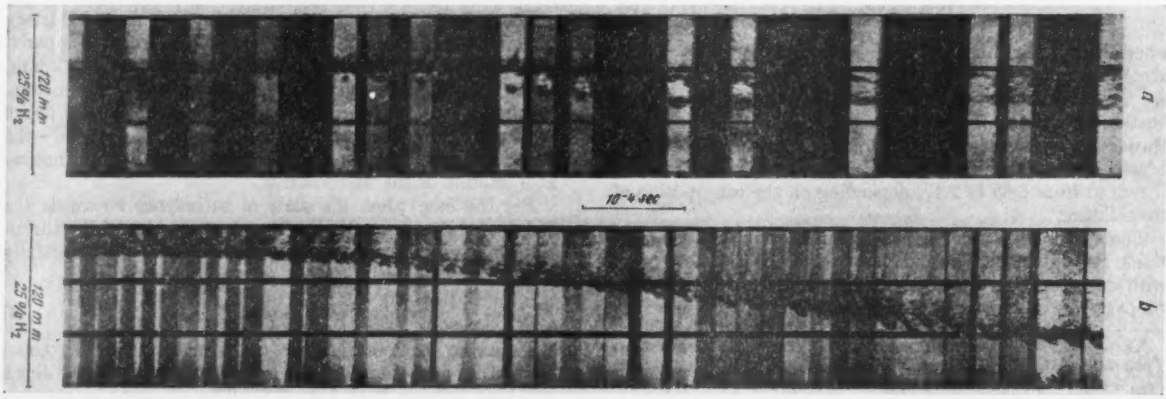

Fig. 5 Formation of a new ignition center: a—ahead of the flame front; b—cellular structure of flame front

wave and the flame front is accompanied by a deformation of the latter. In some cases a new ignition center is formed ahead of the flame front, produced by the injection of the reaction products into the fresh gas. The shock wave itself also experiences a change.

2 The produced shock wave can readily pass through the flame front and throw it back. The throwback of the flame is accompanied by a deformation of its front. In a flame front which is meniscus shaped before the encounter with the shock wave, there is produced a dent which imparts to it a characteristic tulip shaped form. The structure of the flame front is also changed, for the front becomes covered with cells that increase considerably the combustion surface.

A long comet-like "loop" extends behind the flame front, in which the mixture is afterburned. The increase in the surface of the flame leads to an increase in its propagation speed. The new encounter between the shock wave and the flame causes a new deformation of the flame front, etc., making it possible to speak of a periodic change in the shape of the flame front in combustion with ripples. In passing through the flame front and the comet-like loop behind it, the front of the shock wave becomes curved, and resumes the initial form after emerging from the zone of the "loop."

Measurement of the Speed of Propagation of Turbulent Combustion

K. I. SHCHELKIN

A PAPER by Bolz and Burlage (1)[1] published in 1955, is devoted to the influence of turbulence on the speed of flame propagation. It can be shown that the paper contains a principal error in the processing of the experimental data, an error leading to a considerable underestimate of the turbulent speed of combustion propagation; furthermore, the extent of the underestimate is different in different cases. Since reference may be made to this paper when comparing various turbulent combustion theories with experiment, we deem it advisable to analyze this paper in greater detail.

Bolz and Burlage, igniting a jet of homogeneous mixture of commercial methane with air by means of a single spark, produced a small spherical flame, carried by a stream having an equalized velocity profile. By taking successive photographs of the growing spherical flame, they determined the apparent combustion propagation speeds in the absence of walls. The speeds of the flame relative to the uncombusted gas u were calculated by dividing the apparent speed u_a by the increase in volume in combustion at constant pressure C

$$u = \frac{u_a}{c} = u_a \frac{n_0 R_0 T_0}{nRT} \qquad [1]$$

where n_0 is the number of moles, R_0 the gas constant, T_0 the absolute temperature of the uncombusted gas, and n, R and T are the same quantities for the adiabatically expanded combustion products. Under the conditions of the Bolz and Burlage experiments, the ratio of the volume of the combusted gases to the initial volume of the combustible mixture C ranged from 6.65 to 7.47, depending on the composition of the mixture.

The speeds of laminar flame for various mixture compositions, determined by Bolz and Burlage, were in good agreement with data obtained by others. The values of the speeds of propagation of turbulent combustion were not expected by the authors. In some cases, particularly in mixtures with very lean or very rich combustible components, the turbulent speeds were found to be unusually low, even less than normal speeds of flame propagation in the same mixtures. The good reproducibility and sufficient compactness of the results made it impossible to attribute this unexpected result to random measurement errors.

We shall show that the Bolz and Burlage experiments contain a systematic error in the processing of the experimental data, due to the neglect of the width of the combustion zone.

Equation [1] is valid only when the width of the combustion zone is small compared with the radius of spherical flame. The combustion of the gas is still incomplete in the combustion zone, and if its width is comparable with the dimensions of the flame, the expansion of the flame is not determined by the quantity C, which ranges from 6.65 to 7.47, as is suggested by Bolz and Burlage, who believed that the spherical flame contains the products of complete combustion. It is determined instead by a smaller quantity; furthermore, the wider the combustion zone, and the more uncombusted gas it contains, the smaller this quantity.

The width of the combustion zone in the Bolz and Burlage experiments on laminar flames was always small compared with the flame dimensions. It was on the order of 0.2 mm, while the flame measured several dozens of millimeters. However, when measuring the turbulent speeds of flame propagation, the foregoing conditions were not satisfied—the width of the turbulent combustion zone amounting to a noticeable fraction of the flame radius.

For the case when the scale of turbulence l exceeds the width of the laminar combustion zone, the size of the turbulent combustion zone λ can be determined semi-empirically from the expression

$$\lambda = Bl(v/u_n)^m \qquad [2]$$

Here v/u_n is the ratio of the turbulent pulsational component of flow velocity to the normal flame velocity, and B is a constant ranging from 1 to 3.5. The exponent m assumes values between 1 and 0.5, depending on the theory of turbu-

Translated from *Izvestiia Akademii Nauk SSSR, Otdelenie Tekhnicheskikh Nauk, Energetika i Avtomatika* (*Bull. USSR Acad. Sci., Tech. Sci., Div., Power and Automation*), no. 2, 1959, pp. 137–138.

[1] Numbers in parentheses indicate References at end of paper.

lent combustion employed; in the experiments described here, m is probably close to 0.7 or 0.8.

Strictly speaking, Equation [2] applies only when $v >> u_n$, while in this case v is commensurate with u_n. However, for lack of anything better, we shall use Equation [2] to estimate the extent of the turbulent combustion zone, making use of the values of v and u_n listed in Table 4 and values of l from Table 5 of the cited paper. Setting B equal to the average value, 2.25, we obtain for experiments 63 and 66 (for which lowest speed of Table 4 is given) the following values for the width of the zone of turbulent flame

$$\lambda_{63} = 2.25 \times 2.7 \left(\frac{16.4}{26.6}\right)^{0.75} = 5.0 \text{ mm}$$

$$\lambda_{66} = 2.25 \times 2.7 \left(\frac{16.4}{17.4}\right)^{0.75} = 5.8 \text{ mm}$$

These values cannot be neglected compared with the flame dimensions, if we recall that the maximum flame radius does not exceed 30 mm.

For an approximate estimate of the influence of the width of the zone on the quantity C, we can assume the following simplified scheme for the structure of the front: Half the combustion zone is filled with combustion products, while the other half contains uncombusted gas. Under these assumptions, the coefficient C_n, corrected for the zone width, is related to the coefficient C used by Bolz and Burlage, as follows

$$C_n = \frac{C}{(1 - \lambda/2\bar{r})^2 + C[1 - (1 - \lambda/2\bar{r})^2]} \qquad [3]$$

Assuming that the measurements were made at maximum flame radius $\bar{r} = 30$ mm (see Fig. 7 of the cited paper), taking the values of C from Table 4, and using the values of λ as computed above, we obtain for experiments 63 and 66 the values of 0.45 and 0.4 respectively, for the ratio of the corrected to uncorrected coefficient, C_n/C. Taking these values into account, we find that in experiment 63 the speed of turbulent flame propagation was not 24 cm/sec, as indicated in Table 4, but 24/0.42 = 56 cm/sec, whereas the normal velocity in the same mixture is 21.6 cm/sec. In the case of experiment 66, the correction for the width of the zone increases the value of turbulent velocity from 18 cm/sec listed in the table to 45 cm/sec, the normal velocity in the same mixture being 17.4 cm/sec. Analogous corrections for the width of the zone of turbulent combustion should be made for all the experimental points.

It is interesting that the dependence of the flame velocity on its dimensions is clearly seen on the Bolz and Burlage curves in Figs. 7, 14, 15 and 16. As the radius of the flame increases, the radius vs. time curves bend as if the speed of the flame were to increase with time, while actually one should expect a decrease in speed, owing to the damping of the turbulence. Bearing in mind that the flame dimensions were too small for self-turbulization of the combustion front to arise, the unusual course of the curves can be taken to be indirect proof of the influence of the width of the combustion zone on the expansion of the combustion products: As the flame dimensions increase, the value of C_n increases (see Eq. [3]). At a sufficiently large flame radius, C_n goes into C and the apparent speed approaches the asymptotic value—the radius vs. time curve approaches a straight line.

Actually, the corrections for the width of the combustion zone can hardly be accurate, since the width of the combustion zone was not found in the measurements. But even if it were known, the correction would be only approximate, since the distribution of the combustion products over the turbulent flame zone is unknown. The only accurate way of determining the turbulent flame speed in free flow, by the procedure used by Bolz and Burlage, would be to make the measurements at sufficiently large flame sizes, so that the width of the combustion zone could be neglected by comparison.

The remarks made in this communication apply also to measurements of turbulent speed in an inverted cone of turbulent flame.

In our opinion the most accurate measurements, although not free of shortcomings, are measurements in a straight flat cone of a turbulent flame. However, in this case one must estimate the speed of propagation of turbulent combustion from the dimensions of the surface that envelops the forward edge of the flame, rather than from the area of the maximum glow zone, as was done, for example, by Summerfield, Reiter, Kebely and Mascolo (2). To explain the last remark, let us perform an imaginary experiment. Imagine a straight flame cone. We maintain in it a constant speed of propagation of turbulent flame, changing if necessary to pulsational component of the gas flow. To satisfy the condition of invariance of the turbulent flame speed propagation, we increase sharply the width of the combustion zone, say by increasing the scale of turbulence or by reducing the normal flame speed. As the width of the zone of turbulent combustion is increased, all the characteristic dimensions of the combustion zone increase, the upper zone of maximum glow moves away from the mouth of the burner and the surface of this zone increases. Using the procedure of Summerfield et al. we connect the increase in the surface of the zone of maximum glow with the reduction in the speed of propagation of turbulent combustion. Actually, however, there was no reduction whatever in the speed of the flame, and the increase in the zone of maximum glow is due to the increase in the width of the combustion zone, determined by factors other than the speed of propagation of turbulent flame.

References

1 Bolz, R. E. and Burlage, H., "The Influence of Turbulence on Flame Propagation Rates," Jet Propulsion, vol. 25, no. 6, p. 265, 1955.

2 Summerfield, M., Reiter, S. H., Kebely, V. and Mascolo, R. W., "The Structure and Propagation Mechanism of Turbulent Flames in High-Speed Flow," Jet Propulsion, vol. 25, no. 8, p. 377, 1955.

Calculation of Orthotropic Conical Shell for Arbitrary External Load, Using the Method of V. Z. Vlasov

V. A. SIBIRYAKOV

Faculty of Aircraft Structural Mechanics
Moscow Aviation Institute

The conical shell is the component part of most aviation structures. Therefore the knowledge of an elastically loaded and deformed state of such a shell is very important for the solution of many problems. Thus far most papers have been devoted to the strength of conical shells under axially symmetrical loading. The case of arbitrary loading has not been sufficiently considered. The purpose of this paper is to obtain equations for the design of a conical shell, a type of a rocket nose, having nonaxially symmetrical loading.

WE SHALL determine the stressed and deformed state of an orthotropic conical shell, using the general technical theory of Vlasov (1).[1] Starting with the physical hypotheses of this theory pertaining to orthotropic semi-momentless shells of medium length, we shall consider only the transverse bending moments from among all the internal moments.

The equations of equilibrium of an element of shell under these assumptions become

$$\frac{\partial}{\partial z}(rN_1) - kN_2 + A\frac{\partial S}{\partial \theta} + ArX = 0$$

$$A\frac{\partial N_2}{\partial \theta} + \frac{\partial}{\partial z}(rS) + kS + Q_2 + ArY = 0 \qquad \frac{\partial M_2}{\partial \theta} + rQ_2 = 0$$

$$-N_2 + \frac{\partial}{\partial z}(rQ_1) + A\frac{\partial Q_2}{\partial \theta} + ArZ = 0 \qquad kM_2 - ArQ_1 = 0$$

.....[1]

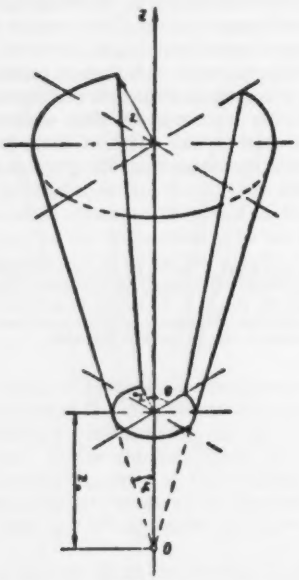

Fig. 1

where

z, θ	=	cylindrical coordinates of the shell (see Fig. 1)
r	=	kz, radius of conical shell
k	=	$\tan \varphi$, tangent of the angle between the generatrix and the axis of the cone
A	=	$\sqrt{1 + k_2}$, coefficient of first quadratic form
N_1, N_2	=	elastic normal forces
S, M_2	=	tangential force and bending moment
Q_1, Q_2	=	shearing forces
X, Y, Z	=	components of the total load vector

The positive directions of forces and displacements are shown in Fig. 2.

Let us make a change of variables which is very convenient in the analysis of conical shells (3), using $z = z_0 e^{\alpha t}$, and let us rewrite Equations [1] in the following form

$$\left(\frac{\partial}{\partial t} + k\right)N_1 - kN_2 + A\frac{\partial S}{\partial \theta} + ArX = 0$$

$$A\frac{\partial N_2}{\partial \theta} + \left(\frac{\partial}{\partial t} + 2k\right)S + Q_2 + ArY = 0 \qquad \frac{\partial M_2}{\partial \theta} + rQ_2 = 0$$

$$-N_2 - \frac{1}{r}\frac{\partial}{\partial t}(rQ_1) + A\frac{\partial Q_2}{\partial \theta} + ArZ = 0 \qquad kM_2 - ArQ_1 = 0$$

.....[2]

Knowing the internal forces and the moments, we can obtain the strain components from the following relations

$$N_1 = Eh\epsilon_1 \quad N_2 = Eh\epsilon_2 \quad S = 0.5Eh\omega \quad M_2 = -\frac{Eh^3}{12}\chi_2 \qquad [3]$$

Translated from *Izvestiia Vysshych Uchebnykh Zavedenii MVO, Aviationnaya Tekhnika* (*Bull. Higher Institute of Learning, Aviation Engng.*), no. 2, 1959, pp. 72–82.

[1] Numbers in parentheses indicate References at end of paper.

where

E = modulus of elasticity of the material
h = thickness of the shell along the generatrix
$\bar{h} = \eta h$, reduced thickness of the shell along the parallel (1)

The strain components are expressed in terms of the components of the total-displacement vector as follows

$$\epsilon_1 = \frac{1}{Ar}\frac{\partial u}{\partial t} \qquad \omega = \frac{1}{r}\frac{\partial u}{\partial \theta} + \frac{1}{A}\frac{\partial}{\partial t}\left(\frac{v}{r}\right)$$

$$\epsilon_2 = \frac{1}{Ar}\left(ku + A\frac{\partial v}{\partial \theta} + w\right)$$

$$\chi_2 = -\frac{1}{A^2r^2}\left(ku + w + k\frac{\partial w}{\partial t} + A^2\frac{\partial^2 w}{\partial \theta^2}\right) \quad \ldots\ldots [4]$$

If we eliminate N_2, Q_1 and Q_2 from Equations [2] we obtain the following system of equations

$$\left(\frac{\partial}{\partial t} + k\right)N_1 - \left(\frac{k^2}{Ar}\frac{\partial}{\partial t} - \frac{Ak}{r}\frac{\partial^2}{\partial \theta^2}\right)M_2 + A\frac{\partial S}{\partial \theta} = Ar(kZ - X)$$

$$\left(\frac{k}{r}\frac{\partial^2}{\partial t \partial \theta} - \frac{A^2}{r}\frac{\partial^2}{\partial \theta^2} - \frac{1}{r}\frac{\partial}{\partial \theta}\right)M_2 + \left(\frac{\partial}{\partial t} + 2k\right)S = Ar\left(A\frac{\partial Z}{\partial \theta} + Y\right) \quad \ldots\ldots [5]$$

After eliminating S we get

$$\left[A^2\left(\frac{\partial^4}{\partial \theta^4} + \frac{\partial^2}{\partial \theta^2}\right) - \frac{k^2}{A}\left(\frac{\partial^2}{\partial t^2} + 3k\frac{\partial}{\partial t} + 2k^2\right)\right]\frac{M_2}{r} + \left(\frac{\partial^2}{\partial t^2} + 3k\frac{\partial}{\partial t} + 2k^2\right)N_1 = P^*$$

$$P^* = -Ar\left(\frac{\partial}{\partial t} + 3k\right)X + A^2r\frac{\partial}{\partial \theta}Y + Akr\left(\frac{\partial}{\partial t} + 3k + \frac{A^2}{k}\frac{\partial^2}{\partial \theta^2}\right)Z \quad \ldots\ldots [6]$$

We shall solve the problem in terms of displacements.

Using the supplementary condition $\epsilon_2 = 0$, considered in Vlasov's monograph (2), expressions [3 and 4] are rewritten

$$N_1 = \frac{Eh}{Ar}\frac{\partial u}{\partial t} \qquad S = \frac{1}{r}\frac{\partial u}{\partial \theta} + \frac{1}{A}\frac{\partial}{\partial t}\left(\frac{v}{r}\right)$$

$$M_2 = -\frac{E\bar{h}^3}{12r^2}\left[k\frac{\partial^2 u}{\partial \theta^2} + \frac{k^2}{A^2}\frac{\partial u}{\partial t} + \frac{1}{A}\frac{\partial}{\partial \theta}\left(A^2\frac{\partial^2}{\partial \theta^2} + 1\right)v + \frac{k}{A}\frac{\partial^2 v}{\partial t \partial \theta}\right] \quad \ldots\ldots [7]$$

Inserting Equations [7] into Equations [5], we separate the variables, eliminate from the system the components of the displacement vector u, simplify the coefficients of the resultant equation, and get as the final result

$$v_n^{IV} - \left[k^2 + \frac{\eta^2\eta^2(A^2n^2 - 1)^2}{6}\left(\frac{h}{kz_0}\right)^2 e^{-2kt}\right]v''_n + \frac{\eta^2A^6n^4(n^2 - 1)^2}{12}\left(\frac{h}{kz_0}\right)^2 e^{-2kt}v_n = -\frac{2A^2k^2z_0^2e^{2kt}}{E \cdot h} \times \left[\frac{An}{2}\left(\frac{d}{dt} + k\right)X_n + \left(\frac{d^2}{dt^2} - \frac{A^2n^2}{2}\right)Y_n - \frac{An}{2}\left(2\frac{d^2}{dt^2} + k\frac{d}{dt} + k^2 - A^2n^2\right)Z_n\right] \quad [8]$$

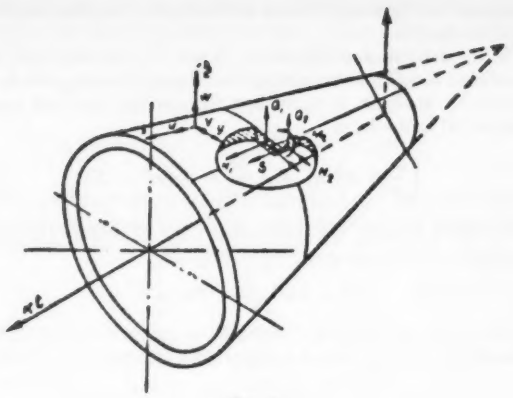

Fig. 2

This equation characterizes the elastically stressed and deformed state of a conical shell with a deformable contour. If we put in this equation $k = 0$, and consequently $kz_0e^{kt} = R$, we obtain the equation

$$v^{IV} - \frac{n^2(n^2 - 1)^2h^2}{6R^2}v'' + \frac{n^4(n^2 - 1)^2h^2}{12R^2}v = -\frac{2R^2}{Eh}\left[n\frac{d}{dt}X + \left(\frac{d^2}{dt^2} - \frac{n^2}{2}\right)Y - \left(\frac{d^2}{dt^2} - \frac{n^2}{2}\right)Z\right]$$

proposed by Vlasov (2) for an orthotropic cylindrical shell of small length.

In the foregoing separation of variables, we had in mind the Fourier expansions

$$N_1 = \sum N_{1n}\cos n\theta \qquad u = \sum u_n \cos n\theta \qquad X = \sum X_n \cos n\theta$$
$$S = \sum S_n \sin n\theta \qquad v = \sum v_n \sin n\theta \qquad Y = \sum Y_n \sin n\theta$$
$$M_2 = \sum M_{2n}\cos n\theta \qquad w = \sum w_n \cos n\theta \qquad Z = \sum Z_n \cos n\theta \quad \ldots\ldots [9]$$

Following Vlasov (1), let us also consider the supplementary conditions $\epsilon_2 = 0$ and $\omega = 0$. Now the expressions [3 and 4], with [9] taken into account, can be rewritten as

$$N_{1n} = \frac{Eh}{A^2n}\left(\frac{d^2}{dt^2} - k\frac{d}{dt}\right)v_n$$

$$M_{2n} = -\frac{E\bar{h}^3}{12A^2n}\left[k^2\frac{d^2}{dt^2} + k^2\frac{d}{dt} - A^4n^2(n^2 - 1)\right]v_n \quad \ldots\ldots [10]$$

If Equations [10] are inserted into Equations [6] and the coefficients simplified, we obtain

$$v^{IV} - k^2v'' + a_0e^{-2kt}v = -\frac{A^2nk^2z_0^2e^{2kt}}{E \cdot h}\left[\left(\frac{d}{dt} + 3k\right)X - AnY - \left(k\frac{d}{dt} + 3k^2 - A^2n^2\right)Z\right] \quad [11]$$

where

$$a_0 = \frac{A^6n^4(n^2 - 1)^2\eta^3}{12} \cdot \left(\frac{h}{kz_0}\right)^2$$

Equation [11] characterizes the elastically stressed and deformed state of a conical shell with deformable contour in the absence of shear deformation. If we put in Equation [11] $k = 0$, and consequently $kz_0e^{kt} = R$, we get the equation

$$v^{IV} + \frac{n^4(n^2 - 1)^2h^2}{12R^2}v = -\frac{nR^2}{Eh}\left[\frac{d}{dt}X - nY + n^2Z\right]$$

proposed by Vlasov (1) for an orthotropic cylindrical shell of medium length.

In the derivation of Equations [8 and 11], starting with the condition $k \leqslant 1$, we have simplified the coefficients, which, as shown by analysis, is equivalent to rewriting the first equation of [5] in the form

$$\left(\frac{\partial}{\partial t} + k\right) N_1 + A\,\frac{\partial S}{\partial \theta} = Ar(kZ - X) \qquad [12]$$

In the following we shall solve only Equation [11]; the homogeneous equation corresponding to it

$$v^{IV} - k^2 v'' + a_0 e^{-2kt} v = 0$$

is solved by successive approximations and written in terms of Bessel functions of complex argument (Thomson functions)

$$v_n = C_1\Phi_{11} + C_2\Phi_{12} + C_3\Phi_{13} + C_4\Phi_{14} + v_n^*$$

where

$$\Phi_{11} = \frac{e^{0.5kt}}{p}\,\mathrm{Im}\,\sqrt{i}\,I_1(\sqrt{i}\,\cdot\varphi)$$

$$\Phi_{12} = kt\Phi_{11} - 0.751 - 5.075\,\frac{e^{0.5kt}}{p}\,\mathrm{Im}\,\sqrt{i}\,I_1(\sqrt{i}\,0.898\,\varphi)$$

$$\Phi_{13} = pe^{0.5kt}\mathrm{Re}\sqrt{i}\,I_1(\sqrt{i}\,\varphi)$$

$$\Phi_{14} = kt\Phi_{13} + e^{kt} - 5.007pe^{0.5kt}\mathrm{Re}\sqrt{i}\,I_1(\sqrt{i}\,0.918\varphi)$$

$$p^4 = \frac{a_0}{k^4}$$

$$\varphi = 2pe^{-0.5kt}$$

.....[13]

Using the condition $\omega = 0$, we get

$$u_n = \frac{1}{An}\left(\frac{d}{dt} - k\right) v_n$$

$$= \frac{k}{An}\,(C_1\Phi_{21} + C_2\Phi_{22} + C_3\Phi_{23} + C_4\Phi_{24} + u_n^*)$$

where

$$\Phi_{21} = -\mathrm{Re}I_0(\sqrt{i}\,\varphi)$$

$$\Phi_{22} = kt\Phi_{21} + \Phi_{11} + 0.751 + 4.562\,\mathrm{Re}I_1(\sqrt{i}\,0.898\,\varphi)$$

$$\Phi_{23} = p^2\,\mathrm{Im}\,I_0(\sqrt{i}\,\varphi)$$

$$\Phi_{24} = kt\Phi_{23} + \Phi_{13} - 4.673p^2\,\mathrm{Im}\,I_0(\sqrt{i}\,0.918\,\varphi)$$

.....[14]

We can next write, on the basis of Equations [3 and 4]

$$N_{1n} = \frac{Ehe^{-kt}}{A^2kz_0n}\left(\frac{d^2}{dt^2} - k\,\frac{d}{dt}\right) v_n$$

$$= \frac{Ehke^{-kt}}{A^2z_0n}\,(C_1\Phi_{31} + C_2\Phi_{32} + C_3\Phi_{33} + C_4\Phi_{34} + N_{1n}^*)$$

where

$$\Phi_{31} = -pe^{-0.5kt}\,\mathrm{Re}\,\sqrt{i}\,I_1(\sqrt{i}\,\varphi)$$

$$\Phi_{32} = kt\Phi_{31} + 2\Phi_{21} + \Phi_{11} + 4.097pe^{-0.5kt} \times \mathrm{Re}\,\sqrt{i}\,I_1(\sqrt{i}\,0.898\,\varphi)$$

$$\Phi_{33} = p^2e^{-0.5kt}\,\mathrm{Im}\,\sqrt{i}\,I_1(\sqrt{i}\,\varphi)$$

$$\Phi_{34} = kt\Phi_{33} + 2\Phi_{23} + \Phi_{13} - 4.284p^2e^{-0.5kt} \times \mathrm{Im}\,\sqrt{i}\,I_1(\sqrt{i}\,0.918\,\varphi)$$

.....[15]

Finally, from the homogeneous equation corresponding to Equation [12], we get

$$S_n = \frac{Ehe^{-kt}}{A^2n^2kz_0}\left(-\frac{d^2}{dt^2} + k\,\frac{d^2}{dt^2}\right) v_n$$

$$= \frac{Ehk^2e^{-kt}}{A^2n^2z_0}\,(C_1\Phi_{41} + C_2\Phi_{42} + C_3\Phi_{43} + C_4\Phi_{44} + S_n^*)$$

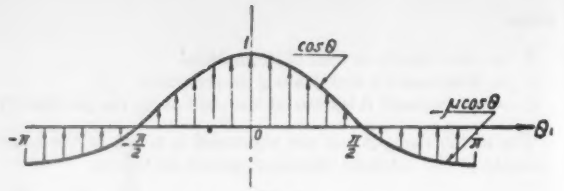

Fig. 3

where

$$\Phi_{41} = p^2e^{-kt}\,\mathrm{Im}\,I_0(\sqrt{i}\,\varphi)$$

$$\Phi_{42} = kt\Phi_{41} - 3\Phi_{31} - \Phi_{21} - \Phi_{11} - 3.688p^2e^{-kt} \times \mathrm{Im}\,I_0\,(\sqrt{i}\,0.898\,\varphi)$$

$$\Phi_{43} = p^4e^{-kt}\mathrm{Re}\,I_0(\sqrt{i}\,\varphi)$$

$$\Phi_{44} = kt\Phi_{43} - 3\Phi_{33} - \Phi_{23} - \Phi_{13} - 3.922p^4e^{-kt} \times \mathrm{Re}\,I_0(\sqrt{i}\,0.918\,\varphi)$$

.....[16]

In analogy with the foregoing, we can, by using the method of successive approximation, obtain an expression for the particular solution of Equation [11], no matter what the right-hand side is.

By way of example we shall consider the case when the component of the external-load vector varies as

$$Z = Z_0 \cdot e^{2kt} \cdot \sum a_n \cos n\theta$$

The law of variation of the external load with the angular coordinate is shown in Fig. 3. It can be represented analytically by the expression

$$\sum a_n \cos n\theta = \bar{a}_0 + a_1 \cos\theta + a_2 \cos 2\theta + a_4 \cos 4\theta + \ldots$$

where

$$\bar{a}_0 = 2(1 - \mu)/\pi$$

$$a_1 = (1 + \mu)/2$$

$$a_2 = 2(1 - \mu)/3\pi$$

$$a_4 = -2(1 - \mu)/15\pi$$

Thus, the right half of Equation [11] will have the form at $X = Y = 0$ of

$$a_n\,\frac{A^2nk^2z_0^2}{Eh}\,Z_0[(\beta + 3)k^2 - A^2n^2]e^{(2+\beta)kt} = qe^{(2+\beta)kt}$$

In those cases when β assumes nonintegral values, the general expression for the particular solution can be written

$$v^* = \frac{q}{k^4}\,I_1^{(2+\beta)}\left[e^{(2+\beta)kt} - p^4e^{\beta kt}\sum_0^\infty\left[(-1)^m p^{4m}e^{-2mkt}\prod_0^m I_1^{(\beta-2m)}\right]\right]$$

where

$$I_1^{(\beta-2m)} = \frac{1}{(\beta - 2m)^2[(\beta - 2m)^2 - 1]} \qquad [17]$$

We can now supplement the system of Equations [13–16] with particular solutions and use this system to determine arbitrarily the integration constants for the specified boundary conditions.

As can be seen from the expression for the coefficient a_0 in Equation [11], the foregoing equations are correct only when $n \geq 2$, but it is easy to check that for the particular values $n = 0$ and $n = 1$ it is possible to obtain from the initial Equations [6 and 7] solutions that are in accord with beam theroy.

As an example, we perform the calculations for the shell

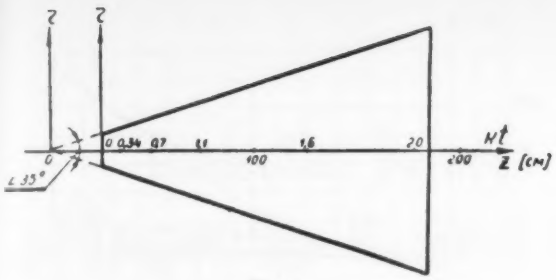

Fig. 4

shown in Fig. 4. It has the following geometrical characteristics

$$r_0 = 7.9 \text{ cm} \qquad k = 0.316$$
$$h = 0.25 \text{ cm} \qquad \eta = 1.0$$
$$l = 160 \text{ cm} \qquad z_0 = 25 \text{ cm}$$

We shall determine only the second-order stresses ($n = 2$), since a preliminary analysis shows that there is no point in going to higher approximations.

From Equations [11 and 13] we get $p^4 = 1.61$, and consequently

$$\varphi = 2.26e^{-kt/2}$$

Let us assume that the shell is cantilever-supported on the right end, and has a diaphragm on the left end. The boundary conditions for this case can be written

$$\text{for } kt = 0 \quad N_{1n}(0) = 0 \qquad \text{for } kt = 2 \quad u_n(2) = 0$$
$$S_n(0) = 0 \qquad\qquad\qquad\qquad v_n(2) = 0$$

In order to determine these conditions, it is necessary to calculate first the functions Φ_i in terms of certain expressions for v_n, u_n, N_{1n} and S_n. However, it must be borne in mind that the Thomson functions used here are taken in the form tabulated in the Jahnke and Emde tables (5), and differ from the functions given by Watson (Bessel Functions) and many other authors.

Let us assume that the load under consideration is characterized by the parameter $\beta = 0.5$. Then

$$v_n^*(2) = 5.210\,\frac{q}{k^4} \qquad N_{1n}^*(0) = -0.485\,\frac{q}{k^4}$$

$$u_n^*(2) = 6.450\,\frac{q}{k^4} \qquad S_n^*(0) = -1.000\,\frac{q}{k^4}$$

The arbitrary constants of integration will be determined from the system of Equations [13–17], which we present in matrix form

C_1	C_2	C_3	C_4	Right side
0.998	−3.329	0.109	7.180	$-v_n^*$
−0.991	4.301	−0.218	0.533	$-u_n^*$
−0.790	2.022	1.396	−8.029	$-N_{1n}^*$
−1.541	6.755	0.966	−7.966	$-S_n^*$

It follows that

$$C_1 = \frac{1}{D}\,[-M_{11}v_n^* + M_{21}u_n^* - M_{31}N_{1n}^* + M_{41}S_n^*]$$

$$C_2 = \frac{1}{D}\,[M_{12}v_n^* - M_{22}u_n^* + M_{32}N_{1n}^* - M_{42}S_n^*]$$

$$C_3 = \frac{1}{D}\,[-M_{13}v_n^* + M_{23}u_n^* - M_{33}N_{1n}^* + M_{43}S_n^*]$$

$$C_4 = \frac{1}{D}\,[M_{14}v_n^* - M_{24}u_n^* + M_{34}N_{1n}^* - M_{44}S_n^*]$$

where

D = the principal value of the determinant
M_{ij} = the minor of the determinant

In this example we obtain

$$C_1 = 16.989\,\frac{q}{k^4} \qquad C_3 = -4.470\,\frac{q}{k^4}$$

$$C_2 = 2.424\,\frac{q}{k^4} \qquad C_4 = -1.899\,\frac{q}{k^4}$$

We next obtain from formulas [13, 14, and 17] the secondary normal and tangential stresses

$$\alpha = \frac{N_{12}}{h} \qquad \tau = \frac{S_2}{h}$$

The final computation results are shown in Figs. 5 and 6.

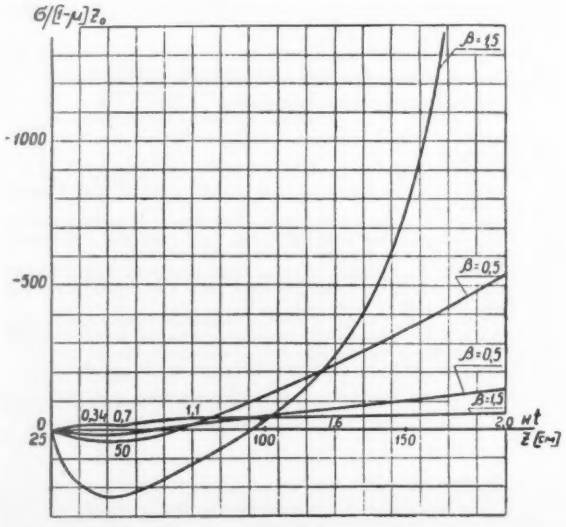

Fig. 5

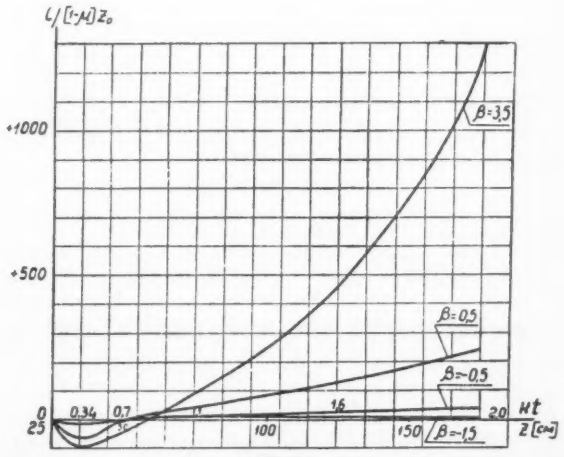

Fig. 6

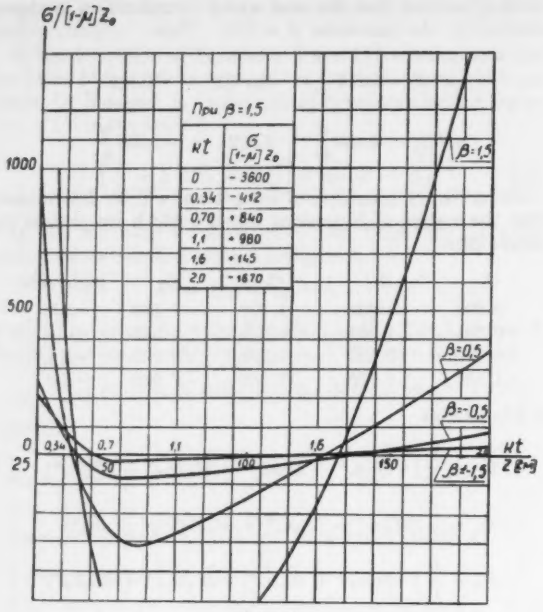

Fig. 7

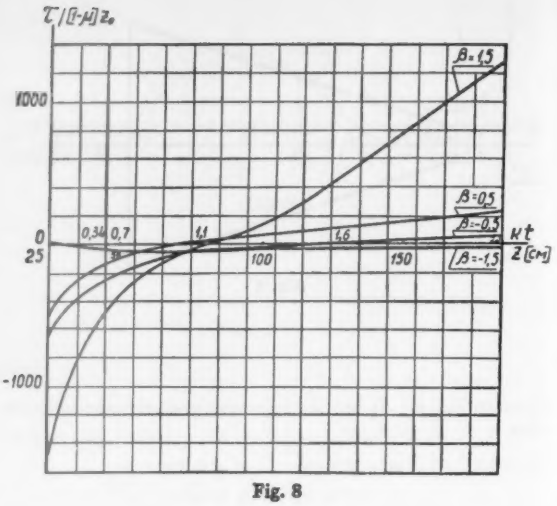

Fig. 8

For comparison, the figures also show lines corresponding to other values of the parameter β.

Let us perform the calculations for the same shell, but for different boundary conditions. Let the shell be cantilever mounted on the right end, and let there be on the left end either a rigid frame that is not subject to flexure, or else a massive ballistic end piece, welded to the shell. The latter circumstance is quite important, for although the left side may move as a part of cantilever beam, the shell cross section cannot distort. In this case the boundary conditions have the form

$$\text{for } kt = 0 \quad v_2(0) = 0 \qquad \text{for } kt = 2 \quad v_2(2) = 0$$
$$u_2(0) = 0 \qquad\qquad u_2(2) = 0$$

The functions f_1 of Equations [13–17] will be calculated (5), in analogy with the foregoing procedure, for the argument $\varphi = 2.26e^{-kt/2}$. To determine the arbitrary constant of integration, we set up the following matrix

C_1	C_2	C_3	C_4	Right side
0.867	−4.912	0.790	−2.074	$-v_n^*(0)$
0.997	−3.329	0.109	7.180	$-v_n^*(2)$
−0.600	4.992	−1.541	6.915	$-u_n^*(0)$
−0.991	4.301	−0.218	0.533	$-u_n^*(2)$

The right side of this matrix, for a load characterized by a parameter $\beta = 0.5$, has the values

$$v_2^*(0) = 0.148\,\frac{q}{k^4} \qquad v_2^*(2) = 5.210\,\frac{q}{k^4}$$

$$u_2^*(0) = 0.280\,\frac{q}{k^4} \qquad u_2^*(2) = 6.450\,\frac{q}{k^4}$$

After performing the necessary calculations, we obtain the values for the arbitrary constants of integration

$$C_1 = 41.781\,\frac{q}{k^4} \qquad C_2 = -2.612\,\frac{q}{k^4}$$

$$C_3 = 8.425\,\frac{q}{k^4} \qquad C_4 = -0.515\,\frac{q}{k^4}$$

We then use Equations [13–17] to find the stresses of interest to us. The results of the calculations are presented in Figs. 7 and 8.

In conclusion let us indicate that the law of distribution of normal stresses along the generatrix (Fig. 5) agrees qualitatively with the results obtained by Kut'inov (4) for a caisson with small taper.

The proposed equations make it possible to determine the stresses produced by internal pressurization of the conical shell and due to the stiffness of the end frames or supports for nonaxially symmetrical loading of the structures. These stresses may be quite considerable. For example, the secondary normal stresses for the structure shown in Fig. 5 are approximately 30 per cent of the stresses calculated by the law of plane sections at $\mu = 0.5$ and $\beta = 0.5$, and 50 per cent of the latter at $\mu = 0$ and $\beta = 0.5$.

At larger values of the parameter β, these figures may increase, since in this case the load assumes the character of a local load near the point of support.

References

1 Vlasov, V. Z., *"Obshchaya teoriya obolochek"* (General Shell Theory), Gostekhizdat, 1949.

2 Vlasov, V. Z., "Contact Problems in the Theory of Shells and Thin-Wall Rods," *Izvestiia Akad. Nauk SSSR, Otd. Tekh. Nauk* (*Bull. USSR Acad. Sci., Div. Tech. Sci.*), no. 6, 1949.

3 L'vin, Ya. B., "Design of Conical Shell for Cyclic Edge Actions," *Inzhinernyi sbornik* (*Engineering Anthology*), vol. XX, USSR Acad. Sci., Div. Tech. Sci., Inst. of Mechanics, 1954.

4 Kut'inov, V. F., "Design of Conical Caisson for Flexure and Torsion, with Allowance for Sweepback," Ministry of Aviation Industry, USSR, Trudy TsAGI (Trans. Central Aero-Hydrodynamical Institute), 1955.

5 Jahnke, E. and Emde, F., "Tables of Functions," Dover, 1945.

Original received January 5, 1959

Connection Between the Flame Temperature Measured by Optical Means and by Other Methods

K. P. VLASOV

It was found in many investigations that optical methods yield higher values of the temperature in the combustion zone of a turbulent flame than other methods. This phenomenon was explained by Kadyshevich et al. (1),[1] who have shown that if the temperature varies with the time at a given point, optical methods give values that exceed the time averaged temperature.

We consider in this paper the use of optical methods (line reversal and infrared pyrometry) to measure the temperatures of turbulent flames. A connection is found between the mean thermodynamic temperature and the temperature obtained by optical data.

From the values of the combustion temperature as measured by reversal of spectral lines it is also possible to calculate the mean square pulsation temperature, caused by insufficient micromixing of the fuel and air, as frequently occurs in ordinary technical apparatus.

TO FIND a quantitative relation between the temperature T_0 measured by optical means and the time averaged thermodynamic temperature T, it is necessary to know the law of variation of the instantaneous value of T with time, $T = f(t)$. Such a law was derived in a recent experimental investigation by N. V. Kokushkin (2). The only temperatures observed were in the turbulent combustion zone, temperatures T_1 of the fresh mixture and temperatures T_2 of the combustion products. The fraction of intermediate temperatures T_3 is negligibly small ($T_2 > T_3 > T_1$). The time averaged temperature is then

$$T = T_1 p_1 + T_2 p_2$$

or

$$T = T_2 p_2 + T_1(1 - p_2) \qquad (p_1 + p_2 = 1) \quad [1]$$

where

p_1 = probability of temperatures T_1 at a given point over a given time interval
p_2 = probability of temperatures T_2

The average optical temperature T_0 is found from the relations

$$\frac{1}{\exp(c_2/\lambda T_0) - 1} = \frac{1}{t_2 - t_1}\int_{t_1}^{t_2} \frac{1}{\exp(c_2/\lambda T(t)) - 1}\, dt \ldots \quad [2]$$

where

$T(t)$ = true temperature
c_2 = the constant in Planck's radiation formula
λ = radiation wave length
t = time

If relation [1] is satisfied, we obtain from Equation [2]

$$\frac{1}{\exp(c_2/\lambda T_0) - 1} = \frac{p_2}{\exp(c_2/\lambda T_2) - 1} + \frac{p_1}{\exp(c_2/\lambda T_1) - 1} \quad [3]$$

Discarding the second term (at T_1, the radiation contribution is small) we get

$$T_0 = \frac{c_2}{\lambda \ln\left(\frac{1}{p_2}\exp\frac{c_2}{\lambda T_2} + 1\right)} \qquad \left(p_2 = \frac{T - T_1}{T_2 - T_1}\right) \quad [4]$$

If the value of the average thermodynamic temperature is known, the value T_0 obtained by a given optical method can be calculated (from the value of λ). The results of such a calculation are shown in Figs. 1 and 2. The calculations show that all optical methods give temperature values higher than the average thermodynamic temperature, and the excess increases with diminishing radiation wave length λ and as p_2 decreases toward the edges of the flame.

It is more interesting to solve the inverse problem, that of determining the average thermodynamic temperature from a measured value of T_0. This can be readily done by transforming Equation [3]

$$p_2 = \frac{\exp(c_2/\lambda T_2) - 1}{\exp(c_2/\lambda T_0) - 1} \quad [5]$$

Since T_2 is known for a specified value of α of a homogeneous mixture, and since T_0 is found experimentally, p_2 can be calculated. (In all cases, complete chemical combustion, $\varphi = 1$, is assumed.)

The results of a similar processing of experimental data of Kadyshevich et al. (1) are shown in Fig. 3.

It can be seen that the temperature profiles, calculated from values of T_0 obtained with an infrared pyrometer, are in good agreement with the results obtained by the chemical analysis method. Matters are worse if the data on the reversal of the spectral lines (Na, Li) are used, owing to the effect of the relative error of the measurements. As is known, the total

Translated from *Izvestiia Akademii Nauk SSSR, Otdelenie Tekhnicheskikh Nauk, Energetika i Avtomatika* (*Bull. USSR Acad. Sci., Div. Tech. Sci., Power and Automation*), no. 3, 1959, pp. 100–103.

[1] Numbers in parentheses indicate References at end of paper.

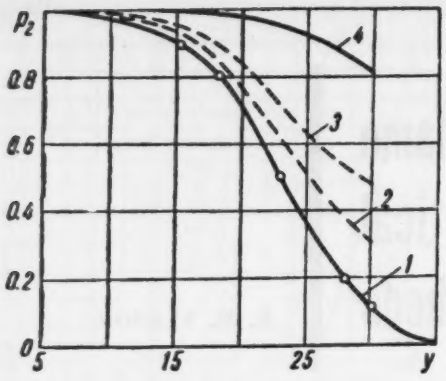

Fig. 1 Comparison of profiles of the mean thermodynamic temperature with the profiles of mean optical temperatures for various wave lengths λ. 1—Profile of thermodynamic temperature; 2—Profile of mean optical temperature, obtained from a specified value of the thermodynamic temperature, $\lambda = 4.3\mu$ (measured by infrared radiation); 3—Profile of mean optical temperature for $\lambda = 2.7\mu$ (measured by infrared radiation); 4—Profile of mean optical temperature, $\lambda = 0.6\mu$ (reversal method)

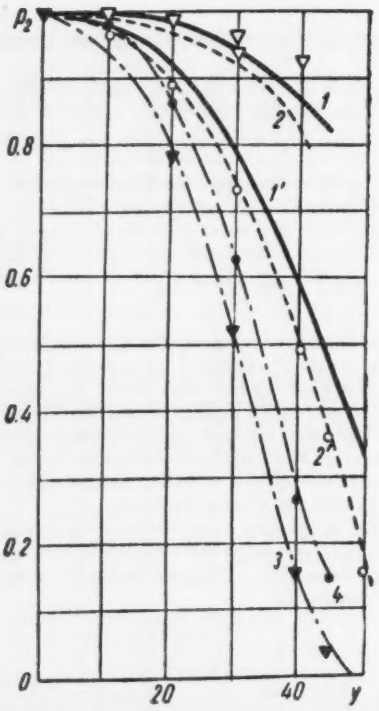

Fig. 2 Comparison of experimental and theoretical temperature profiles in transverse cross section of the turbulent cone of a flame; distance y in millimeters from the axis of the cone ($\alpha = 1.2$). 1,1′—Calculated temperature profile, with the mean thermodynamic temperature taken from the experimental chemical analysis data; 2,2′—Calculated temperature profile, with thermocouple readings used for the average thermodynamic temperature; open triangle—Experimental temperature profile, obtained by reversal of the spectral lines; open circle—Experimental data obtained by the method of infrared radiation; 3—Experimental data obtained by chemical analysis; 4—Experimental data obtained with thermocouple

error in determining the true temperature by optical methods amounts to $\Delta T = 50$–80 deg. Let us estimate the relative error in the determination of p_2. We use the transformed Equation [5] and the simpler Wien equation

$$p_2 = \exp\left(\frac{c_2}{\lambda}\frac{T_0 - T_2}{T_2 - T_0}\right) \qquad [6]$$

The relative error is

$$\frac{\Delta p_2}{p_2} = \frac{c_2}{\lambda}\frac{\Delta T}{T_0^2}$$

($T_{0\,max} = 2400$ deg abs. for $\alpha = 1$.)

In the case of the live reversal method

$$\frac{\Delta p_2}{p_2} = \frac{14{,}320}{0.6}\frac{50 \text{ to } 80^\circ}{2400^2} = 0.21 \text{ to } 0.33$$

for the infrared pyrometer

$$\frac{\Delta p_2}{p^2} = 0.070 \text{ to } 0.045$$

It is seen thus that a small deviation in the experimental value of T_0, as determined by the reversal of the spectral lines, results in a large error in the determination of p_2. Therefore, even if corrections are included in the calculations, this method cannot be recommended to determine the profiles of the average thermodynamic temperature in the transverse cross section of the turbulent cone section of the flame.

Measurements of combustion temperatures by reversal of spectral lines in the range $0.8 \leq \alpha < 1.1$ give temperatures

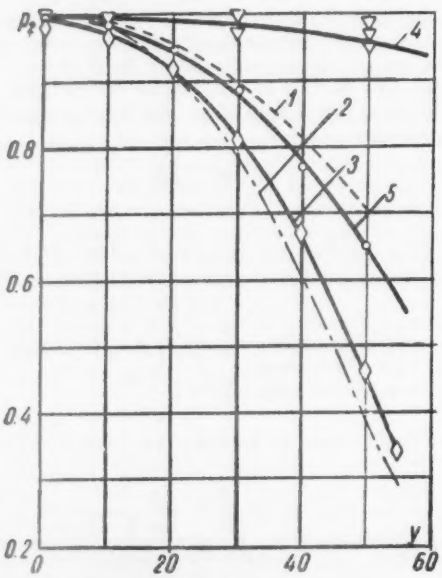

Fig. 3. Comparison of experimental and theoretical temperature profile in transverse cross section of cone of flame ($\alpha = 1.0$). 1—Profile of mean calculated thermodynamic temperature, in which the average optical temperature necessary to determine the thermodynamic temperature is obtained from data on the reversal of the spectral lines; 2—Calculated profile of mean thermodynamic temperature, the optical temperature obtained with infrared pyrometers; 3—Experimental profile of mean thermodynamic temperature based on chemical analysis data; 4—Profile of average optical temperature, experimental, based on data obtained by the reversal method; 5—Profile of average optical temperature, experimental, based on optical parameter data

Table 1

α_c^*	θ_T	θ_z	T_0	ϑ_T^*	ϑ_z^*	ΔT_z	ΔT_T	T_0	ΔT_z	ΔT_T	T_{0T}
1.1	2290	2280	2350	0.10	0.09	70	60	2295	0	5	2280
1.2	2190	2160	2320	0.22	0.13	160	130	2200	35	10	2195
1.3	2100	2010	2260	0.22	0.15	250	160	2115	35	15	2045
1.4	2030	1860	2180	0.29	0.16	320	150	2040	55	10	1915
1.5	1950	1680	2060	0.39	0.12	380	110	1965	140	15	1820

Notes: T_0—by spectral-line reversal T_0—by infrared pyrometer

$\Delta T_z = T_0 - \theta_z$, $\Delta T_T = T_0 - \theta_T$—difference in readings between the optical and true temperatures.

that are considerably higher than the possible theoretical temperatures at a given average value of α. This result was attributed by Kadyshevich et al. (1) to the presence of microirregularities in the composition of the mixture, i.e., to a deviation of the instantaneous values of α from the time averaged ones α^*. (The fuel benzine was injected through a fuel collector made up of 12 nozzles into air preheated to 200 C at a distance of 4000–6000 mm from the point of measurement.) In spite of the fact that, in this case, the mixing should have been complete enough for the parameters to assume their average values, the actual mixing could not be expected to be microscopic. Let us attempt to calculate the possible fluctuation in α, or, more correctly, the corresponding temperature fluctuation in these experiments. As is obvious from the foregoing, the optical methods measure the mean energy of radiation J^*, which corresponds to some average temperature θ.

The instantaneous fluctuation of α about the average value α^* should lead to corresponding fluctuations in the combustion temperature

$$T = \theta + \vartheta \qquad [7]$$

where

θ = average temperature corresponding to α^*
ϑ = instantaneous fluctuation of the temperature due to the instantaneous change in α

We assume that the temperature fluctuations are not too large, $\sqrt{\vartheta^2}/\theta \leq 0.5$, and that they are random. Let us find the running average value of the radiation energy as a function of T. Taking Equation [7] into account, we have

$$J^*(T) = J^*(\theta) + \left(\frac{\partial J}{\partial T}\right)_{T=\theta} \vartheta + \frac{1}{2}\left(\frac{\partial^2 J}{\partial T^2}\right)_{T=\theta} \vartheta^2 \qquad [8]$$

For $J(T)$ we use the Wien formula instead of Equation [2]

$$J(T) = \exp\left(-\frac{c_2}{\lambda} T_0\right)$$

Confining ourselves to three terms in expansion [8], we obtain

$$\exp\left(-\frac{c_2}{\lambda} T_0\right) = \exp\left(-\frac{c_2}{\lambda} \theta\right)\left[1 + \frac{c_2}{\lambda T^2}\left(\frac{c_2}{\lambda \theta^2} - \frac{1}{\theta}\right)\vartheta^2\right] \qquad [9]$$

We now obtain from [8] the mean square pulsation temperature $\sqrt{\vartheta^2}/\theta = \vartheta^*$.

Knowing the value of T_0 (measured by reversal of the spectral lines or by infrared radiation) and the value of θ we can find ϑ^*. Two values were computed:

1 The value of θ_z was found from chemical analysis data (corresponding to ϑ_z^*).

2 θ_T and ϑ_T^* were obtained by thermodynamic calculations, assuming complete combustion ($\varphi = 1.0$). The results are listed in Table 1.

In the right part of the table we give the calculated values of T_0 obtained by infrared methods, assuming that the magnitude of the pulsations of the temperature ϑ^* in the stream is specified and obtained from the left part of the table.

The results obtained show that the temperature fluctuations due to poor mixing are quite considerable, 15 to 30 per cent, and increase with increasing α.

A measurement of T_0 in the combustion product region by reversal of the spectral lines and a comparison of this temperature with the theoretical value (or that obtained by chemical analysis) makes it possible to calculate the possible inhomogeneities in α and the fluctuations of temperature with time. As a result it should also be noted that the use of infrared radiation for the determination of temperature fluctuations due to inhomogeneities of α with time is not convenient in the range of investigated values of α (α = 1.1 to 1.5). The difference between $T_0 - \theta$ is within the limits of the instrumental error of the infrared pyrometer.

References

1 Kadyshevich, A. E., Dubrovskaya, O. N., Merson, Ya. I. and Vlasov, K. P., *"O primenimosti opticheskikh metodov dlya opredeleniya temperatury turbulentnykh plamen" (On the Applicability of Optical Methods for the Determination of the Temperature of Turbulent Flames)*, Oborongiz, 1957.

2 Kokushkin, N. V., *Izvestiia Akad. Nauk SSSR, Otd. Tekh. Nauk (Bull. Acad Sci. USSR, Div. Tech. Sci.)*, no. 8, 1958.

Original submitted July 3, 1958

Transients in Optimal Control Systems

O. M. KRYZHANOVSKII and V. M. KUNTSEVICH

OPTIMAL control systems have recently attracted the attention of many investigators (1 to 10),[1] and principal attention has been paid to the analysis of steady-state oscillations in the system, since the normal operating condition of most optimal control systems is the mode of oscillation about the position of the extremum. To analyze such a mode of steady oscillation in optimal relay systems, use is made of expansion of the periodic solution in a Fourier series, in which a count is taken either of all terms in the series (4,5) or only of one term (8,9). Use can also be made of other methods of finding a periodic solution, similar to the investigation of self-oscillations in simple relay control systems (11).

However, as is known from the general premises of control theory, in order to obtain a complete and all-embracing estimate of a control system, it is necessary to consider also their transients, and this applies in particular to optimal control systems. As will be shown in the following, the investigation of transients in such systems can be carried out in many cases by the well-known methods of nonlinear control system transients as employed in control theory.

The analysis which follows is limited only to control systems in which the extremal characteristic has only one maximum.

1 Let, under certain physical conditions, the extremal characteristic shown in Fig. 1a have the form 1, and let the coordinates of the control system be characterized in magnitude by the position of the point of extremum A. Let us assume that suddenly the physical conditions of the controlled object have changed in such a way, that the extremal characteristic has shifted and taken position 2 in Fig. 1a, with a maximum point O. Transients will then occur in the system, and will continue until the regulated object arrives at the point of new maximum O, or until steady-state oscillations are established about this point. Let us choose the origin of the coordinates in the new position of the maximum and let us write down a system of differential equations for the transients in the optimal system. The initial conditions are determined, as usual, from the static equations, assuming that the object has occupied the old extremum position A or oscillated about this point. We next assume that the change in the physical condition was insignificant and that the control system has been subjected to "a sufficiently small disturbance." Then the equation of the curve with the maximum can be expressed, near the point of maximum, by means of a quadratic function. Here as in ordinary control systems, the concept "sufficiently small disturbance" remains sufficiently broad when investigating the response quality of the transients.

We assume furthermore that the controlled object, which has an extremal characteristic, can be represented by means of an equivalent circuit (Fig. 1b) in which an inertialess link is connected in series with a linear link that takes into account the inertia of the object.

2 Let us consider linear systems of extremal regulation with a proportional element. The equations of the links of the system, as shown in Fig. 1b, have, under the assumptions made, the following form.

The equation of the servo motor is

$$\dot{\mu} = \alpha_1 u \qquad [2.1]$$

The equation of the linear portion of the controlled object is

$$\tau\dot{x} + x = \alpha_2\mu \qquad [2.2]$$

The equation of the nonlinear extremal characteristic of the controlled object (after the disturbance) is

$$\varphi = -\alpha_3 x^2 \qquad [2.3]$$

The equation of the measuring element is

$$u = \frac{d\varphi}{dx} = \frac{\dot{\varphi}}{\dot{x}} \qquad [2.4]$$

where

u, μ, φ, x = functions of time and represent the coordinates that characterize the state of the system

$\alpha_1, \alpha_2, \alpha_3$ = constant coefficients

The initial conditions are determined from the state of the system preceding the disturbance.

Eliminating the variables u, μ and φ from Equations [2.1 to 2.4], we obtain the linear differential equation

$$\tau\ddot{x} + \dot{x} + 2\alpha_1\alpha_2\alpha_3 x = 0 \qquad [2.5]$$

which determines the transients in the system. It is possible to continue the analysis of the transients in the extremal control system with proportional measuring elements, following the known rules of transient analysis (stability, response quality) in ordinary linear control systems. Since the equations of the proportional measuring element of type [2,4] actually reduce to a linear relation between the coordinates x and u, then, if the equations of the servo motor and the object in the control system are linear equations of higher order, the optimal control system will nevertheless be reduced to a linear differential equation of respectively higher order, and can be analyzed in accordance with the general rules.

It is seen from Equation [2.5] that at different values of the amplification coefficients α_1, α_2, α_3, the transients have a damped character, i.e., the system arrives at the maximum point O as $t \to \infty$ and $x \to 0$. The degree of damping is determined here only by the time constant of the object, and the frequency also varies as the amplification coefficient is changed.

3 Let us consider next an optimal control system, which differs from the foregoing one only in that the proportional measuring element is replaced by a relay-type measuring element, the equation of which is of the form

$$u = \operatorname{sign}\frac{d\varphi}{dx} = \operatorname{sign}\frac{\dot{\varphi}}{\dot{x}} \qquad [3.1]$$

The transients in this control system are then described by a system of differential equations [2.1 to 2.3] and [3.1]. Eliminating the intermediate variables from this system of equations, we obtain a nonlinear differential equation in x

$$\tau\ddot{x} + \dot{x} + \alpha_1\alpha_2 \operatorname{sign} x = 0 \qquad [3.2]$$

The transients which are described by Equation [3.2] are

Translated from *Izvestiia Akademii Nauk SSSR, Otdelenie Tekhnicheskikh Nauk, Energetika i Avtomatika* (*Bull. USSR Acad. Sci., Div. Tech. Sci., Power and Automation*), 1959, no. 3, pp. 32–42.

[1] Numbers in parentheses indicate References at end of paper.

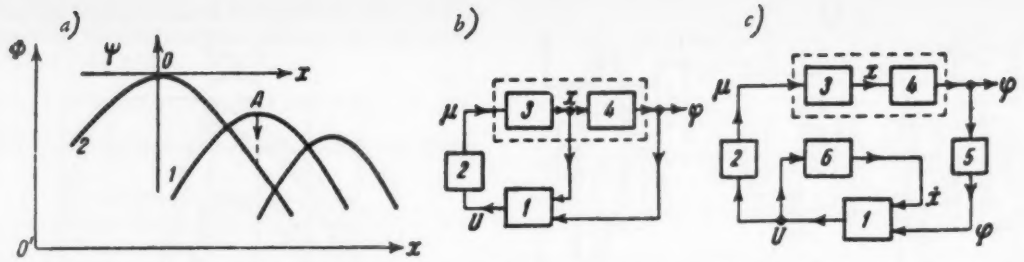

Fig. 1 a—Characteristics of the regulated object; b—structural diagram of optimal control system with direct feedback proportional to x; c—structural diagram of optimal control systems with a model of the linear portion of the regulated object: 1—extremal regulator, 2—actuating motor, 3—linear portion of the regulated object, 4—nonlinear element, 5—linear element, 6—tachometer generator

best analyzed in phase plane x,v, where $v=\dot{x}$.

After integrating Equation [3.2] we obtain the equations of the phase trajectories (Fig. 2a).

$$x = x_0 - \tau(v - v_0) \pm \tau a_1 a_2 \ln\left(\frac{1 \pm v/\alpha_1\alpha_2}{1 \pm v_0/\alpha_1\alpha_2}\right) \qquad [3.3]$$

The plus sign holds here when $x>0$, and the minus sign when $x<0$. The symbols x_0 and v_0 denote the corresponding initial conditions.

Let us examine an optimal control system which may be described by Equations [2.1 to 2.3] and by the following measuring element equations

$$u = \operatorname{sign}\left(\frac{d\varphi}{dx} - \Delta\right) \quad \frac{d}{dt}\frac{d\varphi}{dx} > 0$$
$$u = \operatorname{sign}\left(\frac{d\varphi}{dx} + \Delta\right) \quad \frac{d}{dt}\frac{d\varphi}{dx} < 0 \qquad [3.4]$$

where 2Δ is the width of the hysteresis loop of the two-position polarized relay. Fig. 2b gives the phase trajectories of this system.

For the purpose of plotting we used formulas [3.3] and, according to Equations [3.4], Equation [3.3] holds in the region to the right of the line $EFGH$ when $x>0$, and to the left when $x<0$. As can be seen from Fig. 2b, a stable limit cycle is established in the phase plane, and the system returns to it regardless of the initial conditions.

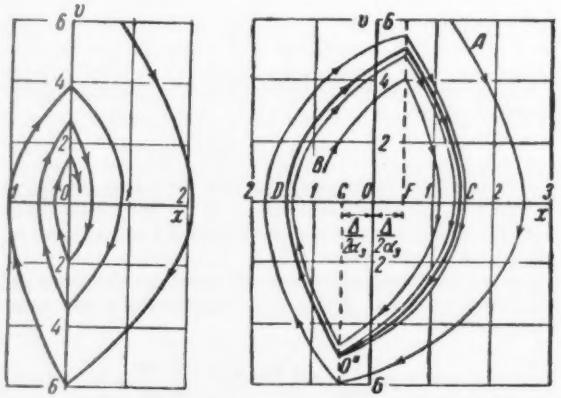

Fig. 2 a—Phase trajectories of optimal system with measuring element described by [3.1], $\alpha_1\alpha_2 = 10$, $\alpha_3 = 0.5$, $\tau = 1$ sec; b—phase trajectories of optimal system with measuring element [3.4], $\alpha_1\alpha_2 = 10$, $\alpha_3 = 0.5$, $\tau = 1$ sec, $\Delta = 0.5$

Let us next analyze an optimal control system (Fig. 3a) with an element of logical action (1,2).

Let us consider the case when it is possible to establish measurement with respect to x. For simplicity we shall assume that relay $2PR$ is ideal but relay $1PR$ is not. Then the

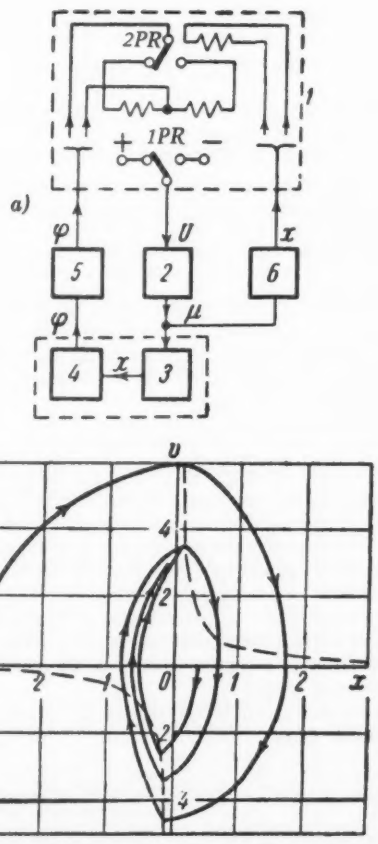

Fig. 3 a—Structural diagram of optimal control system with a logical-action element: 1—logical-action element, 2—actuating motor, 3—linear portion of the regulated object, 4—nonlinear element, 5—differentiator, 6—tachometer generator, $1PR$, $2PR$—two-position polarized relays; b—phase trajectories of optimal control system with logical action element, $\alpha_1\alpha_2 = 10$, $\alpha_3 = 0.5$, $\tau = 1$ sec, $\Delta = 0.5$ (the dotted lines limit the switching boundary)

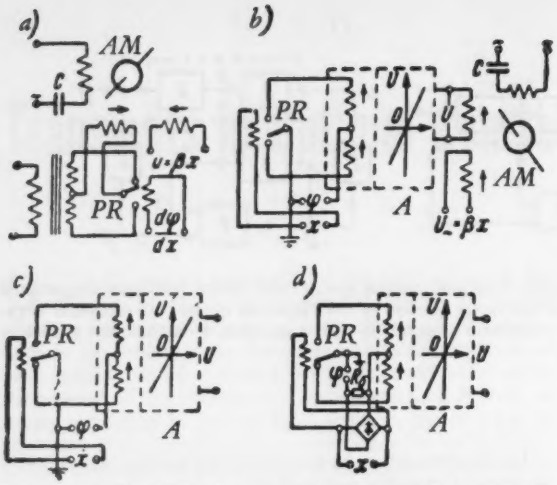

Fig. 4 a—Principal diagram of regulator with measuring element [4.3]; b—principal diagram of regulator with measuring element [4.10]; c—principal diagram of regulator with measuring element [4.11]; d—principal diagram of regulator with measuring element [4.11], *A*—amplifier, *AM*—actuating motor, *PR*—two-position polarized relay

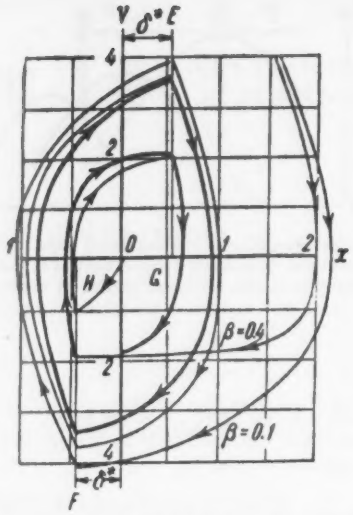

Fig. 5 Phase trajectories of optimal system with measuring element [4.1], $\alpha_1\alpha_2 = 10$, $\alpha_3 = 0.5$, $\tau = 1$ sec, $\Delta = 0.5$

equation for the law of regulation can be written in the form

$$u = \text{sign}\,(\dot{\varphi} + \Delta)\,\text{sign}\,\dot{x} \qquad [3.5]$$

Equation [3.5] can be rewritten, by using [2.3] as

$$u = -\text{sign}\,(2\alpha_3 xv - \Delta)\,\text{sign}\,v \qquad [3.6]$$

Since the control coordinate u can assume values of only $u = \pm 1$, then after reduction, the dynamic equation of the system becomes

$$\tau\ddot{x} + \dot{x} + \alpha_1\alpha_2\,\text{sign}\,u = 0 \qquad [3.7]$$

The phase trajectories of this system are given by Equation [3.3] and the boundary on the phase plane, corresponding to the transition from $x>0$ to $x<0$ and vice versa, is determined from Equation [3.6]. This boundary comprises the two branches of the hyperbola

$$v = (\Delta/2\alpha_3 x) \qquad [3.8]$$

Since the coordinate x is usually not accessible for direct measurement, then to obtain the value of x it is necessary to use an equivalent circuit for the linear portion of the regulated object. The greater the hysteresis loop of the relay $1PR$, the less stringent the accuracy requirements for this equivalence. In individual cases it is merely necessary to introduce time delay in relay $2PR$. It is frequently better to use a model of the linear portion of the controlled object. Fig. 1c shows the block diagram of a control system with an equivalent circuit for the linear portion.

The value of x is determined from Equations [2.1 and 2.2] in operator form

$$px = \frac{a_1 a_2}{\tau p + 1}\,u \qquad [3.9]$$

Consequently, as the time constant of the model τ_m of the link (Fig. 1c) is so chosen that $\tau_m = \tau$, then

$$y = \frac{k}{\tau p + 1}\,u$$

or

$$y = k\dot{x}$$

We note that when using an equivalent circuit for the linear portion of the control object, it is possible to dispense with one of the differentiating elements.

Using the same method of phase-plane transient analysis, it is possible to investigate an optimal control system with a memory for the maximum value of the controlled quantity. The circuit with capacitor recharging (3) used in such systems is essentially none other than the simplest equivalent circuit of the controlled object.

4 Let us consider the improvement in the transient response in optimal control systems, an improvement based on introducing into the control law additional terms containing the velocity $\dot{x}$ in some form or another. The advantage of such a method is that for normal operation of the control system it is necessary in general to have the value of $\dot{x}$, and therefore the introduction of additional feedback proportional to $\dot{x}$ does not raise any technical difficulties.

We illustrate this using as an example an optimal control system with proportional measuring element, described by Equations [2.1 to 2.3] and by the equation of the new measuring element

$$u = \frac{d\varphi}{dx} - \beta\dot{x} \qquad [4.1]$$

Eliminating the intermediate variables from these equations, we obtain

$$\tau\ddot{x} + (1 + \beta\alpha_1\alpha_2)\dot{x} + 2\alpha_1\alpha_2\alpha_3 x = 0 \qquad [4.2]$$

By varying the parameter β it is possible to vary the degree of damping. We recall that this could not be done for Equation [2.5] for the transients in the system [2.1 to 2.4], to which our system reduces when $\beta = 0$.

Let us consider an optimal control system which is described by Equations [2.1 to 2.3] and the equations of a new measuring element

$$u = \text{sign}\left(\frac{d\varphi}{dx} - \Delta\right) - \beta\dot{x} \qquad \frac{d}{dt}\frac{d\varphi}{dx} > 0$$

$$u = \text{sign}\left(\frac{d\varphi}{dx} + \Delta\right) - \beta\dot{x} \qquad \frac{d}{dt}\frac{d\varphi}{dx} < 0 \qquad [4.3]$$

The principal diagram of such a diagram is shown in Fig. 4a. Eliminating the intermediate variables from Equations [2.1 to 2.3] and [4.3], we get

$$\tau\ddot{x} + (1 + \beta\alpha_1\alpha_2)\dot{x} + \alpha_1\alpha_3 \operatorname{sign}(2\alpha_3 x \pm \Delta) = 0 \quad [4.4]$$

from which we determine the equations of the phase trajectories

$$x = x_0 - \frac{\tau}{a}(v - v_0) \pm \frac{\alpha_1\alpha_2\tau}{a^2} \ln\left(\frac{1 \pm av/\alpha_1\alpha_2}{1 \pm av/\alpha_1\alpha_2}\right) \quad [4.5]$$

Here $a=1+\beta\alpha_1\alpha_2$; the plus sign holds for $x>(1/2)\Delta/\alpha_3$, and the minus sign for $x = -(1/2)\Delta/\alpha_3$.

Fig. 5 shows the phase trajectories for the motion of the system based on these formulas, for feedback coefficient values $\beta=0.1$ and $\beta=0.4$. It is seen from this construction that increasing the coefficient β permits not only an increase in the damping of the system, but also reduces the amplitude of the steady-state oscillations.

We shall show further, that if the servo motor is relay controlled, introduction of feedback proportional to $\dot{x}$ also improves the quality of the operation of the extremal system. Let us consider a system described by Equations [2.1 to 2.3] and the following equations for the measuring element

$$\begin{aligned} u &= \operatorname{sign}(u_+ - \Delta) \qquad \dot{u}_+ > 0 \\ u &= \operatorname{sign}(u_+ + \Delta) \qquad \dot{u}_+ < 0 \end{aligned} \quad \ldots\ldots\ldots\ldots\ldots\ldots\ldots\ldots\ldots\ldots [4.6]$$

Here

$$u_+ = \frac{d\varphi}{dx} - \beta\dot{x} \quad [4.7]$$

Since u can assume the values $u=\pm 1$, the phase trajectories for the motion of the system are determined by Equation [3.3] with a plus sign when $u=1$ and a minus sign when $u=-1$.

The switching limits are

$$u_+ - \Delta > 0 \qquad u_+ + \Delta < 0 \quad [4.8]$$

or, using Equation [4.7], are represented in the xv plane in the form of two parallel lines

$$-2\alpha_3 x - \beta v - \Delta > 0 \qquad -2\alpha_3 x - \beta v + \Delta < 0 \quad [4.9]$$

Fig. 6a shows the phase trajectories for $\beta=0.2$ and $\beta=0.4$. It follows from this graph that for a relay controlled servo motor, feedback proportional to $\dot{x}$ improves the stability of the system and decreases the amplitude of steady-state oscillations. At a definite ratio of control system parameters and the value of the coefficient β the transient may become similar to the so-called "gliding mode," in ordinary control systems (11).

Let us note here a characteristic feature of optimal control relay systems. It is known (11) that the introduction of proportional feeback in ordinary relay systems increases the degree of its damping. A similar result is obtained by introduction of derivative feedback (proportional to $\ddot{x}$) in an optimal control system.

Let us consider further still another method of improving the operating quality of an optimal system. We considered before the system [2.1 to 2.4], in which the measuring instrument performed the function of division. However, realization of such a measuring element is quite difficult. Much simpler, in the structural sense, are regulator systems (Figs. 4b, 4c, 4d) in which the measuring elements have the equations

$$u = \dot{\varphi} \operatorname{sign} \dot{x} \quad [4.10]$$

$$u = \dot{\varphi} \operatorname{sign} \dot{x} - \beta\dot{x} \quad [4.11]$$

Let us consider first the optimal system of Fig. 4b. Eliminating the intermediate variables from the system of Equations [2.1 to 2.3] and [4.10], we get

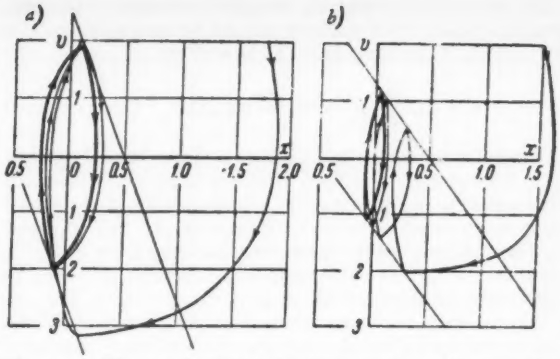

Fig. 6 a—Phase trajectories of optimal system with measuring element [4.6] ($v_0 = 7$, $x_0 = 0.8$), $\alpha_1\alpha_2 = 10$, $\alpha_3 = 0.5$, $\tau = 1$ sec, $\Delta = 0.5$, at $\beta = 0.2$; b—the same but with $\beta = 0.4$

$$\tau\ddot{x} + \dot{x} \pm 2\alpha_1\alpha_2\alpha_3 x\dot{x} = 0 \quad [4.12]$$

Hence, going over to variables x, v, we obtain after integration the phase trajectories (Fig. 7a)

$$v = v_0 - \frac{1}{\tau}(x - x_0) \mp \frac{\alpha_1\alpha_2\alpha_3}{\tau}(x^2 - x_0^2) \quad [4.13]$$

The upper sign in Equations [4.12 and 4.13] holds for $v>0$, and the lower one for $v<0$.

Comparing the quality of the extremal systems, Fig. 1b and Fig. 4b, we conclude that the systems have nearly equal dynamic properties, but the system of Fig. 4b is considerably simpler.

To improve the dynamic of the system of Fig. 4b, we introduce feedback proportional to $\dot{x}$ (Figs. 4c, 4d). The motion in the system is consequently described by Equations [2.1 to 2.3] and [4.11].

Going over to variables x,v we obtain after integration the sought phase trajectories (Fig. 7b)

$$v = v_0 - \frac{1 + \beta\alpha_1\alpha_2}{\tau}(x - x_0) \mp \frac{\alpha_1\alpha_2\alpha_3}{\tau}(x^2 - x_0^2) \quad [4.14]$$

In Equations [4.14], the upper sign holds for $v>0$ and the lower one for $v>0$.

Comparison of Figs. 7a and 7b shows how effective the introduction of additional feedback is.

5 Let us consider a case in which the external characteristic of this system can be approximated, with accuracy sufficient for practical purposes, by straight line segments

$$\varphi = -\alpha_3 x \operatorname{sign} x \quad [5.1]$$

Let us analyze the transients in a system described by Equations [2.1, 2.2, 2.4, and 5.1]. Since

$$\begin{aligned} (d\varphi/dx) &= -\alpha_3 \operatorname{sign} x \\ u &= -\alpha_3 \operatorname{sign} x \end{aligned} \quad \ldots\ldots\ldots\ldots\ldots\ldots\ldots\ldots\ldots\ldots [5.2]$$

and after eliminating the intermediate variables u and μ, we obtain one differential equation

$$\tau\ddot{x} + \dot{x} + \alpha_1\alpha_2\alpha_3 \operatorname{sign} x = 0 \quad [5.3]$$

which indeed describes the transients in the system.

Equation [5.3] differs from [3.2] only in the magnitude of the constant coefficient, and its investigation in the phase plane is analogous. Consequently, the system described by Equations [2.1, 2.2, 2.4, and 5.1] is analogous to the relay system described by Equations [2.1 to 2.3] and [3.1].

Let us consider further the transient processes in the system, describable by Equations [2.1, 2.2, 5.1 and 3.1].

Using [5.2], Equation [3.1] can be written

$$u = \text{sign}\frac{d\varphi}{dx} = \text{sign}\,(-\alpha_3 \text{ sign } x) = -\text{sign } x \qquad [5.4]$$

After eliminating the intermediate variables from Equations [2.1, 2.2 and 5.4], we obtain Equation [3.2], which describes the transients in this system. Consequently, the optimal control system describable by Equations [2.1, 2.2, 5.1 and 3.1] is analogous to the system describable by Equations [2.1, to 2.3 and 3.1]. The transients in the systems differ only in the magnitude of the coordinate φ.

The addition of a term proportional to the velocity $\dot{x}$ into the law of regulation of a system with an object characteristic [5.1] also affects favorably the quality of the transients. To verify this, it is enough to consider a system with a measuring element describable by the equation

$$u = \text{sign}\frac{d\varphi}{dx} - \beta\dot{x} = -\text{sign } x - \beta\dot{x} \qquad [5.5]$$

Let us examine now an optimal system, describable by Equations [2.1, 2.2, 5.1 and 4.10].

Differentiating Equation [5.1], we have $\dot{\varphi} = \alpha_3\dot{x}$ sign x, and then Equation [4.1] can be written in the form

$$u = -\alpha_3\dot{x} \text{ sign } \dot{x} \text{ sign } x \qquad [5.6]$$

Eliminating the intermediate variables from the system [2.1, 2.2 and 5.6], we get

$$\tau\ddot{x} + \dot{x} + \alpha_1\alpha_2\alpha_3\dot{x} \text{ sign } \dot{x} \text{ sign } x = 0 \qquad [5.7]$$

which describes the transients in the system.

Integrating Equation [5.7] in each quadrant of the xv plane, we obtain the equations of the phase trajectories in the form of straight line segments (Fig. 8a)

$$\tau(v - v_0) + (1 \pm \alpha_1\alpha_3\alpha_2)(x - x_0) = 0 \qquad [5.8]$$

The quality of the transients in the system improves as additional feedback proportional to x is introduced. In this case the system is described by Equations [2.1, 2.2, 5.1 and 4.11], whereas the phase trajectories are straight lines (Fig. 8b), whose equations are

$$\tau(v - v_0) + [1 \pm \alpha_1\alpha_3(\alpha_2 \pm \beta)](x - x_0) = 0 \qquad [5.9]$$

The upper sign in Equations [5.8 and 5.9] corresponds to one of the combinations of inequalities of the same sign ($v > 0$, $x > 0$) or ($v < 0$, $x < 0$); the lower one corresponds to one of the inequality combinations of opposite signs ($v > 0$, $x < 0$ or $v < 0$, $x > 0$).

In practice, the case where the extremal characteristic is not symmetrical and can be approximated in the form of straight

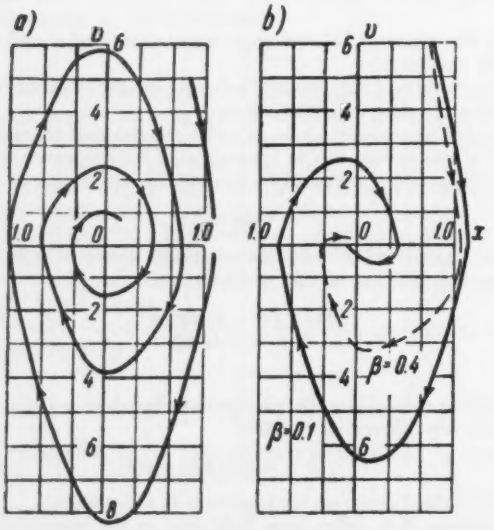

Fig. 7 a—Phase trajectories of optimal system with measuring element [4.10], $\alpha_1\alpha_2 = 10$, $\alpha_3 = 0.5$, $\tau = 1$ sec, $\Delta = 0.5$; b—phase trajectories of optimal system with measuring element [4.11], $\alpha_1\alpha_2 = 10$, $\alpha_3 = 0.5$, $\tau = 1$ sec, $\Delta = 0.5$

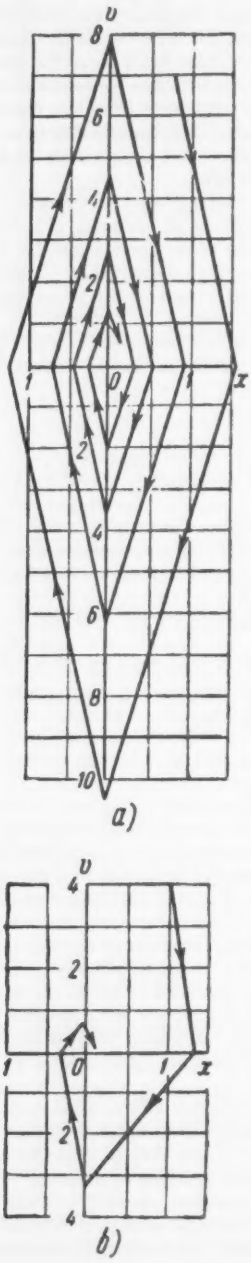

Fig. 8 a—Phase trajectories of optimal system with measuring element [4.10] with the characteristics of the regulated object being approximated by Equation [5.1], $\alpha_1\alpha_2 = 10$, $\alpha_3 = 0.75$, $\tau = 1$ sec; b—phase trajectories of optimal system with measuring element [4.1] with the characteristics of the regulated object being approximated by Equation [5.1], $\alpha_1\alpha_2 = 10$, $\alpha_3 = 0.75$, $\tau = 1$ sec, $\beta = 0.4$

line segments having different slopes

$$\varphi = -\alpha_{31}x \qquad [5.10]$$

when $x>0$

$$\varphi = \alpha_{32}x$$

when $x<0$, is much more frequent than an extremal characteristic approximated by a parabola. In this case the investigation of the transient in the optimal control systems can also be carried out in the phase plane, as was done by Ostrovskii et al. (10).

6 In the papers of Kulebakin (13), and later by others, it was shown that it is possible to improve the dynamics of ordinary servo systems by intoducing error derivatives. This method can be extended also to optimal control systems. This results not only in improved system quality, but considerable simplification of the investigation of the optimal systems.

Let us consider systems in which the object of regulation can be represented by an inertial-less nonlinear link in series with an inertial linear link.

Let the optimal control system be described by Equation [2.1] for the actuating motor, by Equation [2.3] for the object, by

$$x = \alpha_3\mu \qquad [6.1]$$

$$\tau_1\dot{y} + y = \alpha_3\varphi \qquad [6.2]$$

and by the following equation for the measuring element

$$u = \alpha_4\frac{\dot{y}}{\dot{x}} \qquad [6.3]$$

Solving Equations [2.1, 2.3 and 6.1 to 6.3] simultaneously, we get

$$2\tau_1\ddot{x} + \dot{x} + 2\alpha_1\alpha_2\alpha_3\alpha_4\alpha_5 x = 0 \qquad [6.4]$$

This equation differs from Equation [2.5] only in the coefficient preceding the highest order derivative.

Introducing a second derivative into the measuring element of this system, its equation becomes

$$u = \alpha_4\frac{\ddot{y} + \tau_1\dot{y}}{\dot{x}} \qquad [6.5]$$

After eliminating the intermediate variables from Equations [2.1, 6.1, 2.3, 6.2 and 6.5] we obtain the first-order equation

$$\dot{x} + 2\alpha_1\alpha_2\alpha_3\alpha_4\alpha_5 x = 0 \qquad [6.6]$$

Thus, the order of the equation has been reduced, and the quality of the system has improved.

Let us consider now an optimal system in which the object of regulation, jointly with the inertial measuring element, can be represented by a series-circuit comprising a linear, nonlinear and a linear link, and describable by a system of equations [2.1 to 2.3, 6.2 and 6.5].

Solving these equations simultaneously, we obtain a linear differential equation for the dynamics of the system

$$\tau\ddot{x} + \dot{x} + 2\alpha_1\alpha_2\alpha_3\alpha_4\alpha_5 x = 0 \qquad [6.7]$$

analogous to Equations [2.5 and 6.4]. The introduction of the second derivative into the measuring element [6.5] has made it possible to reduce the investigation to that of a linear equation. Were we to consider the same system but with a measuring element [2.4], the dynamic equation of the system would be a third-order nonlinear differential equation, which is, in general, difficult to analyze.

It is easy to show that for the optimal system just considered, additional feedback proportional to $\dot{x}$ improves considerably the dynamic properties of the system. Actually, solving the system of Equations [2.1 to 2.3 and 6.2] together with the equation of the new measuring element

$$u = \alpha_4\frac{\dot{y} + \tau_1\ddot{y}}{x} - \beta\dot{x} \qquad [6.8]$$

we obtain a dynamic equation of the system

$$\tau\ddot{x} + (1 + \beta\alpha_1\alpha_2)\dot{x} + 2\alpha_1\alpha_2\alpha_3\alpha_4\alpha_5 x = 0 \qquad [6.9]$$

in which it is possible to change the damping of the system as desired by varing the coefficient β. A similar optimal system, but with a measuring element of the relay type, describable by the equation

$$u = \alpha_4 \operatorname{sign}\frac{\dot{y} + \tau_1\ddot{y}}{x} \qquad [6.10]$$

is reduced to a dynamic system equation

$$\tau\ddot{x} + \dot{x} + 2\alpha_1\alpha_2\alpha_4 \operatorname{sign} x = 0 \qquad [6.11]$$

analogous to Equation [3.2], the phase-plane solution of which was obtained above. It is easy to show also that introduction of an additional term $-\beta\dot{x}$ into the control Equation [6.10] makes it possible, all other conditions remaining equal, to change the damping of this system.

Systems in which a linear portion having a high order is connected past the nonlinear element are describable by complex nonlinear differential equations. It is easy to show that by introducing into the measuring element of such a system, in a suitable manner, corresponding higher derivatives of the output coordinate of the object of regulation, will make it possible to reduce respectively the order of the overall dynamic equation of the system and thereby simplify the investigation of the system and improve the transient response.

7 Let us consider a system of extremal control with constant time delay, in which the linear portion of the object is described by the equation

$$\tau\dot{x}(t) + x(t) = \alpha_3\mu(t - \tau_3) \qquad [7.1]$$

and the remaining elements of the system are described by Equations [2.1, 2.3 and 2.4]. Eliminating the intermediate variables, the equation of the system becomes

$$\tau(\dot{x})(t) + \dot{x}(t) + 2\alpha_1\alpha_2\alpha_3\dot{x}(t - \tau_3) = 0 \qquad [7.2]$$

Thus, an investigation of the dynamics of such a control system can also be performed by the known methods of general control theory. The improvement in the transient response in this system is attained by introducing additional velocity feedback proportional to $\dot{x}$. In this case the transients are determined by the dynamic equation

$$\tau\ddot{x}(t) + \dot{x}(t) + \beta\alpha_1\alpha_2\dot{x}(t - \tau_3) + 2\alpha_1\alpha_2\alpha_3 x(t - \tau_3) = 0 \qquad [7.3]$$

and a comparison of this equation with Equation [7.2] can demonstrate the suggested improvement in system response.

An investigation of a similar system, but having a relay-type measuring element, such as describable by Equations [2.1, 6.1, 2.3, and 3.4] can be carried out in phase plane. The system is described by the equations

$$\tau\ddot{x}(t) + \dot{x}(t) + \alpha_1\alpha_2 = 0 \quad x(t - \tau_3) > -\Delta \qquad [7.4]$$

$$\tau\ddot{x}(t) + \dot{x}(t) - \alpha_1\alpha_2 = 0 \quad x(t - \tau_3) < \Delta \qquad [7.5]$$

the integration of which yields Equations [3.3], and the switch-

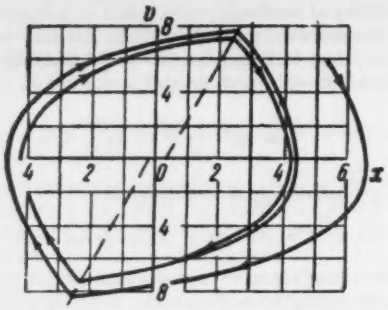

Fig. 9 Phase trajectories of optimal system with delay in the regulated object and with measuring element [3.4], $\alpha_1\alpha_2 = 10$, $\alpha_3 = 0.5$, $\tau = 1$ sec, $\tau_3 = 0.25$ sec, $\Delta = 0.5$

ing limits are of the following form in this case

$$x = \mp\Delta \mp \tau\alpha_1\alpha_3\left[1 + \frac{\tau_3}{\tau} - \exp\frac{\tau_3}{\tau}\right] + \tau\left(\exp\frac{\tau_3}{\tau} - 1\right)v \qquad [7.6]$$

The phase trajectories of such a system are shown in Fig. 9. The introduction of the derivative x into the measuring elements also improve the response of the system.

If the element with the constant lag is connected in the control system past the nonlinear element, something that can occur physically if the lag is built into the measuring element, then the optimal system is describable, for example, by Equations [2.1 to 2.3] together with $\varphi_1(t) = \varphi(t-\tau_3)$.

If a measuring element of type [2.4] is used the investigation of the system becomes quite difficult. On the other hand, if we construct a measuring element with an equation of the form

$$u = \dot{\varphi}_1/\dot{x}_1 \qquad [7.7]$$

where $x_1 = x(t-\tau_3)$, then after eliminating the intermediate variables, the dynamic equation of the system has the form [7.2]. To obtain the function x_1 it is enough to introduce into the model of the linear portion of the regulated object (element 6, Fig. 1c) an element having a constant lag equal to τ_3.

References

1 Ivakhnenko, A. G., "Automatic Control System with Logical-Action Elements—Principal Problems of Automatic Control and Regulation," *Sessiya AN SSSR po nauchn. prob. avtomat. proizvodstva* (session of Academy of Sciences, USSR on Scientific Problems of Automatization of Manufacture), Moscow, 1957.

2 Ivakhnenko, A. G., "Elements of General Theory of Combined Cybernetic Systems," *Avtomatika* (*Automation*), no. 1, 1958.

3 Tsien, H. S., Engineering Cybernetics McGraw-Hill Book Co., Inc., New York, 1954 (Russian Translation, I.I.L., Moscow, 1956).

4 Tsien, H. S. and Serdengecti, S., "Analysis of Peak-holding Optimalising Control," *J. Aeron. Sci.*, no. 8, 1955.

5 Serdengecti, S., "Optimalising Control in the Presence of Noises Interference," JET PROPULSION, no. 6, 1956.

6. Taylor, C. F., "Problems of Nonlinearity in Adaptive or Self-Optimalising Systems," J. R. E. Trans. on Automatic Control, PGAC, July 1958.

7 Cosgriff, R. L. and Emerling, R. A., "Optimizing Control Systems, Application and Industry," no. 35, March 1958.

8 Kuntsevich, V. M. and Akunin, P. I., "Approximate Methods of Determination of Frequency and Amplitude of Self-Oscillations in Extremal-Control Systems," *Avtomatika* (*Automation*), no. 3, 1957.

9 Morosanov, I. S., "Methods of Extremal Control," *Avtomatika i Telemekhanika* (*Automation and Remote Control*), vol. 18, no. 11, 1957 (English translation published by American Instrument Society).

10 Ostrovskii, Yu. I. and Eskin, M. G., "Extremum Regulator for Turbine Drilling of Oil Wells," *Avtomatika i Telemekhanika* (*Automation and Remote Control*), vol. 17, no. 9, 1956.

11 "*Osnovy avtomaticheskovo regulirovaniya, Teoriya*" (Principles of Automatic Control, Theory), edited by V. V. Solodovnikov, Mashgiz, Moscow 1954.

12 Kryshanovskii, V. M. and Kuntsevich, V. N., "Analysis of Extremal-Control System by Investigating Their Transients," *Avtomatika* (*Automation*), no. 3, 1958.

13 Kulebakin, V. S., "Applicability of the Principle of Absolute Invariance in Physical Real Systems," DAN SSSR (Proc. of the Academy of Sciences, USSR), vol. 77, no. 2, 1951.

Original received February 23, 1959

Contribution to the Theory of Inertial Damped Systems With Arbitrary Period, Invariant With Respect to Maneuvering of the Object

V. A. BODNER
V. P. SELEZNOV and
V. E. OVCHAROV

As is known (1,2)[1] inertial systems based on the use of the gyroscopic model of the pendulum of Schuler have the following principal shortcomings: 1 If the compensation conditions are exactly satisfied, the system becomes insensitive to disturbances caused by maneuvering of the object carrying the inertial system, but in the case of non-zero initial conditions undamped oscillations occur in the system (the system is at the stability limit); 2 in the absence of external correction for the drift of the gyroscopes, large errors accumulate in the system with time. The initial deviations of the vertical of an inertial system could be reduced to zero by introducing damping in the system, i.e., by introducing into the equations of motion such terms for which the motion changes from periodic into damped. However, the well-known error rate method of introducing damping by using internal signals leads to violation of the compensation conditions and does not make it possible to obtain rapid damping of the processes. The damping time is comparable here with Schuler's period (84.4 min).

There is nothing unique about these features of inertial systems, for they are characteristic of all single-loop closed systems. It is known that in single-looped systems it is impossible to satisfy the conditions of insensitivity to disturbance (compensation) without violating the stability conditions. To satisfy this insensitivity condition at a given point of the system with respect to definite disturbances it is necessary that the information concerning this disturbance arrive at the point over not less than two channels. If the signals—the carriers of information concerning the disturbances—arriving over one channel are in phase opposition with respect to the signals arriving from another channel, compensation of signals can occur, and the system becomes insensitive to disturbances. Consequently acceleration insensitive systems, having acceptable dynamic properties, should by their very nature be multilooped systems. The additional loops over which the compensation signals are transmitted can be either closed or opened.

This paper contains the theory and principles of construction of damped inertial systems with arbitrary period, insensitive to acceleration with respect to the maneuvering of the object. A theorem is formulated here, which is a generalization of the corresponding theorem by Schuler.

I Methods of Damping Inertial Systems

LET US assume that an object moving at a constant altitude above the Earth (which is assumed to be spherical) carries a gyro platform which is free in azimuth. Let, at the initial instant of time, the plane of the gyro platform be perpendicular to the local vertical. We place on the gyro platform two accelerometers with mutually perpendicular axes, lying in the plane of the platform (Fig. 1). We orient the x and y axes of the coordinate system along the axis of the accelerometer, and the z axis upward along the local vertical.

We denote by α and β small deflections of the gyro vertical from the local vertical, along the x and y axes, respectively, and by V_x and V_y the components of the inertial velocity of the object. If the gyro platform is perpendicular to the local vertical, then the accelerometers mounted on it will measure the components of absolute acceleration, double integration of which yields the displacement components. To maintain the gyro vertical in a position perpendicular to the local vertical, it is necessary to apply to it correcting signals, proportional to the integral of acceleration signals. Thus, the equations of motion of the gyro platform will be

$$\alpha = k_2 \int_0^t k_1 dt \int_0^t (\dot{V}_x - g\alpha)dt - \int_0^t \frac{V_x}{R}\,dt$$

$$\beta = k_2 \int_0^\infty k_1 dt \int_0^\infty (\dot{V}_y - g\beta)dt - \int_0^t \frac{V_y}{R}\,dt \qquad [1.1]$$

where

k_1, k_2 = gains of the integrating elements (Fig. 2)
R = Earth's radius
g = acceleration due to the central forces acting on the gyro platform

Since Equations [1.1] have an identical structure, we shal consider only one of these.

In the derivation of Equations [1.1] it was assumed that the gyro platform rotates about a vertical axis with a velocity $(\omega_E + \dot{\lambda})\sin\varphi$ where ω_E is the angular speed of the Earth's

Translated from *Izvestiia Akademii Nauk SSSR, Otdelenie Tekhnicheskikh Nauk, Energetika i Avtomatika* (*Bull. USSR Acad. Sci., Div. Tech. Sci., Power and Automation*), no. 3, 1959, pp. 11–18.

[1] Numbers in parentheses indicate References at end of paper.

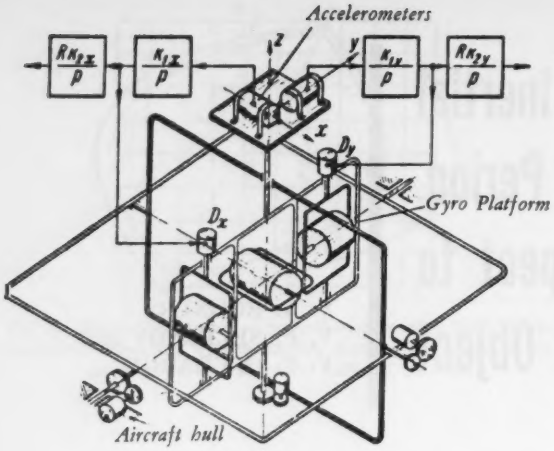

Fig. 1

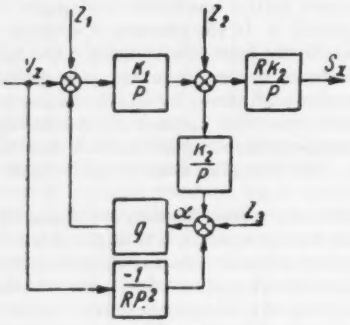

Fig. 2

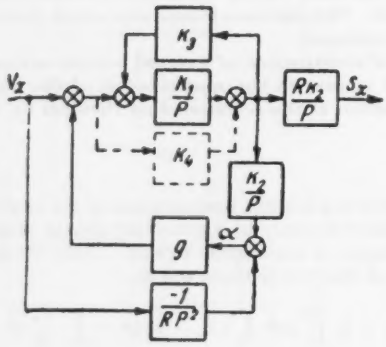

Fig. 3

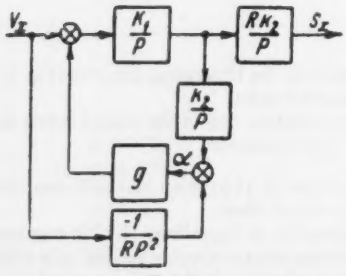

Fig. 4

rotation, φ the local latitude and $\dot{\lambda}$ the rate of change of longitude.

If we differentiate the first equation of system [1.1] with respect to time and rearrange terms, we obtain

$$(p^2 + gk_1k_2)\alpha = \left(k_1k_2 - \frac{1}{R}\right)\dot{V}_z \qquad [1.2]$$

It is shown in the block diagram of the system (Fig. 2) that the accelerometer measures the acceleration $\dot{V}_z - g\alpha$, which after a single integration yields a signal proportional to the velocity. This signal is fed, on the one hand, to the correcting mechanism of the gyro platform, which has a transfer function k_2/p, and on the other hand to an integrator with a transfer function Rk_2/p, to obtain the component of the elapsed distance.

If we satisfy in Equation [1.2] the compensation condition

$$k_1k_2 = \frac{1}{R} \qquad [1.3]$$

we obtain

$$(p^2 + \Omega_0^2)\alpha = 0 \qquad \left(\Omega_0^2 = \frac{g}{R}\right) \qquad [1.4]$$

where Ω_0 is the Schuler frequency.

If condition [1.3] is satisfied, the inertial system is undisturbed by the acceleration of the object. However, under non-zero initial conditions ($\alpha_0 \neq 0$, $\dot{\alpha}_0 \neq 0$), undamped oscillations arise in the system with a frequency Ω_0 and with an amplitude determined by the initial conditions. If the instrument errors are taken into account, the angle α is subject to additional errors.

If the condition $\alpha = 0$ is satisfied, the first integrals of the acceleration components represent, with allowance for the Earth's peripheral velocity, the components of the ground velocity of the object, whereas the second integrals represent the components of the elapsed path. Consequently, it is possible to determine the velocity vector, the position coordinates of the objects and other navigational elements.

To eliminate the undamped oscillation of the inertial system it is necessary to incorporate in it devices that introduce damping of the oscillations. Fig. 3 shows a block diagram of an inertial system in which the damping is produced by including the first (and perhaps also the second) integrator in a positive (dotted) or negative (solid) feedback loop.

The equation of motion of the inertial system with feedback damping has the form

$$(p^2 + 2d\Omega_0 p + \Omega_0^2)\alpha = \frac{2d\Omega_0}{R}V_z \qquad (2d\Omega_0 = k_1k_3) \qquad [1.5]$$

If the damping is produced by positive feedback, the equation of motion will be

$$(p^2 + 2d\Omega_0 p + \Omega_0^2)\alpha = -\frac{k_3k_4}{R}\ddot{V}_z \qquad (2d\Omega_0 = gk_3k_4) \qquad [1.6]$$

It follows from Equations [1.5 and 1.6] that damping by inclusion of the first or second integrator in some sort of feedback loop destroys the insensitivity of the system [1.3]. It is possible to prove the following premise, which is valid in general: Damping of an inertial system by means of any internal coupling destroys the acceleration insensitivity conditions.

It is interesting to note that if the inertial system in which the damping is obtained by internal feedback is incorporated in a closed control loop and made to serve as a position-coordinate transmitter, its damping disappears. In fact, assume that the coordinate η is fed to an autopilot (Fig. 4). The transfer functions of the system in response to a gust of wind, $v_g = U/_gV$, and in response to a signal of a change in setting

η_0, assume the form

$$\frac{y}{\nu_y} = \frac{a_1 p(p^2 + 2d\Omega_0 p + \Omega_0^2)}{p^2(p^2 + 2d\Omega_0 p + \Omega_0^2) + (c_1 p + c_2)(p^2 + \Omega_0^2)} \quad [1.7]$$

$$\frac{y}{\eta_0} = \frac{(c_1 p + c_2)(p^2 + 2d\Omega_0 p + \Omega_0^2)}{p^2(p^2 + 2d\Omega_0 p + \Omega_0^2) + (c_1 p + c_2)(p^2 + \Omega_0^2)} \quad [1.8]$$

where the binomial $c_1 p + c_2$ characterizes the law of control of the autopilot and the dynamics of acceleration in response to an error signal applied to the control system.

Since the coefficients of the polynomial in the denominators of expressions [1.7 and 1.8] are positive, the stability of the system can be estimated from the sign of the determinant

$$\Delta = \begin{vmatrix} c_1 + 2d\Omega_0 & c_1\Omega_0^2 & 0 \\ 1 & \Omega_0^2 + c_2 & c_2\Omega_0^2 \\ 0 & c_1 + 2d\Omega_0 & c_1\Omega_0^2 \end{vmatrix} \quad [1.9]$$

It is easy to see that

$$\Delta = (c_1 + 2d\Omega_0)(c_1\Omega_0 - 2dc_2)\Omega_0^2 - c_1\Omega_0^4 < 0 \ (2dc_2 \gg c_1\Omega_0) \quad [1.10]$$

Consequently, if the inertial system is included in a closed control loop as a coordinate reference, the damping introduced in it by internal feedback vanishes. The closed system thus becomes unstable.

To estimate the character of the divergent transient in the closed system, let us consider in greater detail the denominator of the transfer functions [1.7 and 1.8], which can be approximately factored into

$$\left(p^2 - \frac{2d\Omega_0^2}{c_2} p + \Omega_0^2\right)(p^2 + c_1 p + c_2) \quad [1.11]$$

It follows from this that the system is subject to two motions, a slow one with the frequency of the inertial system, and a fast one with a frequency of the center of mass of the aircraft. These frequencies differ by two orders of magnitude. Furthermore, the inertial system is divergent, while the degree of buildup of the oscillations $2d\Omega_0^2/c_2$ does not exceed several tenths of a per cent during each period (of 84.4 min).

Thus, damping introduced into an inertial system by means of internal feedback, leads to a violation of the acceleration insensitivity condition if the inertial system is used as an indicator, and disappears entirely if the inertial system is used as a control system. It follows therefore that other damping methods must be employed.

2 Use of External Information for Damping and Altering the Period

Let us assume that the inertial system placed on the object receives extraneous[2] discrete (i.e., intermittent in time) information (Fig. 5) which characterizes the actual ground position of the object, its velocity, its acceleration, etc. Over short intervals of time, the extraneous information, which may be received from a radio system or from distance-computing systems, may have a high degree of reliability (accuracy). This information can be used to correct the errors of the inertial system, to introduce damping and to change the period of the system. Let the information be introduced into the system via the input of the first integrator (z_1), the input of the second integrator (z_2) and the input of the gyro platform (z_3). It may also pass first through special filters.

The equation of motion of the system (Fig. 5), with account of the external information, can be represented in the

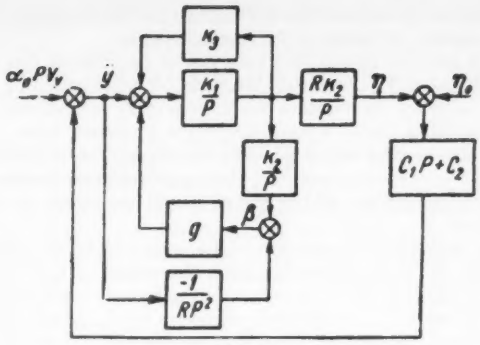

Fig. 5

following form

$$(p^2 + gk_1k_2)\alpha = k_1k_2z_1 + k_2pz_2 + p^2z_3 \quad [2.1]$$

It was assumed in the derivation of this equation that the compensation condition [1.3] was satisfied.

Let us choose the externally derived sources of information z_1, z_2 and z_3 such that the vertical's own motion is damped, and the period of the system is arbitrary and differs from the Schuler period, while the right half of Equation [2.1] differs little from zero. For this purpose we put, for example

$$z_1 = -k(\alpha \pm \Delta_\alpha) - \epsilon(\dot{\alpha} \pm \Delta_{\dot{\alpha}}) \qquad z_2 = 0 \qquad z_3 = 0 \quad [2.2]$$

In expressions [2.2] the angle α and the angle of velocity $\dot{\alpha}$ are determined from

$$\alpha \pm \Delta_\alpha = \frac{s_x - s_{x0}}{R} \qquad \dot{\alpha} \pm \Delta_{\dot{\alpha}} = \frac{V_x - V_{x0}}{R} \quad [2.3]$$

where

V_x, s_x = velocity and the coordinate of the object measured by means of the inertial system

V_{x0}, s_{x0} = velocity and coordinate of the object measured by means, say, of radio devices (external information)

Δ_α, $\Delta_{\dot{\alpha}}$ = the errors in the determination of the angle and angular velocity

It is assumed that the external information on the coordinate and velocity of the object has higher accuracy than the information produced by the inertial system.

If we insert Equations [2.2] into [2.1], we obtain

$$(p^2 + 2d\Omega_0\chi p + \Omega_0^2\chi^2)\alpha = \mp\Omega_0^2(\chi^2 - 1)\Delta_\alpha \mp 2d\Omega_0\chi\Delta_{\dot{\alpha}} \quad [2.4]$$

Here

$$\Omega_0^2 = \frac{g}{R} \qquad 2d\Omega_0\chi = \epsilon k_2 \qquad \chi^2 = 1 + \frac{k}{g}$$

Depending on the sign of the coefficient k, it is possible either to increase ($k < 0$) or decrease ($k > 0$) the period of the inertial system as compared with the Schuler period, without violating the compensation conditions [1.3] (with accuracy to within the errors of the system, due to inaccuracy in the external information). Since Equation [2.4] contains a damping term, the vertical's own motion will be damped.

Thus, we can formulate the following theorem:

Theorem—To construct a damped inertial system with arbitrary period, invariant with respect to maneuvering of the object, it is necessary to introduce into it extraneous information concerning the velocity and coordinates of the object, and to determine the angles and angular velocities of the

[2] Extraneous information is meant to be information on the velocity and coordinates of the position of the object, obtained by means of any system that is not inertial.

vertical on the basis of this information and the corresponding information produced by the inertial system.

The external information need not be continuous, but can be applied only at brief time intervals, for example during the initial display (to eliminate the initial errors), to eliminate the accumulated errors after a prolonged operating time, etc. The time during which the external information is supplied should be as short as possible; during this time the transients due to elimination of the errors should essentially be terminated.

In order for the transients in the system to be terminated within the shortest possible time, the period of the system should be considerably less than that of Schuler's period ($\chi^2 \gg 1$). However, a considerable reduction in the period makes the inertial system sensitive to noise due to the external information. The choice of an optimum coefficient of period reduction d is one of the principal problems of the theory of inertial systems with arbitrary period. The choice of the magnitude of the decrement d is dictated by the requirement that the processes must be damped rapidly, thus calling for, say, $d = 0.7$ to 1.0.

3 Analysis of Errors of Inertial System With Arbitrary Period

The errors Δ_α and $\Delta_{\dot\alpha}$ in the extraneous information, used for the correction, give rise to errors in the inertial system. It is obvious that if $\Delta_\alpha = \Delta_{\dot\alpha} = 0$, the intrinsic errors of this system will vanish after the transients have died down. However, it is impossible to determine by any method whatever the velocity and position of an object without an error, and therefore we shall consider the characteristics of inertial systems in the presence of the foregoing errors.

We consider two typical cases:

1 The errors Δ_α and $\Delta_{\dot\alpha}$ are independent of the time and are constant.

2 The errors are random functions of time.

In the case of constant Δ_α and $\Delta_{\dot\alpha}$, the steady-state error α^0 of the inertial vertical will be

$$\alpha^0 = \mp \frac{\chi^2 - 1}{\chi^2} \Delta_\alpha \mp \frac{2d}{\Omega_0 \chi} \Delta_{\dot\alpha} \qquad [3.1]$$

It follows from this that at large numerical values of the period reduction coefficient $\chi(\chi \gg 1)$, the major source of steady-state error of the system will be the errors in the coordinate information, whereas at small numerical values of χ the decisive errors will be those in object velocity data.

If the inertial system is corrected without changing (reducing) the period, the errors in the object velocity information may prove to be inadmissibly large. This results from the following considerations. Modern navigational systems make it possible to determine the object position over ranges of several hundreds of kilometers with an accuracy up to $\Delta s_{x0} = 1$ km, while the speed can be determined, with the aid of a Doppler system, with accuracy to 0.3–0.4 per cent. Consequently

$$\Delta_\alpha = \frac{\Delta s_{x0}}{R} = \frac{1}{6 \times 10^3} = 0.6' \qquad \Delta_{\dot\alpha} = \frac{0.004 \cdot V_{x0}}{R}$$

or, taking the object velocity to be $V_{x0} = 1$ km per sec

$$\Delta_{\dot\alpha} = \frac{0.004 \times 1}{6 \times 10^3} \approx 0.23 \times 10^{-3} \left(\frac{\text{angular min}}{\text{sec}} \right)$$

Knowing these errors in the external information, we can find the errors in the initial system under various reductions in the period. For $\chi = 1$ we have

$$\alpha^0 = \mp \frac{2d}{\Omega_0} \frac{0.004 V_{x0}}{R} \approx 3.7'$$

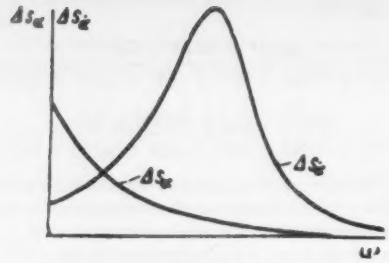

Fig. 6

When the period is reduced by $\chi = 10$, we find

$$\alpha^0 = \mp 0.6' \mp 0.37'$$

i.e., the error does not exceed 1 angular min.

Let us estimate the system errors if the errors Δ_α and $\Delta_{\dot\alpha}$ are random functions of time. After estimating these errors in terms of their spectral densities $\Delta s_\alpha(\omega)$ and $\Delta s_{\dot\alpha}(\omega)$, we can write for the mean-squared error of the vertical

$$\bar{s}_x^2 = \frac{1}{\pi} \int_{-\infty}^{\infty} |\Phi_1(i\omega)|^2 \Delta s_\alpha(\omega) d\omega + \frac{1}{\pi} \int_{-\infty}^{\infty} |\Phi_2(i\omega)|^2 \Delta s_{\dot\alpha}(\omega) d\omega \qquad [3.2]$$

where

$$|\Phi_1(i\omega)|^2 = \frac{\Omega_0^4(\chi^2 - 1)^2}{(\Omega_0^2\chi^2 - \omega^2)^2 + 4d^2\Omega_0^2\chi^2\omega^2} \qquad [3.3]$$

$$|\Phi_2(i\omega)|^2 = \frac{4d^2\Omega_0^2\chi^2}{(\Omega_0^2\chi^2 - \omega^2)^2 + 4d^2\Omega_0^2\chi^2\omega^2} \qquad [3.4]$$

The spectral densities of the errors $\Delta s_\alpha(\omega)$ and $\Delta s_{\dot\alpha}(\omega)$ are determined essentially by the properties of the systems used to measure the quantities s_{x0} and V_{x0}, and by the vibration of the objects on which these systems are mounted. The influence of the object vibrations on the magnitude of the error is particularly substantial when the results of the measurement depend on the position of the object relative to the local vertical. In such cases the oscillations, which are random functions of time, determine to a considerable extent the spectral characteristics of the errors Δd_α and $\Delta s_{\dot\alpha}$. A Doppler system for measuring ground speed is indeed such a system in which the errors are determined by the vibration of the object. When the position coordinates of the object are measured with the aid of radio-navigation systems, the effect of vibrations is less noticeable. Taking the foregoing into account, we can assume for the spectral densities $\Delta s_\alpha(\omega)$ and $\Delta s_{\dot\alpha}(\omega)$ the following expressions (3,4)

$$\Delta s_\alpha(\omega) = \frac{4\beta_1\sigma_\alpha}{\omega^2 + \beta_1^2} \qquad [3.5]$$

$$\Delta s_{\dot\alpha}(\omega) = \frac{4\beta_1\sigma_{\dot\alpha}^2(z^2 + \omega^2)}{(z^2 + \omega^2)^2 - 4\omega_0^2\omega^2} \qquad (z^2 = \beta_1^2 + \omega_0^2) \qquad [3.6]$$

where

β_1 = damping parameter
ω_0 = resonant frequency

Fig. 6 shows plots of the functions Δs_α and $\Delta s_{\dot\alpha}$.

Inserting the expressions [3.3–3.6] into [3.2] we obtain after integrating and transforming

$$\bar{\epsilon}_z^2 = \bar{\epsilon}_{z\alpha}^2 + \bar{\epsilon}_{z\dot{\alpha}}^2 \qquad [3.7]$$

where $\bar{\epsilon}_{z\alpha}$ and $\bar{\epsilon}_{z\dot{\alpha}}$ are the mean-squared values of the errors of the inertial system due to inexact object coordinate and velocity information. With this we have

$$\bar{\epsilon}_{z\alpha}^2 = \frac{\Omega_0\sigma_\alpha^2(\chi^2 - 1)^2(2d\Omega_0\chi + \beta_1)}{\chi^2(\beta_1^2 + \Omega_0^2\chi^2 + 2d\Omega\chi\beta_1)} \qquad [3.8]$$

$$\bar{\epsilon}_{z\dot{\alpha}}^2 = \frac{16d^2\sigma_{\dot{\alpha}}^2[n\Omega_0^2\chi^2\Delta_A + \beta z^2(\Delta_e + \Omega_0^2\chi^2\Delta_D)}{nz^2\Omega_0\chi\Delta} \qquad [3.9]$$

where

$$\begin{aligned}
\Delta &= (z^4 - \Omega_0^4\chi^4)^2 + (2h - \lambda^2)(2hz^2 - \lambda^2\Omega_0^2\chi^2)\\
\Delta_A &= z^2[-(z^4 - \Omega_0^4\chi^4) + (2h - \lambda^2)(z^2 - \lambda^2)]\\
\Delta_e &= z^2(z^4 - \Omega_0^4\chi^4) + (2h - \lambda^2) + (2hz^2 - \Omega_0^4\chi^4)\\
\Delta_D &= z^4 - \Omega_0^4\chi^4 + z^2(2h - \lambda^2)\\
n &= \sqrt{2d^2 - 1 - 2d\sqrt{d^2 - 1}} + \sqrt{2d - 1 + 2d\sqrt{d^2 - 1}}\\
2h &= 2\Omega_0^2\chi^2(2d^2 - 1)\\
\lambda^2 &= 2z^2 - 4\omega_0^2
\end{aligned}$$

Let us analyze the errors $\bar{\epsilon}_z$ and $\bar{\epsilon}_{z\dot{\alpha}}$. It follows from Equation [3.8] that when $\chi = 1$, i.e., in the case of a system with a Schuler period, the position error $\bar{\epsilon}_{z\alpha}$ vanishes. As χ increases, the error $\bar{\epsilon}_{z\alpha}$ increases, and as the period of inertial system is further reduced, it tends to a maximum $\bar{\epsilon}_{z\alpha\,\max}^2 = 2\sigma_\alpha^2$.

The velocity error also depends on χ. If we assume that $d = 1$ and $\beta_1 < \Omega_0$, then as χ ranges from 1 to infinity the error

$$\bar{\epsilon}_{z\dot{\alpha}}^2 = 8\frac{\beta}{\Omega_0}\frac{\sigma_{\dot{\alpha}}^2}{z^2} \text{ for } \chi = 1$$

starts increasing, and reaches a maximum

$$\bar{\epsilon}_{z\dot{\alpha}}^2 = 12\frac{\sigma_{\dot{\alpha}}^2}{z^2} \text{ for } \chi = \frac{\omega_0}{\Omega_0}$$

Upon further increase in the coefficient χ the error begins to decrease, reaching zero at $\chi \to \infty$. Such a character of the dependence of the error $\bar{\epsilon}_{z\dot{\alpha}}$ on χ is explained by the fact that as the frequency of the inertial system increases, the amplitudes of the frequency characteristic decrease in inverse proportion to χ^2, with a total decrease in the spectral density at frequencies above resonance. One must not conclude from this that it is necessary to increase the frequency of the inertial system to values exceeding the resonant frequency ω_0. When the frequency of the inertial system is so increased, additional errors due to angular vibrations of the airplane arise.

The choice of the coefficient χ can be based on the requirement $\Omega_0\chi < \omega_0$. If ω_0 is equal to 0.02 sec^{-1}, then χ is less than 16.3. Apparently, a reduction by a factor of 10 is acceptable.

If the damping parameter β_1 is greater than Ω, the function $\bar{\epsilon}_{z\dot{\alpha}}$ does not have a maximum with respect to χ and decreases monotonically with increasing χ.

4 Influence of the Object Speed on Operation of the Inertial System

It has been assumed up to now that the acceleration g due to the central forces is constant and independent of the velocity V of the object, something that is true at low velocities ($V < 3c$, where c is the velocity of sound). For large velocities the acceleration g, to which the elements in the object are subjected, will be

$$g = g_0 - \frac{V^2}{R}$$

where

g_0 = acceleration due to gravity
V = absolute velocity of the object

It follows therefore that for a velocity

$$V \to \sqrt{g_0 R}$$

the period of the inertial system tends to infinity. Consequently, the inertial system cannot function on an object that moves with the satelloidal velocity. However, if the initial errors are eliminated by using external reference information to reduce the period and the damping, then a large period (infinite in the limit) after cessation of the correction may prove to be a favorable property of the inertial system.

Thus, to construct damped inertial systems with arbitrary period it is necessary to have external information, which can be received by the system either discretely or continuously. In the case of discrete information, the pauses may be arbitrary. One can also conceive of inertial systems in which the extraneous information is used only during the initial instant of operation for initial adjustment (to eliminate initial errors). Such systems then continue to function as Schuler systems.

References

1 Ishlinskii, A. Yu., "On the Theory of the Gyroscopic Pendulum," *Prikladnaya Matematika i Mekhanika* (*Applied Mathematics and Mechanics*), vol. XXI, no. 1, 1957; "Theory of a Two-Gyroscope Vertical," *ibid.*, vol. XXL, no. 6, 1957.

2 Wrigley, W., Woodbury R. and Hovorka J., "Inertial Guidance," IAS Preprint no. 698. New York, 1937.

3 "Teoriya slyedyashchikh sistem" (Theory of Servo Systems), IL, 1951.

4 Besekerskii, V. A. et al., "Proektirovanie sledyashchikh sistem maloi moshchnosti" (Design of Low Power Servo Systems), Sudpromgiz, 1958.

Original received February 18, 1959.

Reviewer's comment: The appearance of this Russian treatment on damping of inertial navigation systems is timely in that a number of American papers have recently been released from security controls (1-4), the work in the classified literature dating back into the 1950's (5–11). An interesting difference in point of view is apparent between the approaches taken in the two countries. The Russian point of view centers around damping of the inertial system and considers the external reference only as a supplement used to suppress the disturbances originating from the total signal damping in the computer loops. In general, American authors treat the problem from the filter viewpoint, looking at the power spectra of both inertial components and the source of reference information.

—C. J. Mundo
American Bosch Arma Corp.

1 Dworetzky, L. H. and Edwards, A., "Principles of Doppler-Inertial Guidance," ARS JOURNAL, vol. 29, no. 12, Dec. 1959, pp. 967–972.

2 Duncan, D. B., "Combined Doppler Radar and Inertial Navigation Systems," *Navigation*, vol 6, no. 5, Spring 1959, pp. 321–327.

3 Stevens, F. and Lynch, F. W., "Aids to Inertial Navigation," *IAS Rev.*, Nov. 1957.

4 Mundo, C. J., "Aided Inertial Systems," *Arma Engng.*, vol. 2, no. 2, Nov. 1957.

5 Blassingame, P., "Optimum Parameters for Automatic Airborne Navigation," MIT Instrumentation Lab Rep. 63–98–T–8, May 1950.

6 Greenwood, I. A., "The Theory of Combined Doppler-Inertial High Precision Navigation Systems," General Precision Labs Tech. Rep. 150, May 10, 1951.

7 Armstrong, J. W. and Dodd, J. M., Jr., "Doppler-Inertial Mixing Systems," Convair Rep. no. FCA 4-089, April 30, 1953.

8 Yachter, M., "Generalized Optimum Transfer Function of a Linear Doppler-Inertial System," General Precision Labs Rep. A14-7, April 18, 1954, part 5, pp. 1–15.

9 Cole, R. D. and Seeley, R., "Inertial and Doppler-Inertial Navigation, Free Azimuth System," Naval Ordnance Test Station, NOTS TP 2058, NavOrd Rep. no. 6377, July 10, 1958.

10 Goldman, C. C. and Hayden, M. L., "Linearly Combined Doppler-Inertial Navigation Systems," WADC Tech. Rep. 52120, June 1952.

11 Clemens, J. E., Kerris, W. and Waselt, F., "Navigational Systems Combining Inertial and Ground Velocity Vector Information," WADC Tech. Rep. 52–76, April 1952.

Thermodynamic Properties of Air in the Temperature Interval From 1000 to 12,000 K and the Pressure Intervals From 0.001 to 1000 atm

E. V. STUPOCHENKO
I. P. STAKHANOV
E. V. SAMUILOV
A. S. PLESHANOV
I. B. ROZHDESTVENSKII

MODERN theory of jet propulsion deals with high temperatures arising when bodies move through the atmosphere at supersonic speeds. In this connection it becomes necessary to study the properties of air under such conditions. There are at present no fully developed experimental methods for direct investigations of the properties of gases at high temperatures. Theoretical calculations therefore become particularly important. Methods of statistical physics, in its quantum-mechanical formulation, along with spectroscopic data, serve as a reliable base for a theoretical calculation of the thermodynamic properties of gas systems and especially of mixtures of gases capable of reacting chemically with each other. An example of such a mixture is air: In addition to the dissociation of O_2 and N_2 and the formation of NO, ionization of both the molecular and the atomic components occur in air at high temperatures.

The thermodynamic functions of air are determined from the thermodynamic parameters of its components and from its composition, which varies with the temperature and pressure. Therefore the problem breaks up into two stages: Calculation of the thermodynamic parameters of the "pure" components, and calculation of the composition of the air and its thermodynamic functions.

The calculation of the thermodynamic parameters of "pure" components reduces to the calculation of statistical sums. For example, the free energy of one mole of a one-component ideal gas is expressed in terms of the statistical sum Q of the internal degrees of freedom of the gas in the following manner

$$F = -NkT \ln \left\{ \frac{eV}{N} \left(\frac{2\pi mkT}{h^2} \right)^{3/2} Q \right\}$$

where

$$Q = \sum_i g_i e^{-\frac{\epsilon_i}{kT}}$$

ϵ_i = energy levels of the gas particles
g_i = statistical weights of the levels
N = number of molecules in gm-mole
k = Boltzmann's constant
h = Planck's constant
m = particle mass
T = absolute temperature
V = volume of gas
e = base of natural logarithms

To determine the composition of the air it is necessary to solve a system of nonlinear algebraic equations, which include the equations of the law of effective masses for each of the possible reactions in the air and for each ionization process, the equation for Dalton's law, the equation of material balance, and the law of charge conservation.

To calculate the thermodynamic functions of a mixture of reacting gases it is necessary to solve two systems of linear equations.

Translated from "Physical Gasdynamics," USSR Acad. Sci., pp. 3–38.

1 Methods of Calculating the Statistical Sums for Atoms, Molecules and Their Ions

The statistical sums of atoms are the simplest in form. Henceforth we shall understand "statistical sums" to mean the statistical sums of the internal degrees of freedom.

In calculating the statistical sums, the energy of the unexcited (ground) state of the atom was assumed to be zero; i.e., we calculated statistical sums of the form

$$Q = g_{\text{nuc}}(g_0 + g_1 e^{-\frac{\epsilon_1}{kT}} + g_2 e^{-\frac{\epsilon_2}{kT}} + \dots)$$

For most atomic systems, several of the first excited levels are located 20,000 cm^{-1} above the ground state, and many of the excited levels are located above this small group of levels, 100,000 cm^{-1} from the ground state. At low temperatures, up to 6000–8000 K, it is possible to neglect the influence of the large number of levels located 100,000 cm^{-1} above the ground level without introducing a noticeable error in the value of this statistical sum. However, at higher temperatures (from 10,000 K and up) such neglect introduces a noticeable error in the values of the statistical sums and their first and second derivatives with respect to the temperature. Thus, for example, for nitrogen at $T = 12{,}000$ K, neglecting the influence of all the levels located above 30,000 cm^{-1}, we would introduce an error of 0.6 per cent in the value of the statistical sum, an error of 1.2 per cent in the value of the first derivative with respect to the temperature, and an error of 18 per cent in the second derivative with respect to the temperature.

In calculating the statistical sums of atoms and their ions, we took into account all the known levels, but instead of using the exact values of ϵ_i of the excited levels, we used values rounded off to three significant figures. The error introduced thereby in Q is estimated in the following manner. We represent ϵ_i in the form

$$\epsilon_i = \epsilon_p + \Delta\epsilon_i^{(p)}$$

where

$$\Delta\epsilon_i^{(p)} \lesssim 1000 \text{ cm}^{-1}$$

The statistical sum becomes

$$Q = \sum_p e^{-\frac{\epsilon_p}{kT}} \sum_i^{(p)} g_i e^{-\frac{\Delta\epsilon_i^{(p)}}{kT}}$$

Expanding $\exp(-\Delta\epsilon_i^{(p)}/kT)$ and retaining the first two

terms of the expansion, we obtain

$$Q = \sum_p e^{-\frac{\epsilon_p}{kT}} \sum_i^{(p)} g_i \left(1 - \frac{\Delta\epsilon_i^{(p)}}{kT}\right)$$

$$\Delta Q = -\sum_p e^{-\frac{\epsilon_p}{kT}} \sum_i^{(p)} g_i \frac{\Delta\epsilon_i^{(p)}}{kT}$$

To calculate the thermodynamic functions it is convenient to use the quantities Q and

$$Q' \equiv T\frac{dQ}{dT} \qquad Q'' = T^2\frac{d^2Q}{dT^2}$$

The formulas for Q, Q' and Q'' have the form

$$Q = g_{\text{nuc}} \sum_p g_p e^{-\frac{\epsilon_p}{kT}} \qquad [1]$$

$$Q' = g_{\text{nuc}} \sum_p g_p \frac{\epsilon_p}{kT} e^{-\frac{\epsilon_p}{kT}} \qquad [2]$$

$$Q'' = g_{\text{nuc}} \sum_p g_p \frac{\epsilon_p}{kT}\left(\frac{\epsilon_p}{kT} - 2\right) e^{-\frac{\epsilon_p}{kT}} \qquad [3]$$

$$g_p = \sum_p^{(p)} g_i$$

The statistical sums for diatomic molecules are of the form

$$Q = g_{\text{nuc}} \sum_l g_l e^{-\frac{\epsilon_l}{kT}} \sum_{v=0}^{v=v\,\max} e^{-\frac{\epsilon_v(l,v)}{kT}} \sum_{J=J\,\min}^{J=J\,\max} (2J+1) e^{-\frac{\epsilon_r(l,v,J)}{kT}} \qquad [4]$$

where ϵ_r, ϵ_v and ϵ_l are the rotational, vibrational and electronic energies of the molecule. In the simplest case, when the resultant electron spin and orbital-momentum projections on the axis joining the nuclei vanish, the rotational energy is given by

$$\epsilon_r = B_v J(J+1) - D_v J^2(J+1)^2 + F_v J^3(J+1)^3 + H_v J^4(J+1)^4 + \ldots \qquad [5]$$

J is the rotational quantum number, which assumes all permissible values up to $J_{\max}(v, l)$. $J_{\max}(v, l)$ is the maximum rotational quantum number at which the molecule is stable.

B_e, D_e, F_e, H_e, α_e, β_e, γ_e and δ_e are constants determined from the analysis of the spectra. The vibrational energy is expressed in the form of the following series

$$\epsilon_v = \omega_0 v - \omega_0 x_0 v^2 + \omega_0 y_0 v^3 + \omega_0 z_0 v^4 + \ldots \qquad [7]$$

where v is the vibrational quantum number, and ω_0, $\omega_0 x_0$, $\omega_0 y_0$ and $\omega_0 z_0$ are spectroscopic constants.

In the calculation of the rotational portion of the statistical sum

$$Q_r = \sum_{J=J\,\min}^{J=J\,\max} (2J+1) e^{-\frac{\epsilon_r}{kT}} \qquad [8]$$

the summation over the rotational quantum numbers is replaced by integation. As a result of this replacement, Q_r is expressed as a series in powers of T with diminishing coefficients. Neglect of the sixth and all other terms of this series does not introduce errors greater than 0.001 per cent in Q_r, 0.008 per cent in Q_r'/T, and 0.3 per cent Q_r''/T^2.

Estimates show that at temperatures above 8000 K a noticeable contribution is made to the statistical sums of the diatomic molecules O_2, N_2, NO, O_2^+, N_2^+ and NO^+ by the energy levels located above the limit of dissociation of the electron ground state of the molecule. In this connection, we took into account in Q_r the finite number of rotational levels. Integration of the rotational portion of the statistical sum was carried out in the limits from $J_{\min}$ to $J_{\max}$. Up to temperatures of 6000–8000 K, we can integrate from $J_{\min}$ to ∞. For molecules made up of identical nuclei (O_2, N_2, O_2^+, N_2^+), we took into account the factor one half in front of the rotational component of the statistical sum. The lower electronic states of the molecules O_2, NO, N_2^+ and O_2^+ have electronic terms that are different from $^1\Sigma$. Therefore, because of the interaction of the spin with K or with the axis, splitting of the rotational levels takes place. Estimates have shown that this splitting, in the temperature interval from 1000 to 12,000 K, can be accounted for by means of a statistical weight for Q_r, calculated under the assumption that there is no splitting, as was indeed done in the calculation of Q_r for all the electronic states. The final formulas for Q_r, Q_r' and Q_r'' are

$$Q_r = b_v T + d_v T^2 + f_v T^3 + h_v T^4 + m_v T^5 - e^{-\frac{hc}{kT}\psi}\{l_v T + p_v T^2 + n_v T^3 + t_v T^4 + \pi_v T^5\}$$

$$Q_r' = b_v T + 2d_v T^2 + 3f_v T^3 + 4h_v T^4 + 5m_v T^5 - e^{-\frac{hc}{kT}\psi}\{(\rho_v+1)l_v T + (\rho_v+2)p_v T^2 + (\rho_v+3)n_v T^3 + (\rho_v+4)t_v T^4 + (p_v+5)\pi_v T^5\}$$

$$Q_r'' = 2d_v T^2 + 6f_v T^3 + 12h_v T^4 + 20m_v T^5 - e^{-\frac{hc}{kT}\psi}\{\rho_v^2 l_v T + (\rho_v^2+2\rho_v+2)p_v T^2 + (\rho_v^2+4\rho_v+6)n_v T^3 + (\rho_v^2+6\rho_v+12)t_v T^4 + (\rho_v^2+8\rho_v+20)\pi_v T^5\} \qquad [8a]$$

where

$$B_v = B_e - \alpha_e\left(v+\frac{1}{2}\right)$$

$$F_v = F_e + \gamma_e\left(v+\frac{1}{2}\right)$$

$$D_v = D_e + \beta_e\left(v+\frac{1}{2}\right)$$

$$H_v = H_e + \delta_e\left(v+\frac{1}{2}\right) \qquad [6]$$

where

$$b_v = \frac{1}{B_v}\frac{k}{hc} \qquad d_v = 2\frac{D_v}{B_v^3}\left(\frac{k}{hc}\right)^2$$

$$f_v = 12\frac{D_v^2}{B_v^5}\left(\frac{k}{hc}\right)^3 \qquad h_v = 120\frac{D_v^3}{B_v^7}\left(\frac{k}{hc}\right)^4$$

$$m_v = 1680\frac{D_v^4}{B_v^9}\left(\frac{k}{hc}\right)^5$$

$$l_v = \left\{\frac{1}{B_v} + 2\frac{D_v}{B_v^3}\psi + 12\frac{D_v^2}{B_v^5}\frac{\psi^2}{2} + 120\frac{D_v^3}{B_v^7}\frac{\psi^3}{6} + 1680\frac{D_v^4}{B_v^9}\frac{\psi^4}{24}\right\}\frac{k}{hc}$$

$$p_v = \left\{2\frac{D_v}{B_v^2} + 12\frac{D_v^2}{B_v^5}\psi + 120\frac{D_v^3}{B_v^7}\frac{\psi^2}{2} + 1680\frac{D_v^4}{B_v^9}\frac{\psi^3}{6^2}\right\}\left(\frac{k}{hc}\right)^2$$

$$h_v = \left\{12\frac{D_v^2}{B_v^5} + 120\frac{D_v^3}{B_v^7}\psi + 1680\frac{D_v^4}{B_v^9}\frac{\psi^2}{2}\right\}\left(\frac{k}{hc}\right)^3$$

$$t_v = \left\{120\frac{D_v^3}{B_v^7} + 1680\frac{D_v^4}{B_v^9}\psi\right\}\left(\frac{k}{hc}\right)^4 \qquad \pi_v = 1680\frac{D_v^4}{B_v^9}\left(\frac{k}{hc}\right)^5$$

$$\psi = B_v J_{max}(J_{max}+1) \qquad \rho_v = \frac{hc}{k}\psi$$

.....[8b]

The vibrational component of the statistical sum

$$Q_v' = \sum_{v=0}^{v=v\ max} e^{-\frac{\epsilon_v}{kT}} Q_r(v) \qquad [9]$$

together with its derivatives, was calculated by direct summation over the entire interval of temperatures from 1000 to 12,000 K over all possible v from 0 to v_{max}. For the vibrational component of the statistical sum and its derivative we used the following formulas

$$Q_v = \sum_{v=0}^{v=v\ max} e^{-\frac{\epsilon_v}{kT}} Q_r$$

$$Q_v' = \sum_{v=0}^{v=v\ max} e^{-\frac{\epsilon_v}{kT}} \left\{\frac{\epsilon_v}{kT} Q_r + Q_r'\right\}$$

$$Q_v'' = \sum_{v=0}^{v=v\ max} e^{-\frac{\epsilon_v}{kT}} \left\{\frac{\epsilon_v}{kT}\left[\left(\frac{\epsilon_v}{kT} - 2\right) Q_r + 2Q_r'\right] + Q_r''\right\}$$

.....[9a]

In the calculation of the electron portion of the statistical sum

$$Q_l = g_{nuc}\sum_l e^{-\frac{\epsilon_l}{kT}} Q_v(l) \qquad [10]$$

we took into account all the known levels located 100,000 cm^{-1} above the ground state of the molecule. The equations for the electronic component of the statistical sum are

$$Q_l = g_{nuc}\sum_l g_l e^{-\frac{\epsilon_l}{kT}}$$

$$Q_l' = g_{nuc}\sum_l g_l e^{-\frac{\epsilon_l}{kT}}\left\{\frac{\epsilon_l}{kT} Q_v + Q_v'\right\}$$

$$Q_l'' = g_{nuc}\sum_l g_l e^{-\frac{\epsilon_l}{kT}}\left\{\frac{\epsilon_l}{kT}\left[\left(\frac{\epsilon_l}{kT} - 2\right) Q_v + 2Q_v'\right] + Q_v''\right\}$$

.....[10a]

2 Spectroscopic Constants Used in Calculation of Statistical Sums

The spectroscopic constants used for the calculation of the atomic and molecular statistical sums are listed in Tables 1 to 7. The sources used in the compilation of this table were essentially in references (1 to 3).[1] We also used the results of later works, which were not included in these collections. The source reference from which the corresponding constants are taken is indicated in each case. The quantities in parentheses were calculated either by solving the wave equation for the given case, or from empirical or semi-empirical formulas. The tables list all the atomic and molecular electronic levels taking into account the calculation of the corresponding statistical sums.

Four, three or two terms of the series of Equation [7] are usually given for spectroscopically investigated electronic states of molecules. The possibility of determining the terms of this series depends on the number of bands that can be observed in the spectra of the corresponding band systems. In those cases where there were not enough spectroscopic data to determine $\omega_0 z_0$ or $\omega_0 l_0$, we did not determine them theoretically. For the NO^+ molecule, we calcu-

[1] Numbers in parentheses indicate References at end of paper.

Table I

ϵ_p, cm^{-1}	g_p	ϵ_p, cm^{-1}	g_p	ϵ_p, cm^{-1}	g_p
		A			
0	1	108700	1	119000	33
93144	5	111700	1	120000	71
93751	3	111800	3	121000	51
94550	1	112100	5	122000	73
95400	3	113500	10	123000	103
104100	2	113000	16	124000	176
105500	7	113700	10	125000	293
105600	5	114100	3	126000	362
106000	8	115000	24	127000	45
107000	1	116700	3	128000	24
107100	3	117000	15		
107300	5	117200	5		
107500	3	118000	12		
		A^+			
0	4	150000	15	190000	16
1432	2	155000	12	192000	8
108723	2	158000	20	193000	10
132000	14	160000	24	195000	50
133000	12	167000	2	196000	26
135000	6	170000	14	199000	30
139000	6	173000	26	200000	35
142200	10	175000	6	205000	14
143000	18	180000	12	209000	4
144700	2	183000	10	213000	10
145700	4	184000	34		
147500	12	186000	24		
149000	18	187000	30		
		O			
0	5	99760	9	123000	14
158,5	3	101150	15	124000	52
226.5	1	102000	8	126000	24
15868	5	102800	29	127000	18
13792	1	103870	9	129000	10
33768	5	105300	48	129800	61
76795	3	106700	57	131000	1
86630	15	107500	48	132000	51
88630	9	108200	96	134000	13
95480	5	108700	48	190000	3
96930	3	113300	15		
97420	45	114000	37		
99090	15	116000	8		
		O^+			
0	4	212700	2	254000	14
26808	6	214200	6	255000	56
26829	4	226800	2	156000	138
40467	6	228700	14	258000	14
120000	12	231200	38	259000	14
166000	10	233000	56	268000	38
185000	12	234000	12	266000	150
189000	6	238700	12	268000	18
195700	2	240400	6	276000	122
203900	2	245900	26	292000	36
207000	30	248200	16		
208400	12	251000	20		
212000	18	253000	28		
		N			
0	4	96800	12	107400	4
19223	6	97800	6	110000	14
19231	4	99660	10	110200	30
28840	6	103700	12	110300	48
83350	12	104200	6	110500	26
86130	2	104600	6	112300	6
86223	4	104700	28	113000	102
88110	6	104900	26	114000	100
88153	4	105000	20	115000	92
88173	2	105100	10	116000	340
93582	2	106500	2		
94800	20	106800	20		
95500	12	107000	12		
		N^+			
0	2	245700	6	334500	10
174,5	4	267200	10	336300	12
57192	2	287600	12	339800	14
57252	4	297000	6	342000	10
57333	6	301090	2	343000	32
101030	10	310000	26	355000	32
131000	2	311700	6	368600	12
145880	2	314200	4	374000	16
146000	4	317600	22	378000	56
186800	4	320800	18	387000	202
203080	10	327000	2		
221300	2	330300	28		
230400	7	332800	22		

lated the quantities $\omega_e x_e$ for all four electronic states and we determined ω_e for the state $^3\Pi$. The constant $\omega_e x_e$ for a known dissociation energy of a given electron state was determined by us under the assumption that the potential energy of the electronic state is described by a Morse function in accordance with the formula

$$\omega_e x_e = (\omega_e^2/4D_e) \qquad [11]$$

1. Molecular nitrogen N_2 — Table 2

$D(N_2)$=78715 cm^{-1}=224984[gcal (15 C)/g-mole (chem)] (references 2 and 6)
$I(N_2)$=125702 cm^{-1}=359283[gcal (15 C)/g-mole (chem)]. From I(N), $D(N_2)$ and $I(N_2^+)$

Name of constant	Electronic state						
	$X^1\Sigma_g^+$	$A^3\Sigma_u^+$	$B^3\Pi_g$	$a'^1\Sigma_u^-$	$a^1\Pi_g$	N	$C^3\Pi_u$
ε_e	0	49756.5	59313.5	60000	68956.6	63959	88984
ω_0	2345.16	1446.46	1719.64	1515.5	1678.959	(1515.5)	2020.00
$\omega_0 x_0$	14.445	13.929	14.47	11.5	13.3181	(11.5)	26.40
$\omega_0 y_0$	0.64958	—0.0261	—	—	—0.95353	(—)	1.158
$\omega_0 z_0$	—0.000509	—0.000614	—	—	—0.002298	(—)	0.5542
B_e	2.010	1.440	1.6380	1.48	1.637	(1.49)	1.8259
α_e	0.01869	0.013	0.0184	0.015	0.0224	(0.015)	0.0197
D_e	$5.8\cdot10^{-6}$	$(5.61\cdot10^{-6})$	$(-5.86\cdot10^{-6})$	$(5.56\cdot10^{-6})$	$(6.14\cdot10^{-6})$	$(5.56\cdot10^{-6})$	$6.0\cdot10^{-6}$
β_e	$-0.001\cdot10^{-6}$	$(-0.154\cdot10^{-6})$	$(-0.0281\cdot10^{-6})$	$(-0.029\cdot10^{6})$	$(0.0645\cdot10^{6})$	$(-0.029\cdot10^{-6})$	$(-0.013\cdot10^{-6})$
ν_m	50	26	30	30	25	30	4
Source reference	(2)	(3)	(2)	(3)	(3)	(3)	(3)

2. Molecular oxygen O_2 — Table 3

$D(O_2)$=41260 cm^{-1}=117930[gcal (15 C)/g-mole (chem)] (reference 7)
$I(O_2)$=38813.7 cm^{-1}=282430[gcal (15 C)/g-mole (chem)]. From I(O), $D(O_2)$ and $D(O_2^+)$

Name of constant	Electronic state						
	$^3\Sigma_g^-$	$^1\Delta_g$	$b\,'^1\Sigma_g^+$	$^1\Sigma_g^-$	$^3\Delta_u$	$A^3\Sigma_u^+$	$B^3\Sigma_u^-$
ε_e	0	7892.39	13120.908	36212.74	—	35780.12	49363.1
ω_0	1568.33	1496.4	1418.7292	633.371	—	758.89	692.08
$\omega_0 x_0$	11.993	12.9	13.9662	17.2056	—	14.635	8.5653
$\omega_0 y_0$	0.0517	—	—0.01075	—0.1205	—	—0.55	—0.37535
$\omega_0 z_0$	—0.00143	—	—	—0.00744	—	—	—
B_e	1.445666	1.4264	1.400416	0.826	—	(0.902)	0.819
α_e	0.015791	0.0171	0.01817	0.02055	—	(0.0245)	0.011
D_e	$4.957\cdot10^{-6}$	4.8652	$5.356\cdot10^{-6}$	$(10.731\cdot10^{-6})$	—	$(3.32\cdot10^{-6})$	$(4.38\cdot10^{-6})$
β_e	$-0.088\cdot10^{-6}$	$-0.0104\cdot10^{-6}$	$-0.077\cdot10^{-6}$	$(0.262\cdot10^{-6})$	—	$(0.96\cdot10^{-6})$	$-0.0784\cdot10^{-6}$
ν_m	36	30	27	13	—	11	21
Source reference	(12)	(13)	(12)	(14)	(14)	(15)	(7)

3. Nitrous oxide NO — Table 4

D(NO)=52477 cm^{-1}=149990 gcal (15 C)/g-mole (chem) (reference 7)
I(NO)=76626.8 cm^{-1}=219015 [gcal (15 C)/g-mole (chem)] (reference 2)

Name of constant	Electronic state					
	$X^2\Pi^1/_2, ^3/_2$	$A^2\Sigma^+$	$B^2\Pi$	$D^2\Sigma^+$	$C^2\Sigma^+$	$E^2\Sigma^+$
ε_e	60.6	44199.2	45440	52817	—	60862.8
ω_0	1889.88	2356.82	1030.15	2304	—	2357.79
$\omega_0 x_0$	13.972	14.48	7.458	23	—	15.87
$\omega_0 \beta_0$	—0.012	—	0.0967	—	—	—
$\omega_0 z_0$	—	—	—	—	—	—
B_e	1.7046	1.9948	1.126	1.9912	—	1.9863
α_e	0.0178	0.0184	0.0152	(0.0243)	—	0.0182
D_e	$5\cdot10^{-6}$	$5.6\cdot10^{-6}$	$2.65\cdot10^{-6}$	$5.8\cdot10^{-6}$	—	$5.6\cdot10^{-6}$
β_e	$0.02\cdot10^{-6}$	$0.02\cdot10^{-6}$	$(0.0405\cdot10^{-6})$	$(-0.063\cdot10^{-6})$	—	$0.02\cdot10^{-6}$
ν_m	38	3	29	25	25	20
Source reference		(8)	(2)	(3)	(3)	(8)

4. Molecular ionized nitrogen, N_2^+ — Table 5

$D(N_2^+)$=70.358 cm^{-1}=201098 gcal (15 C)/g-mole (chem) (reference 9)

Name of constant	Electronic state					
	$X^2\Sigma^+_g$	$(X^2\Sigma^+_g)$	$A^2\Pi$	$B^2\Sigma^+_u$	$(B^2\Sigma^+_u)$	$B'^2\Sigma^+$
ε_e	0	(50470)	9057	25566	(51618)	64547
ω_0	2191.02	(1023.5)	1887.93	2396.22	(1007.5)	2162.8
$\omega_0 x_0$	13.19	(13.24)	14.91	24070	—	—
$\omega_0 y_0$	—0.0303	—	—	—0.6365	—	—
$\omega_0 z^0$	—0.00092	—	—	—0.04949	—	—
B_e	—1.932	(1.315)	1.722	2.083	(1.433)	1.16
α_e	0.02	(0.0192)	0.018	0.0195	(0.0294)	0.05
D_e	$5.75\cdot10^{-6}$	$(7.427\cdot10^{-6})$	$4\cdot10^{-6}$	$(6.15\cdot10^{-6})$	$(13.903\cdot10^{-6})$	$(3.8\cdot10^{-6})$
β_e	$0.29\cdot10^{-6}$	$(-0.0202\cdot10^{-6})$	$(-0.216\cdot10^{-6})$	$(0.216\cdot10^{-6})$	$(0,116\cdot10^{-6})$	$(0.6\cdot10^{-6})$
ν_m	30	37	63	14	37	10
Source reference	(9)	(9)	(10)	(9)	(9)	(3)

We estimated ω_e for $^3\Pi$ from empirical relations. For certain electronic states, owing to interaction with the neighboring ones, it is in general impossible to select a series [7], with a small number of terms, suitable for all the vibration levels. In this case we select two series, one of which corresponds to arrangement of vibrational levels from $v = 0$ to a certain v_k, and the other one from v_{k+1} to v_{max}. This is equivalent to introducing a fictitious electronic state. Such fictitious states are set in parentheses in Tables 1 to 7. The number of spectroscopically investigated vibrational levels for various electronic states is variable and fluctuates from one to several times 10. For the majority of the lowest electronic states usually we investigated a large number of bands, a fact favoring the reliability of calculations based on the spectroscopic data. However, the quantity v_{max} was not determined spectroscopically for the majority of electron states of the molecules O_2, N_2, NO, O_2^+, N_2^+ and NO^+, which were of interest to us. If it is assumed that the arrangement of the vibrational levels above the investigated levels obeys the same law as that of the observed levels, then v_m can be determined from the relation

$$\epsilon_v(v_m) = D_0 \qquad [12]$$

Almost all the v_m listed in Tables 2 to 7 were obtained precisely in this manner. However, Equation [12] had no real positive roots for certain electron states. In such cases v_m was determined from the following considerations. The dissociation energy of any electronic state should be equal to the sum of all the vibrational quanta $\Delta G(v)$ of the given electronic state

$$D_0 = \sum_{v=0}^{v=vm} \Delta G(v) \qquad [12a]$$

In other words, if we plot $\Delta G(v)$ vs. v, then the area bounded by the curve and the coordinate axes should be equal to the dissociation energy of the given electronic state. The solid curve in Fig. 1 corresponds to the investigated values of ΔG for the state $X^2\sum_g^+$ of the molecule N_2^+. If we continue this curve until it intersects the abscissa (dotted curve), then the area under the curve will be found to be less than 70,358 cm^{-1} (dissociation energy of the $X^2\sum_g^+$ state of the N_2^+ molecule). This corresponds to the fact that Equation [12] does not have a satisfactory solution. To obtain an area of 70,358 cm^{-1} under the curve, we make a simple assumption concerning the course of the curve $\Delta G(v)$ above $v = 30$, namely, that $\Delta G(v)$ depends linearly on v, as indicated on the diagram by the dotted line. The constants $\omega_0 x_0$ and ω_0 for the fictitious electronic state were determined from the equations

$$\Delta G = \omega_0 - \omega_0 x_0$$
$$D_0 = \omega_0^2/4\omega_0 x_0 \qquad [12b]$$

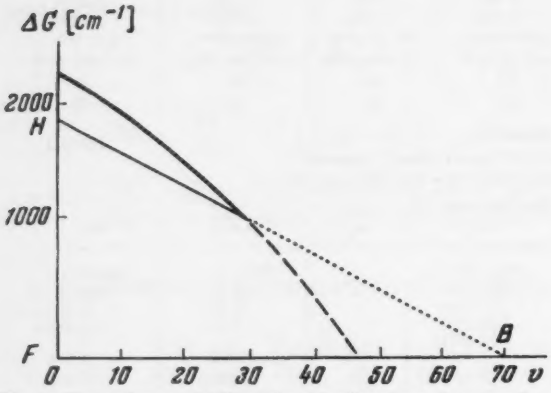

Fig. 1 Dependence of ΔG on the vibrational quantum number for the state $X^2\Sigma$ of the molecule N_2^+

Table 6

5. Molecular ionized oxygen O_2

$D(O_2^+)$=52283 cm^{-1}=149.436 gcal (15 C)/g-mole (chem) (reference 2)

Name of constant	Electronic state			
	$X^2\Pi_g$	$a^4\Pi_g$	$A^2\Pi_u$	$b^4\Sigma^-$
ϵ_e	97.5	31900	383.9	48567
ω_e	1859.87	1025.30	888.6	1179.68
$\omega_e x_e$	16.53	1039	13.4	17.08
$\omega_e y_e$	—	—	—	—
$\omega_e z_e$	—	—	—	—
B_e	1.6722	1.10466	1.0617	1.28729
α_e	0.01984	0.01575	0.01908	0.02206
D_e	$(6.84 \cdot 10^{-6})$	$4.88 \cdot 10^{-6}$	$(5.33 \cdot 10^{-6})$	$5.81 \cdot 10^{-6}$
β_e	$(-0.0356 \cdot 10^{-6})$	$-0.095 \cdot 10^{-6}$	$(-0.0955 \cdot 10^{-6})$	$-0.0185 \cdot 10^{-6}$
v_m	53	27	25	27
Source reference	[2]	[2]	[2]	[2]

Table 7

Ionized nitrous oxide NO^+

$D(NO^+)$=85686.9 cm^{-1}=244911 gcal (15 C)/g-mole (chem).
From I(O), D(NO) and I(NO)

Name of constant	Electronic state			
	$(^1\Sigma^+)$	$(^3\Pi)$	$(^3\Sigma^+)$	$(^1\Pi)$
ϵ_e	0	37000	57000	71000
ω_0	(2334)	(1636)	(1322.4)	(1265)
$\omega_0 x_0$	(16.1)	(14)	(15.6)	(12)
$\omega_0 y_0$	—	—	—	—
$\omega_0 z_0$	—	—	—	—
B_0	(1.90)	(1.54)	(1.35)	(1.31)
α_0	(0.0181)	(0.174)	(0.0196)	(0.0163)
D_0	$(5.4 \cdot 10^{-6})$	$(5.3 \cdot 10^{-6})$	$(5.5 \cdot 10^{-6})$	$(5.5 \cdot 10^{-6})$
β_0	—	—	—	—
v_m	(73)	(59)	(42)	(25)

Table 8

	Name of quantity	Numerical value
1	Velocity of light, km/sec	$c = 299{,}792 \pm 0.8$
2	Number of molecules per g-mole	
	physical (1/g-mole)	$N_{ph} = (6.02472 \pm 0.00036) \cdot 10^{23}$
	chemical	$N_{ch} = (6.02308 \pm 0.00033) \cdot 10^{23}$
3	Planck's constant, erg-sec	$h = (6.6252 \pm 0.0005) \cdot 10^{-27}$
4	Boltzmann's constant, erg/deg	$k = (1.38042 \pm 0.00010) \cdot 10^{-16}$
5	Electron mass, g	$m = (9.1085 \pm 0.0006) \cdot 10^{-28}$
6	$\frac{1}{16}$ of the mass of the oxygen atom, g	$16\ g/(16\ N_{ch}) = 1.66028 \cdot 10^{-24}$
7	Gas constant, erg/g-mole-deg	$R = (8.31662 \pm 0.00038) \cdot 10^7$ erg/mole-deg
		$R_{ch} = (8.31436 \pm 0.00034) \cdot 10^7$ erg/mole-deg
		$R_{ch} = 1.98647 \pm 0.000008$ g-cal (15 C)
8	Gram-calorie, 15 C	1 g-cal (15 C) = 4.1855 abs joule
9	Atmosphere, physical	$1\ atm = 1.01325 \cdot 10^6$ dyne/cm^2

Relations between energy units

	erg	ev	cm^{-1}
erg	1	$0.624192 \cdot 10^{12}$	$5.0347 \cdot 10^{15}$
ev	$1.60207 \cdot 10^{-12}$	1	8.06598
cm^{-1}	$1.98620 \cdot 10^{-16}$	...	1

$$\frac{hc}{k} = 1.43883 \text{ cm-deg}$$

where

ΔG = height of the first vibrational level above the zero level (HF on the diagram)
D_0 = area of the triangle FBH

Not more than four rotational constants are usually determined spectroscopically: B_e, α_e, D_e and β_e. Where there were no data on these constants, they were calculated from the following equations

$$B_e = \frac{h}{8\pi^2 c\mu r_e^2} \qquad [13]$$

$$D_e = \frac{4B_e^3}{\omega_e^2} \qquad [14]$$

$$\alpha_e = \frac{\sqrt{\omega_e x_e B_e^3}}{\omega_e} - \frac{6B_e^2}{\omega_e} \qquad [15]$$

$$\beta_e = -D_e\left(\frac{8\omega_e x_e}{\omega_e} - \frac{5\alpha_e}{B_e} - \frac{\alpha_e^2\omega_e}{24B_e^3}\right) \qquad [16]$$

In most cases the formulas give the correct order of the constants. The rotational constants B_e and D_e cannot always be well represented by Equation [6]. Since the deviations from the ordinary dependence of B_v and D_v on v correspond to the same deviations for the vibrational constants, the introduction of the fictitious electronic states results simultaneously in convenient methods of calculating both the rotational and vibrational parts of the statistical sums.

As already mentioned, the rotational parts of the statistical sums of the molecules were calculated in this investigation for a finite number of values of J. The maximum value of J at which the molecule is still stable was estimated in the following manner.

The potential-energy function of the rotating molecule can be represented by

$$U(r) = D_e(1 - e^{-2\beta\xi})^2 + \frac{h}{8\pi^2 c\mu r^2} J(J+1) \qquad [16a]$$

where

$\xi = (r - r_e)/r_e$
r_e = equilibrium state between the nuclei

and

$$\beta = \frac{\omega_e}{4(B_e D_e)^{1/2}}$$

$$D_e = D_0 + \frac{\omega_e}{2} - \frac{\omega_e x_e}{2} + \ldots$$

$$\ldots\ldots\ldots\ldots\ldots\ldots\ldots\ldots\ldots\ldots\ldots\ldots [16b]$$

$U(r)$ has a maximum located above the dissociation limit. This maximum forms a potential barrier, beyond which there exist stable molecular states with energies greater than the dissociation energy. The position of the maximum for each value of $J(J+1)$ can be found from the condition

$$\frac{\partial U(r)}{\partial r} = 0 \qquad [16c]$$

which after transformation reduces to

$$J(J+1) = \frac{8\pi^2 c}{h}\mu D_e \frac{2\beta}{r_1} r^3(1 - e^{-2\beta\xi})e^{-2\beta\xi} \qquad [17]$$

From the value of r_{max} thus obtained for the given $J(J+1)$ we can calculate

$$U_m = D_e(1 - e^{-2\beta r_m - r_e/r_e}) + \frac{1}{8\pi^2 c\mu r_m^2} J(J+1) \qquad [17a]$$

and from

$$U_m = \omega_e\left(v + \frac{1}{2}\right) - \omega_e x_e\left(v + \frac{1}{2}\right)^2 + \ldots + B_v J(J+1) - D_v J^2(J+1)^2 + \ldots \qquad [18]$$

we can obtain the value of $J(J+1)$ that corresponds to the given v. Equations [17 and 18] were solved graphically.

The scantiest data on spectroscopic constants were those for NO^+.

Not one of the electronic states of NO^+ has yet been investigated spectroscopically. There are only data on the location of the first four electronic states, obtained from a spectroscopic investigation of the Rydberg series of NO^+. For three out of these four electronic states, the existence of which we have verified from the convergence of the Rydberg series of NO^+, we know the values of ω_e, also obtained from spectra of NO. For the lower electronic state we know also the equilibrium internuclear distance

$$r_e = 1.073 \text{ Å} \qquad [18a]$$

The method of electronic impact was used to determine the ionization energy of NO, found to be 9.5 ev. From this, using the equation

$$I(NO) + D(NO^+) = D(NO) + I(O) \qquad [18b]$$

we can obtain

$$D(NO^+) = D(NO) + I(O) - I(NO) = 10.5 \text{ ev} \qquad [18c]$$

All this disjointed information was gathered together by Rosen (3). The calculation of the statistical sums of NO^+ on the basis of such information may lead to an error, due to lack of knowledge of the electronic terms, by factors of two, three, or four. We therefore attempted first to determine the types of electronic terms of the known four electronic states. One method of determining the possible types of electronic terms is to construct the electronic configurations by successive addition of the electrons. Such a compilation of the electronic configurations for the molecules can be carried out in two limiting cases; first, when the distance between nuclei is small compared with the distance between the electron and the nucleus, and second when the distance between nuclei is large compared with the distances between the electrons and the nucleus.

For the atoms N and O^+ "joined" together ($r_e \to 0$), we would obtain the following sequence of filling of the electron shells

$$(1s\sigma)^2(2s\sigma)^2(2p\sigma)^2(2p\pi)^4(3s\sigma)^2(3p\sigma)^2 \qquad [18d]$$

For the N and O^+ atoms far apart we would obtain the following sequence of filling of the electron shells

$$(\sigma 1s_O)^2(\sigma 1s_N)^2(\sigma 2s_O)^2(\sigma 2s_N)^2(\sigma 2p_O)^2(\pi 2p_O)^4 \qquad [18e]$$

The order of arrangement of the electrons in an actual NO^+ molecule will be intermediate between the system in which the internuclear distance approaches zero, and in a system in which it goes to infinity. The NO^+ system is isoelectronic relative to the molecules N_2 and CO, which have 14 electrons each. For the lower electronic state of $CO(^1\Sigma^+)$ the value of r_e is 1.1289 Å, and for $N_2(^1\Sigma^+)$ it equals 1.094 Å. For the lower electronic state of NO^+, as already mentioned, $r_e = 1.073$ Å. This gives us the right to assume that the lower electronic configuration of NO^+ will coincide with the lower electronic configurations of CO and N_2

$$KK(\sigma 2s_O)^2(\sigma 2s_N)^2(\pi 2p_O)^4(\sigma 2p_N)^2 \qquad [18f]$$

An important argument in favor of such a lower electronic configuration of NO^+ is the fact that it corresponds to the removal of one upper electron $\pi 2p_N$ from the NO molecule,

which has a lower electronic configuration

$$KK(\sigma 2s_O)^2(\sigma 2s_N)^2(\pi 2p_O)^4(\sigma 2p_N)^2(\pi 2p_N) \qquad [18g]$$

This method of determining the electronic configuration (we have in mind the method of removing the electron from the electronic ground state of the un-ionized molecule) is found to be valid in examples of other molecules (for example, determination of the electronic states of N_2^+).

The first excited electronic configuration of NO^+ may be, apparently

$$KK(\sigma 2s_O)^2(\sigma 2s_N)^2(\pi 2p_O)^4(\sigma 2p_O)(\pi 2p_N) \qquad [18h]$$

or

$$KK(\sigma 2s_O)^2(\sigma 2s_N)^2(\pi 2p_O)^4(\sigma 2p_O)(\sigma 2p_N) \qquad [18i]$$

Removal of one of the $\sigma 2p_O$ electrons of NO results in the electronic configuration

$$KK(\sigma 2s_O)^2(\sigma 2s_N)^2(\pi 2p_O)^4(\sigma 2p_O)(\pi 2p_N) \qquad [18j]$$

which coincides with the first of the possible excited electronic configurations of NO^+. One can therefore assume the electronic configuration

$$KK(\sigma 2s_O)^2(\sigma 2s_N)^2(\pi 2p_O)^4(\sigma 2p)(\pi 2p_N) \qquad [18k]$$

to be the first excited electronic configuration of NO^+.

The next excited electronic configuration of NO^+ may be

$$KK(\sigma 2s_O)^2(\sigma 2s_N)^2(\pi 2p_O)^4(\sigma 2p_O)(\sigma 2p_N) \qquad \text{I}$$

or

$$KK(\sigma 2s_O)^2(\sigma 2s_O)^2(\pi 2p_O)^2(\sigma 2p_O)^2(\pi 2p_N) \qquad \text{II}$$

or

$$KK(\sigma 2s_O)^2(\sigma 2s_N)^2(\pi 2p_O)^2(\sigma 2p_O)^2(\sigma 2p_N) \qquad \text{III}$$

Removal of the $(\pi 2p_O)$ electron of the NO molecule leads to an electron configuration

$$KK(\sigma 2s_O)^2(\sigma 2s_N)^2(\pi 2p_O)^2(\sigma 2p_O)^2(\pi 2p_N)$$

which coincides with the second of the possible excited electronic configurations of NO^+ from the series (I, II, III). We thus conclude that the possible electron configurations of NO^+ are:

Normal state

$$KK(\sigma 2s_O)^2(\sigma 2s_N)^2(\pi 2p_O)^4(\sigma 2p_O)^2$$

First excitation

$$KK(\sigma 2s_O)^2(\sigma 2s_N)^2(\pi 2p_O)^4(\sigma 2p_O)(\pi 2p_N)$$

Second excitation

$$KK(\sigma 2s_O)^2(\sigma 2s_N)^2(\pi 2p_O)^2(\sigma 2p_O)^2(\pi 2p_N)$$

Corresponding to these electronic configurations are the following terms:

Normal state $^1\sum^+$
First excitation $^1\Pi$; $^3\Pi$
Second excitation $^1\sum^+$; $^1\sum^-$; $^1\Delta$; $^3\sum^+$; $^3\sum^-$; $^3\Delta$

The possible electronic terms can also be obtained from the products of the dissociation of the NO^+ molecule, by using the Wigner-Witmer moment-summation rules. In Table 9 we list the possible products of dissociation of NO^+, the possible electronic terms corresponding to them, and the relative arrangement of the limits of dissociation.

Comparing Table 9 with the possible terms obtained from the electronic configurations, we can state that the term of the normal state of NO^+ is the term $^1\sum^+$. Of the remaining terms of the first limit of dissociation

$$^3\sum^+ \quad ^5\sum^+ \quad ^7\sum^+$$

Table 9

Dissociation products	Possible electrical terms	Height of the dissociation limits for various products above the limit of the lower electronic state, cm^{-1}
$N(^4S) + O^+(^4S)$	$^1; ^3; ^5; ^7\Sigma^+$	0
$N^+(^3P) + O(^3P)$	$^1; ^3; ^5\Sigma^+$ (2); $^1; ^3; ^5\Sigma^-$; $^1; ^3; ^5\Pi$ (2); $^1; ^3; ^5\Delta$	7508.3
$N(^2P) + O^+(^4S)$	$^3; ^5\Sigma^+$; $^3; ^5\Pi$; $^3; ^5\Delta$	19223
$N^+(^3P) + O(^1D)$	$^3\Sigma^-$ (2); $^3\Sigma^+$; $^3\Pi$ (3); $^3\Delta$ (2); $^3\Phi$	23376

the only stable one is apparently $^3\sum^+$, since it has only one pair of uncompensated spins. The terms $^5\sum^+$ and $^7\sum^+$, as in the case of the N_2 molecule, are unstable, since the number of uncompensated spins predominates in them over the number of compensated spins. We are led to the same result also by the fact that the terms $^5\sum^+$ and $^7\sum^+$ are not included among the terms obtained on the basis of comparison of the electronic configurations. The term $^3\sum^+$ is encountered in Table 9 in all four cases. However, to satisfy the rule of noncrossing of the electronic terms, it is necessary to assume that term $^3\sum^+$ of the second excited electronic state has dissociation products

$$N(^4S) + O^+(^4S)$$

The term of the first excited electronic state $^3\Pi$ is encountered in Table 9 for the dissociation products

$$N^+(^3P) + O(^3P)$$
$$N(^2D) + O^+(^4S)$$
$$N^+(^3P) + O(^1E)$$

Using the noncrossing rule, it can be said that $^3\Pi$ has dissociation products $N^+(^3P) + O(^3P)$. The same dissociation products are possessed, apparently, also by the term $^1\Pi$, since it is not encountered in any of the rows of Table 9 (with the exception of the second one).

We can thus apparently state the following. Located far above the ground state $^1\sum^+$ of the NO^+ molecule are the terms $^1\Pi$, $^3\Pi$ and $^3\sum^+$, which are relatively close to each other. This is connected with the fact that the orbital

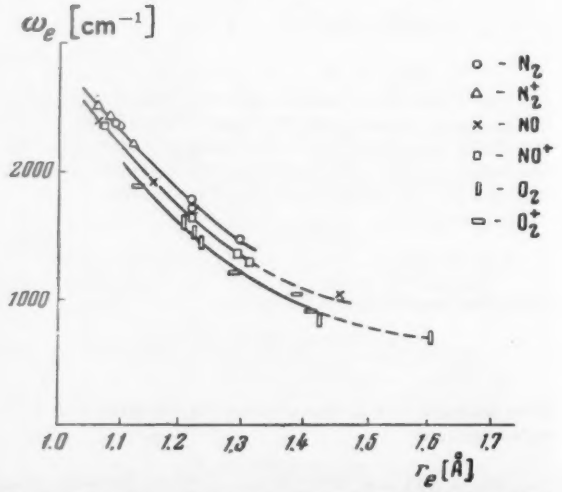

Fig. 2 Dependence of r_e on ω_e for N_2, N_2^+, NO, NO^+, O_2 and O_2^+

$(\pi^2 P_N)$ is quite far above the closed electronic configuration of NO^+. The orbitals $\sigma 2P_O$ and $\pi 2P_O$, from which the terms $^1\Pi$, $^3\Pi$ and $^3\Sigma^+$ are obtained, lie close to each other. Using the Hund rule, by which the state with the greatest multiplicity lies below the remaining ones, we can say that $^3\Pi$ lies below $^1\Pi$. The state $^3\Sigma^+$ is apparently located above $^3\Pi$. It cannot be located below $^3\Pi$, since it is obtained by transfer of a deeper electron from the orbital $\pi 2P_O$ to the orbital $\pi 2P_N$, whereas $^3\Pi$ is obtained by transfer of an electron from the orbital $\sigma^2 P_O$ to the orbital $\pi 2P_N$. This is supported also by the fact that r_e for NO is less than r_e for CO for the lower electronic state; i.e., the molecule NO is closer than CO to the limiting case $r_e \to 0$, and with this the orbital $\sigma 2P_O$ becomes more and more remote from $\pi 2P_O$. The term $^1\Pi$ is apparently located above $^3\Pi$. The only proof in favor of such a relative placement of $^3\Sigma^+$ and $^1\Pi$ is the analogous placement of the states $^3\Sigma^+$ and $^1\Pi$ in the isoelectronic molecules CO and N_2. It must also be noted that the states $^3\Sigma^+$ and $^1\Pi$ are high (respectively 57,000 and 71,000 cm^{-1}), and an error in the choice of the term results in either a factor 3 or a factor 2 in front of the statistical sum of the electronic state with $T = 57{,}000\ cm^{-1}$.

To calculate the rotational part of the statistical sum it is necessary to have at least values of r_e from which to calculate the quantity B_e. For NO^+, we know r_e for the state $^1\Sigma^+$. An estimate of the values of r_e for the three other states was made from empirical laws. For the molecules N_2, N_2^+, O_2, O_2^+ and NO we noted the following regularity. The dependence of r_e on ω_e for the electronic states located not more than 70,000 cm^{-1} above the ground state, is a relatively smooth descending curve. With this, all the values of r_e fall on one curve for N_2 and N_2^+, and on another parallel curve for O_2 and O_2^+. The curve for NO lies between the N_2, N_2^+ and O_2, O_2^+ curves. One known value of r_e for NO fits satisfactorily on the curve for NO. From the curve for NO we determined all the missing values of r_e for NO^+. Fig. 2 shows all the curves and points from which the values of r_e for NO^+ were taken.

3 Effect of Ionization, Coulomb Interaction and Degeneracy of Electron Gas on Values of Thermodynamic Functions

We shall show below that it is possible to neglect the Coulomb interaction between the charged particles when estimating the degree of ionization. Let us denote by N_0, N_1, $N_2, \ldots, N_n, \ldots, N_m$ the number of neutral, singly-, doubly-, . . . , n-fold ionized atoms per gram-mole of the gas; we denote by N the total number of atoms in a gram-mole of gas

$$N = N_0 + N_1 + N_2 + \ldots + N_n + \ldots + N_m$$

by N_e the number of electrons in a gram-mole of gas, and by

$$\alpha_0 = \frac{N_0}{N} \qquad \alpha_1 = \frac{N_1}{N} \ldots \alpha_n = \frac{N_n}{N} \ldots \alpha_m = \frac{N_m}{N}$$

The ionization process can be considered as a system of chemical reactions

$$A^+ + e \rightleftarrows A + I(A) \tag{1}$$

$$A^{++} + e \rightleftarrows A^+ + I(A^+) \tag{2}$$

$$A^{n(+)} + e \rightleftarrows A^{(n-1)(+)} + I[A^{(n-1)(+)}] \tag{n}$$

$$A^{m(+)} + e \rightleftarrows A^{(m-1)(+)} + I[A^{(m-1)(+)}] \tag{m}$$

The condition of thermodynamic equilibrium for such a system of reactions is expressed in the form of a system of algebraic equations

$$\frac{C_n C}{C_{n-1}} = \frac{K_p^{(n)}}{p} \qquad (n = 1, 2 \ldots m)$$

where $C_0, C_1, \ldots, C_n, \ldots, C_m$ are concentrations of the neutral, singly-, doubly-, and m-fold ionized atoms in a gram-mole of gas and

C = concentration of the electrons
$K_p^{(m)}$ = equilibrium constants for the corresponding reaction, depending on the potentials of the ionization and the temperature
p = pressure

and

$$C = N_e/(N + N_e)$$

$$C_0 = N_0/(N + N_e)$$

$$\ldots C_n = N_n/(N + N_e)$$

$$\ldots C_m = N_m/(N + N_e)$$

The m equations of equilibrium and the $m + 1$ unknown must be supplemented by the condition

$$1 = C_0 + C_1 + \ldots + C_4 + \ldots + C_m + C$$

and the law of conservation of charge

$$N_e = N_1 + 2N_2 + \ldots + nN_n + \ldots + mN_m$$

which expressed in terms of the concentrations becomes

$$C = C_1 + 2C_2 + \ldots + nC_n + \ldots + mC_m$$

Transforming from concentrations to degrees of ionization, $\alpha_0, \alpha_1, \ldots, \alpha_m$, we obtain the following system of $m + 1$ equations for $m + 1$ unknowns.

$$\frac{\alpha_n(\alpha_1 + 2\alpha_2 + \ldots + n\alpha_n \ldots + m\alpha_m)}{(1 + \alpha_1 + 2\alpha_2 + \ldots + n\alpha_n + \ldots + m\alpha_m)\alpha_{n-1}} = \frac{K_p^{(n)}}{p}$$

$$n = 1, 2 \ldots m$$

$$\alpha_0 + \alpha_1 + \ldots + \alpha_n + \ldots + \alpha_m = 1$$

A calculation of the equilibrium constants shows that usually

$$K_p^{(n)} \gg K_p^{(n+1)}$$

and the ionization process proceeds, therefore, in steps as the temperature is increased. First the gas is practically all singly ionized, then it is all doubly ionized, and so on. With such an ionization process, direct calculations show that the system of $m + 1$ equations for $\alpha_0, \alpha_1, \ldots, \alpha_n, \ldots \alpha_m$ becomes considerably simpler. When the $(n - 1)$th degree of ionization is complete and the nth degree of ionization begins, the following relations hold

$$\alpha_n + \alpha_{n-1} = 1$$
$$\alpha_{n+1} = \alpha_{n+2} = \alpha_{n+3} = \ldots = \alpha_m = 0$$
$$\alpha_{n-2} = \alpha_{n-3} = \ldots = \alpha_0 = 0$$

With this, the $(m + 1)$th equation for α becomes a system of two equations for α_{n-1} and α_n

$$\frac{\alpha_n[(n-1)\alpha_{n-1} + n\alpha_n]}{[1 + (n-1)\alpha_{n-1} + n\alpha_n](1 - \alpha_n)} = \frac{K_p^{(n)}}{p}$$

$$\alpha_{n-1} + \alpha_n = 1$$

After transforming, we obtain

$$\alpha_n = -\frac{n-1}{2} + \sqrt{\left(\frac{n-1}{2}\right)^2 + \frac{nK_p^{(n)}}{p + K_p^{(n)}}}$$

$$\alpha_{n-1} = 1 - \alpha_n$$

When $n = 1$, the expression obtained goes into the well-known Saha formula

$$\alpha_1 = \frac{1}{\sqrt{1 + (p/K_p^{(1)})}}$$

Table 10 gives the results of the estimates for α_0, α_1 and α_2. The estimates were made for nitrogen. The ionization potentials of N, O and A as well as the ionization potentials of N^+, O^+ and A^+ are approximately equal. Therefore Table 10 is suitable also for estimating the ionization of O and A.

The deviation of the gas from an ideal gas, due to Coulomb interaction, is characterized in the Debye-Huckel approximation by a correction term in the equation of state of the ionized gas

$$p = \frac{kT}{V}\sum_n N_n - \frac{e^3}{3V^{3/2}}\sqrt{\frac{\pi}{kT}}\left(\sum_n N_n z_n^2\right)^{3/2}$$

where

z_n = positive or negative numbers, characterizing the charge of the corresponding ion

N_n = number of particles of the nth sort in a gram-mole of gas; the index n is not connected with the multiplicity of ionization

The results of the calculations of the corrections are listed in Table 11.

It is seen from Table 11 that up to temperatures of approximately 12,000 to 14,000 K one can neglect the Coulomb interaction in the pressure interval from 0.001 to 1000 atm. The degree of degeneracy of the electron gas is characterized by the parameter

$$D = \frac{h^3 n_0}{2(2\pi mkT)^{3/2}}$$

where n_0 is the electron density.

Table 10

P, atm	0.001		0.01		0.1		1		10		100		300		1000	
α % / T °K	α_1	α_2	α_1	α_2	α_1	α_2	α_1	α_2	α_1	α_2	α_1	α_2	α_1	α_2	α_1	α_2
6000	0.16	0														
7000	1.4	0														
12000	97	0	78	0	36	0	12		4							
14000	100	0	97	0	78	0	37		12							
15000	99	1	100	0	95	0										
18000	86	14	98	2	100	0										
20000	45	55	88	12	99	1	95.6	0			65	35	86	14	99	1
22000	13	87	57	43	92	8	99	1	100	0						
24000	3	97	16	84	67	33	96	4	99.5	0.5	38	62	66.5	33.5	75.6	24.4

Table 11

T	p	Δ p	$\frac{\Delta p}{p}$
12 000	0.001	$0.7 \cdot 10^{-6}$	0.07%
14 000	0.01	$13.6 \cdot 10^{-6}$	0.14%

Table 12

	c		c		c
N_2	0	Ar	0	N_2^+	359 283
O_2	0	N^+	447 889	O_2^+	282 430
NO	21 467	O^+	372 901	NO^+	219 015
N	112 492	Ar^+	363 307		
O	58 965	e^-	0		

At $T = 25{,}000$ K and $p = 1000$ atm we have $D = 0.003 \ll 1$; i.e., we can neglect the degeneracy of the electron gas.

4 Formulas for Calculation of Enthalpy, Specific Heat and Equilibrium Constants in Temperature Interval from 1000 to 12,000 K

It was shown in Section 3 that at these temperatures the gas can be considered ideal, and therefore the formulas for the calculation of the enthalpy and heat content have the form

$$H = RT\left(\frac{5}{2} + \frac{Q'}{Q}\right) + C$$

$$C_p = R\left[\frac{5}{2} + 2\frac{Q'}{Q} + \frac{Q''}{Q} - \left(\frac{Q'}{Q}\right)^2\right]$$

where R is the gas constant, and the values of the constant C are given in Table 12, in g-cal (15 C)/g-mole (chem).

The formulas for the equilibrium constants are of the form:

For the reaction $2N \rightleftarrows N_2 + D(N_2)$

$$K_p = 0.474542T^{4/3}\frac{Q_N^2}{Q_{N_2}}e^{-113{,}257/T}\ \text{atm}$$

For the reaction $2O \rightleftarrows O_2 + D(O_2)$

$$K_p = 0.579281T^{3/2}\frac{Q_O^2}{Q_{O_2}}e^{-59{,}366/T}\ \text{atm}$$

For the reaction $N + O \rightleftarrows NO + D(NO)$

$$K_p = 0.522569T^{3/2}\frac{Q_N Q_O}{Q_{NO}}e^{-75{,}505/T}\ \text{atm}$$

For the reaction of ionization $A^+ + e \rightleftarrows A + I(A)$

$$K_p = 6.57936 \cdot 10^{-7}\,T^{3/2}\frac{Q_{A^+}}{Q_A}e^{-I(A)/T}\ \text{atm}$$

where

$I(N)$ = 168,840 deg
$I(O)$ = 157,036 deg
$I(A)$ = 182,890 deg
$I(N_2)$ = 180,864 deg
$I(O_2)$ = 142,176 deg
$I(NO)$ = 110,253 deg

5 Solution of Equations of Chemical Equilibrium of Ideal Gas Systems

For a thermodynamic analysis of reacting gas systems it is necessary to calculate first the composition of these systems. The principal solution of this problem is known. However, in the case of a large number of reactions and components, a direct solution of the corresponding equations leads to cumbersome derivations which are difficult to visualize.

In this section of the article we discuss briefly a method of symmetrizing the equations of chemical equilibrium with and without allowance for ionization

It is known that the closed system of equations of chemical equilibrium (ECE) of an ideal gas system consisting of non-ionized[2] components, containing a different types of atoms, consists of one equation of Dalton's law (EDL), $a - 1$ equations of material balance (EMB), and $r = k - a$ equations using the law of mass action (LMA). Here r is the number of reactions that proceed in this system.

[2] The case of ionized components will be considered later.

We introduce the symbols:

K_i = component i ($i = 1, \ldots, k$)
A_m = atom m ($m = 1, \ldots, a$)
n_{im} = number of A_m in the molecule K_i
ν_{si} = stoichiometric coefficient of K_i in the reaction s ($s = 1, \ldots, r$)

The molecule K_i has the form $\sum_{m=1}^{a} n_{im}A_m$, while the reaction $s - \sum_{i=1}^{k} \nu_{si}K_i = 0$. The ECE have the form

$$\sum_{i=1}^{k} x_i = 1 \qquad \text{(EDL)} \qquad [19a]$$

$$\sum_{i=1}^{k} n_{im}x_i \Big/ \sum_{i=1}^{k} n_{i1}x_i = p_{m1} \qquad \text{(EMB)} \qquad [19b]$$

$$K_{p,s+1}p^{-\nu_s} = \prod_{i=1}^{k} x_i^{\nu_{si}} \qquad \text{(LMA)} \qquad [19c]$$

where

p_{m1} = constant
$p_{11} = 1$

The physically obvious uniqueness of the solution of the ECE was proved in (15).

Equation [19] is difficult to solve because of the nonlinearity of Equation [19c] and the asymmetry of Equations [19a and 19b].

The principal numerical methods used to solve the ECE are the iteration method and the Newton-Rafson method. The need for using numerical methods in solving Equation [19] arises from the nonlinearity of Equation [19c]. We iterate here the a components whose content predominates in the region of the p-T diagram where the solution of Equation [19] is sought (we have in mind here the values of x_i). Different regions of the p-T diagram have different sets of such components.

We shall henceforth segregate the set of the so-called predominating components, the number of which equals the number of various types of atoms, i.e., a. This set is assumed ordered in such a way that the mth component of the set has the maximum content of the mth type of atom, compared with all other components. Under this definition, this set may contain components the absolute content of which is small. We shall assume that the predominating components are the first a components from among a total of k components. The asymmetry of [19a and 19b] is removed by solving them with respect to the predominating components, i.e., by obtaining symmetrical equations for the concentrations of the predominating component (EPC). For this purpose we introduce the concentration of the predominating components x_m^0 in the absence of the remaining components, where x_m^0 are determined from [19a] or [19b]:

$$\sum_{m=1}^{a} x_m^0 = 1 \qquad \frac{n_{mm}x_m^0}{n_{i1}x_1^0} = p_{m1} \qquad (p_{1i} = 1) \qquad [19d]$$

From this, obviously

$$x_m^0 = \frac{p_{m1}}{n_{mm}} \Big/ \sum_{m=1}^{a} \frac{p_{m1}}{n_{mm}} \qquad [20]$$

We furthermore introduce

$$\Phi_0 = \sum_{l=a+1}^{k} x_l \qquad [21a]$$

$$n_{mm}\Phi_m = \sum_{i=1}^{k} n_{im}x_i - n_{mm}x_m \qquad [21b]$$

In view of the foregoing definition of the predominating components, $n_{mm} \neq 0$. Then [19a and 19b] assume the form

$$\sum_{m=1}^{a} x_m = 1 - \Phi_0$$

$$\frac{x_m + \Phi_m}{x_l + \Phi_l} = \frac{x_m^0}{x_1^0} \qquad [21c]$$

From this we readily obtain the EPC that are equivalent to the EDL and the EMI

$$x_m = x_m^0\Phi - \Phi_m \qquad [22a]$$

where

$$\Phi = 1 + \sum_{m=1}^{a} \Phi_m - \Phi_0 = 1 + \sum_{i=1}^{k} x_i \left(\sum_{m=1}^{a} \frac{n_{im}}{n_{mm}} - 1 \right) \qquad [22b]$$

The EPC becomes simple if each K_m consists of only A_m. Then $n_{lm} = 0$ ($l \neq m$; $l, m = 1, \ldots, a$) and Equations [21b and 22b] become

$$n_{mm}\Phi_m = \sum_{l=a+1}^{k} n_{lm}x_l \qquad [21b']$$

$$\Phi = 1 + \sum_{m=1}^{a} \Phi_m - \Phi_0 = 1 + \sum_{l=a+1}^{k} x_i \left(\sum_{m=1}^{a} \frac{n_{im}}{n_{mm}} - 1 \right) \qquad [22b']$$

In this case the EPC express the concentrations of the predominating components in terms of the concentrations of the remaining components. Since in most applications the LMA make it possible to express the concentrations of the remaining components in terms of the concentrations of the predominating components, the systems [22a and 19c] are suitable for generalized iteration. We note that it is always possible, by combining Equations [19c], to recast the LMA in the most symmetrical form, which permits a simple expression of the remaining components in the term of the predominating ones.

The calculation of the iterations, which is known to be purely algebraic, is simple, but since the iterations converge only in the centers of the regions where the components predominate on the p-T diagram, their application is limited in character. The Newton-Rafson method is much more promising.

The principal advantage of this method is that the region of its applicability goes far beyond the boundaries of that region of the p-T diagram where the components, relative to which the EPC are solved, predominate. This is connected with the differential character of the method. The amount of calculation necessitated by this method is considerably less than that involved in simple calculations based on the EDL, ENI and the unreduced LMA, thanks to the symmetry of the ETC and of the reduced LMA, provided the components are suitably numbered and the computation program is suitably detailed. Finally, the Newton-Rafson method gives information necessary for the calculation of the specific heats, the velocity of sound and other thermodynamic functions of the reacting gas systems in the equilibrium state.

We shall detail in the following a program for the calculation of the ionizations of arbitrary orders of all k components. Bearing in mind that the composition is independent of the specific choice of the complete system of independent reactions, we can write the equations of the ionization equilibrium, with allowance for n-fold ionization, as

$$\frac{x_{k+1}x_e}{x_1} = \frac{1}{p}K_{p,\,k+1} \ldots \frac{x_{nk+1}x_e^n}{x_1} = \frac{1}{p^n}K_{p,\,nk+1}$$

$$\frac{x_{2k}x_e}{x_k} = \frac{1}{p}K_{p,\,2k} \ldots \frac{x_{(n+1)k}x_e^n}{x_k} = \frac{1}{p^n}K_{p,(n+1)k}$$

..... [23a]

where x_e is the concentration of the electrons

$$x_e = \sum_{t=1}^{n} t \sum_{i=1}^{k} x_{ti+i} \qquad [23b]$$

Equation [23b] expresses the law of conservation of electron charge.

Multiplying [23b] by x_e and making use of [23a], we obtain

$$x_e^2 = \sum_{t=1}^{n} \frac{1}{x_e^{t-1}} \frac{t}{p^t} \sum_{i=1}^{k} K_{ti} \qquad [24a]$$

where

$$K_{ti} = K_{p,\,ti+i} x_i \qquad [24b]$$

If $x_1, \ldots, x_k$ are known, then for specified values of $K_{p,\,ti+i}$, Equation [24a] is an algebraic equation of degree $n - 1$ in x_e. It is generally solved by numerical methods. For the first-order ionization we have

$$x_e = \sqrt{\frac{1}{p} \sum_{i=1}^{k} K_{ti}} \qquad [24c]$$

After determining x_e, the ionized components are found from the equation

$$x_{ti,\,ki} = \frac{1}{p^t} \frac{K_{ti}}{x_e^t} \qquad [24d]$$

The program for solving the general ECR is as follows: We specify the predominating components $x_1, \ldots, x_a$; the transformed Equations [19c] are used to find $x_{a+1}, \ldots, x_k$; Equation [24a] is used to find x_e, and Equation [23a] is used to find $x_{k+1}, \ldots, x_{(n+1)k}$. We then apply the Newton-Rafson method to Equation [22a], obtaining new values of $x_1, \ldots, x_a$, and so on until the necessary accuracy is attained.

6 Thermodynamic Analysis of Reacting Ideal Gas Systems in Equilibrium State

Let us consider first the calculation of molecular and specific heats C_p and C_v for systems of reacting ideal gases in equilibrium.[3]

The calculation of these quantities is discussed in (16). It will be shown below that this calculation is exact.

The formulas for the specific heats c_p and c_v have the form

$$c_p = \left(\frac{\partial h}{\partial T}\right)_p \qquad c_v = \left(\frac{\partial u}{\partial T}\right)_v \qquad [25a]$$

where h and u are the specific enthalpy and internal energy of the system. Multiplying and dividing Equation [25a] by the constant mass of the system $M = \mu N$ ($\mu = \sum_{i=1}^{K} \mu_i x_i$ = molecular weight of the system, $N = \sum_{i=1}^{K} N_i$ = number of moles in the system), we get

$$\frac{C_p}{\mu} = \left(\frac{\partial \frac{H}{\mu}}{\partial T}\right)_p \qquad \frac{C_v}{\mu} = \left(\frac{\partial \frac{u}{\mu}}{\partial T}\right)_v \qquad [25b]$$

or

$$C_p = \frac{1}{N}\left(\frac{\partial \sum_{i=1}^{K} H_i N_i}{\partial T}\right)_p \qquad C_v = \frac{1}{N}\left(\frac{\partial \sum_{i=1}^{K} U_i N_i}{\partial T}\right)_v \qquad [26]$$

where

K = number of components, of which the first k are the un-ionized components

[3] The molecular quantities are denoted by capital letters and the specific by corresponding lower case letters.

μ_i = molecular weight of the component i
N_i = number of moles of the component i
x_i = N_i/N, the concentration of the component i
H_i, U_i = molar enthalpy and internal energy of the same component

The symmetrical equations of chemical equilibrium (ECE) consist of symmetrical equations of the predominating components (EPC) and the reduced equations of the laws of mass action (LMA); see Section 5

$$x_m = x_m^0 \Phi - \Phi_m (m = 1, \ldots, a) \qquad \text{(EPC)} \qquad [27a]$$

$$K_{p,\,a+s} p^{-\nu_s} = \prod_{i=1}^{K} x_i^{\nu_{si}} (s = 1, \ldots, R) \qquad \text{(EEML)} \qquad [27b]$$

where

a = number of different atoms of the system
R = number of independent reactions, of which the first r are ordinary reactions, and the remaining ones are ionization reactions

If we go over from x_i to N_i and use the equation of state $pV = NRT$, then Equations [27] assume the following form

$$N_m + \Psi_m = \text{constant} \qquad [28a]$$

$$K_{p,\,a+s} \left(\frac{V}{RT}\right)^{\nu_s} = \prod_{i=1}^{K} N_i^{\nu_{si}} \qquad [28b]$$

Here Ψ_m stands for Φ_m when x_i is replaced by N_i.

From Equations [25–28] we obtain

$$C_p = \sum_{i=1}^{K} C_{pi} x_i + \left\{\sum_{i=1}^{K} H_i y_i + H\Sigma_p\right\}$$

where

$$\Sigma_p = \frac{1}{N}\left(\frac{\partial N}{\partial T}\right)_p = -\frac{1}{\mu} \sum_{i=1}^{K} \mu_i y_i$$

$$y_i = \left(\frac{\partial x_i}{\partial T}\right)_p$$

$$C_v = \sum_{i=1}^{K} C_{pi} x_i - R + \left\{\sum_{i=1}^{K} H_i v_i - RT\Sigma_v\right\}$$

$$\Sigma_v = \frac{1}{N}\left(\frac{\partial N}{\partial T}\right)_v = \sum_{i=1}^{K} v_i$$

$$v_i = \frac{1}{N}\left(\frac{\partial N_i}{\partial T}\right)_v$$

Thus, the calculation of C_p and C_v reduces to finding y_i and v_i, respectively. Taking logarithms and then differentiating Equation [27b] with respect to T, with p held constant, we obtain

$$y_m = x_m^0 \bar{\Phi} - \bar{\Phi}_m \qquad [29a]$$

$$\frac{Q_{a+s}}{RT^2} = \sum_{i=1}^{K} \nu_{si} \frac{y_i}{x_i} \qquad [29b]$$

The bars denote the substitution of y_i for x_i. In Equation [29b] we use the well-known relation

$$\frac{d \ln K_{p,\,a+s}}{dT} = \frac{Q_{a+s}}{RT^2} \qquad [29c]$$

where $Q_{a+s} = \sum_{i=1}^{K} \nu_{si} H_i$ is the heat of the reaction s.

Analogously, we obtain from [28] at V = constant

$$v_m + \bar{\Psi}_m = 0 \qquad [30a]$$

$$\frac{\Delta U_{a+s}}{RT^2} = \sum_{i=1}^{K} \nu_{si} \frac{v_i}{x_i} \qquad [30b]$$

where

$$\Delta U_{a+s} = \sum_{i=1}^{K} \nu_{si} U_i = Q_{a+s} - \nu_s RT \qquad [30c]$$

Here the bars denote the substitution of v_i for x_i. A direct solution of systems [29 and 30] is not advisable. It is simpler to first find y_a from Equation [29a] and v_a from [38], and find from these the values of $y_{a+1}, \ldots, y_K$ from [29b] and of $v_{a+1}, \ldots, v_K$ from Equation [30b]. Such a sequence of operation (from the EPC to the LMA), which is natural for the forms [29 and 30], is rational when $a < R$. When $a > R$ we should use the reverse sequence of operation (from the EECM to the EPC). Actually, at $a > R$ one can confine one's self to a solution of only the LMA, transformed in a suitable manner. The case $a > R$ will be considered somewhat later.

Retur ing to Equations [29 and 30], we note the substantial obvious circumstance: The matrix of the solution based on Equation [29a] coincides with the matrix of the last step in the determination of δx_m by the Newton-Rafson method by means of Equation [27a].

To calculate c_p when $a > R$ we begin with the system

$$N_m + \bar{\Psi}_m = \text{constant} \qquad [31a]$$

$$K_{p,s} p^{-\nu_s} = \sum_{i=1}^{K} N_i^{\nu_{si}} N^{-\nu_s} \qquad [31b]$$

which differs from Equation [30] by the obvious substitution and the replacement of the index of K_p. We note that the conditions of conservation of the number of atoms of each kind must be observed for each reaction (see Section 5)

$$\sum_{i=1}^{K} \nu_{si} n_{im} = 0 \qquad [32]$$

To calculate C_p from Equation [26] it is necessary to determine $u_i = (1/N)(\partial N_i/\partial T)_p$. After taking the logarithm of [31b], differentiation of Equation [31] with respect to T, with p held constant, yields a system of linear equations for u_i

$$\sum_{i=1}^{K} n_{im} u_i = 0 \qquad [33a]$$

$$\frac{Q_s}{T^2} = \sum_{i=1}^{K} \nu_{si} \frac{u_i}{x_i} - \nu_s \sum_{i=1}^{K} u_i \qquad [33b]$$

If we furthermore represent u_i in the form

$$u_i = \sum_{s=1}^{R} \nu_{si} \Gamma_s \qquad [34]$$

then Equations [33] are automatically satisfied by virtue of Equation [32].

To determine Γ_s, we derive the system of equations

$$\frac{Q_s}{RT^2} = \sum_{t=1}^{R} \frac{\Gamma_t}{F_{st}} \qquad [35]$$

where

$$\frac{1}{F_{st}} = \sum_{i=1}^{K} \frac{\nu_{si}\nu_{ti}}{x_i} - \nu_s \nu_t \qquad [35a]$$

From Equation [25] we obtain for C_p, the following formula

$$C_p = \sum_{i=1}^{K} C_{pi} x_i + \sum_{s=1}^{R} Q_s \Gamma_s \qquad [36]$$

To calculate C_p for $a > R$ we start, as before, with Equations [28], that is to say with Equations [30], which are written in transformed form, in analogy with Equations [33]

$$\sum_{i=1}^{K} n_{im} v_i = 0 \qquad [37a]$$

$$\frac{\Delta U_s}{RT^2} = \sum_{i=1}^{K} \nu_{si} \frac{v_i}{x_i} \qquad [37b]$$

Here, too, the index of ΔU has been changed.

Further operations are analogous to the calculation of C_p, and we obtain for the representation of

$$v_i = \sum_{s=1}^{R} \nu_{si} \gamma_s \qquad [38]$$

equations that permit us to determine γ_s

$$\frac{\Delta U_s}{RT^2} = \sum_{t=1}^{R} \frac{\gamma_s}{f_{st}} \qquad [39]$$

where

$$\frac{1}{f_{st}} = \sum_{i=1}^{k} \frac{\nu_{si}\nu_{ti}}{x_i} = \frac{1}{F_{st}} + \nu_s \nu_t \qquad [39a]$$

From Equation [25] we obtain for C_v

$$C_v = \sum_{i=1}^{K} C_{vi} x_i + \sum_{s=1}^{R} \Delta U_s \gamma_s \qquad [39b]$$

Epstein (16), who proposed a system analogous to the foregoing for $a > R$ for the calculation of C_p and C_v, did not obtain the systems [35 and 39], inasmuch as he implied material independence, which in general is incorrect.

The term "materially independent reactions" denotes reactions for which the corresponding sets of components do not overlap. (Each reaction has its own corresponding set of components, which participate in this reaction.)

Epstein determined Γ_s and γ_s from the equations

$$\Gamma_s = \frac{Q_s}{RT^2} F_{ss} \quad \gamma_s = \frac{\Delta U_s}{RT^2} f_{ss} \qquad [39c]$$

without solving, thus, the systems [35 and 39]. If the interaction of the reactions is weak, Epstein's calculations are sufficiently accurate. This occurs when the regions of the maximum intensities of all the reactions do not overlap on the p-T diagram. For a single reaction in this system, naturally, Epstein's calculation is correct. It is therefore no wonder that theory and experiment are in good agreement in the experiments of McCollum (17), where only the reaction $2NO_2$–$N_2O \rightleftarrows O$ was investigated. As to the strongly interacting reactions, naturally, Epstein's calculations are not valid for them. In the calculation of the specific system of reactions discussed in this paper, we found a discrepancy up to 40 per cent between the values of the specific heats calculated by the proposed scheme and those calculated by Epstein's scheme, over a sufficiently large region of the p-T diagram.

We note that it follows from Equation [35a] that the material independence of the reaction is not a sufficient condition for the correctness of Epstein's scheme in the calculation of C_p. In fact, this calculation leads only to $\nu_{si}\nu_{ti} = 0$ $(s \neq t)$. It is obviously necessary to have also the condition that the number of particles be constant during the occurrence of all the reactions, with the exception of one. This last condition reduces to $\nu_s = 0$, where s runs through all the values from 1 to R, with the exception of a single one. The material independence of the reactions is sufficient for Epstein's scheme to be correct only in the calculation of C_v, as can be seen from Equation [39a].

The formula for the velocity of sound is (16)

$$a = \sqrt{\gamma \frac{RT}{\mu} \cdot \frac{1 + \frac{T}{N}\left(\frac{\partial V}{\partial T}\right)_s}{1 + \frac{T}{N}\left(\frac{\partial N}{\partial T}\right)_p}} \qquad [40]$$

The value of the velocity of sound, calculated in accordance with the proposed scheme, differs from the value given by Epstein's scheme, although this difference is less than that obtained in the calculation of the specific heats.

Let us turn now to an examination of other thermodynamic characteristics.

It is easy to see that the solutions of the systems [29 and 30] make it possible to find partial derivatives with respect to T, with t or V held constant, for all quantities that characterize the investigated system. We shall confine ourselves to a mention of the following equations

$$\left(\frac{\partial h}{\partial T}\right)_p = C_p - H\Sigma_p$$

$$\left(\frac{\partial h}{\partial T}\right)_s = c_v + \frac{R}{\mu}(1 + T\Sigma_s)$$

$$\left(\frac{\partial \rho}{\partial T}\right)_p = -\frac{\rho}{T}(1 + T\Sigma_p)$$

Analogously, we can obtain $(\partial s/\partial T)_{p,v}$.

If derivatives with respect to T of H_i of orders higher than the first are specified, it is possible to find for the quantities partial derivatives with respect to T (with p or V constant) of higher orders, but not exceeding the order of the derivative of H_i with respect to T. Corresponding systems can be obtained, by differentiation of suitable order, of the systems [29 and 30].

We can find equally well the partial derivatives of arbitrary quantities with respect to p or ρ for T = constant. For example, to investigate the Joule-Thomson effect, it is essential to know $(\partial u/\partial \rho)_T$, the equation for which is

$$\left(\frac{\partial u}{\partial \rho}\right)_T = \frac{1}{\mu}\sum_{i=1}^{K} U_i v_i = \frac{1}{\mu}\left[\sum_{i=1}^{K} H_i v_i - RT\Sigma_v\right]$$

where

$$v_i = \frac{1}{N}\left(\frac{\partial N_i}{\partial \rho}\right)_T \qquad \Sigma_v = \sum_{i=1}^{K} v_i$$

The corresponding system for v_i differs little in structure from the system [30], namely: All the Q_{s+1} vanish identically and T is replaced by ρ; i.e., it is possible to calculate $(\partial u/\partial \rho)_T$ by using the ready-made program for solving the system [30].

Finally, using the properties of Jacobians (18), we can calculate the first-order partial derivatives of any arbitrary quantity (f) with respect to another arbitrary quantity (x) for constant third derivatives of quantity (y).

We note that the partial derivatives of any quantities with respect to arbitrary quantities at T = constant can be found for an order as high as desired.

7 Discussion of Results

On the basis of the procedure expounded in the previous sections for the calculation of the thermodynamic properties of a mixture of gases capable of reacting chemically and capable of being ionized, the authors have calculated the thermodynamic properties and the composition of atmospheric air in the temperature range from 1000 to 12,000 K and in the pressure range from 0.001 to 1000 atm.

The volumetric composition of air under normal conditions was assumed to be as follows: N_2—78.08 per cent, O_2—20.95 per cent, with all the other components replaced by argon. The error in such an approximation is offset by the variation of the composition of air with altitude.

Preliminary estimates and subsequent exact calculations have shown the following:

1 Up to 6000 K, at pressures from 0.001 to 1000 atm, we can neglect the effect of ionization on the thermodynamic properties and the composition of the air.

2 From 6000 to 12,000 K it is possible to neglect the effect of ionization other than that of first order. In connection with this, the temperature interval from 1000 to 12,000 K is broken up into two stages: From 1000 to 6000 K without allowance of ionization; from 6000 to 12,000 K with allowance for single ionization of all the components.

The calculation relative to T is carried out every 100 deg K (a total of 111 values of T). The calculation with respect to p is in accordance with the following scale:

From $1 \times 10k$ to $2 \times 10k$—every $0.2 \times 10k$
From $2 \times 10k$ to $5 \times 10k$—every $0.5 \times 10k$
From $5 \times 10k$ to $10 \times 10k$—every $1 \times 10k$

where $k = -3, -2, -1, 0, 1$ and 2 (a total of 16 points for each order of p—a total of 97 values of p for each temperature). A total of 10,767 points was calculated.

In the temperature interval from 1000 to 6000 K six values of the molar fractions of N_2, O_2, NO, N, O and A were calculated at each point. In the interval of temperatures from 6000 to 12,000 K were calculated 13 values of molar fractions of N_2, O_2, NO, N, O, A, N_2^+, O_2^+, NO^+, N^+, A^+ and e. In the interval of temperatures from 1000 to 12,000 K, the following functions were calculated at each point, in addition to the composition of the air:

h—enthalpy (g-cal/g)
u—internal energy (g-cal/g)
s—entropy (g-cal/g-deg)
μ—molecular weight (g/g-mole)
c_p—specific heat for constant pressure (g-cal/g-deg)
c_v—specific heat at constant volume (g-cal/g-deg)
a—velocity of sound (m/sec)
ρ—density (g/cm^3)

The results of the calculations were used to plot 44 curves, of which we include in this article curves for x_{N_2}, x_{O_2}, x_{NO}, x_N, x_O, x_A, x_e, h, c_p, a, μ and s (Figs. 3–10) as functions of the temperature for pressures 0.001, 1 and 1000 atm.

An analysis of the composition of the air based on these curves shows that an increase in the temperature increases the content of first the atomic and then the ionized components; an increase in pressure, on the contrary, leads to a reduction in the contents of the ionized and atomic components and to an increase of the molecular components. For all pressures, an increase in temperature develops first the reaction of dissociation of molecular oxygen. The dissociation of N_2 begins considerably later, since N_2 has almost twice the dissociation energy of O_2. The reaction of production of NO occurs simultaneously with the reaction of dissociation of O_2. Usually the content of NO in air reaches, with increasing temperature, a maximum value during the time when the dissociation reaction of O_2 is the most vigorous, after which the content of NO decreases with increasing temperature.

The ionization of atomic and molecular components begins in practice with 6000 K. As the temperature is increased, the percentage of ionized components increases, and at p = 0.001 atm and T = 12,000 K the air is found to be fully ionized.

The enthalpy and entropy curves increase monotonically with T and decrease monotonically with increasing p. It is possible to segregate on the enthalpy curves sections where the enthalpy increases markedly. The first such increase, measuring from the beginning of the curve, is due to the dis-

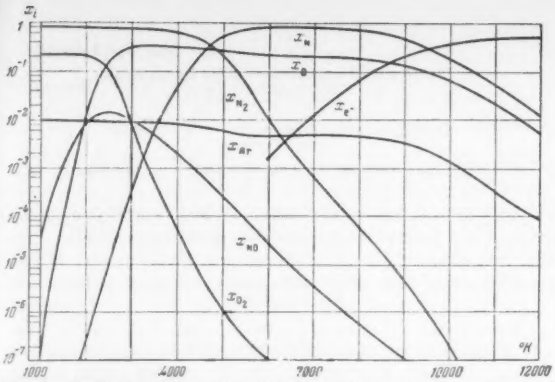

Fig. 3 Molar fractions of molecular and atomic components of air and electrons as a function of temperature at $p = 0.001$ atm

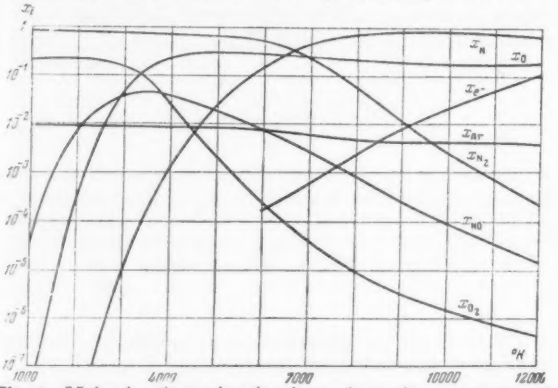

Fig. 4 Molar fractions of molecular and atomic components of air and electrons as a function of the temperature at $p = 1$ atm

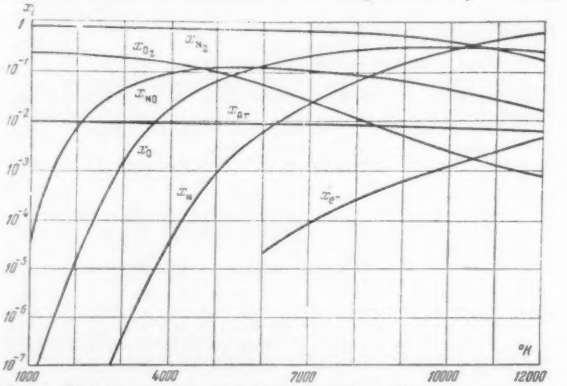

Fig. 5 Molar fractions of molecular and atomic components of air and electrons as a function of the temperature at $p = 1000$ atm

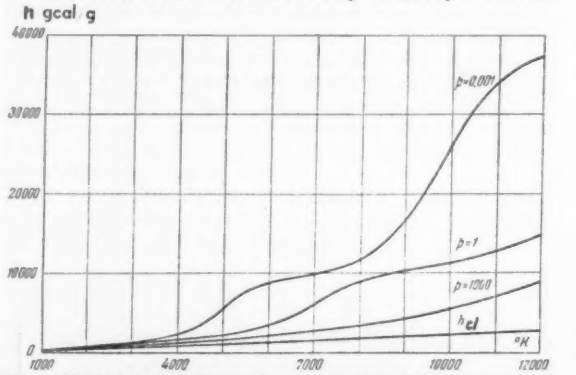

Fig. 6 Enthalpy of air in gcal/g as a function of the temperature at $p = 0.001$, 1 and 1000 atm. For comparison, the value of h calculated from Equation [41] is shown

sociation of N_2, and the second is due to the ionization of the components of the air.

The curves for the specific heats have several maxima. The first maximum from the beginning of the curve corresponds to the dissociation of O_2, the second to that of N_2 and the third to ionization.

The molecular weight of the air diminishes with increasing temperature. The curves for μ have sections where they decrease rapidly. The first section from the start of the curve is due to dissociation of O_2, the second to that of N_2 and the third to ionization of the components of the air.

The curve for the density is not reproduced here, in view of its practical linear dependence on the pressure.

The curves for enthalpy, specific heat, velocity of sound and molecular weight show also for comparison the values of h, c_p, a and μ calculated in accordance with the following formulas

$$h = \frac{7}{2}\frac{RT}{\mu} \qquad c_p = \frac{7}{2}\frac{R}{\mu} \qquad a = \sqrt{1.4\,\frac{RT}{\mu}} \qquad \mu = 28.966 \text{ [41]}$$

These values of the thermodynamic functions, as follow for example from the curves, differ considerably from the true values.

The authors have calculated the values of c_p, c_v, γ and a for 25 points using the Epstein scheme. Table 13 lists the results of the comparison of the calculations based on Epstein's schemes and on the scheme used by the authors. The comparison is given for c_p and c_v. The differences in γ and α, calculated in accordance with the two schemes, can be neglected in practice, something that cannot be done obviously as regards to c_p and c_v.

The mathematical accuracy of the calculations of the thermodynamic functions and of the composition of the air is quite high and exceeds the physical accuracy. The sources of physical errors are inaccuracies in the calculation of the thermodynamic functions of the components of the air, the approximate nature of the determination of the composition of the air, mentioned at the beginning of this section, and also a certain incorrectness in the Clapeyron equation at low temperatures and high pressures (owing to corrections of van der Waals kind) and at high temperatures (owing to corrections of the Debye-Hückel kind, which take into account the Coulomb interaction of the ionized particles and electrons).

The computations were performed on a high speed electronic computer, constructed at the Institute of Precision Mechanics and Computer Engineering of the USSR Academy of Sciences.

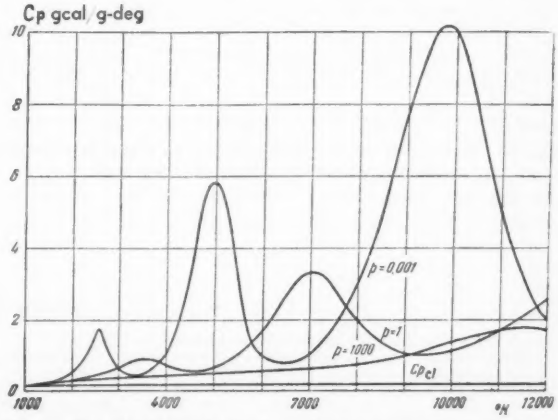

Fig. 7 Specific heat of air at constant pressure in gcal/g-deg as a function of the temperature at $p = 0.001$, 1 and 1000 atm. The value of c_p calculated from Equation [41] is shown for comparison

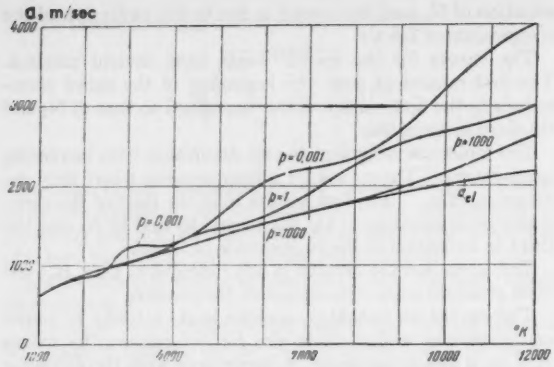

Fig. 8 Velocity of sound in m per sec as a function of the temperature at p = 0.001, 1 and 1000 atm. The values of the velocity of sound calculated from Equation [41] are shown for comparison

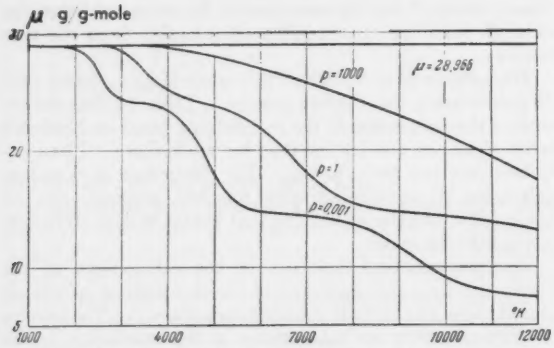

Fig. 9 Molecular weight of air as a function of the temperature at p = 0.001, 1 and 1000 atm. The value μ = 28.966 is shown for comparison

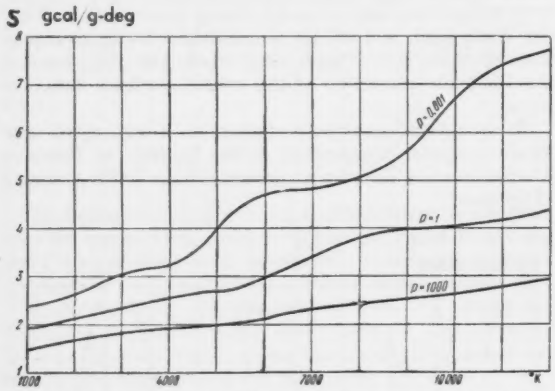

Fig. 10 Entropy of the air in gcal/g-deg as a function of the temperature at p = 0.001, 1 and 1000 atm

Table 13

Degree of approximation of the Epstein scheme

$$\omega_I = \frac{I_{Eps} - I}{I} \cdot 100\%$$

p = 0.001 atm							
T °K	6000	7000	8000	9000	10000	11000	12000
ω_{c_p}	1.99	12.4	15.5	12.9	7.19	2.29	0.471
ω_{c_v}	2.46	14.0	16.8	15.5	10.9	4.30	1.01
p = 0.1 atm							
T °K	6300	7300	8300	9300	10300	11300	
ω_{c_p}	0.327	0.970	7.10	11.8	13.1	12.3	
ω_{c_v}	0.474	1.40	8.34	13.0	14.6	14.6	
p = 10 atm							
T °K	6500	7500	8500	9500	10500	11500	
ω_{c_p}	16.1	3.80	0.914	0.821	3.52	7.25	
ω_{c_v}	16.8	4.29	1.45	1.61	4.68	8.56	
p = 1000 atm							
T °K	6700	7700	8700	9700	10700	11700	
ω_{c_p}	24.5	29.2	35.8	17.0	8.84	4.56	
ω_{c_v}	27.2	30.0	37.8	17.9	10.1	6.01	

The results of the calculations were published, in the form of tables of thermodynamic functions and of the composition of air in the interval of temperatures from 1000 to 20,000 K and the interval of pressures from 0.001 to 1000 atm, in (19).

References

1 Moore, C. E., "Atomic Energy Levels," 1949.
2 Herzberg, G., "Spectra of the Diatomic Molecules," 1951.
3 Rosen, B., "Données spectroscopiques concernant les molecules diatomiques," Paris, 1951.
4 Vukalovich, M. P., "Termodinamicheskie svoistva gazov" (Thermodynamic Properties of Gases), Moscow, 1953.
5 Dumond, J. W. M. and Cohen, E. R., *Revs. Mod. Phys.*, vol. 25, p. 691, 1953.
6 Douglas, A. E., *J. Chem. Phys.*, 1953.
7 Brix, P. and Herzberg, G., *Canad. J. Phys.*, vol. 32, p. 112, 1954.
8 Teast, M. W., *Canad. J. Phys.*, vol. 28, p. 488, 1950.
9 Douglas, A. E., *Canad. J. Phys.*, vol. 30, p. 302, 1952.
10 Douglas, A. E., *Astrophys. J.*, vol. 117, p. 380, 1953.
11 Herzberg, G., *Astrophys. J.*, vol. 108, p. 163, 1948.
12 Herzberg, G., *Astrophys. J.*, vol. 105, p. 353, 1947.
13 Herzberg, G., *Canad. J. Phys.*, vol. 31, p. 657, 1953.
14 Herzberg, G., *Canad. J. Phys.*, vol. 30, p. 185, 1952.
15 Zel'dovich, Ya. B., "Proof of Uniqueness of Solution of the Equations of the Law of Effective Mass," *Zhurnal fizicheskoi khimii* (*J. Phys. Chem.*), vol. XI, 685, 1938.
16 Epstein, P. S., "A Textbook of Thermodynamics," Wiley, N.Y., 1937.
17 McCollum, E.D., *J. Amer. Chem. Soc.*, vol. 49, p. 28, 1927.
18 Landau, L. and Lifshitz, E. M., "Statisticheskaya fizika" (Statistical Physics), GITTL, 1951.
19 Predvoditetev, A. S., et al., "Tablitsy termodinamicheskikh funktsii vozdukha v intervale temperatur ot 1000 do 12000° K i intervale davlenii ot 0.001 do 1000 atm." (Tables of Thermodynamic Functions of Air in the Temperature Interval from 1,000 to 12,000°K and in the Pressure Interval from 0.001 to 1000 atm), USSR Academy of Sciences Press, 1957.

(*Continued from page 64*)

reactions. In a typical rocket motor (3)

$$a = 0.061 \qquad b = 3.75 \qquad c = 0.0655$$

$$x_e = 0.052 \qquad \Delta H/RT^2 = 6.06 \times 10^{-3} \text{ for } 1900\text{K}$$

Using this data, dx_e/dT is found to be -2.66×10^{-5} mole per deg. The approximate solution of Equation [11] yields $x \backsimeq 0$. Accordingly, we conclude that the reaction is frozen at chamber exit in agreement with the conclusion of Penner (3).

An Approximate and Quicker Procedure for Estimating the Nature of the Flow

This is based on an approximate solution of Equation [2] which enables the computation of the composition at any instant. We shall illustrate this procedure by considering the reaction

$$N_2 + 2NO_2 \underset{k_b}{\overset{k_f}{\rightleftharpoons}} N_2 + N_2O_4$$

Recently Wegener has experimentally studied this reaction in a supersonic nozzle (4), and hence it is suitable for comparison between theory and experiment. Let c and d be the initial concentrations of nitrogen peroxide and nitrogen, respectively. Let y be the amount of NO_2 decomposed at any instant. Then

$$\frac{dy}{dt} = d\left[k_f(c - y)^2 - k_b \cdot \frac{y}{2}\right]$$

At equilibrium

$$k_f = k_b \cdot \frac{y_e}{2(c - y_e)^2}$$

where the subscript e stands for equilibrium value. Hence we can write

$$\frac{dy}{(y_e - y)(c^2 - yy_e)} = \frac{d \cdot k_b}{2(c - y_e)^2} \cdot dt \qquad [12]$$

where k_b, the rate of decomposition of N_2O_4, is given by (5)

$$k_b \equiv 10^{16} \cdot e^{-13000/RT} \text{ litre mole}^{-1} \cdot \text{sec}^{-1}$$

Equation [12] can be integrated provided y_e and the cooling rate are assumed to be constant. There would be no serious error in assuming the constancy of cooling rate across the nozzle. y_e, in general, will not be constant, but an average value can be taken for the purpose of integration. A better way would be to perform integration in successive steps, where y_e may be reasonably constant. The integral on the right-hand side of Equation [12] is difficult to evaluate by ordinary methods. Graphical integration may be adopted, but in the present case an approximate solution was found by plotting log k_b against log T using the relation (5) between T and k_b between the region of 400 and 200 K, which is involved in the experiment.

Fig. 1 shows that for the decomposition of N_2O_4 between these temperatures, the curve is a straight line to the first approximation. It follows, therefore

$$k_b = Q \cdot T^m \qquad [13]$$

where Q and m are constants. From the graph it is found that

$$m = 23.5 \qquad Q = 1.168 \times 10^{-5}$$

Substituting the value of k_b from Equation [13] into Equation [12] and integrating, we obtain

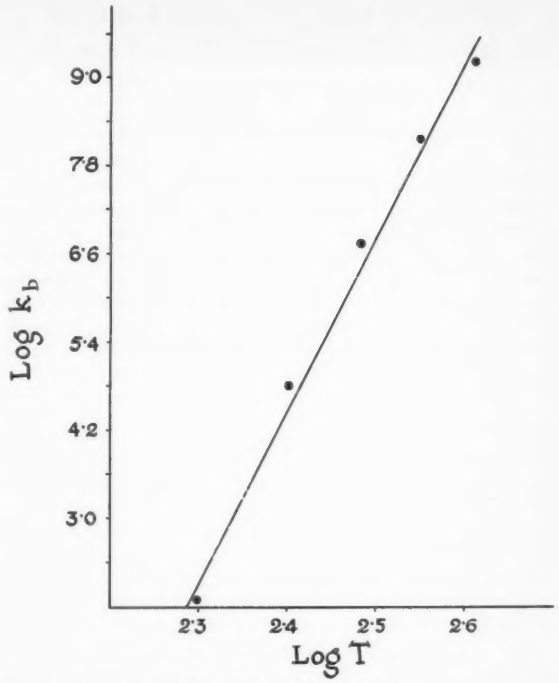

Fig. 1 Approximate functional relationship between rate constant and temperature

$$\ln \frac{c^2 - yy_e}{y_e - y} \cdot \frac{y_e}{c^2} = \frac{d}{2} \cdot \frac{c + y_e}{c - y_e} \cdot \frac{1}{m + 1} \cdot Q \cdot T^{m+1} + \text{constant} \qquad [14]$$

The constant of integration was evaluated from the condition that $y = 0$ when $T = 400$ K, which corresponds to chamber temperature of the experiment. From Wegener's data we have

$$c = 6.09 \times 10^{-4} \text{ mole cc}^{-1}$$
$$d = 6.029 \times 10^{-2} \text{ mole cc}^{-1}$$
$$y_e = 5.48 \times 10^{-4} \text{ mole/litre}$$

In his experiments, the cooling rate was of the order of 10^6 C per sec. Substitution of these values in Equation [14] yields $y \backsimeq y_e$. Since the average value of y_e would lie between its corresponding values at 400 and 220 K, the concentration of NO_2 actually present will really be intermediate between the concentrations predicted by assuming near-equilibrium and frozen flows. This prediction agrees satisfactorily with the experimental results of Wegener.

The method given above is approximate to the extent that an average value of x_e is used. Nevertheless, it can give an approximate idea of the composition at any cross section of the nozzle.

References

1 Penner, S. S., "Maintenance of Near Equilibrium During Isentropic Expansions Through a Nozzle," *J. Amer. Chem. Soc.*, vol. 71, 1949, p. 788.
2 Rastogi, R. P. and Denbigh, K. G., "The Error in Thermodynamic Predictions as a Function of the Displacement From Equilibrium," *Chem. Engng. Sci.*, vol. 7, 1958, p. 261.
3 Altmann, D. and Penner, S. S., "Chemical Reaction During Adiabatic Flow Through a Rocket Nozzle," *J. Chem. Phys.*, vol. 17, 1949, p. 56.
4 Wegener, P. P., "Measurement of Rate Constants of Fast Reactions in a Supersonic Nozzle," *J. Chem. Phys.*, vol. 28, 1958, p. 724.
5 Carrington, T. and Davidson, N., "Shock Waves in Chemical Kinetics: The Rate of Dissociation of N_2O_4," *J. Phys. Chem.*, vol. 57, 1953, p. 418.

Effects of Diffusion and Chemical Reaction on Convective Heat Transfer[1]

DANIEL E. ROSNER[2]

AeroChem Research Laboratories, Princeton, N. J.

The notion of an "effective" thermal conductivity for reacting gaseous mixtures is applied to the prediction of convective heat transfer rates when dissociation, diffusion and atom recombination take place within a laminar boundary layer in quasi-equilibrium. The result for the forward stagnation region of a cool blunt nosed body is compared to recent solutions of the boundary layer equations with particular regard to the explicit dependence on the Lewis number.

THE THEORETICAL and experimental work in (1 through 4)[3] has indicated that existing convective heat transfer data can be applied successfully to situations in which diffusion and gas phase chemical reaction take place at quasi-equilibrium provided that the ordinary thermal conductivity and specific heat are replaced by suitably augmented values which account for these physical and chemical effects. The *explicit* consequences of an ultra-simplified version of this approach are briefly examined here for the case of stagnation point heat transfer with a partially dissociated free stream. The computational work of (5) is then available for comparison.

In a partially dissociated diatomic gas, if thermal diffusion and other secondary diffusion processes are neglected, the energy flux vector can be written in the "undissociated" form

$$\vec{J}_Q = -\lambda_{eq} \text{ grad } T \qquad [1]$$

where the "equilibrium" thermal conductivity λ_{eq} is related (2) to the ordinary "frozen" conductivity λ_f through

$$\frac{\lambda_{eq}}{\lambda_f} = 1 + (Le_f)\left[\left(\frac{C_{peq}}{C_{pf}}\right) - 1\right] \qquad [2]$$

To apply this result to convective heat transfer problems, we note that ordinary low speed heat transfer data may be expressed in the Stanton form

$$\dot{q}_\lambda = (St_\lambda)\rho_e U_e C_{p,avg}(T_e - T_w) \qquad [3]$$

where (for gases) the dimensionless Stanton number is usually a power function of the Prandtl number. When dissociation, diffusion and atom recombination occur, the average specific heat and Prandtl number alone will then embody the principal physical and chemical effects. This naturally suggests the application of Equations [2 and 3], but, for the purpose of obtaining an *explicit* correlation equation, we further introduce

$$(C_{peq})_{avg} = (h_e - h_w)/(T_e - T_w) \qquad [4a]$$

$$(C_{pf})_{avg} = (\bar{h}_e - \bar{h}_w)/(T_e - T_w) \qquad [4b]$$

It is through the ratio of these two quantities that a "chemical" energy parameter of the form $\alpha_e Q/(h_e - h_w)$ explicitly enters this class of problems. Furthermore, if the degree of dissociation corresponding to the wall temperature is negligible, the ratio of equilibrium to frozen Prandtl number then becomes

$$\frac{Pr_{\lambda,eq}}{Pr_{\lambda,f}} = \left\{1 + [(Le_f) - 1]\frac{\alpha_e Q}{h_e - h_w}\right\}^{-1} \qquad [5]$$

This approach is now applied to an important particular case. For the laminar flow at the blunt nose of a body of revolution, St_λ can be approximated by Sibulkin's (6) incompressible fluid formula, applied to the stagnation region behind the normal shock

$$St_\lambda = 0.763(\rho_e U_e)^{-1}(\beta\rho_e\mu_e{}^{1/2})(Pr_{\lambda,f})^{-0.6} \qquad [6]$$

where, for heat transfer purposes, $\rho_e\mu_e$ has been introduced for $(\rho\mu)_{avg}$. Combining Equations [4, 5 and 3], we then immediately predict that the equilibrium heat transfer rate should be given by a correlation equation of the form

$$\dot{q} = 0.763(\beta\rho_e\mu_e)^{1/2}(Pr_{\lambda,f})^{-0.6}(h_e - h_w) \times \left\{1 + [(Le_f) - 1]\frac{\alpha_e Q}{h_e - h_w}\right\}^{0.6} \qquad [7]$$

It is now interesting to compare this conclusion with recent numerical solutions to the complete laminar boundary layer equations. For the comparable case, Fay and Riddell (5) have correlated their results with the equation

$$\dot{q} = 0.763\left(\frac{\rho_w\mu_w}{\rho_e\mu_e}\right)^{0.1}(\beta\rho_e\mu_e)^{1/2}(Pr_{\lambda,f})^{-0.6}(h_e - h_w) \times \left\{1 + [(Le_f)^{0.52} - 1]\frac{\alpha_e Q}{h_e}\right\} \qquad [8]$$

Apart from the familiar correction factor for variable $\rho\mu$, formulas [7 and 8] differ mainly in the form of the Lewis number dependence. In Table 1, the two Lewis number "augmentation" factors are compared for three values of the "chemical" energy parameter $\alpha_e Q/(h_e - h_w)$ and six values of the Lewis number.

With regard to the effects of Lewis number, it is seen that Equation [7] yields results which are higher than Equation [8] by less than 2.75 per cent for Lewis numbers in the neighborhood of 1.4; however, the departures increase with increasing Lewis number. Equation [7] also leads to the important conclusion that if recombination *does* take place, the

Table 1 Lewis number augmentation factors for convective heat transfer

$\frac{\alpha_e Q}{h_e - h_w}$	Le_f	Eq. [7]	Eq. [8]
	1.0	1.000	1.000
	1.2	1.030	1.025
0.25	1.4	1.059	1.048
	1.6	1.088	1.069
	1.8	1.116	1.089
	2.0	1.143	1.108
	1.0	1.000	1.000
	1.2	1.059	1.050
0.50	1.4	1.116	1.096
	1.6	1.170	1.138
	1.8	1.224	1.179
	2.0	1.275	1.217
	1.0	1.000	1.000
	1.2	1.088	1.075
0.75	1.4	1.170	1.143
	1.6	1.250	1.208
	1.8	1.326	1.268
	2.0	1.399	1.325

Received June 23, 1959.

[1] This research was supported by the U. S. Air Force through the Air Force Office of Scientific Research of the Air Research and Development Command under contract no. AF 49(638)-300, as well as Wright Air Development Center contract no. AF 33(616)-6216.

[2] Research Scientist. Member ARS.

[3] Numbers in parentheses indicate References at end of paper.

resulting heat transfer rate, for the Lewis numbers shown, is about the same whether the recombination takes place at equilibrium within the gas phase *or* at a "fully" (7) catalytic surface. Using the result of (7) and Equation [7], this is seen by computing values of the ratio

$$\frac{\{1 + [(Le_f)^{0.6} - 1][(\alpha_e Q)/(h_e - h_w)]\}}{\{1 + [(Le_f) - 1][(\alpha_e Q)/(h_e - h_w)]\}^{0.6}} \qquad [9]$$

This ratio never departs from unity by more than 1.4 per cent over the range of parameters shown in Table 1. In contrast to the comparable ratio

$$\frac{1 + [(Le_f)^{0.63} - 1][(\alpha_e Q)/(h_e - h_w)]}{1 + [(Le_f)^{0.52} - 1][(\alpha_e Q)/(h_e - h_w)]} \qquad [10]$$

suggested by the work of Fay and Riddell, the ratio [9] has the interesting property of tending toward unity for all values of the Lewis number when $\alpha_e Q/(h_e - h_w) \to 1$, and it is always slightly *less* than unity.

Nomenclature

C_p = specific heat at constant pressure
D_{12} = binary diffusion coefficient for atoms in the gas mixture
$\bar{h}$ = sensible or "frozen" enthalpy of the mixture
h = enthalpy of the mixture
$\vec{J}$ = flux vector
Le = "frozen" Lewis number $D_{12}\rho C_{pf}/\lambda_f$; assumed constant
Pr = Prandtl number
Q = heat of recombination, assumed constant
St = Stanton number
T = absolute temperature
U = fluid velocity relative to body
α = mass fraction of atoms in mixture
β = inviscid velocity gradient at the nose
ρ = density of fluid
λ = thermal conductivity of mixture
μ = absolute viscosity of fluid
grad = gradient operator

Subscripts

avg = average
e = at outer edge of boundary layer
eq = equilibrium
f = chemically "frozen"
Q = pertaining to energy transport
w = at the wall (surface of cool body)
λ = pertaining to ordinary thermal conduction

References

1 Langmuir, I., "The Dissociation of Hydrogen into Atoms," *J. Amer. Chem. Soc.*, vol. 34, 1912, p. 860 ff., also vol. 34, 1912, p. 1310 ff.
2 Butler, J. N. and Brokaw, R. S., "Thermal Conductivity of Gas Mixtures in Chemical Equilibrium," *J. Chem. Phys.*, vol. 26, no. 6, 1957, p. 1636 ff.
3 Brokaw, R. S., "Correlation of Turbulent Heat Transfer in a Tube for the Dissociating System $N_2O_4 \rightleftarrows 2\ NO_2$," NACA RM E57K19a, March 1958.
4 Schotte, W., "Heat Transfer to a Gas Phase Chemical Reaction," *Ind. Engng. Chem.*, vol. 50, no. 4, 1958, pp. 683–690.
5 Fay, J. A. and Riddell, F. R., "Theory of Stagnation Point Heat Transfer in Dissociated Air," *J. Aeron. Sci.*, vol. 25, no. 2, 1958, p. 73.
6 Sibulkin, M., "Heat Transfer Near the Forward Stagnation Point of a Body of Revolution," *J. Aeron. Sci.*, vol. 19, no. 8, Aug. 1952, pp. 570–571.
7 Rosner, D. E., "Similitude Treatment of Hypersonic Stagnation Heat Transfer," ARS JOURNAL, vol. 29, 1959, pp. 215–216.

Uncertainty in a Calculated Specific Impulse Due to an Uncertainty in the Heat of Formation of the Propellant

L. J. GORDON[1]

Aerojet-General Corp., Sacramento, Calif.

THE CALCULATED specific impulse of a propellant is necessarily dependent on the heat of formation of its components. Although these heats of formation are fairly accurately known for most propellant materials, there is a reasonable uncertainty in many values.[2] Fortunately, however, the uncertainties in the heats of formation of propellant components are small compared to heats of combustion of the propellants so that the errors in the calculated specific impulses are small. A relation between the uncertainty in the heat of formation and the uncertainty in the specific impulse in terms of parameters usually calculated for a particular propellant is

$$\frac{dI_s}{d\Delta H_f} = \frac{K}{I_s}\left(1 - \frac{T_e}{T_c}\right)$$

where

I_s = specific impulse
ΔH_f = enthalpy of formation of propellant
T_c = chamber temperature
T_e = exhaust temperature
K = appropriate energy conversion factor

Received July 6, 1959.

[1] Assistant Senior Engineer, Solid Propellant Research Dept. Member ARS.

[2] For example, ΔH_{f298} of NH_4ClO_4, NBS Circular 500, is −69.42 kcal/mole; older value listed in Perry's Handbook is −78.1 kcal/mole.

A derivation of the equation, a set of units for K, and a numerical example is given as follows.

Although specific impulses are often calculated from the common approximate formula involving the heat capacity ratio, average molecular weight, etc., more accurate values are obtained from enthalpy-entropy calculations. In these calculations it is assumed that combustion is isenthalpic and the expansion process is isentropic. The path of such a process can be depicted on an enthalpy-entropy diagram such as Fig. 1, where the curves *ab* and *cd* represent the chamber and exhaust isobars. Assume that the uncertainty in ΔH_f is such that the paths 1–2 and 3–4 in Fig. 1 represent the expansion processes for the two enthalpies of formation ΔH_f and $\Delta H_f + \delta\Delta H_f$ respectively.

The respective heats released to become kinetic energy are then

$$Q = H_1 - H_2$$

$$Q + \delta Q = H_3 - H_4$$

From Fig. 1 it is seen that

$$\delta Q = (H_3 - H_6) - (H_5 - H_2)$$

At any point on the H-S diagram realize that the slope of a constant pressure line

$$\left(\frac{dH}{dS}\right)_p = \frac{(dH/dT)_p}{(dS/dT)_p} = \frac{C_p}{C_p/T} = T$$

so that

$$\frac{H_3 - H_6}{S_6 - S_1} = T_c$$

$$\frac{H_5 - H_2}{S_4 - S_2} = T_e$$

and

$$H_5 - H_2 = T_e/T_c(H_3 - H_6)$$

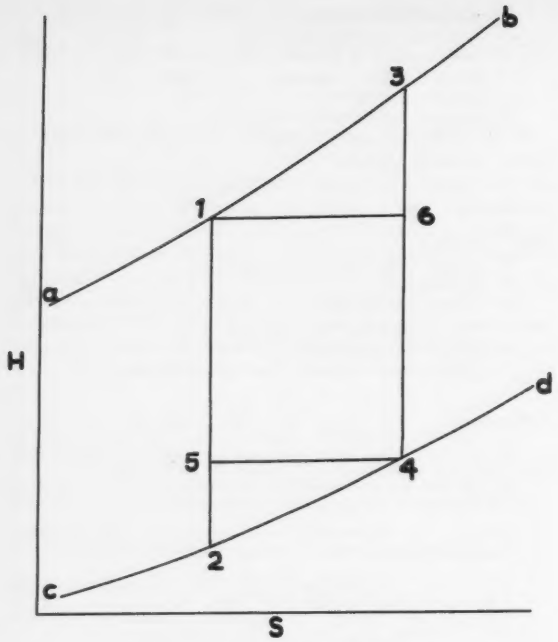

Fig. 1 Enthalpy-entropy diagram

Solving for δQ results in

$$\delta Q = H_3 - H_6\left(1 - \frac{T_e}{T_c}\right) = \delta\Delta H_f\left(1 - \frac{T_e}{T_c}\right)$$

$$\frac{dQ}{d\Delta H_f} = \left(1 - \frac{T_e}{T_c}\right)$$

The relationship between Q and specific impulse is

$$I_s = 29.5Q^{1/2}\ \text{lbf-sec/lbm}$$

when Q and ΔH_f are given in units of kcal/100 gm. Therefore

$$\frac{dI_s}{d\Delta H_f} = \frac{29.5}{2Q^{1/2}}\left(1 - \frac{T_e}{T_c}\right) = \frac{(29.5)^2}{2I_s}\left(1 - \frac{T_e}{T_c}\right)$$

As an example of the uncertainty, one finds that when

$$I_s = 270\ \text{lbf-sec/lbm}$$
$$T_c = 3500\ \text{K}$$
$$T_e = 2200\ \text{K}$$

an uncertainty of 20 kcal/100 gm in the heat of formation of a component which is 40 weight per cent of the propellant yields an uncertainty in I_s of

$$\frac{(29.5)^2}{2(270)}\left(1 - \frac{2200}{3500}\right)(8) = 3.5\ \frac{\text{lbf-sec}}{\text{lbm}}$$

High temperature shifting equilibrium heat capacities are about 80 cal/100 gm-deg K, so that the corresponding uncertainty in T_c is

$$8000/80 = 100\ \text{K}$$

a number small enough so as to not seriously affect the accuracy of using a constant value of $[1 - (T_e/T_c)]$ over the short $\delta\Delta H$ range.

That the fractional uncertainty in I_s is independent of the expansion ratio, P_e/P_c, may be shown by rewriting the foregoing expression

$$dI_s = \frac{(29.5)^2}{2I_s^2}\left(1 - \frac{T_e}{T_c}\right)d\Delta H_f$$

and substituting into it the approximate expression for I_s

$$I_s = 29.5\left\{\bar{C}_p T_c[1 - (P_e/P_c)^{(\gamma-1)/\gamma}]\right\}^{1/2}$$

yielding

$$\frac{dI_s}{I_s} = \frac{d\Delta H_f}{2\bar{C}_p T_c}$$

and as long as the average heat capacity $\bar{C}_p$ does not vary with the expansion ratio, and T_c is not changed appreciably, dI_s/I_s remains constant.

It is also apparent that the mathematic derivation used here is applicable to calculating the effects on specific impulse of heat losses and of the propellant initial temperature.

Transient and Steady-State Behavior of an Idealized Solar Powered Heat Exchanger

J. W. TATOM[1]

Chance Vought Aircraft, Inc., Dallas, Texas

The differential equation describing the transient and steady-state behavior of an idealized solar heat exchanger is developed. The equation is solved for the three possible operating conditions, and the steady-state temperature is defined.

SOLAR energy is an important source of power for space vehicles. To collect and utilize this energy, a typical power generation system would include a collector, heat exchanger and some device for converting thermal energy into useful work. Abrupt changes in vehicle energy level requirements and discontinuities in collection of the solar energy have made the transient and steady-state behavior of the heat exchanger an important factor in the system operation.

If the solar heat exchanger can be assumed to have a uniform temperature at any instant in time and if the vehicle power requirements P are maintained at a constant level, the following expression describes the thermal behavior of the heat exchanger[2]

$$\dot{q}_{\text{net}} = \dot{q}_{\text{in (solar)}} - \dot{q}_{\text{out (radiation}} - \dot{q}_{\text{power output}}$$

which written in differential form is

$$W_h\frac{dh}{d\tau} = SA_m\alpha_h(1 - \alpha_m) - \sigma\epsilon_h A_h T_h^4 - P \qquad [1]$$

Received July 14, 1959.

[1] Propulsion Engineer.

[2] The heat exchanger is considered alone as the reference body and does not include the weight of any working fluid which may pass through or around it.

We note that

$$dh = CdT$$

Since the specific heat for solids is generally a function of temperature, it is assumed that

$$C = C_1 + C_2T + C_3T^2 + C_4T^3$$

where C_1, C_2, C_3 and C_4 are determined experimentally. Hence Equation [1] becomes

$$\frac{dT}{d\tau} = \frac{\sigma\epsilon_h A_h}{W_h}\left[\frac{1 - \dfrac{P}{SA_m\alpha_h(1-\alpha_m)}}{\left(\dfrac{\sigma}{S}\right)\left(\dfrac{A_h}{A_m}\right)\dfrac{\epsilon_h}{\alpha_h(1-\alpha_m)}} - T_h^4\right] \qquad [2]$$

Three possible modes of operation for the heat exchanger are indicated from Equation [2]. They are when

(a) $SA_m\alpha_h(1-\alpha_m) > P$

(b) $SA_m\alpha_h(1-\alpha_m) < P$

(c) $SA_m\alpha_h(1-\alpha_m) = P$

Case (a) corresponds to transient operation which ultimately stabilizes at some equilibrium temperature T_e. Case (b) corresponds to a transient operation, which if continued and were physically possible, would result in the heat exchanger temperature going to absolute zero. Case (c) is equivalent to simple radiation cooling, where the temperature approaches zero asymptotically. Integrating Equation [2] for Case (a)

$$\Delta\tau = \frac{W_h N^3}{4\sigma\epsilon_h A_h}\left\{\left(C_1 + \frac{C_2}{N^2}\right)\ln\left|\frac{1+NT_2}{1+NT_1}\cdot\frac{1-NT_2}{1-NT_1}\right| + \frac{C_3}{N}\ln\left|\frac{1+N^2T_2^2}{1+N^2T_1^2}\cdot\frac{1-N^2T_2^2}{1-N^2T_1^2}\right| + 2\left(C_1 - \frac{C_3}{N^2}\right)[\tan^{-1}NT_2 - \tan^{-1}NT_1] - \frac{C_4}{N^3}\ln\left|\frac{1-N^4T_2^4}{1-N^4T_1^4}\right|\right\} \qquad [3]$$

where

$$N = \left[\frac{\left(\dfrac{\sigma}{S}\right)\left(\dfrac{A_h}{A_m}\right)\dfrac{\epsilon_h}{\alpha_h(1-\alpha_m)}}{1 - \dfrac{P}{SA_m\alpha_h(1-\alpha_m)}}\right]^{1/4}$$

Integrating Equation [2] for Case (b)

$$\Delta\tau = \frac{W_h M^3}{4\sqrt{2}\,\sigma\epsilon_h A_h}\left\{\left(C_1 - \frac{C_3}{M^2}\right)\ln\left|\frac{M^2T_1^2 + MT_1\sqrt{2} + 1}{M^2T_2^2 + MT_2\sqrt{2} + 1}\cdot\frac{M^2T_1^2 - MT_1\sqrt{2} + 1}{M^2T_2^2 - MT_2\sqrt{2} + 1}\right| + \frac{2\sqrt{2}\,C_2}{M}[\tan^{-1}M^2T_1^2 - \tan^{-1}M^2T_2^2] + 2\left(C_1 + \frac{C_3}{M^2}\right)\left[\tan^{-1}\frac{MT_1\sqrt{2}}{1-M^2T_1^2} - \tan^{-1}\frac{MT_2\sqrt{2}}{1-M^2T_2^2}\right] + \frac{\sqrt{2}\,C_4}{M^3}\ln\left|\frac{1+M^4T_1^4}{1+M^4T_2^4}\right|\right\} \qquad [4]$$

where

$$M = \left\{\frac{\left(\dfrac{\sigma}{S}\right)\left(\dfrac{A_h}{A_m}\right)\dfrac{\epsilon_h}{\alpha_h(1-\alpha_m)}}{\dfrac{P}{SA_m\alpha_h(1-\alpha_m)} - 1}\right\}^{1/4}$$

and

$$T_1 > T_2$$

Integrating Equation [2] for Case (c)

$$\Delta\tau = \frac{W_h}{\sigma\epsilon_h A_h}\left\{\frac{C_1}{3}\left[\frac{1}{T_2^3} - \frac{1}{T_1^3}\right] + \frac{C_2}{2}\left[\frac{1}{T_2^2} - \frac{1}{T_1^2}\right] + C_3\left[\frac{1}{T_2} - \frac{1}{T_1}\right] + C_4[\ln T_2 - \ln T_1]\right\} \qquad [5]$$

Steady-state operation would be possible only for the conditions of Case (a), since both (b) and (c) result in the system temperature ultimately going to or approaching absolute zero. In Case (a) an equilibrium state can exist, and the system approaches this condition asymptotically as $dT/d\tau$ approaches zero. By setting $dT/d\tau$ equal to zero in Equation [1], the equilibrium temperature of the heat exchanger can be found. Hence

$$T_e = \left[\frac{1 - \dfrac{P}{SA_m\alpha_h(1-\alpha_m)}}{\left(\dfrac{\sigma}{S}\right)\left(\dfrac{A_h}{A_m}\right)\dfrac{\epsilon_h}{\alpha_h(1-\alpha_m)}}\right]^{1/4} = \frac{1}{N} \qquad [6]$$

Although the expressions above are true only for an idealized situation, they provide insight into the general behavior of an actual solar heat exchanger, an understanding of the important parameters involved, and an approximate method for calculating performance. A study of this idealized behavior will facilitate more efficient design and provide a greater appreciation of the problems to be faced.

It should be noted that the assumption of instantaneous temperature uniformity becomes more valid if the heat exchanger is small, the transient operation time is large and/or if the thermal diffusivity of the heat exchanger material is high.

Nomenclature

α_h	=	solar absorptivity of solar heat exchanger
α_m	=	solar absorptivity of solar collector
A_h	=	external area of solar powered heat exchanger
A_m	=	normal projected area of solar collector
C_n	=	constants used in equation for specific heat of heat exchanger

C = specific heat of heat exchanger
$dT/d\tau$ = rate of change of temperature with respect to time
ϵ_h = surface emissivity of solar powered heat exchanger
h = specific enthalpy of heat exchanger
M = general modulus used to describe behavior of solar heat exchanger under nonstabilizing transient conditions
N = general modulus used to describe behavior of solar heat exchanger under stabilizing transient conditions
P = power generation term
σ = Stephan-Boltzmann constant, 0.174×10^{-8} Btu/hr ft^2 R^4
S = solar radiation constant at 9.3×10^7 miles, 425 Btu/hr ft^2
τ = time, hr
T = temperature, R
W_h = weight of heat exchanger, lb

Steady-State Behavior of Extended Surfaces in Space

J. W. TATOM[1]

Chance Vought Aircraft, Inc., Dallas, Texas

The differential equation describing the thermal behavior of a uniform extended surface receiving and losing heat by radiation alone is developed. The equation is solved for three sets of boundary conditions, and a solution is indicated for several others.

THE TWO heat transfer phenomena, conduction and radiation, working together establish the equilibrium temperature of many systems in space. Hence, a study of the two in combination is important and necessary to the solution of numerous present day and future heat transfer problems.

Consider the steady-state behavior of a rod[2] protruding from some body at temperature T_0 into a solar radiation field. Assuming that the conduction heat flow is one-dimensional, the physical properties of the rod are constant and the effect of neighboring bodies is neglected, the following differential equation may be used to describe the thermal behavior of the rod

$$\frac{d^2T}{dX^2} = \frac{\sigma\epsilon CT^4}{kA} - \frac{S\alpha D \sin\theta}{kA} \qquad [1]$$

This equation can be integrated to give

$$X = \int_T^{T_0} \frac{dT}{\sqrt{\frac{2\sigma\epsilon CT^5}{5kA} - \frac{2S\alpha D(\sin\theta)T}{kA} + K}} \qquad [2]$$

Received July 14, 1959.

[1] Propulsion Engineer.

[2] The following material can be applied to any constant cross-sectional area extended surface. The rod was used for illustrative purposes alone.

This general integral cannot be formally evaluated, and numerical methods must be employed in the solution. However, for the special case of an infinitely long rod with $\theta = 0$ (Case a, Table 1), Equation [2] can be integrated. The resulting solution is

$$T = [T_0^{-3/2} + \sqrt{9\sigma\epsilon C/10kA}\ X]^{-2/3} \qquad [3]$$

and

$$\dot{q}_{x=0} = \sqrt{(2/5)kA\sigma\epsilon C}\ (T_0)^{5/2} \qquad [4]$$

This solution is applicable to rods of relatively large effective length (defining effective length as $Le = \sqrt{\beta\epsilon C/kA}\ L$), because their temperature distribution approaches that of an infinite rod.

In Table 1, Case (b) can be evaluated easily by the substitution $\zeta = T/T_L$, and Equation [2] becomes

$$X = \sqrt{\frac{5kA}{2\sigma\epsilon CT_L^3}} \int_\zeta^{\zeta_0} \frac{d\zeta}{\sqrt{\zeta^5 - 1}} \qquad [5]$$

Applying Equation [3] as a first approximation, and using the tabulated values of the integral presented in Table 2, an iteration procedure can be used to determine T_L. Knowing T_L and noting that

$$X = \sqrt{\frac{5kA}{2\sigma\epsilon CT_L^3}} \left(\int_1^{\zeta_0} \frac{d\zeta}{\sqrt{\zeta^5 - 1}} - \int_1^{\zeta} \frac{d\zeta}{\sqrt{\zeta^5 - 1}} \right) \qquad [6]$$

the intermediate values of temperature can be determined.

By making the substitution

$$r = \zeta \Big/ \left(1 - \frac{5\sigma\epsilon AT_L^3}{2kC}\right)^{1/5} \qquad [7]$$

Case (c) can be reduced to a form which can be integrated.

The temperature for large values of X along an infinite rod receiving energy from solar radiation does not tend to zero, but approaches some equilibrium value. The equilibrium tem-

Table 1 Values of the integration constant K for $\theta = 0$ and $\pi/2$

Rod	Boundary condition	K
(a) infinite, $\theta = 0$	$-kA \frac{dT}{dX}_{x\to\infty} = 0,\ T_{x\to\infty} = 0$	0
(b) finite, insulated end, $\theta = 0$	$-kA \frac{dT}{dX}_{x=L} = 0$	$-\frac{2}{5}\frac{\sigma\epsilon CT_L^5}{kA}$
(c) finite, uninsulated end, $\theta = 0$	$-kA \frac{dT}{dX}_{x=L} = \sigma\epsilon AT_L^4$	$-\frac{2}{5}\frac{\sigma\epsilon CT_L^5}{kA}\left[1 - \frac{5\sigma\epsilon AT_L^3}{2kC}\right]$
(d) infinite, $\theta = \pi/2$	$-kA \frac{dT}{dX}_{x\to\infty} = 0,\ T_{x\to\infty} = \left[\frac{S\alpha D}{\sigma\epsilon C}\right]^{1/4}$	$\frac{8}{5}\frac{S\alpha D}{kA}\left[\frac{S\alpha D}{\sigma\epsilon C}\right]^{1/4}$
(e) finite, insulated end, $\theta = \pi/2$	$-kA \frac{dT}{dX}_{x=L} = 0$	$-\frac{2}{5}\frac{\sigma\epsilon CT_L^5}{kA} + \frac{2S\alpha DT_L}{kA}$
(f) finite, uninsulated end, $\theta = \pi/2$	$-kA \frac{dT}{dX}_{x=L} = \sigma\epsilon AT_L^4$	$\left(\frac{\sigma\epsilon}{k}\right)^2 T_L^8 - \frac{2}{5}\frac{\sigma\epsilon CT_L^5}{kA} + \frac{2S\alpha DT_L}{kA}$

Table 2 Tabulation of the integral

$$I = \int_1^{\zeta} \frac{d\zeta}{\sqrt{\zeta^5 - 1}}$$

ζ	I	ζ	I
1.00	00000	1.75	0.62083
1.01	0.08915	1.80	0.63313
1.02	0.12616	1.85	0.64452
1.03	0.15407	1.90	0.65512
1.04	0.17653	1.95	0.66498
1.05	0.19705	2.00	0.67432
1.06	0.21399	2.10	0.69126
1.07	0.23076	2.20	0.70614
1.08	0.24570	2.30	0.71937
1.09	0.26049	2.40	0.73133
1.10	0.27351	2.50	0.74205
1.12	0.29756	2.60	0.75168
1.14	0.31957	2.70	0.76053
1.16	0.33960	2.80	0.76850
1.18	0.35773	2.90	0.77582
1.20	0.37477	3.00	0.78255
1.25	0.41270	3.20	0.79441
1.30	0.44542	3.40	0.80454
1.35	0.47399	3.60	0.81325
1.40	0.49916	3.80	0.82084
1.45	0.52161	4.00	0.82754
1.50	0.54228	4.20	0.83343
1.55	0.56058	4.40	0.83866
1.60	0.57770	4.60	0.84332
1.65	0.59316	4.80	0.84750
1.70	0.60759	5.00	0.85126

perature is governed by the expression

$$S\alpha D \sin\theta = \sigma\epsilon C T_{x\to\infty}^4 \qquad [8]$$

and therefore

$$T_{x\to\infty} = [(S\alpha D/\sigma\epsilon C)\cdot\sin\theta]^{1/4} = U^{1/4} \qquad [9]$$

Hence for a rod in the vicinity of the Earth receiving solar radiation perpendicularly and assuming $\alpha = \epsilon$

$$T_{x\to\infty} = 528.04 \text{ R}$$

The ratio

$$U = \left[\frac{S\alpha D}{\sigma\epsilon C}\cdot\sin\theta\right]$$

when substituted into Equation [2] for Cases (d), (e) and (f) respectively, results in the following expressions

$$X = \sqrt{\frac{5kA}{2S\alpha D}}\int_T^{T_0} \frac{dT}{\sqrt{(1/U)T^5 - 5T + 4U^{1/4}}} \qquad [10]$$

$$X = \sqrt{\frac{5kA}{2S\alpha D}}\int_T^{T_0} \frac{dT}{\sqrt{(1/U)(T^5 - T_L{}^5) - 5(T - T_L)}} \qquad [11]$$

$$X = \sqrt{\frac{5kA}{2S\alpha D}} \times \int_T^{T_0} \frac{dT}{\sqrt{(1/U)(T^5 - T_L{}^5) - 5(T - T_L) + 5\sigma\epsilon D T_L{}^8/8kU}} \qquad [12]$$

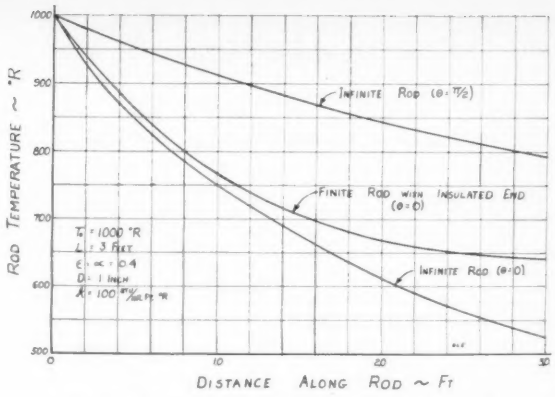

Fig. 1 Temperature distribution along a 3-ft rod

which can be solved by numerical means together with, in Cases (e) and (f), an iterative technique.

To demonstrate numerically these expressions, Fig. 1 presents the temperature distribution along a rod treated as: Infinite ($\theta = 0$); finite, with an insulated end ($\theta = 0$), and infinite ($\theta = \pi/2$).

Thus the thermal behavior of simple extended surfaces in space can be predicted by using the previously developed equations. Application of the procedures and techniques to more complicated situations should provide a basis for exact calculations.

Nomenclature

α	= solar absorbtivity of a body
A	= area through which heat can be transferred by conduction
β	= dimensional constant in definition of effective length
C	= circumference of extended surface
dT/dx	= rate of change of temperature with respect to distance
d^2T/dx^2	= second derivation of temperature with respect to distance
D	= diameter
ϵ	= surface emissivity
k	= thermal conductivity
K	= general constant in extended surface radiation-conduction expression
L	= length
$\dot{q}$	= rate per unit time per unit area at which heat is transferred
r	= constant used in integral of finite rod with uninsulated end
σ	= Stephan-Boltzmann constant, 0.174×10^{-8} Btu/hr ft² R⁴
S	= solar radiation constant at 9.3×10^7 miles from the sun, 425 Btu/hr ft²
U	= general constant for surface in radiation field
T	= temperature, R
θ	= angle between an extended surface and the sun's rays
X	= distance
ζ	= dimensionless parameter, used in integration of expression [5]

Analytical Estimates for Optimum Transfer Paths

H. MUNICK[1] and R. McGILL[2]

Grumman Aircraft Engineering Corp., Bethpage, N. Y.

THIS paper essentially extends the work of Lawden (1).[3] The problem considered is the minimization of characteristic velocity, or the amount of fuel consumed, using two impulses.

Lawden studied the case of transfer from an elliptic orbit to a higher energy circular orbit. Consider a space vehicle traveling in an elliptic orbit with velocity components (u, v) resolved perpendicular to and along the radius vector. Suppose at some point on this elliptic orbit the space vehicle is at a distance α from the focus, with velocity components (u_0, v_0).

Suddenly an impulse is applied, giving rise to new components of velocity (u_1, v_1). The vehicle then goes into a new elliptical orbit, the transfer ellipse. Upon arrival at the higher energy circular orbit, a second impulse is applied, correcting the space vehicle's velocity components to those of a circular orbit at a distance β from the focus. The characteristic velocity is given by

$$\sqrt{(u_1 - u_0)^2 + (v_1 - v_0)^2} + \sqrt{[u_2 - (\mu/\beta)^{1/2}]^2 + v_2^2} \quad [1]$$

Lawden then defines dimensionless parameters x, y by

$$u_1 = x\sqrt{\mu/\alpha} \qquad v_1 = y\sqrt{\mu/\alpha} \quad [2]$$

$$u_0 = x_0\sqrt{\mu/\alpha} \qquad v_0 = y_0\sqrt{\mu/\alpha} \quad [3]$$

This transformation reduces the problem to minimizing

$$\sqrt{(x - x_0)^2 + (y - y_0)^2} + \sqrt{x^2 - 2r^{3/2}x + y^2 + 3r - 2} \quad [4]$$

subject to

$$(1 - r^2)x^2 + y^2 \geq 2(1 - r) \quad [5]$$

where $r = \alpha/\beta$.

For the case where r is approximately unity, an analytic estimate can be given. An example of this is transfer from anywhere on a nearly circular orbit to a higher energy neighboring circular orbit (see Fig. 1). A second example is transfer from the near apogee region of an elliptic orbit to a higher energy circular orbit (see Fig. 2).

Case 1

Consider a small quantity $\epsilon > 0$. Let

$$r = 1 - \epsilon \quad [6]$$

Rewrite Equation [4] as

$$\sqrt{(x - x_0)^2 + (y - y_0)^2} + \sqrt{(x - r^{3/2})^2 + y^2 + (3r - 2 - r^3)} \quad [7]$$

Using Equation [6], and omitting terms in ϵ of order higher than one, Equations [7 and 5] become

$$\sqrt{(x - x_0)^2 + (y - y_0)^2} + \sqrt{[x - 1 + (3/2)\epsilon]^2 + y^2} \quad [8]$$

$$x^2 + (y^2/2\epsilon) \geq 1 \quad [9]$$

Equations [8 and 9] can be given a geometric interpretation. The first member of [8] represents the distance from (x, y) to (x_0, y_0), the second the distance from (x, y) to $[1-(3/2)\epsilon, 0]$. The constraint given by Equation [9] says (x, y) must lie on or outside the ellipse given by the equality in Equation [9]. As is presented in Fig. 3, any point on the dashed line connecting (x_0, y_0) to $[1 - (3/2)\epsilon, 0]$ gives the minimum characteristic velocity. Once (x_{opt}, y_{opt}) is found $(u_{1,opt}, v_{1,opt})$ is given by Equation [2]. From Lawden's results the second impulse is determined.

A second case of interest occurs for r slightly greater than unity (see Fig. 4).

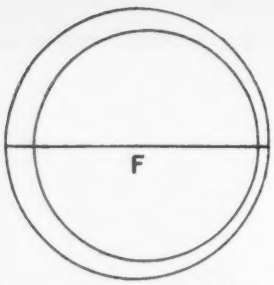

Fig. 1 Transfer from nearly circular orbit to a circular orbit

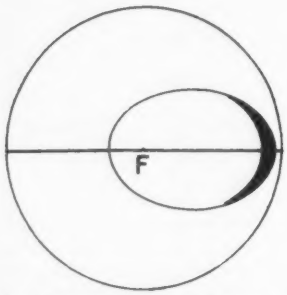

Fig. 2 Transfer from near apogee region to a circular orbit

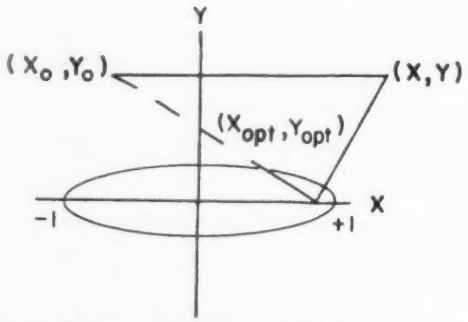

Fig. 3 Optimum solution for r slightly less than unity

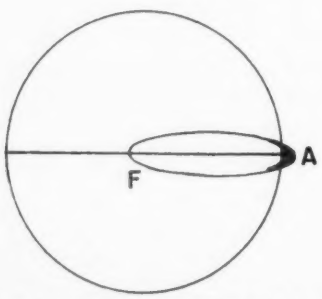

Fig. 4 Transfer from outside of circular orbit to circular orbit

Received June 4, 1959.

[1] Dynamics Group, Research Mathematician. Member ARS.

[2] Systems Section, Research Dynamicist.

[3] Numbers in parentheses indicate References at end of paper.

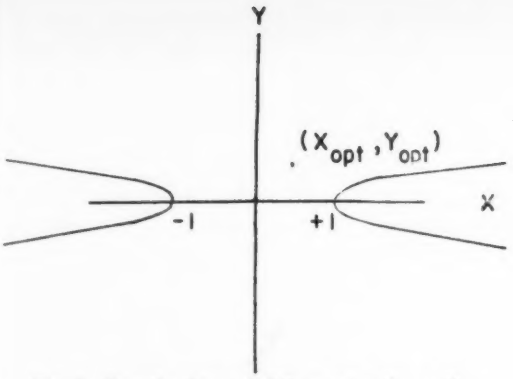

Fig. 5 Transfer for r slightly greater than unity

Case 2

Consider a small quantity $\epsilon > 0$

$$r = 1 + \epsilon \qquad [10]$$

To a first-order approximation Equations [8 and 9] become

$$\sqrt{(x - x_0)^2 + (y - y_0)^2} + \sqrt{\{x - [1 + (3/2)\epsilon]\}^2 + y^2} \qquad [11]$$

$$x^2 - \frac{y^2}{2\epsilon} \leqq 1 \qquad [12]$$

The solution to this minimum problem, owing to constraint [12], is given by some (x, y) in the region (see Fig. 5) between the two branches of a hyperbola. There are two subcases here of interest:

1 Coordinate (x_0,y_0) lies inside the branch containing $[1 + (3/2)\epsilon, 0]$. The minimum is given by the point of nearest tangency of an ellipse with foci at (x_0, y_0), $(1 + (3/2)\epsilon, 0)$, and the branch of the hyperbola (see Fig. 6). Courant and Robbins (2) have treated this type of minimum problem.

2 Coordinate (x_0,y_0) lies anywhere in the plane outside of the region given by subcase 1. For this situation the answer is found by joining (x_0,y_0) to $[1 + (3/2)\epsilon, 0]$ and choosing any (x, y) on this line lying in the region (see Fig. 7).

A different case of interest is for r close to zero. An example of this is transfer of a space vehicle near the Earth's surface to a higher energy circular orbit at a considerable distance from the Earth's surface (see Fig. 8).

Case 3

Consider a small quantity $\epsilon > 0$. Let

$$r = \epsilon \qquad [13]$$

Neglecting terms in ϵ higher than first order, Equations [4 and 5] become

$$\sqrt{(x - x_0)^2 + (y - y_0)^2} + \sqrt{x^2 + y^2 - 2 + 3\epsilon} \qquad [14]$$

$$x^2 + y^2 - 2 \geqq -2\epsilon \qquad [15]$$

Lawden concludes in his analysis that the answer to the minimum problem occurs on the boundary given by the equality in Equation [15]. This reduces Equation [14] to

$$\sqrt{(x - x_0)^2 + (y - y_0)^2} + \sqrt{\epsilon} \qquad [16]$$

From Equation [16] we observe the answer is given as the intersection point of the normal from (x_0,y_0) to the circle given by the equality in Equation [15].

Lawden's results are confirmed if a geometric interpretation is given to Equations [14 and 15] (see Fig. 9). The first member of Equation [14] gives the distance from (x, y) to

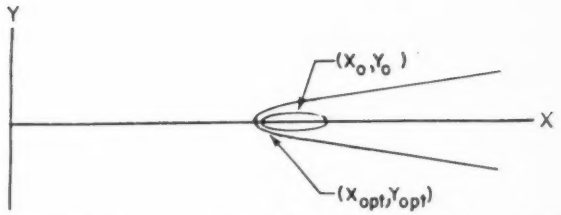

Fig. 6 Optimum transfer for (x_0, y_0) lying inside branch of hyperbola

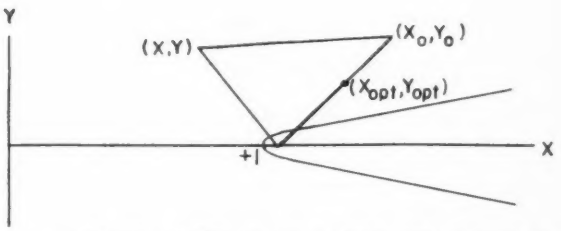

Fig. 7 Optimum solution for (x_0, y_0) lying outside branch of hyperbola

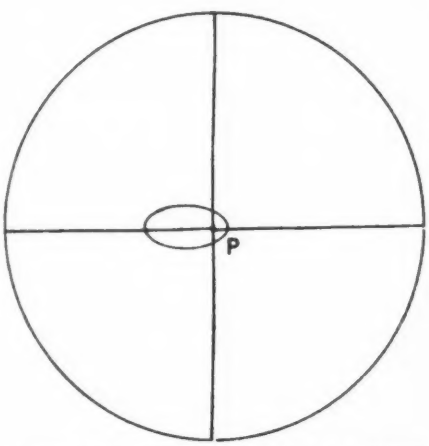

Fig. 8 Transfer from near Earth's surface to a distant circular orbit

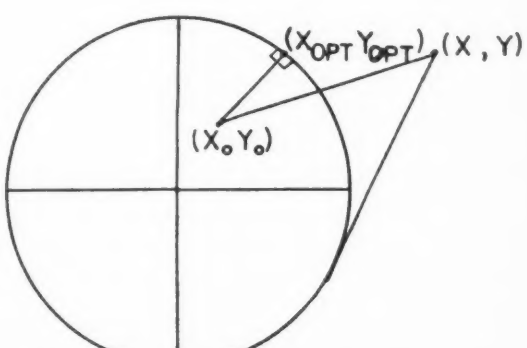

Fig. 9 Optimum solution for transfer from near Earth's surface to a distant circular orbit

(x_0, y_0), the second gives the length of the tangent from (x, y) to the boundary curve given by the equality in Equation [15]. The normal distance is less than the sum of any other two distances.

Acknowledgment

The authors would like to thank G. E. Taylor of the Dynamics Group for his efforts in helping complete this problem.

Nomenclature

u = velocity component perpendicular to the radius vector
v = velocity component along the radius vector
α = distance from focus of point on elliptic orbit
β = radius of higher energy circular orbit
μ = gravitational constant
x = dimensionless parameter related to u
y = dimensionless parameter related to v
r = ratio of α to β
ϵ = small positive quantity

References

1 Lawden, D. F., "Entry into Circular Orbits—I," *J. Brit. Interplanet. Soc.*, vol. 10, no. 1, pp. 5–17, Jan. 1951.

2 Courant, R. and Robbins, H., "What Is Mathematics?," Oxford University Press, New York, pp. 338–341.

Projected Orbits of 24-hr Earth Satellites

LOUIS B. WADEL[1]

Chance Vought Aircraft, Inc., Dallas, Texas

The projected orbit of a 24-hr Earth satellite is a "figure 8," oriented north-south and centered at the Equator. This path is calculated in terms of latitude and longitude as a function of the angle made by the satellite's orbital plane with the Earth's equatorial plane. If this angle is zero, the path reduces to a single point on the Equator.

A SATELLITE in a circular orbit about the Earth (assumed spherically symmetrical) will have a period of rotation equal to the Earth's rotational period if its altitude above the surface of the Earth equals approximately 22,000 miles (1).[2] If the orbit lies in the plane of the Equator and the satellite moves eastward, the projection of the orbit upon the Earth's surface consists of a single stationary point on the Equator.

If the orbit makes an angle α with the equatorial plane, the orbit's projection is a closed "figure 8" path, oriented north-south, centered at the Equator which it crosses at 12-hr intervals, and reaching extreme latitudes of $\pm\alpha$. Detailed properties of this path are calculated below as a function of α.

The projected path will be obtained by first calculating the projected orbit's great circle path in terms of latitude and longitude for a fictitious nonrotating Earth, and then modifying the results to account for the Earth's rotation. The general equation for a great circle is (2)

$$\cos\phi = c_1 \sin\phi \cos\theta + c_2 \sin\phi \sin\theta \qquad [1]$$

where

θ = east longitude
ϕ = 90 deg − λ
λ = north latitude

Crossing of the Equator may be assumed to occur at $\theta = 0$, and the resultant path shifted later to any other crossing point desired. The Equation [1] must be satisfied by the point $\theta = 0$, $\phi = 90$ deg, requiring $c_1 = 0$, and consequently

$$c_2 \tan\phi \sin\theta = 1 \qquad [2]$$

Differentiating Equation [2] and setting $d\phi/d\theta = 0$ yields

$$c_2 = \cot\phi_m = \tan\lambda_m = \tan\alpha \qquad [3]$$

where ϕ_m is minimum ϕ obtained, corresponding to λ_m, maximum latitude reached. The great circle Equation [2] can now be expressed as

$$\tan\alpha \tan\phi \sin\theta = 1$$

or

$$\tan\alpha \cot\lambda \sin\theta = 1 \qquad [4]$$

On the surface of a sphere the equation for differential element of arc length ds is given (2) by

$$(ds)^2/R_e^2 = [1 + \sin^2\phi(d\theta/d\phi)^2](d\phi)^2 \qquad [5]$$

where R_e = radius of the sphere (Earth).

Equation [5] may be divided by $(dt)^2$ and, for the present case of constant speed travel, ds/dt set equal to a constant V. Then, utilizing the relation [4] between ϕ and θ, Equation [5] may be integrated to yield

$$\sin\lambda = \sin\alpha \sin(V/R_e)t = \sin\alpha \sin\omega_e t = \sin\alpha \sin 2\pi t \qquad [6]$$

where

ω_e = angular velocity of Earth in radians per day = 2π
t = time in days measured from time of Equator crossing

Equation [4] may be rearranged as

$$\sin\theta = \cot\alpha \tan\lambda \qquad [7]$$

Once α is specified, latitude can be calculated as a function of time from Equation [6], and then longitude (for a nonrotating Earth) calculated from Equation [7]. The actual geographi-

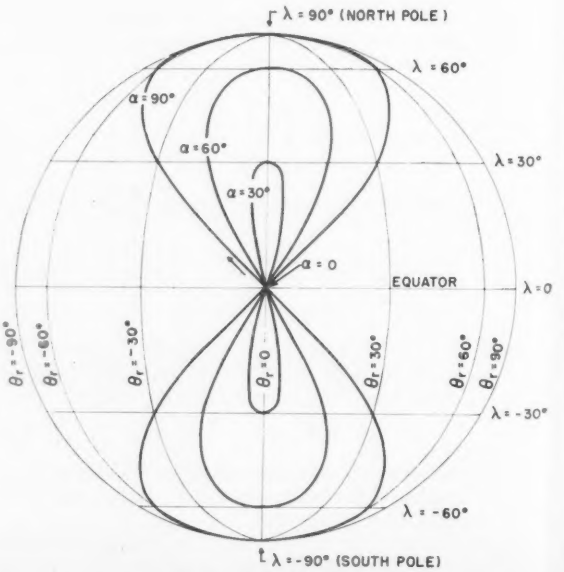

Fig. 1 Projected orbits

Received July 1, 1959.

[1] Supervisor, Missile Systems Evaluation.

[2] Numbers in parentheses indicate References at end of paper.

cal path projected on the surface of the rotating Earth has the same latitude as calculated above, but the longitude θ_r must be obtained from

$$\theta_r = \theta - \omega_\oplus t = \theta - 2\pi t \qquad [8]$$

Note also that the angle the projected path makes with the Equator is not α for the rotating Earth case.

By differentiating Equation [8], setting $d\theta_r/dt = 0$, and utilizing Equations [6] and [7], θ_{rm}, the first extreme value of θ_r, is found to occur at t_m, where

$$\sin 2\pi t_m = \frac{\sqrt{1 - \cos \alpha}}{\sin \alpha} \qquad [9]$$

and the corresponding value of θ_{rm} may be obtained from Equations [6, 7 and 8]. Knowing that $\lambda_m = \alpha$ (occurring for $\theta_r = 0$) and calculating θ_{rm} (and the corresponding λ as a by-product) as described previously allows quick sketches to be made of any projected paths of interest. Conditions of symmetry reduce the problem to calculating the first quarter period. Fig. 1 shows several such paths. The special case of $\alpha = 90$ deg (i.e., a polar orbit) is not included by Equation [4] which thereupon degenerates, but may be found (for the first quarter period) by setting $\theta = 0$, so that $\theta_r = -2\pi t$, and $\lambda = 2\pi t$.

References

1 Staff, Select (Congressional) Committee on Astronautics and Space Exploration, "Space Handbook: Astronautics and Its Applications," U. S. Government Printing Office, Washington, D. C., 1959.

2 Franklin, P., "Methods of Advanced Calculus," McGraw-Hill Book Co., Inc., New York, 1944.

Satellite Librations of Large Amplitude

W. B. KLEMPERER[1]

Douglas Aircraft Co., Inc., Santa Monica, Calif.

THE PROBLEM of small amplitude libration oscillations of satellites or pendulous devices aboard satellites has been treated in *Astronautica Acta* (1),[2] and it is further pursued by two Technical Notes in the present issue (2). How such oscillations behave when their amplitudes grow large has been discussed by Schindler (3). The purpose of the present remark is to add to the discussion the relatively simple exact solution of the simplified differential equation of motion of a dumbbell-shaped instrument of dimensions small compared to the radius of a circular orbit in which it is carried aboard a satellite and allowed to swing in the plane of the orbit.

The equation of motion then takes the form $\ddot{\phi} = -3\Omega^2 \times \sin \phi \cos \phi$ (where ϕ is the angular excursion from the local vertical and Ω the angular velocity of the orbital motion). It is once integrated by multiplying both sides of the equation by $2\dot{\phi}$ to yield the energy equation $\dot{\phi}^2 = \dot{\phi}_0^2 - 3\Omega^2 \sin^2 \phi$, where $\dot{\phi}_0$ is the angular velocity during the passage through the vertical $\phi = 0$. This immediately reveals that the maximum amplitude to be attained will be given by $\sin \phi_{max} = \dot{\phi}_0/\sqrt{3}\,\Omega$ and the motion is oscillatory only if $\dot{\phi}_0 < \sqrt{3}\,\Omega$; otherwise the dumbbell pendulum will swing past the horizontal and tumble. Furthermore it is readily seen that if the

Received July 17, 1959.

[1] Staff Assistant to Chief Engineer, Missiles and Space Systems. Member ARS.

[2] Numbers in parentheses indicate References at end of paper.

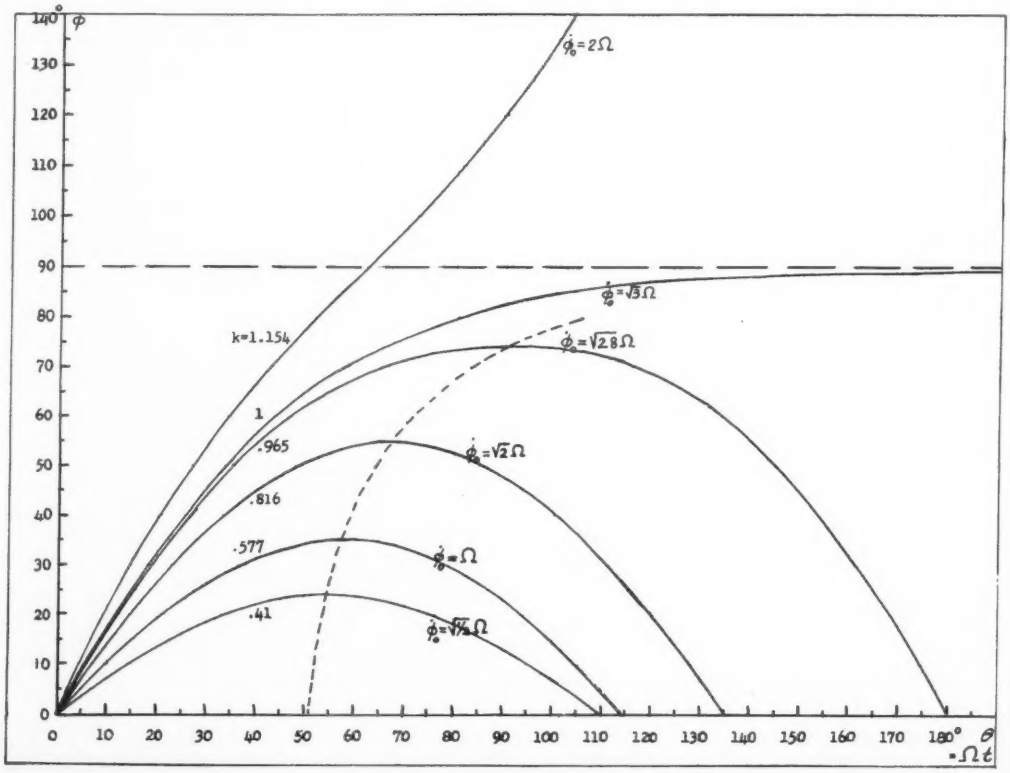

Fig. 1 Satellite librations

initial disturbance is deliberately made so that $\dot{\phi}_0 = \Omega$, as one might want it in order to stop the absolute rotation for a short period while taking telescopic time exposure photographs of distant celestial objects from aboard the satellite, then the swing amplitude will become $\phi_{max} = \sin^{-1}\sqrt{1/3} = 35.3$ deg. This is a case for which it might also be interesting to compute the time required for the pendulum to return to $\phi = 0$ where the speed would be brought back to $\dot{\phi} = 0$; this time turns out to be equal to the time it requires the satellite to travel over two radians of its orbit.

The solution of the time history of the pendulous motion is the integral of the reciprocal of the square root of the energy equation spelled out previously

$$t = \int d\phi/\sqrt{\dot{\phi}_0^2 - 3\Omega^2 \sin^2\phi}$$

For $\dot{\phi}_0 = k\sqrt{3}\,\Omega$, when $k > 1$, this reduces itself to the complete elliptic integral

$$t = (1/k\sqrt{3}\Omega) \int_0^{\pi/2} d\phi/\sqrt{1 - (1/k)^2 \sin^2\phi}$$

and the result is a continuous tumbling at a cyclically varying rate. If $k < 1$, the substitution $\sin\phi = k \sin\psi$ transforms the expression into the incomplete elliptic integral

$$t = (1/\sqrt{3}\Omega) \int d\psi/\sqrt{1 - k^2 \sin^2\psi}$$

for which the solution is periodic.

Three cases are of special interest:

1 $k = \sqrt{1/3} = 0.577$, which means $\dot{\phi}_0 = \Omega$ and for which the swing to maximum amplitude takes the same time as for the satellite to travel one radian.

2 $k = 0.965$ for which the period of the oscillation is the same as that of the orbit.

3 The borderline case for $k = 1$ or $\dot{\phi}_0 = \sqrt{3}\Omega$ for which the motion aperiodically and asymptotically approaches the horizontal. In this case the elliptic integral degenerates into the simple form

$$t = (1/\sqrt{3}\Omega) \int_0^{\phi} \sec\phi\, d\phi = (1/\sqrt{3}\,\Omega) \ln \tan(\pi/4 + \phi/2)$$

Fig. 1 depicts the time history of the motion plotted in terms of excursion ϕ against the angle $\theta = \Omega t$ subtended by the satellite orbital motion in the meantime, for the three special cases just described and for several other example cases, one of lesser and one of intermediate amplitude and one tumbling.

Incidentally, the motion of the dumbbell, as here described, is of a character closely related to that of a conventional pendulum of length l swinging from an Earth-fixed fulcrum, for which the equation of motion to large excursion is $\ddot{\phi} = -(g/l)\sin\phi$; this is solved by the same kinds of elliptic integrals, but with the argument $\phi/2$ instead of ϕ.

These derivations, interesting as they are, are limited to the dumbbell configuration. If analogous reasoning were applied to the case of a more compact body then the motion would appear slowed down by an appropriate factor. Furthermore, the findings apply strictly to a satellite in circular orbit around a central body endowed with a spherically symmetrical gravity field. If the orbit is elliptical or if the field has quadrupole character or possesses anomalies, pertubations enter into the picture.

References

1 Klemperer, W. B. and Baker, R. M. L., Jr., "Satellite Librations," *Astronautica Acta*, vol. III, fasc. 1, 1957, pp. 16–27 and vol. III, fasc. 3.

2 Baker, R. M. L., Jr., "Librations on a Slightly Eccentric Orbit," ARS JOURNAL, vol. 30, no. 1, Jan. 1960, pp. 124–126; "Plane Libration of a Prolate Ellipsoidal Shell," *ibid.*, pp. 126–128.

3 Schindler, G. M., "On Satellite Liberations," ARS JOURNAL, vol. 29, no. 5, May 1959, pp. 368–370.

Librations on a Slightly Eccentric Orbit[1]

ROBERT M. L. BAKER Jr.[2]

University of California, Los Angeles, Calif.

Aside from an idealized circular orbit assumed by Klemperer and Baker, satellite libration phenomena, and hence passive stability also, occur with bodies traveling on orbits of small but finite eccentricity. In such a case, the motion of the satellite about a position of stable equilibrium is found to be a solution to Mathieu's equation with an amplitude in radians less than or equal to the orbital eccentricity.

IMPLICIT in the analysis of a paper by Klemperer and Baker (1),[3] which dealt with the libration in the orbit plane of an idealized dumbbell and a solid ellipsoid, was a constant angular rotation of the dumbbell system at a velocity of n radians per unit time, (i.e., n stands for the mean daily motion).[4] Of course, such a constant rotational velocity did not affect the dynamical equations of the system, since the orbit was perfectly circular and the geocenter effectively rotated about the dumbbell exactly in step with the dumbbell's constant rotation. In the case of an elliptical orbit the geocenter does not keep pace with this constant angular velocity but rather leads it from the perigee to apogee and lags it from apogee to perigee. See Fig. 1. This angle of lead or lag is simply the difference between the true anomaly v and the mean anomaly M of the satellite; i.e., the constantly rotating axis of the dumbbell makes one revolution per orbital period, and therefore its angle with respect to an inertial direction in space is simply $M = M_0 - n(t - t_0)$, where

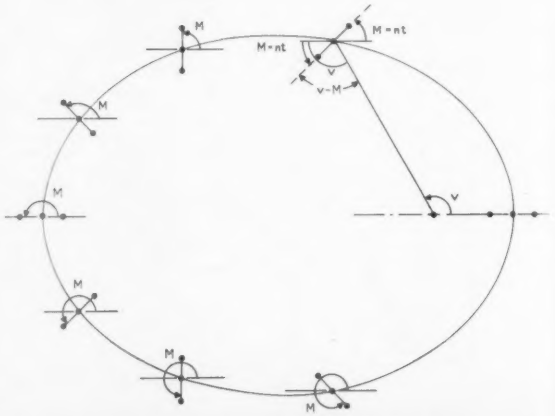

Fig. 1 Motion of a uniformly rotating dumbbell (no librations)

Received July 1, 1959.

[1] This paper presents the results of a study initiated at Douglas Aircraft Co. in 1957 and continued at Aeronutronic Systems, Inc., in June 1958, and published by Aeronutronic Systems as Report no. U-225, dated July 3, 1958.

[2] Acting Assistant Professor of Astronomy; also Staff Member, Aeronutronic Systems, Inc., Newport Beach, Calif. Member ARS.

[3] Numbers in parentheses indicate References at end of paper.

[4] The notation used in this note differs from that of the referenced report (1) in that L replaces e (the half-length of the dumbbell arm), n replaces Ω (the angular velocity of the orbital revolution), F_G replaces G (magnitude of the gravitational force), and $k_s^2\, m/r^2$ replaces $mg\, R^2/r^2$ for the variation of the gravitational force.

M_0 is the value of the mean anomaly at the epoch t_0, and n is the mean daily motion in radians per unit time.

As a result of their different distances from the geocenter, the two spheres suffer different attractions

$$F_{G1} = k_e^2\, m/r_1^2 \qquad [1a]$$

$$F_{G2} = k_e^2\, m/r_2^2 \qquad [1b]$$

where

F_G = gravitational force
k_e = geocentric gravitational constant
m = mass of a dumbbell sphere
r = radial distance from the geocenter

Subscripts 1 and 2 refer to dumbbell spheres 1 and 2.

The respective leverages a_1 and a_2 of these attractive forces are now

$$a_1 = [r\, L \sin(\phi + v - M)]/r_1 \qquad [2a]$$

$$a_2 = [r\, L \sin(\phi + v - M)]/r_2 \qquad [2b]$$

as can readily be seen from Fig. 2, where L is the half-length of the dumbbell connecting rod and ϕ is the angular departure from the constantly rotating reference axis (ϕ is measured negatively).

Hence, the net torque due to the different attraction forces is

$$T = F_{G1}\, a_1 - F_{G2}\, a_2 = k_e^2\, m\, r\, L \sin(\phi + v - M)\,(1/r_1^3 - 1/r_2^3) \qquad [3]$$

The centrifugal force torques cancel out and contribute nothing.

So long as the dimension L is very small compared to any orbital radius r, the individual radii can be approximated by $r_1 \cong r - L\cos(\phi + v - M)$ and $r_2 \cong r + L\cos(\phi + v - M)$. Introducing these into Equation [3] and expanding the reciprocal cubes into a series of power terms, we find that the torque equation becomes

$$T = (6k_e^2 mL2/r^3)\sin(\phi + v - M)\cos(\phi + v - M) \qquad [4]$$

For an elliptical orbit of small eccentricity, e, r can be expressed approximately as

$$r \cong a\,(1 - e\cos M) \qquad [5]$$

Expanding $1/r^3$ for small eccentricity e, we find that

$$T = (6k_e^2/a^3)\, mL^2\,(1 + 3e\cos M)\sin(\phi + v - M) \times \cos(\phi + v - M) \qquad [6a]$$

Furthermore, assuming the angle $(\phi + v - M)$ to be small, we have

$$T = (6k_e^2/a^3)\, mL^2\,(1 + 3e\cos M)\,(\phi + v - M) \qquad [6b]$$

From (2), p. 171, Equation [64]

$$v - M \cong 2e\sin M$$

Also, it should be noted that

$$k_e^2\, P^2 = (2\pi)^2 a^3 \quad \text{or} \quad k_e^2/a^3 = (2\pi/P)^2 = n^2$$

(P is the period of the orbit.) Therefore

$$T = 6n^2\, mL^2\,[(1 + 3e\cos M)\,(\phi + 2e\sin M)] \qquad [6c]$$

where terms of order e^2 are neglected.

If the dumbbell is allowed to swing in response to this torque, the result will be an angular acceleration $\ddot{\phi}$ (in the uniformly rotating reference coordinate system) governed by

$$T = -2\, m\, L^2\, \ddot{\phi} \qquad [7]$$

the minus sign arising because ϕ has been counted negatively. Equating [6c and 7], we find that the part $2\, m\, L^2$

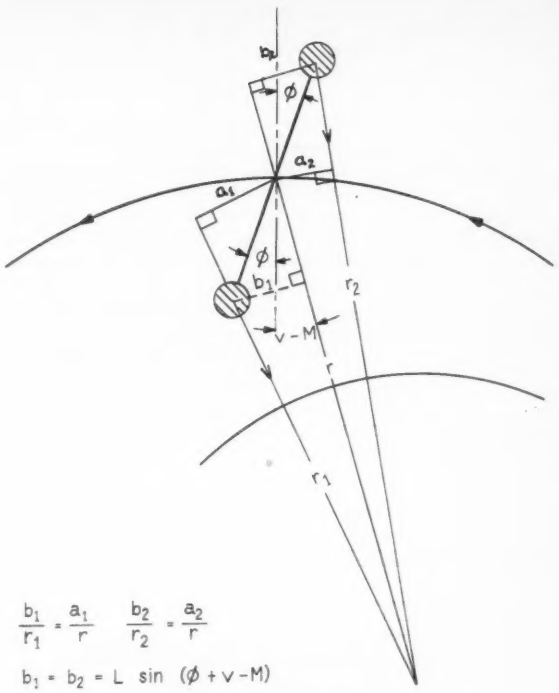

Fig. 2 Dumbbell librations of an eccentric orbit

cancels out and

$$\ddot{\phi} = -3n^2(1 + 3e\cos M)\,\phi + 2e\sin M \qquad [8a]$$

or

$$\ddot{\phi} + 3n^2(1 + 3e\cos nt)\,\phi = -6n^2 e\sin nt \qquad [8b]$$

If z, α and q are defined as

$$z \triangleq \frac{M}{2} = \frac{M_0 + n(t - t_0)}{2} = \frac{n}{2}\,t,\ (M_0 = n\,t_0)$$

$$\alpha \triangleq 12$$

$$q \triangleq (9/4)\,e$$

then Equation [8] becomes

$$\frac{d^2\phi}{dz^2} + (\alpha + 16\,q\cos 2z)\,\phi = -\frac{32}{3}\,q\sin 2z \qquad [9]$$

which is the canonical form of Mathieu's equation with a forcing function of $-(32/3)\,q\sin 2z$; see (3).

The prolate spheroid analysis follows along very similar lines. Utilizing the relations from (1), it is readily seen that

$$\ddot{\phi} + 3n^2 K^2(1 + 3e\cos nt)\,\phi = 6n^2 e K^2\sin nt \qquad [10]$$

where

$$K^2 \triangleq \epsilon^2/(2 - \epsilon^2)$$

and ϵ is the eccentricity of the prolate spheroid. Thus

$$\alpha = 12K^2$$

$$q = (9/4)\,K^2 e$$

The solution of Mathieu's equation follows along two somewhat different lines. Its application to physics involves finding the appropriate constant values of α (depending of course on q) such that the equation possesses a periodic solu-

tion. Problems of this type arise in connection with tidal waves in a cylindrical vessel having an elliptic boundary, certain forms of steady vortex motion in an elliptic cylinder, the decay of magnetic force in a metal cylinder, etc. (4). For astronomical problems (such as determining the motion of the lunar perigee) α and q are known constants and one attempts to solve for the (usually) aperiodic function.[6]

In our general discussion of libration, both of these problems are relevant. With the geometry and orbit of the moon or of the satellite specified, we can only determine the (usually) aperiodic motion. However, if the orbit parameters and the moment of inertia of the satellite can be varied then we may choose to seek out the constants of the system leading to a periodic solution. Because of the complications arising from the forcing functions, an analytical solution to the problem is not very promising and recourse to an electronic computer is indicated. Such work has been carried out by Stocker and Vachino (6) and by Robinson (7).

Tne author wishes to acknowledge the many helpful suggestions and comments made by Drs. W. B. Klemperer, Eric Durand and L. G. Walters during the preparation of this note.

[6] Actually Hill's equation is used in lunar theory. It is a slightly more general relation involving an infinite series in cos $2nz$. See (5).

References

1 Klemperer, W. B. and Baker, R. M. L., Jr., "Satellite Librations," *Astronautica Acta*, vol. III, fasc. 1, 1957, pp. 16–27 and vol. III, fasc. 3.
2 Moulton, F. R., "Introduction to Celestial Mechanics," Macmillan Co., New York, 1914.
3 Margenau, H. and Murphy, G. M., "The Mathematics of Physics and Chemistry," D. Van Nostrand Co., Princeton, N. J., 1956.
4 Whittaker, E. T. and Watson, G. N., "A Course of Modern Analysis," Cambridge University Press, New York, 1953.
5 Smart, W. M., "Celestial Mechanics," Longmans, Green and Co., New York, 1953.
6 Stocker, T. A. J. and Vachino, R. F., "The Two-Dimensional Librations of a Dumbbell-Shaped Satellite in a Uniform Gravitational Field," Thesis, USAF Institute of Technology, Wright-Patterson Air Force Base, Ohio.
7 Robinson, A. C., "On the Three-Dimensional Librations of a Dumbbell-Shaped Satellite Over an Oblate Earth," WCLJY Internal Memo 58-54, Wright-Patterson Air Force Base, Ohio.

Plane Libration of a Prolate Ellipsoidal Shell[1]

ROBERT M. L. BAKER Jr.[2]

University of California, Los Angeles, Calif.

A satellite in the form of a thin prolate ellipsoidal shell contained between two similar ellipsoids is assumed to resolve in a steady circular orbit around the Earth. It rotates essentially so as to show the same pole of its major axis to the Earth, except for a small angular oscillation (libration) superimposed on this rotation and, consequently, behaves in a similar fashion to the solid ellipsoid analyzed by Klemperer and Baker.

LET A Cartesian coordinate system uvw be defined as having its origin in the mass center of the satellite, its w axis coincident with the radius vector from the geocenter, while the v and u axes are in and normal to the plane in which an oscillation of the long figure axis ($a - a'$) of the ellipsoid against the radius vector axis w lies. (This plane may be conceived as coincident with the plane of the orbit, but the solution is not confined to this restriction.) See Fig. 1. At the instant t the angular excursion between a and w shall be denoted by ϕ. In order to break down the mass of the thin ellipsoidal shell into infinitesimal particles it is convenient also to introduce a cylindrical coordinate system X, y, θ, solidly and symmetrically anchored in the ellipsoid, where X is the axial coordinate, y the radius in the body of revolution which assumes the value Y_1 at the inner surface and Y_2 at the outer surface, and θ is the azimuth angle counted from the u direction, as illustrated in Fig. 2.

An increment of mass in the prolate ellipsoid having a density ρ is

$$dm = \rho\, y\, d\theta\, dy\, dX \qquad [1]$$

The distance of this increment above (or below) the uw plane is

$$w = X \cos\phi + y \sin\theta \sin\phi \qquad [2]$$

See Fig. 3.

For every small ϕ this is, with close approximation

$$w = X + (y \sin\theta)\phi \qquad [3]$$

Since the prolate ellipsoid is symmetrical about the vw plane, it suffices to consider the moment of $2dm$ integrated from $\theta = -\pi/2$ to $+\pi/2$, and acting on the arm L which is the distance from the projection of the increment dm on the vw plane to the center of mass. If dF is the incremental force acting on $2dm$ and α is the angle of L with respect to the v

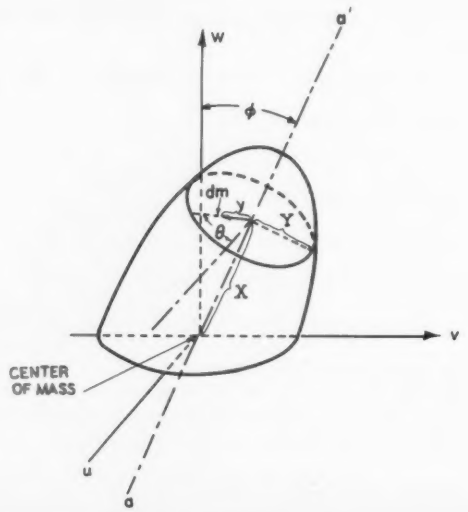

Fig. 1 Coordinate system

Received July 1, 1959.

[1] This paper presents the results of a study initiated at Douglas Aircraft Co. in 1957 and continued at Aeronutronic Systems, Inc. in June 1958, and published by Aeronutronic Systems as Report no. U-225, dated July 3, 1958.

[2] Acting Assistant Professor of Astronomy; also Staff Member Aeronutronic Systems, Inc., Newport Beach, Calif. Member ARS.

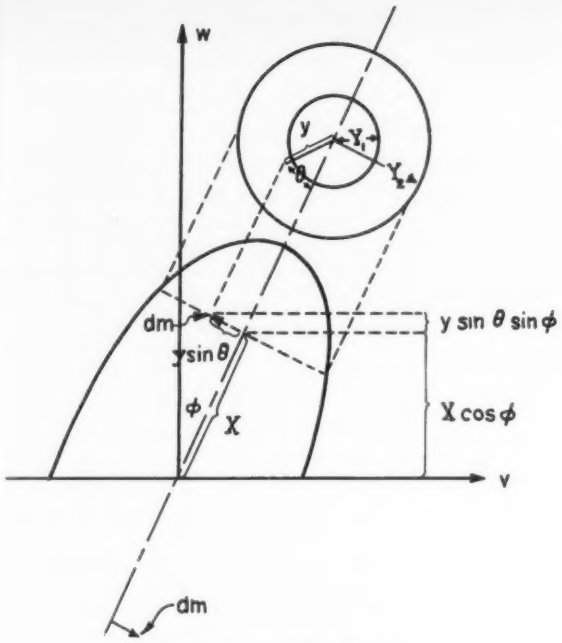

Fig. 2 Symmetrical masses

axis, then the incremental moment $= L\,dF\cos\alpha$, where the leverage is, as readily gleaned from Fig. 4

$$L\cos\alpha = X\sin\phi - y\sin\theta\cos\phi \qquad [4a]$$

which for small ϕ is approximately

$$L\cos\alpha = X\phi - y\sin\theta \qquad [4b]$$

Analogous to Equation [2] of Klemperer's and Baker's paper,[3] the incremental torque due to the symmetrical pair of increments of mass above and below the uv plane as per Equation [4a] (situated symmetrically with respect to the center of mass of the ellipsoid) is

$$dT = 2dmrL\cos\alpha(1/r_1^3 - 1/r_2^3)k_e^2 \qquad [5]$$

where

$$r_1 = r[1 - (L/r)\sin\alpha]$$

and

$$r_2 = r[1 + (L/r)\sin\alpha] \qquad [6]$$

Approximately

$$1/r_1^3 \cong (1/r^3)[1 + (3/r)L\sin\alpha]$$

and

$$1/r_2^3 \cong (1/r^3)[1 - (3/r)L\sin\alpha] \qquad [7]$$

Noting that for the circular orbit $k_e^2/r^3 = n^2$, we find that the incremental restoring moment caused by the antisymmetrical pair of symmetrical $2dm$ acting on the leverage [4a] now reads

$$dT = 2dmn^2\cdot 6(X\cos\phi + y\sin\theta\sin\phi)\cdot (X\sin\theta - y\sin\theta\cos\phi) \qquad [8a]$$

and for small ϕ

$$dT \cong 12dmn^2(X + y\phi\sin\theta)\cdot(X\phi - y\sin\theta)$$
$$= 12dmn^2(X^2\phi - Xy\sin\theta - y^2\phi\sin^2\theta) \qquad [8b]$$

[3] Klemperer, W. B. and Baker, R. M. L., Jr., "Satellite Librations," *Astronautica Acta*, vol. 3, fasc. 1, 1957, pp. 16–27, and vol. 3, fasc. 3.

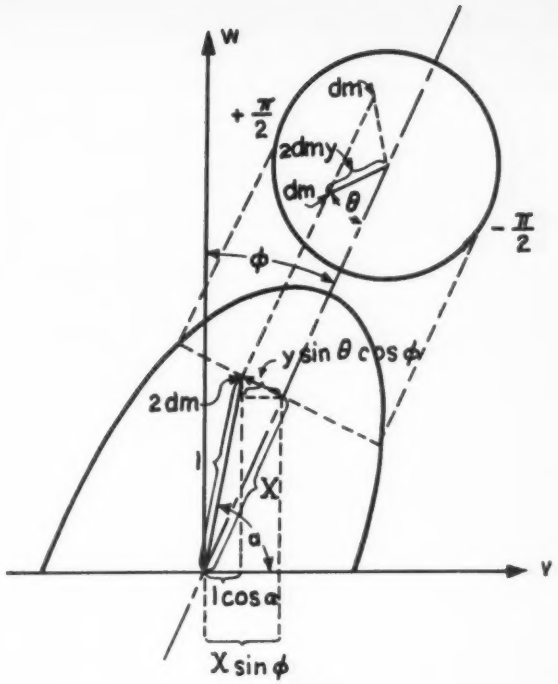

Fig. 3 Geometry

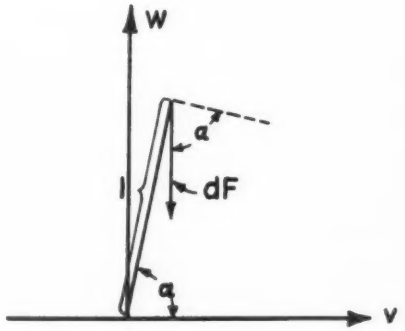

Fig. 4 Lever arm

The torque equation becomes

$$I\ddot{\phi} = -12n^2\rho\int_{-\pi/2}^{\pi/2}d\theta\int_0^a dX\int_{Y_1}^{Y_2}dy\,(X^2\phi - Xy\sin\theta - y^2\phi\sin^2\theta)y$$

Integrating θ from $-\pi/2$ to $\pi/2$, we find that the $\sin\theta$ drops out and

$$I\ddot{\phi} = -12n^2\rho\pi\phi\int_0^a dX\int_{Y_1}^{Y_2}ydy(X^2 - y^2/2)$$
$$= -6n^2\rho\pi\phi\left[\int_0^{a_2}(Y_2^2X^2 - Y_2^4/4)dX - \int_0^{a_1}(Y_1X^2 - Y_1^4/4)dX\right] \qquad [9]$$

For the generatrix ellipse $Y_1^2/b_1^2 + X^2/a_1^2 = 1$, where a_1 and b_1 are the semimajor and semiminor axes of the inner surface. Therefore

$$Y_1^2 = b_1^2 - (b_1/a_1)^2X^2 \quad 1\to 2 \qquad [10]$$

The integral of Equation [9] is for either surface

$$-(b^4/4)\cdot\int_0^a dX + (b^2 + b^4/2a^2)\cdot\int_0^a X^2dX - (b^2/a^2 + b^4/4a^2)\cdot\int_0^a X^4dX = \frac{2}{15}ab^2(a^2 - b^2) \quad [11]$$

$$I\ddot{\phi} = -n^2\pi\rho(4/5)[a_2b_2^2(a_2^2 - b_2^2) - a_1b_1^2(a_1^2 - b_1^2)]\phi \quad [12a]$$

Let the semi-axes of the inner and outer ellipsoidal surfaces be

$$a_1 = a,\ b_1 = b \text{ and } a_2 = a(1 + \mu),\ b_2 = b(1 + \mu)$$

therefore

$$I\ddot{\phi} \cong -n^2\pi\rho(4\cdot 5/5)\mu\, ab^2(a^2 - b^2)\phi \quad [12b]$$

where μ^2 has been neglected.

For a thin ellipsoidal shell

$$I = m(a^2 + b^2)/3 \quad [13]$$

$$m = (4/3)\pi\rho(a_2b_2^2 - a_1b_1^2) \quad [14a]$$

$$\cong (4/3)\pi\rho\ 3\mu ab^2 \quad [14b]$$

Therefore

$$\ddot{\phi} = \frac{-n^2\pi\rho 4\mu ab^2(a^2 - b^2)}{4\pi\rho\mu ab^2(a^2 + b^2)/3}\phi = -n^2\,3\,\frac{(a^2 - b^2)}{(a^2 + b^2)}\phi \quad [15]$$

which is less than the frequency of the dumbbell by the fraction $\sqrt{(a^2 - b^2)/(a^2 + b^2)}$, the same result as obtained for the solid homogeneous prolate ellipsoid found in Klemperer's and Baker's paper[3] Equation [20].

Introducing the numerical eccentricity ϵ of the prolate-ellipsoidal shell by the notation

$$\epsilon^2 \triangleq (a^2 - b^2)/a^2$$

we have

$$\sqrt{\frac{a^2 - b^2}{a^2 + b^2}} = \sqrt{\frac{\epsilon^2}{(2 - \epsilon^2)}} \triangleq K \quad [16]$$

Consequently, the frequency of the shell libration is given by

$$\omega = n\sqrt{3}\,K \quad [17]$$

The suggestions and contributions to this note made by W. B. Klemperer are gratefully acknowledged.

Effect of Thrust Misalignment on Gyro-Stabilized Vehicles

RUSSELL P. NAGORSKI[1]

Aerojet-General Corp., Azusa, Calif.

Consideration of thrust misalignment is a well-known factor in many flight control system dynamic analyses. This same undesired influence, if uncompensated, has the effect of causing the deviation of the velocity vector from the prescribed flight path with its attendant lateral excursion. The purpose of this paper is to present an analytical development of the significant expressions that effect the flight profile due to thrust misalignment.

Conventional Gyro-Stabilized Flight Control System

A TYPICAL control system can be represented as shown in Fig. 1 where the component time constants, small relative to the vehicle control period, are neglected.

The angular displacement θ is indicated by a displacement gyro; the angular rate $\dot{\theta}$ by a rate gyro; the summation of both in turn defines the orientation of the thrust vector γ. The orientation γ causes an angular acceleration of the vehicle to close the loop. From Fig. 1 a set of differential equations defining the motion can be established

$$K_1\theta + K_2\dot{\theta} = \gamma \quad [1]$$

$$-K_3\ddot{\theta} + \epsilon = \gamma \quad [2]$$

An expression for the vehicular axis orientation in the time domain can be deduced by equating Equations [1 and 2], thus

$$\theta(t) = \frac{\epsilon}{K_1}\left[1 + e^{at}\left(\frac{a}{b}\sin bt - \cos bt\right)\right] \quad [3]$$

where

$$a = -K_2/2K_3$$

$$b^2 = \frac{1}{K_3}\left(K_1 - \frac{K_2^2}{4K_3}\right)$$

Similarly an expression for the thrust vector orientation can be given by

$$\gamma(t) = \epsilon\{1 - e^{at}[\cos bt - (a/b)\sin bt]\} \quad [4]$$

The equation defining the time history of the lateral velocity vector component is derived by the basic equation

$$V_x(t) = T\int\frac{\gamma(t)}{M}\,dt \quad [5]$$

Neglecting the transient terms of Equation [4] and assuming a time-based function of mass of the form

$$M = M_0(1 - \alpha t) \quad [6]$$

the integrated solution to Equation [5] is seen to be

$$V_x(t) = (-T\epsilon/M_0\alpha)\ln(1 - \alpha t) \quad [7]$$

Subsequently, a further integration defines the lateral excursion, which is simply

$$X(t) = (T\epsilon/M_0\alpha^2)[(1 - \alpha t)\ln(1 - \alpha t) + \alpha t] \quad [8]$$

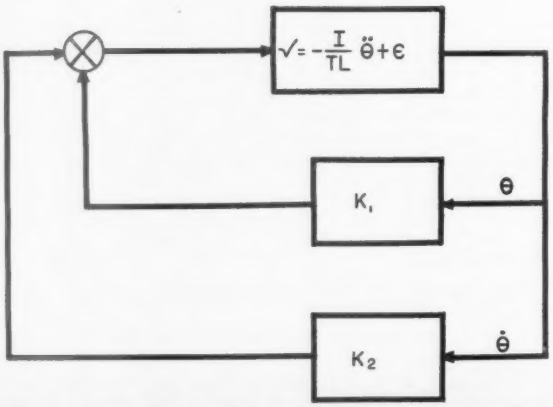

Fig. 1 Conventional attitude stabilization system schematic

Received July 13, 1959.

[1] Guidance and Communications Section, Systems Division. Member ARS.

In order to illustrate the utility of Equations [7 and 8], the following typical illustration is presented using the performance data from a typical booster stage using a 4.5ks-115000 solid in a particular multistaged vehicle:

Initial mass of combined stages, $M_0 = 240$ slugs.
Vehicle mass at burnout of booster stage, $M_{b0} = 122$ slugs.
Thrust (assumed constant during 4.5 sec burning period), $T = 115{,}000$ lb.
Possible thrust misalignment, $\epsilon = 1/2$ deg $= 0.0087$ radians.
Burning time, $T = 4.5$ sec.
Velocity at burnout, $V = 2{,}300$ fps.

Therefore

$$1 - \alpha t = (M_0 - M_{b0})/M_0 = 0.493$$

and

$$\alpha t = 0.507$$

also

$$\alpha = 0.113 \text{ sec}^{-1}$$

Substituting these values in Equation [7] results in $V_x = 26.1$ fps. Therefore the deviation of the velocity vector is seen to be $\psi = 26.1/2300 = 0.0135$ radian or 0.77 deg, a significantly large figure.

A similar substitution in Equation [8] would provide the lateral excursion with the parameters given. This is, however, usually considered of secondary importance, since many of the present-day missions have relatively large coast periods; consequently, the trajectory accuracy is essentially dependent on the velocity vector attitude accuracy as well as its magnitude.

Modified Gyro-Stabilized Flight Control System

If the dynamics of the system previously described were changed so as to include a linear acceleration feedback to the summing amplifier by means of a body mounted accelerometer, the schematic form would appear as shown in Fig. 2.

By the method of derivation previously demonstrated, a series of equations denoting the vehicle characteristics in the time domain can be evolved. These are

$$\theta(t) = \frac{\epsilon(1 - K_4)}{K_1}\left[1 + e^{ct}\left(\frac{c}{d}\sin dt - \cos dt\right)\right] \qquad [9]$$

where

$$c = -K_2/2K_3(1 - K_4)$$

$$d^2 = \frac{K_1}{K_3(1 - K_4)} - \frac{K_2^2}{4K_3^2(1 - K_4)^2}$$

and

$$\gamma(t) = \epsilon(1 - K_4)\{1 - e^{ct}[\cos dt - (c/d)\sin dt]\} \qquad [10]$$

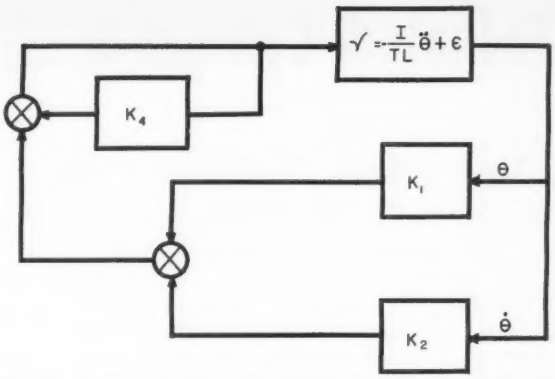

Fig. 2. Attitude stabilization system schematic with lateral acceleration feedback

Neglecting transient terms as before

$$V_x(t) = [-T\epsilon(1 - K_4)/M_0\alpha] \ln (1 - \alpha t) \qquad [11]$$

$$X(t) = [T\epsilon(1 - K_4)/M_0\alpha^2]\{(1 - \alpha t) \ln (1 - \alpha t) + \alpha t\} \qquad [12]$$

Here the usefulness of an acceleration feedback is illustrated, namely, that any finite positive value of accelerometer gain will tend to attenuate the undesired effect caused by thrust misalignment. In practice, the objective of the system engineer is to negate the effect of thrust misalignment by introducing an acceleration feedback as shown here with a unity gain value.

Nomenclature

I = moment of inertia, slug-ft^2
K_1 = displacement gain constant
K_2 = rate gain constant, sec
K_3 = dynamic constant $= I/Tl$, sec^2
K_4 = acceleration gain constant
l = moment arm, ft
M = instantaneous mass, slugs
M_0 = mass at time $t = 0$, slugs
M_{b0} = mass at burnout, slugs
t = time, sec
V = velocity along the principle axis, fps
V_x = velocity normal to the principle axis, fps
α = normalized flow rate, sec^{-1}
γ = orientation of the effective thrust vector, radian
θ = angular attitude displacement, radian
$\dot{\theta}$ = angular rate, radian/sec
ψ = velocity vector deviation due to thrust misalignment, radian

Technical Comments

Cutoff Impulse or Equivalent Time

S. L. BRAGG[1]

Rolls-Royce Ltd., Derby, England

IN A RECENT note, Kelly (1)[2] discussed the effect of the thrust termination process on the range dispersion of a ballistic missile. He concluded that variations of the cutoff impulse and of the missile mass at cutoff both contributed to appreciable dispersions. However, as is shown below, it is comparatively simple to arrange the guidance system so that errors due to the first source of variability are reduced and those due to the second source completely eliminated.

Suppose that the cutoff impulse, instead of being quoted directly as the actual impulse

$$I_{co} = \int_{c.o.}^{\infty} F\, dt$$

is specified by the equivalent cutoff time t_{co} defined by the equation

$$t_{co} = \frac{1}{F_{co}} \int_{c.o.}^{\infty} F\, dt = \frac{I_{co}}{F_{co}}$$

where F_{co} is the thrust just before cutoff. This equivalent time is, as it were, an overrun time. It is the time for which the motor would have to run at full thrust after the cutoff signal was given, in order to produce an impulse equal to the actual integrated cutoff value.

In conventional guidance systems the nominal cutoff impulse and nominal missile mass at cutoff are used to calculate the nominal increment in final velocity $(\Delta U_f)_{\text{nominal}} = (I_{co})_n/(M_{co})_n$. (The effect of the change in missile mass during cutoff is negligible.) The guidance system is arranged to signal cutoff when the missile velocity reaches a value $(\Delta U_f)_{\text{nominal}}$ less than the required one. Deviations of either I_{co} or M_{co} from the nominal values produce proportional error in ΔU_f.

Suppose on the other hand that the guidance system is arranged to measure the momentary missile acceleration a (as is inevitable in all inertial systems) and is arranged to signal cutoff when the missile velocity reaches a value at_{co} less than the required one. This value will vary slightly from flight to flight, compensating automatically for the variations of missile mass at cutoff.

For example a higher than nominal mass at cutoff will yield a low acceleration at that time. On the proposed system cutoff will then automatically be signaled at a slightly higher missile velocity than normal, so the final velocity will be correct.

Although errors due to variations in missile mass at cutoff are eliminated in this way, errors due to the variability of t_{co} will remain. These, however, are likely to be *smaller* than the errors arising from the variability of I_{co}. This is because variability of cutoff impulse arises from two main sources—variation of the sequencing and valve operating times, and variation of the thrust level of the engine at cutoff. The first source produces identical variabilities in I_{co} and t_{co}, but since the second source would be expected to increase I_{co} in the same proportion as F_{co}, it has *no* effect on t_{co}.

The proposed system has also a secondary advantage. It is unnecessary to alter the constants involved in computing the correct time to give the cutoff signal when an alternative range (that is, missile mass at cutoff) is required.

It is interesting to note that if we apply the analysis of Rodean (2) for instantaneous stoppage of propellants to a fixed geometry thrust chamber in vacuo, we find that

$$t_{co} = 2m_c/(k+1)\dot{m}$$

where

k = specific heat ratio
m_c = mass of gas in the chamber under steady running conditions
$\dot{m}$ = corresponding outflow rate

However, it appears unlikely that main propellant valves can in practice be closed in a time appreciably smaller than the gas residence time so this particular relation is of academic interest.

Received July 20, 1959.

[1] Chief Performance Engineer, Rocket Division. Member ARS.

[2] Numbers in parentheses indicate References at end of paper.

References

1 Kelly, A. J., "Effect of Thrust Termination Process Upon Range Dispersion of a Ballistic Missile," ARS JOURNAL, vol. 29, no. 6, June 1959, pp. 432–440.

2 Rodean, H. C., "Rocket Thrust Termination Transients," ARS JOURNAL, vol. 29, no. 6, June 1959, pp. 406–409.

Note on "Interplanetary Trajectories Under Low Thrust Radial Acceleration"

H. K. KARRENBERG[1]

Systems Corporation of America, Los Angeles, Calif.

THIS note presents corrections and additions to Copeland's[2] derivations of ϕ and τ for the specific cases, $\alpha = 1/9$ and $\alpha = 1/6$, and for the generalized case, $\alpha > 1/8$.

For the case $\alpha = 1/9$, Equations [21 and 22] should respectively read

$$\phi = \frac{3}{2} F\left(\theta, \frac{1}{2}\right) + \arctan \frac{3}{2} \frac{\tan\theta}{\sqrt{1 - (1/4)\sin^2\theta}}$$

$$\tau = 9F\left(\theta, \frac{1}{2}\right) - 6E\left(\theta, \frac{1}{2}\right)$$

For $\alpha > 1/8$, Equations [27 and 28] should respectively read

$$\tau = \frac{2}{\sqrt{2\alpha}} \left[\frac{1+\cos\theta}{\sin\theta} \sqrt{1 - k^2 \sin^2\theta} - F(\theta, k) + E(\theta, k) \right] + \text{constant}$$

$$\phi = \arcsin(k \sin\theta) - (1/\sqrt{8\alpha}) F(\theta, k) + \text{constant}$$

Received Aug. 17, 1959.

[1] Member Scientific Staff.

[2] Copeland, J., "Interplanetary Trajectories Under Low Thrust Radial Acceleration," ARS JOURNAL, vol. 29, no. 4, April 1959, pp. 267–271.

In order to conform with the previous cases the following two equations should be added for $\alpha = 1/6$

$$\tau = 2\sqrt{3}\left[\frac{1+\cos\theta}{\sin\theta}\sqrt{1-\frac{3}{4}\sin^2\theta} - F\left(\theta, \frac{\sqrt{3}}{2}\right) + E\left(\theta, \frac{\sqrt{3}}{2}\right) + F\left(\pi, \frac{\sqrt{3}}{2}\right) - E\left(\pi, \frac{\sqrt{3}}{2}\right)\right]$$

$$\phi = \text{arc sin}\left(\frac{\sqrt{3}}{2}\sin\theta\right) - \frac{\sqrt{3}}{2}F\left(\theta, \frac{\sqrt{3}}{2}\right) + \frac{\sqrt{3}}{2}F\left(\pi, \frac{\sqrt{3}}{2}\right)$$

In the middle of the right-hand column of p. 270,[2] the equation for r which indicates when escape velocity is reached should read

$$r = 1 + 1/2\alpha$$

Nomenclature

ϕ = angle subtended at sun between vehicle and point of departure from Earth's orbit
τ = nondimensional time
α = nondimensional vehicle acceleration
F = elliptic integral of the first kind
E = elliptic integral of the second kind

Use of Inert Gases in Flame Stabilization

P. ROY CHOUDHURY[1] and ALI BULENT CAMBEL[2]

Northwestern University, Evanston, Ill.

DIFFERENT aspects of the phenomena associated with the stabilization of premixed flames by gaseous jets have been reported previously in this Journal (1)[3] and elsewhere (2).

Received Oct. 1, 1959.

[1] Now Assistant Professor of Mechanical Engineering, University of Southern California, Los Angeles.

[2] Professor and Chairman of Mechanical Engineering. Fellow Member ARS.

[3] Numbers in parentheses indicate References at end of paper.

In earlier publications we had suggested that a small critical zone governs the mechanism of stabilization and that inert gases may not be useful as stabilizing media. Since then we have performed some experiments which indicate the need for modifying these descriptions.

Our studies indicate that in addition to the critical zone, there must be considered the influence of a diffusion and mixing interface as suggested in (2). Furthermore, we find that argon, nitrogen, carbon dioxide and helium may be used as stabilizer gases. However, we noticed that the behavior of carbon dioxide and helium was erratic.

The data obtained with argon and nitrogen are plotted in Fig. 1 and compared with those for air. As may be seen, two different pressures and three grid sizes are compared.

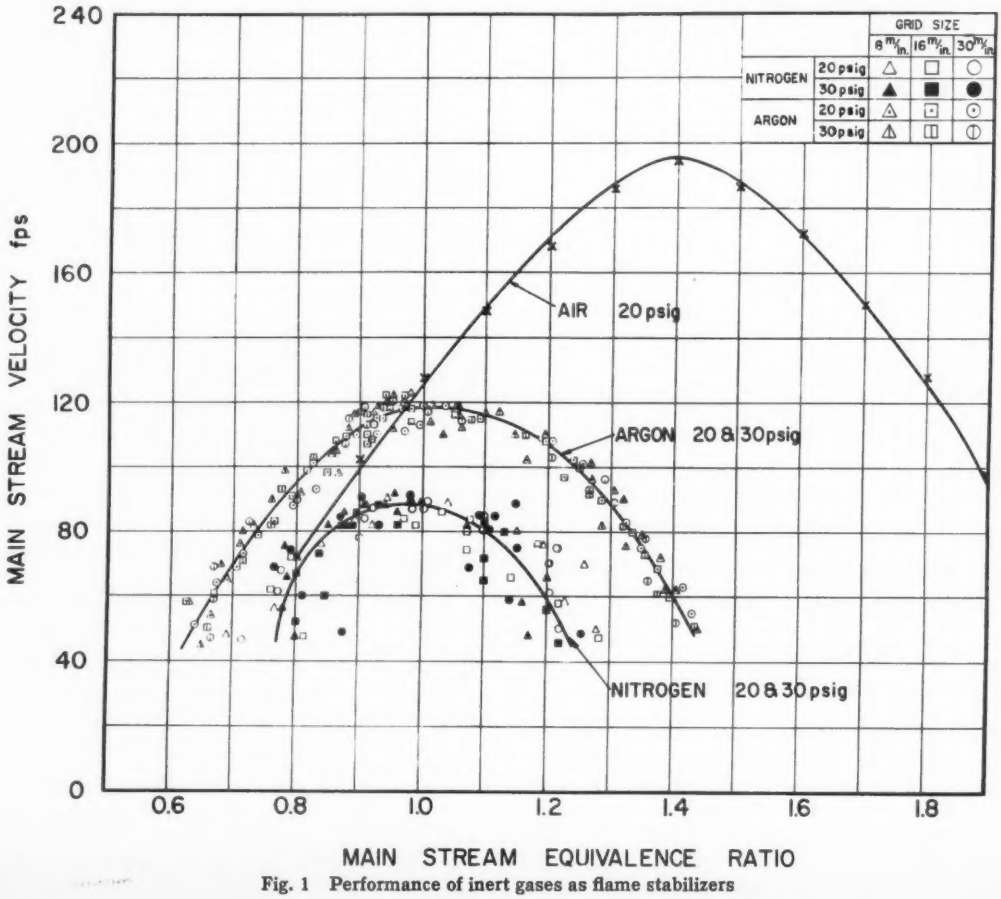

Fig. 1 Performance of inert gases as flame stabilizers

Neither factor influences the performance systematically. The ineffectiveness of the grid size variation is understandable because hot wire anemometry indicated very high levels of turbulence in the stagnation zone.

The fact that inert gases may be used as stabilizers suggests that in addition to the chemistry, the fluid mechanics and the associated transport phenomena must be considered seriously. Probably among the principal difficulties in doing this are the many little known aspects of jet interaction and the meager knowledge concerning the turbulent and convective terms of transport properties.

References

1 Schaffer, A. and Cambel, A. B., "Continued Investigation of the Opposing Jet Flameholder," JET PROPULSION, vol. 26, 1956, pp. 576–578.

2 Cambel, A. B. "A Review of Flame Stabilization by Means of Gaseous Jets," Combustion and Propulsion, Third AGARD Colloquium, Pergamon Press, New York, 1958, pp. 541–554.

Addendum to "Thermal Protection of a Re-Entry Satellite"[1]

SINCLAIRE M. SCALA[2]

General Electric Co., Philadelphia, Pa.

IN AN EARLIER study (1),[3] the author presented an analysis of the total mass transfer required at the forward stagnation point of a re-entry satellite. Included were transpiration cooling, vaporization cooling ($\Gamma = 0.25$) and sublimation.

In a more recent study (2), the author presented analyses of the ablation of quartz-like refractories, thermosetting reinforced plastics, a thermoplastic material (Teflon), and graphite, under the conditions of hypersonic re-entry.

It is interesting therefore to compare the total mass loss requirements for all of the cases treated in (1 and 2). This is done in Fig. 1.

It is seen that Teflon produces the greatest, and graphite the least mass loss, and all of the other materials treated fall between these upper and lower limits.

However, it must be noted that Teflon ablates in a quasi-steady fashion during re-entry and hence requires a relatively thin insulation layer behind the ablating layer. Graphite behaves primarily as a heat sink material, which also undergoes surface combustion, and thus the curve marked graphite represents only the mass ablated, not the total required for insulation.

The curve marked "vaporization cooling $\Gamma = 0.25$," in (1), Fig. 5, coincides with the curve marked quartz, and hence is not shown here in Fig. 1. It is also remarked that the curve marked "transpiration cooling" in (1), Fig. 5, inadvertently included the weight of the porous wall while in Fig. 1 only the mass of air actually injected into the boundary layer is shown. This mass requirement is truly optimistic because of the weight of the porous wall, the storage tanks, and flow regulating equipment required.

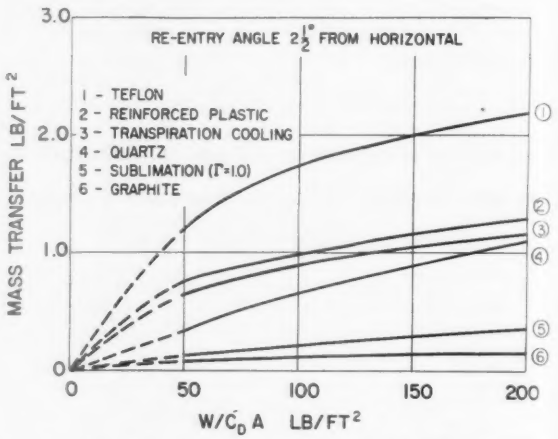

Fig. 1 Total mass transfer at stagnation point of re-entry satellite

Note also that although the quartz and the reinforced plastic seem equally competitive on a total mass loss basis, the depth of thermal penetration will be larger for quartz than for typical reinforced plastics, since the former has a higher thermal diffusivity (3).

References

1 Scala, S. M. "Thermal Protection of a Re-Entry Satellite," ARS JOURNAL, vol. 29, no. 9, Sept. 1959, pp. 670–672.

2 Scala, S. M. "A Study of Hypersonic Ablation," Tenth International Astronautical Federation Congress Preprint, London, England, Aug. 29–Sept. 5, 1959.

3 Steg, L. "Materials for Re-Entry Heat Protection of Satellites," ARS Preprint 836-59, June 1959.

Received Nov. 4, 1959.

[1] This work was performed under the auspices of the USAF Ballistic Missile Division, Contract no. AF 04(647)-269.

[2] Manager, High Altitude Aerodynamics, Missile and Space Vehicle Department. Member ARS.

[3] Numbers in parentheses indicate References at end of paper.

Comment on "Adiabatic Wall Temperature Due to Mass Transfer Cooling With a Combustible Gas"

D. B. SPALDING[1]

Imperial College, London, England

IN A COMMENT (1)[2] on a technical note by Sutton (2) I omitted a factor of 2 which is used by that author in applying the flat plate boundary layer solutions to the axisymmetrical stagnation point. This error is corrected in Fig. 1, which corresponds to Fig. 2 of (1), and which relates the dimensionless mass transfer rate at the stagnation point to the dimensionless driving force.

Sutton's curves, which are valid for constant properties, are those marked (2) and (3); the former, valid for $Pr = 1$, corresponds to Fig. 2 of (2); the latter embodies a correction for $Pr = 0.7$ (3). Comparison with curve (1), recommended in (1) as the exact solution for the constant-property laminar axisymmetric stagnation point, shows that the error associated with the use of the flat plate solutions is considerably less than was suggested in (1).

In plotting Fig. 1, the opportunity has been taken to introduce data presented by other authors, with particular reference to the influence of property variations in the boundary layer. Accordingly the viscosity and density appearing in the ordinate expression require definition; in Fig. 1 the values

Received Nov. 16, 1959.

[1] Professor of Heat Transfer.

[2] Numbers in parentheses indicate References at end of paper.

at the outer "edge" of the boundary layer are employed, namely μ_e and ρ_e.

Curve (1a) represents constant-property solutions from the paper by Reshotko and Cohen (4). Since these were obtained by interpolation in the same exact solutions as those underlying curve (1), the two curves naturally exhibit only minor differences. Reshotko and Cohen also obtained exact solutions of the boundary layer equations valid for variable properties; their results for $T_w/T_e = 0.25$ are plotted as curve (4) on Fig. 1.

Also plotted, as individual points, are the variable-property solutions of Howe and Mersman (5), who assumed: $\mu\alpha T^{0.7}$, $k\alpha T^{0.85}$, $c_p\alpha T^{0.19}$, $\rho\alpha T^{-1}$. The remarkable feature of these results is that, though T_w/T_e varies between 0.25 and 4, the points all lie close to the constant-property curves (1) and (1a). This behavior contrasts with that exhibited by curve (4). The difference may perhaps be attributable to the different property variations assumed by Reshotko and Cohen, e.g., $\mu\alpha T$; their assumptions are rather less in accordance with the properties of air than are those of Howe and Mersman.

The small influence of the temperature ratio on the mass transfer relation, when the properties are inserted at their "outer edge" values, is also exhibited by the solutions of Fay and Riddell (6). These authors considered heat transfer in the absence of mass transfer, a case which represents the $B \to 0$ limit of the present problem. Their results may be expressed as

$$\left(\frac{\dot{m}''}{B}\right)_{B\to 0}\left(\mu_e\rho_e\frac{du_e}{dx}\right)^{-1/2} = 0.957\left(\frac{\mu_w\rho_w}{\mu_e\rho_e}\right)^{0.1} \qquad [1]$$

This asymptotic relation is drawn on Fig. 1 as a broken line marked (5), for the case in which $\mu_w\rho_w/\mu_e\rho_e = 1$. The effect of temperature ratio is easily seen to be small; indeed it is nonexistent if one makes the Reshotko-Cohen assumption: $\mu\rho$ is independent of temperature.

Considering the results represented on Fig. 1 as a whole, it appears that the relations represented by curves (1) or (1a) may be used with some confidence for variable-property boundary layers provided that μ and ρ carry the suffix e.

In conclusion I would like to mention that Fig. 1 (the *h-f* diagram) of (1) was inaccurately plotted. A more careful working out of the numerical example discussed in (1) has shown that $B = 1.725$ with combustion and 1.42 without.

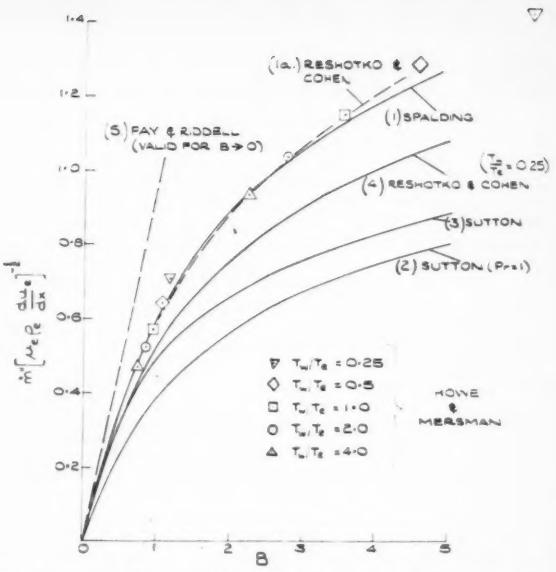

Fig. 1 Curves for prediction of mass transfer rate at laminar axisymmetric stagnation point. All curves are calculated for $Pr_w = 0.7$ and $T_e/T_w = 1$ unless otherwise stated

Nomenclature

- B = "transfer number" or driving force for mass transfer (*N.B.* the name "enthalpy ratio" for this quantity is insufficiently general; for B may be written in terms of concentrations and involve neither enthalpy nor temperature)
- c_p = specific heat of gas at constant pressure
- k = thermal conductivity of gas
- $\dot{m}''$ = mass transfer rate per unit area (e.g., in lbm/ft²h)
- u_e = velocity in gas stream at outer "edge" of boundary layer
- x = distance along surface from stagnation point
- Pr = Prandtl number
- T = absolute temperature of gas
- μ = dynamic viscosity of gas
- ρ = density of gas

Subscripts

- e = in gas stream just outside boundary layer
- w = in gas immediately in contact with surface

References

1 Spalding, D. B., "Adiabatic Wall Temperature Due to Mass Transfer Cooling With a Combustible Gas," ARS JOURNAL, vol. 29, no. 9, Sept. 1959, pp. 666–668.

2 Sutton, G. W., "Adiabatic Wall Temperature Due to Mass Transfer Cooling With a Combustible Gas," ARS JOURNAL, vol. 29, no. 2, Feb. 1959, pp. 136–137.

3 Sutton, G. W., private communication.

4 Reshotko, E. and Cohen, C. B., "Heat Transfer at the Forward Stagnation Point of Blunt Bodies," NACA TN 3513, July 1955.

5 Howe, J. T. and Mersman, W. A., "Solutions of the Laminar Compressible Boundary Layer Equations With Transpiration Which Are Applicable to the Stagnation Regions of Axi-symmetric Blunt Bodies," NASA TN D-12, Aug. 1959.

6 Fay, J. A. and Riddell, F. R., "Theory of Stagnation Point Heat Transfer in Dissociated Air," *J. Aeron. Sci.*, vol. 25, 1958, p. 73.

New Patents

George F. McLaughlin, *Contributor*

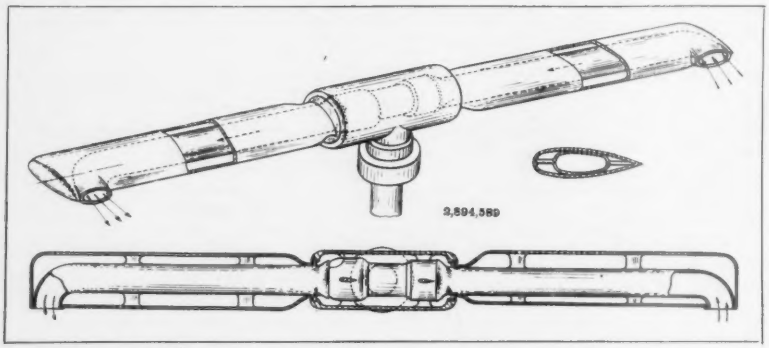

Jet propelled helicopter rotor (2,894,589). F. F. Ehrich, Philadelphia, Pa., assignor to Westinghouse Electric Corp.

Ramjet or turbojet engine mounted in the rotor hub. Blade tips have openings for receiving the incoming air and for discharging motive exhaust gases. The air intake receives the supply of air for the engine by "ram effect" with attendant aerodynamic advantages.

Jet propulsion device for operation through fluid medium (2,891,381). F. Zwicky, Pasadena, Calif., assignor to Aerojet-General Corp.

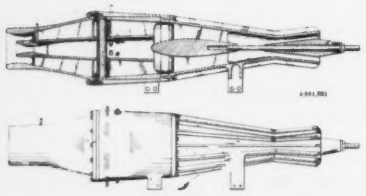

Reaction engine with an automatically operable valve dividing an elongated passageway into two parts, and located between the inlet opening and exhaust nozzle. A shorter duct located in the passageway comprises a vestibule and combustion chamber.

Guided missile (2,892,600). W. K. Ergen, Oak Ridge, Tenn., assignor to the U. S. Army.

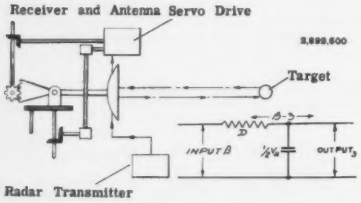

Means cooperating with a control gyroscope whereby a missile may be turned from its vertical path into the horizontal, at a predetermined altitude, without the application of precessing forces to the gyroscope, and without change of position of the gyro spin axis relative to the vertical.

Method for generating impulses in electric detonators (2,889,776). U. Gunther, Zurich, Switzerland, assignor to Inventa A.G. Fuer Forschung und Patentverwertung.

Production of high induction potential for fuses by the interruption of a magnetic circuit. One leg of a U-shaped permanent magnet contains an explosive charge which is detonated upon impact with a target. Destruction of the magnet interrupts the circuit.

Method of operating rotary wing aircraft including jet driven rotors (2,889,887). P. H. Stanley, Glenside, Pa., assignor to Autogiro Co. of America.

Rotors driven at blade tip speed of between 680 and 760 fps controlling the craft by controlling the rotor blade path. Variations of attack angle from all causes is kept within the bucket range of the rotor blade section.

Target assignment for radar tracking apparatus (2,891,244). J. J. Pastoriza, Boston, Mass., assignor to the U. S. Air Force.

Application to a tracking means of a pair of voltages proportional to the coordinates of the selected target and a plan position indicator for displaying the targets. The assignment system consists of an electrically resistive overlay for the plan position indicator. A manually controlled switch applies the voltages to the selected tracking means.

Signal tracking device (2,891,245). J. H. Coogan and R. Klein, Arcadia, Calif., assignors to the U. S. Navy.

Selective filter comprising a balanced modulator adapted to receive a Doppler signal subject to constant variations in frequency within a predetermined range. The output of a local oscillator is connected to the modulator, suppressing the local oscillator contents of its output, and producing a constant intermediate frequency signal.

External flow jet flap (2,891,740). J. F. Campbell, Warwick, Va.

Trailing edge flap on a wing rearward of a jet engine suspended in a pod. The exhaust of the engine travels upward and strikes the flap when the flap is in the deflected position.

Self-cooled turbine drive (2,893,204). R. J. Anderson and J. T. Hamrick, Parkview, Ohio, assignors to Thompson Ramo Wooldridge, Inc.

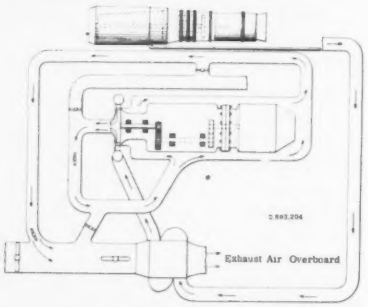

Integrated cooling system for the generator and other temperature critical components. Ram air or regeneratively cooled turbine discharge air is circulated around the components within a shroud.

Shaped cavity explosive charge (2,892,407). N. A. MacLeod, Altadena, Calif.

Cylindrical outer shell with an inwardly extending metal-conical liner at one end and a flat base at the other end. Detonation waves in a primer are transmitted to the main explosive charge, collapsing the liner progressively, and increasing the velocity of the penetrating jet.

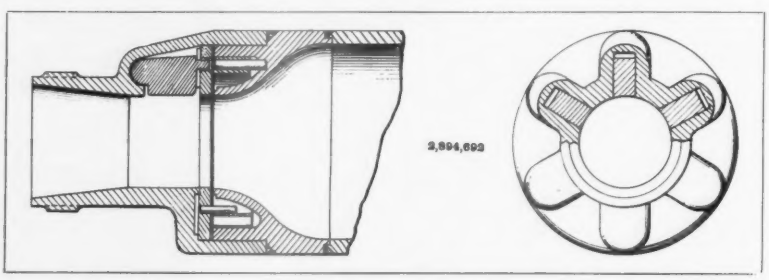

Nozzle (2,894,692). J. H. Ledbetter, H. J. Kircher and R. J. Novotny, Rockaway, N. J., assignors to Thiokol Chemical Corp.

Variable area nozzle for rockets having provision for controlling the gas pressures evolved from burning solid propellants in accordance with temperature. The nozzle throat area is varied in accordance with ambient temperature.

EDITOR'S NOTE: Patents listed above were selected from the Official Gazette of the U.S. Patent Office. Printed copies of patents may be obtained from the Commissioner of Patents, Washington 25, D. C., at a cost of 25 cents each; design patents, 10 cents.

Book Reviews

Ali Bulent Cambel, Northwestern University, *Associate Editor*

Elements of Physical Metallurgy, by A. G. Guy, Addison-Wesley Publishing Co., Inc., Reading, Mass., 1959, 544 pp. $9.50.

Reviewed by DONALD S. CLARK
California Institute of Technology

A review of any book is nothing more than a person's opinion. There cannot be an absolute evaluation of a book. However, a reviewer can judge the logic of the presentation, its accuracy and its completeness in relation to the title. There are problems of evaluation even on this basis, since no two people may envision the same scope of a subject or the same order of presentation. This book presents accurate information on the subject of physical metallurgy. It presents somewhat more than the elements. Those who master the material contained in this book should have a good grasp of the principles of the subject.

This reviewer cannot agree with the order of presentation of the material. The quantitative approach to the subject is good. However, the mathematical approach is overdone in some instances. The author develops some of the relations in kinetic theory, but leaves the matter hanging in the air without direct application. There is an indication that the relation may be referred to later in a discussion of nucleation. It might be preferable to develop these relations if, as and when they are to be applied.

The sequence of presentation is somewhat confusing at times. For example, the chapter on phase diagrams includes radiography, fractures and nondestructive testing. Why these subjects should be included with phase diagrams is not clear. This approach tends to create a hodgepodge impression and may cause some confusion to students.

Proper care in logical presentation is not maintained. The first mention of steel appears on page 19 but it is not defined at this point. The definition does not come until page 213, and this is not listed in the index. There is a tendency to mention subjects before they are explained. For example, reference to the eutectoid reaction for the hardening of alloys in the iron-iron carbide system is referred to on page 199, but the subject is discussed in detail beginning on page 465. The first discussion is supposedly in connection with the general treatment of phase diagrams, whereas the latter one is specifically devoted to the heat treatment of steel. For some individuals this approach may be good; for others it may be a little confusing.

The illustrations are in general very good and appropriate. The index has some deficiencies of incompleteness. The publisher has made an error in the index in that "Sp" appears after "Su." This causes a little difficulty in referring to the index.

In general, the book is an interesting approach to the subject and will be found to be a reliable text.

High Temperature Effects in Aircraft Structures, edited by Nicholas John Hoff, Pergamon Press, New York, 1958, 357 + vii pp. $12.

Reviewed by JAMES J. KAUZLARICH
Worcester Polytechnic Institute

This book is AGARDograph 28 published for and on behalf of the Advisory Group for Aeronautical Research and Development, North Atlantic Treaty Organization. Its purpose is to bring up to date the general state of knowledge concerning aerodynamic heating and its effects on aircraft structures. In accomplishing this end, the editor has persuaded 17 outstanding scientists to write review articles on special topics allied with the book's title. (A list of topics and authors is given at the end of this review.)

The several authors have not developed their subject in a textbook style. Rather, they have presented results in as succinct a form as possible, but being careful to reference all information.

The presentation is far from wordy and must be read carefully. In light of the difficulty of reading this book, the publishers should have used a larger print.

The chapter on materials by Pol Duwez sets the tone of the materials section of the book. The introduction defines three fundamental types of crystalline inorganic materials according to their atomic bonds as metallic, ionic and hard metals. The important physical properties pertinent to the subject are next discussed, and the remainder of the chapter is used to discuss particular materials with respect to characteristics of importance to the subject. The succeeding chapters on plastics and glasslike materials are organized in similar manner.

A discussion of creep and relaxation in metals and of plastics follows. The problem of creep is considered from a mechanical model point of view, where it is shown that an arrangement of springs and dashpots can describe the behavior of actual solids for a sequence of stresses or strains. Much space is used in explaining the form of the creep curves in terms of dislocation theory of the plastic deformation of crystals. The discussion proceeds to a review of the strengths that may be exhibited by available materials under typical conditions.

Another important section of the book is concerned with thermal buckling and creep buckling. The various theoretical approaches are discussed and applied to idealized problems. The analysis is compared to experimental results, and it is brought out that much research is needed on this subject.

This reviewer cannot help but wonder if this book is really making an important contribution to the scientific literature. Actually there is a great deal of simple cataloguing of information. In some sections there is a strong indication of the author's insight into his subject, but the abbreviated form of the presentation does not foster much of this. Of course, almost every chapter could easily have been expanded to book size.

The complete listing of chapters with respective authors are: 1. Introduction, N. J. Hoff, Stanford University; 2. External Sources of Heat, Martin H. Bloom, Polytechnic Institute of Brooklyn; 3. Heat Transmission in the Structure, Frederick V. Pohle, Polytechnic Institute of Brooklyn; 4. Materials for High Temperature Aircraft Structures, Pol Duwez, California Institute of Technology; 5. Non-metallic Structural Materials at High Temperatures, C. Gurney, University College of South Wales and Monmouthshire; 6. Glass-like Structural Materials at High Temperatures, Ivan Peyches, Cie. St. Gobain; 7. Creep and Relaxation in Metals, N. P. Allen, National Physical Laboratory; 8. Creep and Stress Relaxation of Plastics, William N. Findley, Brown University; 9. Fatigue of Structural Materials at High Temperatures, B. J. Lazan, University of Minnesota; 10. Thermal Stress, L. Broglio and P. Santini, University of Rome; 11. Buckling Caused by Thermal Stresses, A. van der Neut, Technische Hogeschool Delft; 12. Stress Distribution in the Presence of Creep, N. J. Hoff, Stanford University; 13. Creep Buckling, B. Fraejis de Veubeke, Université de Liège; 14. Influence of Aerodynamic Heating on Aeroelastic Phenomena, R. L. Bisplinghoff and John Dugundji, Massachusetts Institute of Technology; 15. Experimental Methods in High Temperature Structural Research, J. Taylor, Royal Aircraft Establishment; 16. Models and Analogs, R. R. Heldenfels, NACA Langley Aeronautical Laboratory.

Guided Missiles, Operations, Design, and Theory, sponsored by the Dept. of the Air Force, McGraw-Hill Book Co., Inc., New York, 1958, 575 pp.

Reviewed by LAWRENCE S. BROWN
Grumman Aircraft Engineering Corp.

This book is a reproduction of an Air Force manual on guided missiles fundamentals, compiled in 1955 by the instructors and staff of the Air Training Command's school for missiles at Lowry A.F.B., Colorado. In the foreword, Lt. Gen. C. T. Myers, USAF, states: "While seemingly complex, this book is little more than a primer in a field where science and technology move in their highest form." This appears to be a fair statement although "voluminous" would be a better word than "complex."

Coverage of the subject is quite complete as indicated by the following para-

phrase of the contents: The story of guided missiles, aerodynamics, propulsion, physics, control components, guidance components, control systems, guidance systems, trajectory considerations, tactics and instrumentation. The book is of high potential value to the general technician or to the specialist engineer who wants a briefing (or a reference) on matters other than his specialty. It is unfortunate that the first chapter was not de-oriented from Air Force usage. In the recount of foreign developments, the name of Wernher von Braun is conspicuously omitted. The last half of the chapter describes the USAF organization for development of guided missiles, but is silent about how the administration of development of a Polaris or Pershing is handled. This is, of course, of little scholastic importance, but tends to annoy an unbiased taxpayer.

The technical treatment of the balance of the subjects is excellent, although not uniform in level of coverage. The section entitled: "How optical and electronic principles work together" (following a section on Optics) is particularly unique, as is the section on computer units of guidance systems. The illustrations—schematics, block and circuit diagrams, and pictorial—are far superior to those of most similar publications.

Progress in Elementary Particle and Cosmic Ray Physics, Vol. IV, edited by J. G. Wilson and S. A. Wouthuysen, Interscience Publishers Inc., New York, 1958, 470 pp. $12.50.

Reviewed by S. F. Singer
University of Maryland

This is the fourth volume in a series which deals with cosmic ray physics. However, the subject is now divided into two main branches. One is concerned with the nuclear interactions of the extremely high particles which the cosmic radiation furnishes us, and with the new and strange elementary (i.e., subatomic) particles produced in these nuclear interactions. Thanks to the development of high energy accelerators some of these nuclear interactions can now be reproduced in the laboratory, and it was therefore thought best to discuss the elementary particle physics using both cosmic ray and accelerator data. The first three chapters are concerned with this general area. The first by D'Espagnat and Prentki of the European Nuclear Center in Geneva discusses aspects of the strong interactions of the new particles. This is a highly technical paper which reviews the existing theories. Strong interactions are of the type that occur in connection with nuclear forces, whereas the so-called weak interactions are associated with radioactive data decay.

The second chapter by Walker of the University of Wisconsin discusses properties and production of K-mesons. The K-meson is a particle discovered only about 10 years ago; its mass is approximately 900 times that of the electron. It decays into lighter mesons, the so-called pi-mesons and mu-mesons which in turn decay into electrons and neutrinos. Because of the short lifetime of the K-particles (of the order of 10^{-8} sec) their study is extremely difficult. There exist also neutral K-mesons which have a lifetime of 10^{-10} sec.

The third chapter by Fowler and Wolfendale of the University of Bristol and the University of Durham, England, respectively, deals with interactions of mu-mesons which were the first mesons discovered. Their interaction, however, with nuclei is very weak, and for this reason the number of interactions is small and experiments are rather difficult. However, when a mu-meson is captured by a positive nucleus into an orbit, then the chance of a nuclear interaction becomes greater because of the close proximity and the long time available. In many respects, therefore, a mu-meson behaves like a heavy electron, its mass roughly 210 times that of the electron.

The next two chapters deal with an aspect of cosmic rays which is becoming of importance to astrophysicists. In studying the time variations and origin of cosmic rays we really deal with the problem of how these highly energetic particles are produced in nature, in other words, the electromagnetic properties of the solar system and the galaxy. A review of geomagnetics is first, since it forms the basis of much of the analysis of the cosmic radiation. The first half of the review deals with our present knowledge of the primary radiation, its composition the energy spectra of the primary protons, the primary alpha particles and the heavier primaries. An outstanding problem with the primary radiation is the occasional absence of low energy cosmic rays, and one of the puzzling features, of course, is the mechanism which removes them from the solar system, or at least from the vicinity of the Earth. The second part discusses the time variations of cosmic rays, in particular the increases associated with solar flares, the decreases associated with some magnetic storms and variations during the sunspot cycle. Attempts are made to account for the existing theories and to present a coherent picture of the reason for these time variations. It turns out that these time variations give us a tool of studying the interplanetary space, in particular the existence of magnetic and electric fields in the interplanetary space. The cosmic rays, being charged particles, are deflected by magnetic fields and thus act as probes. Of particular interest to space operations are the discussions of the intensity increase with altitude, its dependence on latitude, the penetration characteristics of primary cosmic rays as a function of their energy and charge, and a discussion of the cosmic ray albedo.

The last chapter is by Ginzburg of the USSR Academy of Science in Moscow. It deals with the origin of cosmic radiation and describes mainly the theoretical work of Shklovski and of Ginzburg in trying to tie together the production of cosmic rays and production of radio noise in one theory. These views have been strikingly confirmed in recent astronomical work on the polarization of the light from the Crab nebula supernova. The chapter discusses the motion of cosmic ray particles in interstellar space and their interactions with interstellar gas. The electrons which are the final end product of these occasional nuclear interactions are then held to be responsible for the emission of radio noise by gyrating in the interstellar magnetic fields. Finally, the possibility that supernovae and novae are the actual sources of cosmic rays are discussed. It is interesting to see that many of the outstanding problems defined by the authors have found their experimental realization in the cosmic ray experiments in Sputnik III.

Technical Literature Digest

M. H. Smith, *Associate Editor*
The James Forrestal Research Center, Princeton University

Propulsion and Power (Non-Combustion)

An Ion Source Operated by High Frequency Pulses, by G. S. Malkiel' and B. I. Sukhanov, *Instruments and Experimental Techniques* (*Translation of Pribory i Tekhnika Eksperimenta*), no. 3, May-June 1958, pp. 431–436.

A 20-30 Kilovolt Ion Gun, by L. N. Bykhovskaia, *Instruments and Experimental Techniques* (*Translation of Pribory i Tekhnika Eksperimenta*), no. 2, March-April 1958, p. 228.

A Source of Negative Hydrogen Ions, by Iu. M. Khirnyi, *Instruments and Experimental Techniques* (*Translation of Pribory i Tekhnika Eksperimenta*), no. 2, March-April 1958, p. 231.

Propellants and Combustion

What Is Specific Impulse Worth?, by Earl R. Hinz, *Inst. Aeron. Sci., Rep.* 59–23, Jan. 1959, 20 pp.

Editor's Note: Contributions from Professors E. R. G. Eckert, J. P. Hartnett, T. F. Irvine Jr. and P. J. Schneider of the Heat Transfer Laboratory, University of Minnesota, are gratefully acknowledged.

Mechanisms of the Autodecomposition of Liquid Acetylenic Monopropellants, by *Experiment, Inc.*, Oct. 1958, 10 pp.

Growth of Disturbances in a Flame-generated Shear Region, by Perry L. Blackshear Jr., *NACA Rep.* 1360, 1958, 46 pp.

The Inflammability of Magnesium, Aluminum and Magnesium-aluminum Alloy Dusts, by A. L. Godbert and L. O. Would, *Gt. Brit., Ministry of Fuel and Power, Res. Rep.* 113, Feb. 1955, 16 pp.

Methane-Oxygen-Fluorine Flames; Spectroscopic and Calorimetric Studies, by J. J. Ball, D. E. Mann, B. A. Thrush, G. T. Armstrong C. F. Coyle and L. A. Krieger, *Wright Air Dev. Center, Tech. Rep.* 58-541 (*ASTIA AD* 204802), Oct. 1958, 63 pp.

Investigation of a Resonant Combustor Concept, by R. M. Lockwood, *Hiller Aircr. Corp., Adv. Res. Div., Rep.* ARD-219, Dec. 1958, 23 pp.

Combustion Instability in Liquid Propellant Rocket Motors, Twenty-fourth Quarterly Progress Report for the Period 1 Feb.–30 April 1958, *Princeton Univ., Dept. Aeron. Engng., Rep.* 216x, June 1958, 19 pp.

Combustion Instability in Liquid Propellant Rocket Motors, Twenty-fifth Quarterly Progress Report for the Period 1 May to 31 July 1958, *Princeton Univ., Dept. Aeron. Engng., Rep.* 216y, Nov. 1958, 59 pp.

A Bibliography of the Electrically Exploded Wire Phenomenon, by William G. Chace, *Air Force Cambridge Res. Center, Geophys. Res. Directorate, Res. Note* 2 (*AFCRC-TN*-58-457; *ASTIA AD* 152-640), Nov. 1958, 69 pp.

The Reaction of B_2, O_2 (1) and Carbon at Elevated Temperatures, by P. M. Rentzepis and D. White, *Ohio State Univ., Res. Found., Tech. Rep.* 691-1, Jan. 1959, 9 pp.

Chemical Nature of Propergolic Liquids; the Boranes and Their Preparation, by P. Duhaut, *Inst. Franc. du Petrole, Rev. et Ann. des Combustibles Liquides,* vol. 13, Nov. 1958, pp. 1563–1581. (In French.)

Powders for Self-propulsion, by G. Reure, *Inst. Franc. du Petrole, Rev. et Ann. des Combustibles Liquides,* vol. 13, Nov. 1958, pp. 1582–1589. (In French.)

The Ignition of Explosives by Radiation, by J. Eggert, *J. Phys. Chem.*, vol. 63, Jan. 1959, pp. 11–14.

A Thermoanalytical Study of the Binary Oxidant System Barium Perchlorate-Potassium Nitrate, by Virginia D. Hogan and Saul Gordon, *J. Phys. Chem.*, vol. 63, Jan. 1959, pp. 93–95.

The Thermal Decomposition of Dimethyl Peroxide: The Oxygen-Oxygen Bond Strength of Dialkyl Peroxides, by Philip L. Hanst and Jack G. Calvert, *J. Phys. Chem.*, vol. 63, Jan. 1959, pp. 101–103.

Thermodynamic Properties of Gases at High Temperature: 1. Chemical Equilibrium Among Molecules, Atoms and Atomic Ions Considered as Clusters, by Harold W. Wooley, *J. Res. Nat. Bur. Standards,* vol. 61, Dec. 1958, pp. 469–490.

Correction for Instrumental Drift in Flame Photometry, by Barry W. Mulligan and Alan F. Haught, *J. Res. Nat. Bur. Standards,* vol. 61, Dec. 1958, pp. 499–502.

Explosively Induced Nonuniform Oblique Shocks, by John O. Erdman, *Phys. Fluids,* vol. 1, no. 6, Nov.-Dec. 1958, pp. 535–540.

Burning Characteristics of Standard Propellants between 21°C and −51°C, by Joel Harris and Lester Shulman, *Picatinny Arsenal, Samuel Feltman Res. and Engng. Labs., Tech. Rep.* 2558 (*ASTIA AD* 202577), Nov. 1958, 34 pp.

The Effect of Explosive Mixtures upon Impact Sensitivity, by James Edward Sinclair, *Naval Postgrad. School, Tech. Rep.* 16, March 1957, 28 pp.

Taliani Tests for Assessment of Stability of Solid Propellants, by Carl Boyars, Kermit Atlas, J. G. Tuono and W. Gough, *NAVORD Rep.* 5688 (*Naval Propellant Plant TR* 106), Nov. 1958, 26 pp.

Research on the Ignition of Solid Propellants, Second Quarterly Progress Report for the Period 15 Aug.–15 Nov. 1958, *Princeton Univ., Dept. Aeron. Engng. Rep.* 433b, Jan. 1959, 16 pp., 1 fig.

The Mechanism of the Autodecomposition of Certain Liquid Acetylenic Compounds, by U. V. Henderson, Lloyd E. Line Jr., I. R. King and J. T. Scheurich, *Experiment Inc.*, TP-140, Dec. 1958, 14 pp.

Infrared Analysis of Exhaust from a Gas Generator Employing Unsymmetrical Demethylhydrazine, by R. F. Muraca, *Calif. Inst. Tech., Jet. Prop. Lab., Progr. Rep.* 20–348, Feb. 1958, 11 pp.

A Ramp Type Testing Circuit for Electric Explosive Devices, by A. H. Klein and T. D. Phillips, *Naval Propellant Plant, Mem. Rep.* 155, Nov. 1958, 15 pp.

Analysis of Heat-driven Oscillations of Gas Flows, by H. J. Merk, *Appl. Sci. Res.*, Sect. A, vol. 8, no. 1, 1958, pp. 1–27.

Experimental Study of a Reversed Jet Flameholder, by G. A. Agoston, A. W. Noon and T. D. Witherly, *Combustion and Flame,* vol. 2, Dec. 1958, pp. 333–367.

On the Decomposition Flame of Liquid Ozone-Oxygen Mixtures in a Tube, by R. Sandri, *Combustion and Flame,* vol. 2, Dec. 1958, pp. 348–352.

Spectroscopic Studies on Temperature Gradients in Flames, by R. H. Tourin, *Combustion and Flame,* vol. 2, Dec. 1958, pp. 353–364.

Confined Jets and Recirculation Phenomena with Cold Air, by R. Curtet, *Combustion and Flame,* vol. 2, Dec. 1958, pp. 383–411.

On the Calculation of Properties of Gases at Elevated Temperatures, by I. Amdur and J. Ross, *Combustion and Flame,* vol. 2, Dec. 1958, pp. 412–420.

Burning Times of Liquid Fuel Drops in a Convection-radiation Field, by E. G. Masdin and R. H. Essenhigh, *Combustion and Flame,* vol. 2, Dec. 1958, pp. 443–446.

The Hydrogen Diffusion Flame as an Inflammable Gas Detector, by P. D. Edwards and R. Long, *Combustion and Flame,* vol. 2, Dec. 1958, pp. 446–449.

A Note on the Influence of the Lewis Number on Flame Stability, by J. Menkes, *Combustion and Flame,* vol. 2, Dec. 1958, pp. 449–452.

Apparatus for the Detection of Vibrations in Combustion Chambers, by M. Trechans and N. Manson, *Inst. Franc. du Petrole. Rev. et Ann. des Combustibles Liquides,* vol. 13, Sept. 1958, pp. 1345–1348. (In French.)

Reaction of Oxygen Atoms with Nitric Oxide, by Paul Harteck, Robert R. Reeves and Gene Mannella, *J. Chem. Phys.*, vol. 29, Dec. 1958, pp. 1333–1335.

Composition of Nitrogen Oxide Equilibria, by Eleanora van Beek-Visser, *J. Chem. Phys.*, vol. 29, Dec. 1958, pp. 1358–1360.

Detonation-product Equation of State Obtained from Hydrodynamic Data, by W. Fickett and W. W. Wood, *Phys. Fluids,* vol. 1, no. 6, Nov.-Dec. 1958, pp. 528–534.

Spray Combustion and Atomization, by F. A. Williams, *Phys. Fluids,* vol. 1, no. 6, Nov.-Dec. 1958, pp. 541–545.

Spectrographic Study of a Flame Stabilized in a Flow, by M. Barrere and Mme. S. Barrere, *Récherche Aéron.*, no. 67, Nov.-Dec. 1958, pp. 11–20. (In French.)

Effect of Additives on the Flammability of Hydrocarbon-Air Mixtures at Reduced Pressure, by M. Guinet, *Récherche Aéron.*, no. 67, Nov.-Dec. 1958, pp. 43–52.

A Study of Oxidation of Hydrogen Based on Flashback of Hydrogen-Oxygen-Nitrogen Burner Flames, by Burton D. Fine, *NASA Memo.* 12–23–58E, Jan. 1959, 31 pp.

Combustion of Elemental Boron, by Claude P. Talley, *J. Aero/Space Engng.* vol. 18, June 1958, pp. 37–40.

Combustion Instability in Solid Propellant Rocket Motors, by E. W. Price, *Astronautica Acta,* vol. 5, no. 1, 1959, pp. 63–72.

The Thermal Decomposition of Hydrogen Peroxide Vapours, by D. E. Hoare, J. B. Protheroe and A. D. Walsh, *Astronautica Acta,* vol. 5, no. 1, 1959, pp. 548–557.

Thermal Explosions. Part I. Induction Periods and Temperature Changes Before Spontaneous Ignition, by P. Gray and M. J. Harper, *Astronautica Acta,* vol. 5, no. 1, 1959, pp. 581–590.

Nitrogen Isotopic Fractionation Between Nitric Acid and the Oxides of Nitrogen, by L. L. Brown and G. M. Begun, *J. Chem. Phys.*, vol. 30, May 1959, pp. 1206–1209.

Configuration Interaction in the Lithium Hydride Molecule. I. A Determination AO Approach, by A. M. Karo and A. R. Olson, *J. Chem. Phys.*, vol. 30, May 1959, pp. 1232–1240.

Configuration Interaction in the Lithium Hydride Molecule. II. An SCF LCAO-MO Approach, by A. M. Karo, *J. Chem. Phys.*, vol. 30, May 1959, pp. 1241–1248.

LCAO-MO Study of B_2, by Alice A. Padgett and Virginia Griffing, *J. Chem. Phys.*, vol. 30, May 1959, pp. 1286–1291.

Heat of Formation of Boron Trichloride, by Walter H. Johnson, Richard C. Miller and Edward J. Prosen, *J. Res. Nat. Bur. Standards,* vol. 62, May 1959, pp. 213–219.

Design Tips for Cryogenic Storage Vessels, by G. F. Sulfrian, *Space Aeron.*, vol. 31, June 1959, pp. 79–80, 82, 84, 86.

Joint Army-Navy Air Force Solid Propellant Rocket Static Test Panel, Bulletin of the Sixth Meeting, Addenum, Solid Propellant Information Agency, Aug. 1958, 30 pp. Contents:

A Dynamic Pressure Calibrator, by D. P. Johnson, pp. 1–9.

Some Measurements of Instrumentation Errors in the Static Testing of Rocket Motors, by W. R. Beakley and R. A. E. Westcott, pp. 11–13.

Inspection of Large Rocket Grains, by Ernest E. Leist and Leonard C. Walther, pp. 15–20.

Accident Investigation, by Joseph G. Thibodaux Jr., pp. 21–25.

A Hermetically-Sealed Igniter Safety for Rockets, by E. M. Kane, pp. 27–30.

Relation of Droplet Consumption Rates to Liquid Strand Consumption Rates, by G. A. Mead, ARS JOURNAL, vol. 29, June 1959, pp. 440–442.

The Vibration and Decomposition of

the Ozone Molecule, by E. K. Gill and K. J. Laidler, *Faraday Soc., Trans.*, vol. 55, May 1959, pp. 753–759.

Autoignition of Liquid Fuel Sprays, by G. J. Mullaney, *Ind. Engng. Chem.*, vol. 51, June 1956 (Partial Contents), pp. 779–782.

Heat of Mixing in the System Nitrogen-Methane, by Helmut Knapp, *Ind. Engng. Chem.*, vol. 51, June 1956 (Partial Contents), pp. 783–786.

NACA Research on Slurry Fuels, by M. L. Pinns, W. T. Olson, H. C. Barnett and R. Breitwieser, *NACA Rep.* 1388, 1958, 24 pp.

Infrared Method for Determining Small Amounts of Dipentaerythritol Hexanitrate in PETN, by Walter E. Fredricks and Frank Pristera, *Picatinny Arsenal, Feltman Res. and Engng. Labs, TN* 30, April 1959, 3 pp.

Some Physical Properties for the System Nitrogen Tetroxide-Nitric Oxide, by Donat B. Brice and Norman Fishman, ARS JOURNAL, vol. 29, May 1959, pp. 354–357.

Burning Rate of an H-Atom Propellant, by Howard B. Palmer, ARS JOURNAL, vol. 29, May 1959, p. 365.

Initiation of Detonations, by Harmon W. Hubbard and M. H. Johnson, *J. Appl. Phys.*, vol. 30, no. 5, May 1959, pp. 765–769.

Performance Limits of Classical Solid Propellants, by R. Eugel, *Phys. Rev.*, vol. 113, March 1, 1959, pp. 14–18.

Most Favorable Shapes for Solid Propellants, by V. T. Bödewadt, *Phys. Rev.*, vol. 113, March 1, 1959, pp. 19–24.

Simultaneous Detonation along a Line, by John O. Erkman, *Stanford Res. Inst. Poulter Labs. Tech. Rep.* 001–59, April 15, 1959, 8 pp.

Recent Developments in Spark Ignition, by E. L. Litchfield and M. V. Blanc, *Bur. Mines, Rep. of Investigations* 5461, 1959, 9 pp.

Communication of Flame Through Cylindrical Channels, by H. G. Wolfhard and A. E. Bruzak, *Bur. Mines, Rep. of Investigations* 5457, 1959, 22 pp.

Studies of Deflagration to Detonation in Propellants and Explosives, by C. M. Mason, F. C. Gibson, C. R. Summers and F. H. Scott, **Quarterly Report,** *Bur. Mines,* Jan. 1, 1959–March 31, 1959, 8 pp.

High Power Pulse Steepening by Means of Exploding Wires, by G. S. Janes and H. Koritz, *Avco Res. Lab., Res. Rep.* 50, April 1959, 19 pp.

Exploratory Investigation of Aerodynamic Flameholders for Afterburner Application, by Helmut F. Butze and Allen J. Metzler, *NASA Memo* 4-9-59E, May 1959, 7 pp.

Some Development Problems with Large Cryogenic Propellant Systems, by Daniel A. Heald, *SAE Preprint* 59S, March 31–April 3, 1959, 7 pp.

Research on Burning Rate Control Factors in Solid Propellants, by Kimball P. Hall and E. Karl Bastress, Initial progress report for the period 1, Jan. 1959–March 1959, *Princeton University Dept. of Aero. Engng. Rep.*, 446-a. Jan.-March 1959, 19 pp.

Thermodynamic Charts for the Combustion Products of Nitric Acid and Kerosene, by W. H. Williams, *Gt. Brit. Aeron. Res. Council, Rep. & Mem.* 2982 (formerly A.R.C. Technical Rep. 16505; Royal Aircraft Establishment, TN R.P.D. 33), 1959, 8 pp.

Methods for Preparing Small Particles of Metals and Salts, by Abraham Rotkowitz, *Naval Propellant Plant, Res. and Development Dept. Mem. Rep.* 156, Dec. 1958, 15 pp.

Kinetics of the Decomposition of Nitric Oxide in the Range 700–1800°, by Edward L. Yuan, John I. Slaughter, William B. Koerner and Farrington Daniels, *J. Phys. Chem.*, vol. 63, June 1959, p. 952.

Combustion Instability; Causes and Cures, by Kurt R. Stehling, *Space/Aeron.*, vol. 32, July 1959, p. 46.

Storable Liquid Propellants Look Good for Drone Rockets, by R. P. Reul, *Space/Aeron.*, vol. 32, July 1959, p. 75.

The Stability of Propellants and the Theory of Thermal Ignitions, by Irvin Glassman, *Princeton Univ., Dept. Aeron. Engng., Rep.* 460, May 1959, 18 pp. (*AFOSR* TN-59-586; *ASTIA AD* 217–185).

Survey of Hydrogen Combustion Properties, by Isadore L. Drell and Frank E. Belles, *NACA Rep.* 1383, 1958, ii, 34 pp.

Effect of Ozone Addition on Combustion Efficiency of Hydrogen-Liquid-Oxygen Propellant in Small Rockets, by Riley O. Miller and Dwight D. Brown, *NASA Memo* 5-26-59E, June 1959, 18 pp.

The Effect of Pressure on the Burning Velocity of Various Gas Mixtures (Measured by the Soap Bubble Method), by William A. Strauss and Rudolph Edse, *Wright Air Development Center, Tech. Rep.* 58-464, Dec. 1958, 38 pp. (*ASTIA AD* 211 031). (Ohio State University Rocket Research Laboratory.)

Studies in the Reactions of High Energy Atoms and Molecules, by R. A. Marcus, *Wright Air Development Center, Rep.* 59–24, Jan. 1959, 30 pp. (*ASTIA AD* 209–533). (Brooklyn Polytechnic Institute.)

Combustible-Gas Analyzers for High-Temperature Operation, by Nelson W. Hartz, *Instruments and Control Systems,* vol. 32, June 1959, p. 886.

Measurement of the Rate of Dissociation of Oxygen, by Stanley R. Brown, *J. Chem. Phys.*, vol. 30, June 1959, p. 1380.

Combustion Instability: Acoustic Interaction with a Burning Propellant Surface, by R. W. Hart and F. T. McClure, *J. Chem. Phys.*, vol. 30, June 1959, p. 1501.

Vibrational Relaxation Times in Oxygen, by Morris Salkoff and Ernest Bauer, *J. Chem. Phys.*, vol. 30, June 1959, p. 1614.

Fluid Dynamics, Heat Transfer and MHD

A Simple Method for Determining Heat Transfer, Skin Friction, and Boundary Layer Thickness for Hypersonic Boundary-Layer Flows in Pressure Gradient, by Mitchel H. Bertram and William V. Feller, *NASA Memo* 5-24-59L, June 1959, 60 pp.

The Electric Conductivity of a Partially Ionized Gas, by A. C. Pipkin, *Maryland University, Inst. for Fluid Dynamics and Appl. Math., TN* BN-170, April 1959 (*AFOSR TN* 59–189; *ASTIA AD* 215842), 30 pp.

Axisymmetric Stagnation Point Mass Transfer Cooling, by H. Hoshizaki and H. J. Smith, *General Research in Flight Sciences, Jan. 1958–Jan. 1959, vol. I, Fluid Mechanics, Viscous Flows, Lockheed Aircraft Corp., Missiles and Space Division, Rep.* LMSD-48381, Jan. 1959, 217 pp., pp. 45–114.

The Effect of Vehicle Deceleration on a Melting Surface, by D. M. Tellep, *General Research in Flight Sciences, Jan. 1958–Jan. 1959, vol. I, Fluid Mechanics, Viscous Flows, Lockheed Aircraft Corp., Missiles and Space Division, Rep.* LMSD-48381, Jan. 1959, 217 pp., pp. 115–154.

On the Application of Liepmann's Heat Transfer Formula, by R. M. Mark, *General Research in Flight Sciences, Jan. 1958–Jan. 1959, vol. I, Fluid Mechanics, Viscous Flows, Lockheed Aircraft Corp., Missiles and Space Division, Rep.* LMSD-48381, Jan. 1959, 217 pp., pp. 155–164.

Heat Transfer Measurements on a Basic Hemisphere-Cylinder in the Lockheed Three-Inch Shock Tube, by R. W. Rutowski and D. Weimer, *General Research in Flight Sciences, Jan. 1958–Jan. 1959, vol. I, Fluid Mechanics, Viscous Flows, Lockheed Aircraft Corp., Missiles and Space Division, Rep.* LMSD-48381, Jan. 1959, 217 pp., pp. 165–178.

Stagnation Point Heat Transfer in Partially-Ionized Argon, by R. W. Rutowski, *General Research in Flight Sciences, Jan. 1958–Jan. 1859, vol. I, Fluid Mechanics, Viscous Flows, Lockheed Aircraft Corp., Missiles and Space Division, Rep.* LMSD-48381, Jan. 1959, 217 pp., pp. 179–205.

Investigation of the Thermal Boundary Layer and the Diffusion of Ions into the Thermal Boundary Layer at the End Wall of a Shock Tube, by W. C. Marlow, II, *General Research in Flight Sciences, Jan. 1958–Jan. 1959, vol. I, Fluid Mechanics, Viscous Flows, Lockheed Aircraft Corp., Missiles and Space Division, Rep.* LMSD-48381, Jan. 1959, 217 pp., pp. 207–217.

Magnetohydrodynamic Effects in Aerodynamic Flows, by W. R. Sears, ARS JOURNAL, vol. 29, June 1959, pp. 397–406.

Chemical Reactions in Supersonic Flow, by F. A. Williams, ARS JOURNAL, vol. 29, June 1959, pp. 442–443.

On Turbulent Supersonic Diabatic Wakes, by R. H. Page, ARS JOURNAL, vol. 29, June 1959, pp. 443–445.

Effect of a Nonisothermal Free Stream on Boundary Layer Heat Transfer, by E. M. Sparrow and J. L. Gregg, *J. Appl. Mech.*, vol. 26, June 1959, pp. 161–171.

The Effects of Combined Electric and Magnetic Fields on Hypersonic Couette Flow, by Z. O. Bleviss, *Douglas Aircraft Co., Inc., Santa Monica, Calif., Rep.* SM 23314, Oct. 1958, 47 pp.

Approximate Methods for Predicting Separation Properties of Laminar Boundary Layers, by N. Curle and S. W. Skan, *Aeron. Quart.*, vol. VIII, Aug. 1957, pp. 257–268.

Some Finite Difference Solutions of the Laminar Compressible Boundary Layer Showing the Effects of Upstream Transpiration Cooling, by John T. Howe, *NASA Memo* 2-26-59A, Feb. 1959, 33 pp.

Boundary Layer Transition on Hollow Cylinders in Supersonic Free Flight as Affected by Mach Number and a Screw-Thread Type of Surface Roughness, by James S. Carlton, *NASA Memo* 1-20-59A, Feb. 1959, 49 pp.

Skin Friction in the Compressible Laminar Boundary Layer with Heat Transfer and Pressure Gradient, by R. E. Luxton and A. D. Young, *NASA* N-68367*, July 7, 1958, 21 pp.

A Survey and Correlation of Data on Heat Transfer by Forced Convection at Supersonic Speeds, by R. J. Monaghan, *NASA* N-28412X*, 1958, 43 pp.

Heat Transfer and Boundary Layer

Measurements in a Region of Supersonic Flow Separation and Reattachment, by A. Naysmith, *NASA* N-66506*, May 1958, 14 pp.

Chemical Reaction in Laminary Boundary Layer—Instantaneous Reaction, by O. E. Potter, *Inst. Chem. Engrs, Trans.* vol. 36, no. 6, Dec. 1958, pp. 415–421.

Viscous Aerodynamic Characteristics in Hypersonic Rarefied Gas Flow, by Ronald F. Probstein and Nelson H. Kemp, *Avco Mfg. Corp., Res. Rep.* 48, March 1959.

Heat Transfer in the Turbulent Incompressible Boundary Layer I—Constant Wall Temperature, by W. C. Reynolds, W. M. Kays and S. J. Kline, *NASA Memo* 12-1-58W, Dec. 1958, 36 pp.

Heat Transfer in the Turbulent Incompressible Boundary Layer II—Step Wall Temperature Distribution, by W. C. Reynolds, W. M. Kays and S. J. Kline, *NASA Memo* 12-2-58W, Dec. 1958, 38 pp.

Heat Transfer in the Turbulent Incompressible Boundary Layer III—Arbitrary Wall Temperature and Heat Flux, by W. C. Reynolds, W. M. Kays and S. J. Kline, *NASA Memo* 12-3-58W, Dec. 1958, 52 pp.

Example of Unsteady Laminar Boundary Layer Flow, by I. Tani, *Tokyo Univ., Aeron. Res. Inst.*, vol. 24, no. 2, Rep. 331, June 1958, pp. 31–42.

Radiation Attenuation Method of Measuring Density of a Two-Phase Fluid, by Michael and Swanson Petrick and S. Bernet, *Rev. Sci. Instr.*, vol. 29, Dec. 1958, pp. 1079–1085.

Pressure Drop and Heat Transfer in a Duct with Triangular Cross-Section, by E. R. G. Eckert and T. F. Irvine Jr., *University of Minnesota Heat Transfer Laboratory Tech. Rep.* 22, April 1959, 39 pp. (WADC Tech Rep. 59-222).

Influence of Radiation on Convection in Noncircular Ducts, by T. F. Irvine Jr., *ASME Paper* 58-A-155 for meeting Nov. 30–Dec. 5, 1958, 16 pp.

Experimental Study of the Stability of Pipe Flow, I, Establishment of an Axially Symmetric Poiseuille Flow, by E. Reshotko, *Jet Propulsion Lab., Calif. Inst. of Tech., Pasadena, Prog. Rep.* 20-364, Oct. 24, 1958.

Variational Method for Fully Developed Laminar Heat Transfer in Ducts, by E. M. Sparrow and R. Siegel, *ASME Paper* 58-A-92, Nov. 30–Dec. 5, 1958, 8 pp.

Details of Exact Low Prandtl Number Boundary-Layer Solutions for Forced and for Free Convection, by E. M. Sparrow and J. L. Gregg, *NASA Memo* 2-27-59E, Feb. 1959, 45 pp.

Heat Transfer, Recovery Factor, and Pressure Distributions Around a Cylinder Normal to a Supersonic Rarefied Air Stream, Pt. 1, Experimental Data, by O. K. Tewfik and W. H. Giedt, *Univ. Calif. Inst. Engng. Res., Tech. Rep.* HE-150-162, Series 20–124, Jan. 30, 1959.

Experiments on Stability of Viscous Flow Between Rotating Cylinders—I, Torque Measurements, by R. J. Donelly, *Royal Soc. Proc.*, vol. 246, no. 1246, Aug. 19, 1958, pp. 312–325.

The Variation of Flow Resistance in Rapidly Rotating Tubes, by L. Kisbocskoi, *Acta Technica Academiae Scientiarum Hungaricae,* vol. 22, nos. 1–2, 1958, pp. 121–128.

Refractory-Metal Thermocouples Containing Rhenium, by Chester T. Sims, Gordon B. Gaines and Robert I. Jaffee, *Rev. Sci. Instr.*, vol. 30, no. 2, Feb. 1959, pp. 112–115.

Emittance and Reflectance in the Infrared, an Annotated Bibliography, by Dorothy E. Crowley, *Univ. Mich., Willow Labs., Ann Arbor, Mich., Rep.* 2389-15-S, April 1959, 154 pp.

Radiation from Hot Air, by J. Keck, J. Camm, B. Kivel and T. Wentink Jr., *Avco Mfg. Corp., Res. Rep.* 42, Feb. 1959.

Effects of Temperature Gradients on Self-Absorption of Infrared Radiation in Hot Gases, by Richard H. Tourin, *Warner and Swasey Res. Corp., N. Y., Sci. Rep.* 1 (AFCRC TN-58-462), July 1958, 21 pp.

Thermal Diffusion Effects in Laminar Boundary Layers of Binary Mixtures, by A. A. Hayday, T. F. Irvine Jr. and E. R. G. Eckert, *Heat Transfer Lab., Univ. Minn.*, April 21, 1959, 10 pp.

Low Prandtl-Number Free Convection, by J. L. Gregg and E. M. Sparrow, *Zeitschrift fur Angewandte Mathematik und Physik,* vol. 9a, no. 4, Nov. 1958, p. 383.

On the Free Convection from a Horizontal Plate, by K. Stewartson, *Zeitschrift fur Angewandte Mathematik und Physik,* vol. 9a, no. 3, Sept. 1958, p. 276.

Effects of Gravitational Electromagnetic Fields on Fluid Motion, Chia-Shun Yih, *Quart. Appl. Math.*, vol. 16, no. 4, Jan. 1959, p. 409.

Thermodynamic Properties and Calculated Rocket Performance of Hydrogen to 20,000° K, by D. Altman, *Jet Propulsion Lab., Calif. Inst. of Tech., Rep.* 20–106, Sept. 3, 1956, 28 pp.

Thermal Conductivity and Thermoelectric Power of Germaniumsilicon Alloys, by M. C. Steele and F. D. Rosi, *J. Appl. Phys.*, vol. 29, no. 11, Nov. 1958, p. 1517.

Temperature Distribution of the Thin-Walled Hollow Cylinder at Radiating Temperature, by Y. Ito, *J. Appl. Phys., Japan,* vol. 26, no. 1, Jan. 1957, pp. 29–36.

Relation Between Gas Absorptivities and Emissitivities, by D. Olfe and S. S. Penner, *J. Appl. Phys.*, vol. 30, no. 1, Jan. 1959, p. 125.

Infrared Absorptivities and Emissivities of Gases, by A. Thomson, W. J. Hooker and S. S. Penner, *J. Appl. Phys.*, vol. 30, no. 1, Jan. 1959, p. 124.

Measurements of Total Hemispherical Emissivity of Various Oxidized Metals at High Temperature, William R. Wade, *NACA TN* 4206, March 1958.

Mass-Transfer from Single Solid Spheres—I. Transfer at Low Reynolds Numbers by E. H. Garner and R. B. Keey, *Chem. Engng. Sci.*, vol. 9, nos. 2/3, Nov. 1958, p. 119.

The Mechanism and Application of Effusion Cooling, by P. Grootenhuis, *J. Royal. Aeron. Soc., London,* vol. 63, no. 578, Feb. 1959, pp. 73–89.

Effects of Oscillating Flow on Heat Transfer in a Tube, by D. T. Harrje, *Calif. Inst. Tech. Jet Propulsion Lab., Prog. Rep.* 20-362, Aug. 27, 1958. 29 pp.

Stagnation Point Melting and Ablation, by Theodore R. Goodman and Charles Chin, *Air Force Office of Scientific Research,* TN-59-390, March 30, 1959 (*Allied Research Associates, Inc.*), 21 pp.

A Further Note on Hypersonic Stagnation Point Flow with a Magnetic Field, by Nelson H. Kemp, *Avco Research Lab., Res. Rep.* 53, April 1959, 15 pp.

On the Flow of a Conducting Fluid Past a Magnetized Sphere, by G. S. S. Ludford and J. D. Murray, *Maryland Univ. Institute for Fluid Dynamics and Applied Mathematics, TN* BN-169, April 1959, 20 pp.

Considerations in the Application of Evaporative Cooling Systems to Hypersonic Vehicles, by Eli Kaplan, *SAE Preprint* 54 T, March 31–April 3, 1959, 7 pp.

Radiant Energy Transfer from Nonisothermal Molecular Emitters with Non-Overlapping Dispersion Lines, by D. Olfe, *Calif. Inst. Tech. Daniel and Florence Guggenheim Jet Propulsion Center, Tech. Rep.* 31, April 1959, 12 pp.

Reaction Rate Distributions on Catalytic Surfaces, by D. E. Rosner, *Aero-Chem. Res. Labs., Inc.*, TM 12 (*AFOSR TN* 59-432; *ASTIA AD* 214794), Dec. 1958, 4 pp.

Compressible Flow Tables K = 1.26. Stagnation Temperature Change Without Friction, by C. Hoebich, *Army Rocket and Guided Missile Agency, Ordnance Missile Labs. Division,* ARGMA TH 1H1N-2, Feb. 1959, 87 pp.

Low Density Supersonic Diffuser Performance, by Arthur M. Collins. *Calif. Univ. Inst. Engng. Res. Tech. Rep.*, HE-150–164, Jan. 15, 1959, 16 pp.

Disturbance Phenomena in Probe Measurement of Ionized Gases, by T. Okuda and K. Yakamoto, *J. Phys. Soc. Japan,* vol. 13, no. 10, Oct. 1958, pp. 1212–1224.

Temperature Error Associated with Embedded Thermocouples, by A. R. Thomas, B. Schurin and J. C. Morris, *Rev. Sci. Instr.*, vol. 29, no. 11, Nov. 1958, pp. 1054–1046.

Thermal Properties of High-Voltage Insulants, by P. H. G. Allen, *Proc. Inst. Elec. Engrs.* vol. 105, pt. C, no. 7 (monograph 250), March 1958, pp. 35–45.

Radiation from a Toroidal Stabilized Pinch, by S. A. Colgate, J. P. Ferguson and H. P. Furth, *Univ. Calif., Lawrence Radiation Lab.*, UCRL-5036 Suppl., June 19, 1958.

Use of Fiber Specimens for Infrared Absorption Measurements, by R. D. B. Fraser, *J. Optical Soc. Amer.*, vol. 48, no. 12, Dec. 1958, p. 1017.

Adiabatic Wall Temperature Downstream of a Single, Tangential Injection Slot, by J. H. Chin, S. C. Skirvin, L. E. Hayes and A. H. Silver, *ASME, Paper* 58-A-107.

Heat Transfer to Flowing Helium by Blowing and Stable Film Evaporation, by P. Grassman, A. Karaguuis, J. Kopp and T. Frederking, *Kaeltetechnik,* vol. 10, no. 7, July 1958, pp. 206–8. (In German.)

Heat Transfer in a Cross Flow Nuclear Reactor, by Charles L. Larson, *Nuclear Science and Engng.*, vol. 4, Nov. 1958, p. 607.

Shape of Initial Portion of Boundary of Supersonic Axisymmetric Free Jets at Large Jet Pressure Ratios, by E. S. Love and L. P. Lee, *NACA TN* 4195, Jan. 1958, 29 pp.

Low Reynolds Number Aerodynamics of Flapped Airfoils at Supersonic Speeds, by James L. Amick and Gerard F. Carvalho, *WADC Tech. Rep.* 58–466 (*ASTIA AD* 155854), Sept. 1958.

A Note on the Interaction of a Normal Shock Wave With a Thermal Boundary Layer, by John P. Appleton and Hubert J. Davies, *J. Aero/Space Sci.*, vol. 25, no. 11, Nov. 1958, p. 722.

Stagnation-Point Heat Transfer to Blunt Shapes in Hypersonic Flight, Including Effects of Yaw, by A. J. Eggers, Jr., C. F. Hansen and B. E. Cunningham, *NACA TN* 4229, April 1958, 54 pp.

On the Solution of the Laminar Bound-

ary-Layer Equations, by Melvin Epstein, *J. Aero/Space Sci.*, vol. 26, no. 1, Jan. 1959, p. 58.

Turbulent Heat Transfer by Forced Convection with Large Temperature Difference, by Tomoshiga Hara and Jun Okushi, *Trans. Japan Soc. Mech. Engrs.*, vol. 24, no. 140, April 1958, pp. 219–223.

Approximate Method for Calculating Laminar Boundary-Layer Using Energy Thickness, by K. Hatta, *Trans. Japan Soc. Mech. Engrs.*, vol. 24, no. 145, Sept. 1958, pp. 636–641.

Heat Transfer and Reynold's Analogy in a Turbulent Flow with Heat Release, by R. Hunziker, *Zeitschrift fur Angewandte Mathematik und Physik*, vol. 9a, no. 4, Nov. 1958, p. 307.

Turbulent Heat Transfer Through a Highly Cooled, Partially Dissociated Boundary Layer, by Peter H. Rose, Ronald F. Probstein and Mac C. Adams, *J. Aero/Space Sci.*, vol. 25, no. 12, Dec. 1958, p. 751.

On Formation of Magneto-Hydrodynamic Shock Waves, by S. Segre, *Nuovo Cimento*, vol. 9, no. 6, Sept. 16, 1958, pp. 1054–1057.

Viscous Dissipation in Low Prandtl Number Boundary-Layer Flow, by E. M. Sparrow and J. L. Gregg, *J. Aero/Space Sci.*, vol. 25, no. 11, Nov. 1958, p. 717.

Unsteady Laminar Boundary Layers in an Incompressible Flow, by K. T. Yang, *J. Appl. Mech.*, vol. 25, no. 4, Dec. 1958, p. 421.

Turbulent Heat-Transfer Coefficients in the Vicinity of Surface Proturbances, by Richard J. Wisniewski, *NASA Memo* 10-1-58E, Oct. 1958.

A Review of Two Phase Heat Transfer, by J. G. Collier, *Atomic Energy Res. Estab. (Gt. Brit.)* (AERE Rep. CER-2496; HX. 4918), May 1958, 93 pp.

The Role of Surface Conditions in Nucleate Boiling, by Peter Griffith and John D. Wallis, *Mass. Inst. of Tech., Division of Industrial Cooperation*, Tech. Rep. 14, Dec. 1, 1958.

Wetting Effects on Boiling Heat Transfer; the Copper-Stearic Acid System, by W. B. Harrison and Zelvin Levine, *AIChEJ*, Dec. 1958, pp. 409–412.

Time Variation of Nucleate Boiling Heat Transfer of Water, by Fumio Hirano and Kaneyasu Nishikawa, *Trans. Japan Soc. Mech. Engrs.*, vol. 24, no. 148, Dec. 1958, pp. 978–983.

Approximation of the Eigenvalues for Heat Transfer in Turbulent Tube Flow, by Robert D. Cess, *J. Aero/Space Sci.*, vol. 25, no. 11, Nov. 1958, p. 723.

Analysis of Turbulent Flow and Heat Transfer in Non-Circular Passages, by Robert G. Deissler and Maynard F. Taylor, *NACA TN* 4384, Sept. 1958.

Analytical and Experimental Investigation of Temperature Recovery Factors for Fully Developed Flow of Air in a Tube, by R. G. Deissler, W. F. Weiland and W. H. Lowdermilk, *NACA TN* 4376, Sept. 1958.

Rearrangement of the Temperature Field in Flow Around a Bend, by E. R. G. Eckert and T. F. Irvine Jr., *Trans. ASME*, vol. 80, no. 8, Nov. 1958, p. 1765.

Heat Transfer in Rarefied Gases, by T. Fujimoto and K. Takao, *Trans. Japan Soc. Mech. Engrs.*, vol. 24, no. 145, Sept. 1958, pp. 642–655.

Magneto-Gasdynamic Channel Flow, by Edwin L. Resler Jr. and William R. Sears, *Zeitschrift fur Angewandte Mathematik und Physik*, vol. 9b, nos. 5/6, March 17, 1958, pp. 509–518.

Effect of Magnetic Field on Forced Convection Heat Transfer in a Parallel Plate Channel, by Robert Siegel, *J. Appl. Mech.*, vol. 25, no. 3, Sept. 1958, pp. 415–416.

Approximate Three-Dimensional Solutions for Transient Temperature Distribution in Shells of Revolution, by Maurice A. Brull and Jack R. Vinson, *J. Aero/Space Sci.*, vol. 25, no. 12, Nov. 1958, p. 742.

The Radial Flow of Heat in an Infinite Cylinder, by T. P. Newcomb, *British J. of Appl. Phys.*, vol. 9, no. 11, Nov. 1958, p. 456.

The Effect of Free Stream Turbulence on the Heat Transfer from Cylinders, by R. A. Seban, *WADC Tech. Rep.* 57-480, Sept. 1957, 32 pp.

Slip-Flow Heat Transfer from Cylinders in Subsonic Airstreams, by Lionel V. Baldwin, *NACA TN* 4369, Sept. 1958.

Free-Molecule Probe and Its Use for the Study of Leading Edge Flows, by J. A. Laurmann, *Phys. Fluids*, vol. 1, no. 6, Nov.-Dec. 1958, p. 469.

Convection Free Instrument for Measuring Infrared Radiation in the Atmosphere, by R. L. Aagard, *Rev. Sci. Instr.*, vol. 29, no. 11, Nov. 1958, pp. 1011–1016.

Effect of Spin on Natural Convection in Mercury Heated From Below, by D. Dropkin and S. Globe, *J. Appl. Phys.*, vol. 30, no. 1, Jan. 1959, p. 84.

Heat Transfer from a Vertical Flat Sur-

face by Laminar Free-Convection (The case where the physical properties of fluid depend on the temperature, and the surface has an arbitrary temperature distribution in vertical direction), by Tetsu Fujii, *Trans. Japan. Soc. Mech. Engrs.*, vol. 24, no. 148, Dec. 1958, pp. 964–972.

Stagnation-point Shielding by Melting and Vaporization, by Leonard Roberts, *NASA Rep.* 10 April 1959, 55 pp.

Channel Turbulent Flow of an Electrically Conducting Fluid in the Presence of a Magnetic Field, by Paul S. Lykoudis, *Purdue Univ., School of Aeron. Engng., Rep.* A-59-4, March 1959, 19 pp.

The Splitting of a Small Discontinuity in Magnetohydrodynamics, by G. Ia. Liubarskii and R. V. Polovin, *Soviet Phys. JETP*, vol. 35 (8), May 1959, pp. 901–902.

Cyclic Acceleration of Particles in High Frequency Fields, by V. I. Veksler and L. M. Kovrizhnykh, *Soviet Phys. JETP*, vol. 35 (8), May 1959, pp. 781–782.

Low Frequency Oscillations of a Plasma in a Magnetic Field, by K. N. Stepanov, *Soviet Phys. JETP*, vol. 35 (8), May 1959, pp. 808–811.

Construction of Exact Discontinuous Solutions of the Equations of One Dimensional Gas Dynamics and Their Applications, by V. P. Korobeinikov and E. V. Riasonov, *J. Appl. Math. Mech. (Translation of Prikladnaya Matematika i Mekhanika)*, vol. 22, no. 2, 1958, pp. 362–367.

Supersonic Profiles with Minimum Drag, by Iu. D. Shmyglevskii, *J. Appl. Math. Mech. (Translation of Prikladnaya Matematika i Mekhanika)*, vol. 22, no. 2, 1958, pp. 368–374.

Self-Similar Solutions of the Laminar Boundary Layer Equations for a Compressible Fluid Including Heat Transfer, by A. Sh. Dorfman, N. I. Pol'skii and P. N. Romanenko, *J. Appl. Math. Mech. (Translation of Prikladnaya Matematika i Mekhanika)*, vol. 22, no. 2, 1958, 375–382.

On the Interaction Between Small Disturbances and Discontinuities in Magnetohydrodynamics and on the Stability of Shock Waves, by V. M. Kontorovitch, *Soviet Phys. JETP.*, vol. 35 (8), May 1959, pp. 851–858.

Calculation of Axisymmetrical Reacting Jets at Minimum Gravity, by L. E. Sternin, *Akad. Nauk, SSSR, Izvestiia, Otdelenie Tekh. Nauk, Mekhanika i Mashinostroenie*, no. 1, 1959, pp. 41–45. (In Russian.)

Shock Waves in Multi-Component Media, by G. M. Liakhov, *Akad. Nauk, SSSR, Izvestiia, Otdelenie Tekh. Nauk, Mekhanika i Mashinostroenie*, no. 1, 1959, pp. 46–49. (In Russian.)

On the Motion of Thin Rigid Bodies Under the Influence of Shock Wave Forces, by S. S. Grigorian, *Akad. Nauk, SSSR, Izvestiia, Otdelenie Tekh. Nauk, Mekhanika i Mashinostroenie*, no. 1, 1959, pp. 165–166. (In Russian.)

Favorable Interference of Wings and Fuselage at Hypersonic Speeds, by G. L. Grodzovskii, *Akad. Nauk, SSSR, Izvestiia, Otdelenie Tekh. Nauk, Mekhanika i Mashinostroenie*, no. 1, 1959, pp. 170–173.

Streamlined Bodies in Non-Ideal Gas Flows at High Supersonic Speeds, by G. A. Luibmov, *Akad. Nauk, SSSR, Izvestiia, Otdelenie Tekh. Nauk, Mekhanika i Mashinostroenie*, no. 1, 1959, pp. 173–176. (In Russian.)

Strong Point Blasts in a Compressible Medium, by N. N. Kochina and N. S. Mel'nikova, *J. Appl. Math. Mech. (Translation of Prikladnaya Matematika i Mekhanika)*, vol. 22, no. 1, 1958, pp. 1–19.

On Exact Solutions of Certain Gas-Dynamical Equations, by S. S. Grigorian, *Soviet Phys. Doklady*, vol. 3, no. 4, July-Aug. 1959 (Russian original, vol. 121, nos. 1–6), pp. 732–735.

On Compression Waves in Magnetohydrodynamics, by S. V. Iordanskii, *Soviet Phys. Doklady*, vol. 3, no. 4, July-Aug. 1959 (Russian original, vol. 121, nos. 1–6), pp. 736–742.

Similarity-Type One-Dimensional Motions of a Conducting Gas in a Magnetic Field, by V. P. Korobeinikov, *Soviet Phys. Doklady*, vol. 3, no. 4, July-Aug. 1959 (Russian original, vol. 121. nos. 1–6), p. 743.

Concerning Riemann Waves in Magnetohydrodynamics, by A. G. Kulikovskii, *Soviet Phys. Doklady*, vol. 3, no. 4, July-Aug. 1959 (Russian original, vol. 121, nos. 1–6), pp. 743–746.

On the Character of Arc Discharges in Inert Gases, by V. N. Egerov, V. N. Kolesnikov and N. N. Sobolev, *Soviet Phys. Doklady*, vol. 3, no. 4, July-Aug. 1959 (Russian original, vol. 121, nos. 1–6), pp. 775.

Comparison of Decay Rates of Plasma in Hydrogen and Deuterium, by G. I. Glotova, V. L. Granovskii and V. L. Savoskin, *Soviet Phys. JETP*, vol. 35(8), no. 6, June 1959.

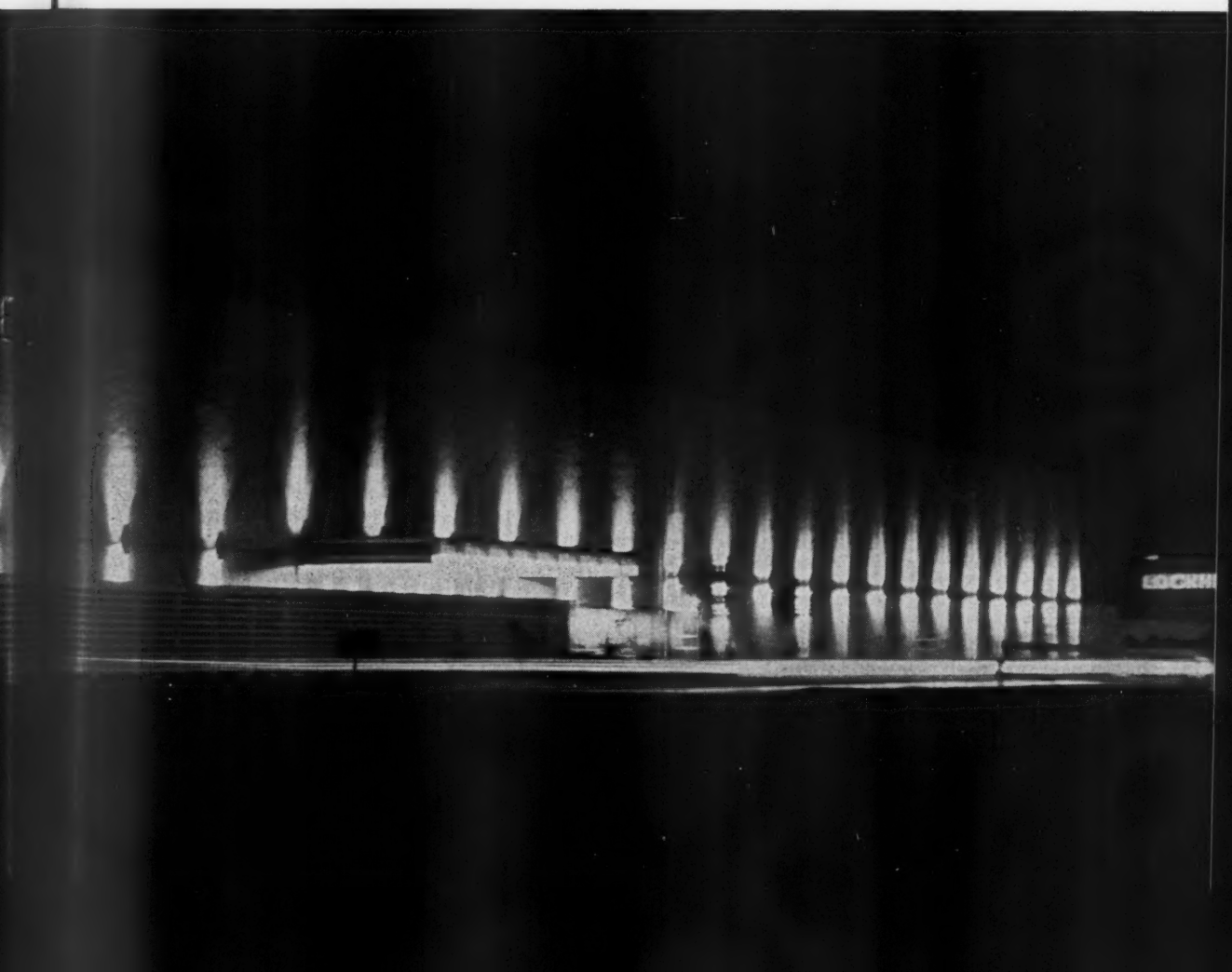

On Ablation for the Recovery of Satellites, by S. Georgiev, H. Hidalgo and M. Adams, *Avco Mfg. Corp., Avco Res. Lab., Res. Rep.* 47, March 1959, 14 pp.

Flight Mechanics

On the Solution of a Degenerate Variational Problem and the Optimum Climb of a Cosmic (Space) Rocket, by V. A. Egerov, *J. Appl. Math. Mech.* (*Translation of Prikladnaya Matematika i Mekhanika*), vol. 22, no. 1, 1958, pp. 20–36.

Flight Mechanics of Low-thrust Spacecraft, by Frank M. Perkins, *J. Aero/Space Sci.*, vol. 26, May 1959, pp. 291–297.

Planetary Orbit Chart, by Francis P. Callahan Jr., *J. Appl. Phys.*, vol. 30, March 1959, pp. 444–445.

The Next Fifteen Years of Rocketry and Rocket Mail to the Moon, by Dr. Harold W. Ritchey, *Thiokol Astronaut*, vol. 1, no. 1, 1959, pp. 12–15.

Nearly Circular Transfer Trajectories for Descending Satellites, by George M. Low, *NASA Rep.* 3, 1959, 43 pp.

Optimal Transfer between Two Coplanar Terminals in a Gravitational Field, by Louis G. Vargo, *Ramo-Wooldridge Corp., Space Tech. Labs.*, 1959, 10 pp.

Contributions of the Explorer to Space Technology, by J. E. Froehlich, *Calif. Inst. Tech., Jet Prop. Lab., External Publication* 526, July 1958, 24 pp.

The Escape Trajectory for a Vehicle in the Earth Moon Gravity Field, by Lester W. Roane, IAS Student Branch Paper Competition, 1958; First Award Papers, by *Inst. Aeron. Sci.*, Minta Martin Aeron. Student Fund, 1958, 127 pp., pp. 70–80.

Correction of Epoch Error in Circular Orbits, Part I: Correction by Tangential Transfer, by Lawrence Berman, *Mass. Inst. Tech.* (*AFOSR TN* 59-62; *ASTIA AD* 209494), Feb. 1959, 10 pp.

Perturbations of a Twenty-four Hour Satellite Orbit, by Don Lautman, *Avco Mfg. Corp., Avco Res. Lab., Res. Rep.* 43, March 1959, 12 pp.

Satellite Orbit Mechanics, by Harry Esses, *Aero/Space Engng.*, vol 18, April 1959, pp. 48–54.

Three-dimensional Satellite Orbits with Emphasis on Re-entry Dynamics and Oblateness Effects, by Jack N. Nielsen, *Aero/Space Engng.*, vol. 18, April 1959, pp. 60–66.

Application of Astronomical Perturbation Techniques to the Return of Space Vehicles, by Robert M. L. Baker Jr., ARS Journal, vol. 29, March 1959, pp. 207–211.

Motion Units to Simplify Space Travel Computations, by Bemrose Boyd, ARS Journal, vol. 29, March 1959, p. 216.

A Short Form Method for Determining Near-circular Orbit Quantities, by Joseph N. Benezra, ARS Journal, vol. 29, March 1959, pp. 216–219.

Methods for Predicting the Orbits of Near Earth Satellites, by D. G. King-Hele and Mrs. D. M. C. Walker, *J. Brit. Interplanet. Soc.*, vol. 17, Jan.-Feb. 1959, pp. 2–13.

Perturbation of Elliptic Orbits by Atmospheric Contact, II: Some Deductions from Observations of the Orbits of the First Russian Satellites, by T. R. F. Nonweiler, *J. Brit. Interplanet. Soc.*, vol. 17, Jan.-Feb. 1959, pp. 14–20.

Meteoritic Dust and Ground Simulation of Impact on Space Vehicles, by Donald H. Robey, *J. Brit. Interplanet. Soc.*, vol. 17, Jan.-Feb. 1959, pp. 21–30.

Vehicle Design, Testing and Performance

Microminiaturized Payloads Open Paths for Space Research, by Howard A. Wilcox, Astronautics, vol. 4, May 1959, pp. 20, 95.

Designing Small Space Payloads, by R. G. McCarty, Astronautics, vol. 4, May 1959, p. 24–25, 96–97.

Piggyback Missile Research Packages, by Lt. Col. Gene M. DeGiacomo, Astronautics, vol. 4, May 1959, p. 32.

Micromodules Make Their Bow, by H. J. Laiming and J. W. Knoll, Astronautics, vol. 4, May 1959, pp. 34–35.

Score—First Communications Satellite, by Marshall I. Davis and George N. Krassner, Astronautics, vol. 4, May 1959, pp. 37–39, 88, 91–92, 94–95.

Microminiaturization in a Space Vehicle Frequency Standard, by Patrick E. Lannan, Astronautics, vol. 4, May 1959, pp. 40–41, 110.

Flight Testing Spacecraft, by R. Schock and R. F. Lander, *Electronics*, vol. 32, March 27, 1959, pp. 53–57.

Flight Into Space, by Hollingsworth Franklin Gregory, *Aero/Space Engng.*, vol. 18, April 1959, pp. 37–39.

The Growing Problems in the Space Program, by H. Guyford Stever, *Aero/-*

Space Engng., vol. 18, April 1959, pp. 40–42.

Guidance and Control

An Attitude Control System for Space Vehicles, by Walter Haeussermann, ARS JOURNAL, vol. 29, March 1959, pp. 203–207.

Instrumentation and Communications

Electronic and Communications Aspects of Space Flight, by Louis N. Ridenour and Bruno W. Augenstein, *Aero/Space Engng.*, vol. 18, April 1959, pp. 55–59.

High-Accuracy Frequency Meter, by R. I. Utiamyshev, *Instruments and Experimental Techniques* (*Translation of Pribory i Tekhnika Eksperimenta*), no. 3, May-June 1958, pp. 386–389.

Multichannel Timing System, by A. A. Vasil'ev and I. I. Grigor'ev, *Instruments and Experimental Techniques* (*Translation of Pribory i Tekhnika Eksperimenta*), no. 3, May-June 1958, pp. 390–394.

On the Application of Multistage Electron-Optical Image Amplifiers in Astrophysics, by M. M. Butslov, E. K. Zavoiskii', A. A. Kaliniak, V. B. Nikonov, V. V. Prokof'eva and G. E. Smolkin, *Soviet Phys. Doklady*, vol. 3, no. 4, July-Aug. 1959 (Russian original, vol. 121, nos. 1–6), p. 693.

The Measurement of Phase Differences (A Review), by V. P. Kovalev, *Instruments and Experimental Techniques* (*Translation of Pribory i Tekhnika Eksperimenta*), no. 2, March-April 1958, pp. 173–183.

An Instrument for Measuring Microsecond Intervals of Time, by B. A. Predein, *Instruments and Experimental Techniques* (*Translation of Pribory i Tekhnika Eksperimenta*), no. 2, March-April 1958, p. 208.

Stabilization of Magnetic Fields with the Help of a Cathode Ray Tube, by V. V. Zhukov and N. N. Semashko, *Instruments and Experimental Techniques* (*Translation of Pribory i Tekhnika Eksperimenta*), no. 2, March-April 1958, p. 218.

Measurement of the Variation of the Phase Path of a Signal Reflected from the Ionosphere, by L. A. Drachev, *Instruments and Experimental Techniques* (*Translation of Pribory i Tekhnika Eksperimenta*), no. 2, March–April 1958, p. 238.

Vacuum Flowmeter, by M. I. Basalaev and N. Ia. Basalaeva, *Instruments and Experimental Techniques* (*Translation of Pribory i Tekhnika Eksperimenta*), no. 2, March-April 1958, p. 260.

Method of Controlling the Operation of an Ion Source, by G. M. Osetinskii, *Instruments and Experimental Techniques* (*Translation of Pribory i Tekhnika Eksperimenta*), no. 2, March-April 1958, p. 291.

Investigation of the Focusing Properties of an Ion Extraction System in a High Frequency Ion Source, by A. N. Serbinov, *Instruments and Experimental Techniques* (*Translation of Pribory i Tekhnika Eksperimenta*), no. 3, May-June 1958, p. 360.

A Multichannel System for Radioactive Telemetering, by A. A. Bragin, V. N. Mikhailovskii and A. N. Svenson, *Instruments and Experimental Techniques* (*Translation of Pribory i Tekhnika Eksperimenta*), no. 3, May-June 1958, p. 377.

A Magnetic Analyzer for the Study of Nuclear Reactions, by G. F. Timushev, *Instruments and Experimental Techniques* (*Translation of Pribory i Tekhnika Eksperimenta*), no. 1, Jan.-Feb. 1958, pp. 21–29.

A Differential Time Analyzer for Measuring Time Intervals of 10^{-8} to 10^{-10} Sec., by E. E. Berlovich, *Instruments and Experimental Techniques* (*Translation of Pribory i Tekhnika Eksperimenta*), no. 1, Jan.-Feb. 1958, p. 74.

A Method of Automatic Compensation in Measuring Low Gas Pressures, by V. I. Bakhtin, *Instruments and Experimental Techniques* (*Translation of Pribory i Tekhnika Eksperimenta*), no. 1, Jan.-Feb. 1958, p. 96.

Atmospheric and Space Physics

Observation of Nuclear-Active Particles of Cosmic Radiation with Energy $\geq 10^{13}$ ev, by E. A. Murzina, S. I. Nikol'skii and V. I. Iakovlev, *Soviet Phys. JETP*, vol. 35 (8), May 1959, pp. 906–907.

On the Question of Antigravitation, by Iu. A. Aleksandrov, V. A. Andreev and I. I. Bondarenko, *Soviet Phys. JETP*, vol. 35 (8), May 1959, p. 911.

Measurement of Cosmic-Ray Intensity in the Stratosphere at Various Altitudes and Latitudes, by A. N. Charakhch'ian and T. N. Charakhch'ian, *Soviet Phys. JETP*, vol. 35 (8), May 1959, pp. 761–771.

The Acceleration of Cosmic Rays in a Fluctuating Magnetic Field, by V. M. Baikov and R. G. Avalov, *Soviet Phys. JETP*, vol. 35 (8), May 1959, pp. 826–828.

Investigation of Nuclear Disintegration Produced by the Charged Component of Cosmic Radiation, by G. V. Khrimian, *Soviet Phys. JETP*, vol. 35 (8), no. 5, May 1959.

The Earth and Inertial Space, Part I: Motions of the Earth, by Richard H. Parvin, *Aero/Space Engng.*, vol. 18, April 1959, pp. 34–36.

Human Factors and Bio-Astronautics

Implications of Space Radiations in Manned Space Flight, by Wright H. Langham, *Inst. Aeron. Sci., Rep.* 59-52, Jan. 1959, 19 pp.

Training in Preparation for Man High I, by Joseph W. Kittinger Jr., *Inst. Aeron. Sci., Rep.* 59-81, Jan. 1959, 7 pp.

Some Fundamental Problems Associated with Injecting, Orbiting and Recovering a Man from Orbit, by R. C. Hakes, *Inst. Aeron. Sci., Rep.* 59-80, Jan. 1959, 10 pp., 14 figs.

Temperature Equilibria in Space Vehicles, by Robert Cornog, *Ramo-Wooldridge Corp., Space Tech. Labs.*, 1958, 12 pp.

Crew Escape from Space Vehicles—and Survival, by Hugo F. Mohrlock and Earl A. Kops, *Aero/Space Engng.*, vol. 18, April 1959, p. 79–82.

BASIC RESEARCH AT LOS ALAMOS INCLUDES NUCLEAR PLATE STUDIES OF HIGH ALTITUDE RADIATION PHENOMENA.

Index to Advertisers